Cranfield

College of Aeronautics Report No. 8702
March 1987

The Redesign of the College of Aeronautics Whirling Arm Facility

by D.I.T.P. Llewelyn-Davies

College of Aeronautics
Cranfield Institute of Technology
Cranfield, Bedford MK43 0AL, England

Cranfield
College of Aeronautics Report No. 8702
March 1987

The Redesign of the College of Aeronautics Whirling Arm Facility

by D.I.T.P. Llewelyn-Davies

College of Aeronautics
Cranfield Institute of Technology
Cranfield, Bedford MK43 0AL, England

ISBN 0 947767 56 8

£7.50

SUMMARY

This report traces the history of the development of the Whirling Arm method of aerodynamic testing and in particular that of the CoA Whirling Arm, which also had been used recently for research on hovercraft.

Recently it was decided to revert to aerodynamic testing and to modify the facility for this purpose. Previous experience had shown that the swirl generated in the test chamber by the rotation of the arm was unacceptably high for aerodynamic work. The opportunity was therefore taken to modify the structure to reduce the swirl at the same time as a suitable method of supporting models in the tunnel was designed and installed.

Although the whirling arm method of test is unusual these days, it is particulary suitable for the determination of the rotary derivatives of an aircraft and the measurement of the characteristics of bodies etc in curved flows. As the problems presented by the presence of swirl in the test chamber and the effects of centrifugal force on the measurement of the forces and pressures on the models are not generally encountered, the basic reasons that controlled the redesign of the facility are described in detail so that this report can act as a "primer" for future users of the facility.

Some assessment has been made of the accuracy that can be achieved in the measurement of forces and pressures under normal operating conditions and possible methods of improving the unsteadiness of the flow approaching the model and breaking up the wing trailing vortices before they encounter the model are discussed.

CONTENTS

1.0 INTRODUCTION

For some years the C o A whirling arm facility has been engaged on hovercraft research programmes. When these concluded recently, it was decided to remove the specialised support systems etc and to modify the facility to make it suitable for aerodynamic research programmes.

Although the whirling arm was the preferred facility for making measurements on captive models from the middle of the 18th century until the beginning of the 20th century, it is an unusual facility these days. It presents many problems that are additional to those encountered in windtunnels and which must be considered carefully at the outset if good quality research work is to be possible. The C o A whirling arm was acquired in the 1950's when the National Physical Laboratory decided to dispose of their whirling arm to make the space available for other facilities. This whirling arm was the third in the series of whirling arms used by the N.P.L. It is therefore instructive to review their development as it highlights many of the problems to which satisfactory solutions have to be found.

This report reviews the development of the N.P.L whirling arms and thus derives a specification for the changes to the present design that are considered necessary. The reasons for the design and structural modifications are discussed as is the new instrumentation system and the special model design and manufacturing techniques that have to be used. The aerodynamic and structural characteristics of the revised design have also been evaluated.

2.0 THE DEVELOPMENT OF WHIRLING ARMS

In a whirling arm facility a model is mounted on one end of a counterbalanced arm which is rotated about a vertical axis. Although a model mounted from the end of the arm can easily be moved through the air in a regulated manner so that it should be possible to measure the forces and/or the pressure distribution over it, there are several limitations to the technique. The main ones are:-

a) The path of the model is circular not straight and the speed of the airstream encountered by the model varies with radius.

b) The model is subjected to quite high centrifugal loading. Because of this it is preferable for the models used for the measurement of forces to be light in weight as the aerodynamic loads have to be measured in the presence of the centrifugal forces which can be large in comparison. Another effect of centrifugal force which is not so obvious is that in making pressure measurements, a correction has to be made for the effect of the variation with radius of the centrifugal force on the mass of air in the pressure tubes.

c) When the arm is rotating especially inside a building, the motion of the arm induces a flow in the neighbourhood of the model which is in the same direction as the direction of rotation thus reducing the speed of the model through the air as compared with the circumferential speed.

The circular path of the model was not of great importance in the early days of the technique as much of the work done was either on compact ballistic shapes, e.g. ball ammunition, or was to establish general principles. In any case, as no more accurate method of model testing was available until the latter part of the 19th century, any reasonably accurate and repeatable measurements were better than none at all. However in these days, aerodynamic testing should be limited to those in which curved flow is an essential feature.

Once the implications of centrifugal loadings are realised, their effects can be minimsed and allowed for by a mixture of suitable model design, test techniques and calculation.

The swirl induced in the building in the path of the model is deleterious in that both the forces and pressures to be measured on the model vary as the square of the approach speed of the air. In addition it is not axiomatic that the swirl is solely circumferential in direction, in which case the radial components give rise to an inclined incident flow over the model and deviations over the model length from the assumed curved flow.

2.1 The first NPL whirling arm, 1908 - 1925 (ref 1)

The first NPL whirling arm (Fig 1) did not differ greatly in concept from the original whirling arm built by Benjamin Robins in 1746 (ref 2), except that an electric motor was used to drive it at speeds of up to 30 rpm instead of the system of falling weights used by Robbins which incidently was an integral part of his measurement system. The arm consisted of a lightweight wirebraced triangulated tubular structure with a flat plate, or table, at one end of the arm and a counterweight at the other end to dynamically balance the arm about its axis of rotation. The model which had a maximum design weight of 15 lb (6.8 kg) was attached to the table at the design radius of 30.0 ft (9.14 m). In order to be able to test independently of the weather the arm was housed inside a large shed which was 80 ft (24.4 m) square.

The initial programme of work intended for the facility was to measure the variation of propeller performance with forward speed (ref 3). It was realised that as the propellers had a relatively large diameter, the incident speed would not be uniform, but as at that time airships were still considered to be the most promising form of aeronautical transport, this deficiency was actually regarded as an advantage as the arm would provide a flow that would approximate to the actual flow field in which the propellers would be operating in the neighbourhood of the airship hull as compared with the straight uniform flow provided by a wind tunnel.

However, much of the published work of the time (refs 4&5) concerned itself with the measurement of the swirl in the building and the calibration of anemometers and pitot-static tubes, subjects which were mutually dependent.

The swirl speed in the buiding was about 3 ft/sec (0.9 m/sec) so as the anemometers only began to work at about half that speed, their calibration presented some difficulties. The method used (ref 4) was to attach the anemometer to the table on the arm and rotate the arm at a slow speed. Then assuming that the swirl speed varied linearly with rotational speed, the then current experimental determination of swirl speed of 35 fpm (11.5 m/minute) at an arm rotational speed of 500 fpm (152.4 m/minute) was used as a basis for correcting the circumferential speed. This revised calibration was then used to remeasure the swirl speed in the building which was found to vary linearly with rotational speed (as assumed) and to have a value of approximately 7.4% of the rotational speed.

An alternative method of measuring the swirl speed was also employed using a pitot tube on the end of the arm and making use of the correction to pressure measurements due to the effect of centrifugal force on the air in the pressure tubes (ref 5). If a pressure tube is open to atmospheric pressure, p, at the centre of the arm, then at radius R the pressure will be

$$p + 1/2\rho R^2\Omega^2$$

or

$$p + 1/2\rho V^2$$

where V is the circumferential speed at radius R. A pitot tube at the same radius will read a pressure of

$$p + 1/2 v^2$$

where v is the approach speed of the air (i.e the difference between the circumferential and swirl speeds). Hence as the difference between the two pressures is fairly large, being proportional to the difference between the squares of two moderately large numbers, it can be measured accurately and hence the swirl speed can be determined. Using this technique good agreement with the anemometer method was obtained as reported in ref 5.

Little of the work done by the whirling arm after this has been published, but some extremely interesting work was done by Jones (ref 6) on the calculation and measurement of the loading distributions on a 4:1 prolate spheroid in straight and curved flow. For the tests in curved flow the model was supported under the table at the end of the arm by a rear support sting attached to a rear extension to the table (Fig 1), this method of support being chosen to minimise support inteference. Good agreement was obtained between the theoretical and experimental results except over the rear of the body where the flow separated due to the high adverse pressure gradient and sting interference.

2.2 The second NPL whirling arm, 1925-c1942.

It would appear that by the early 1920s, it had been decided that the whirling arm should concentrate on the type of tests for which it was uniquely suited, i.e the rotary derivatives of an aircraft and in particular m_q, l_p and n_r. The usual way of measuring these derivatives was by means of oscillatimg a model in a wind tunnel. Both free and forced oscillation techniques were used but neither method measures the derivatives directly as a correction has to be made because of the incidence changes during the oscillation. In consequence of the appreciable time taken for the downwash field from the wings to reach the tailplane, the effective incidence of the tailplane does not correspond to that expected from the incidence of the wing at the same instant. A correction for this can be applied with some confidence if the wing is completely unstalled during the oscillation, especially if the rate of change of downwash over the tailplane is linear with incidence. However once the stall is approached or past, the corrections necessarily become uncertain with a corresponding uncertainty in the values of the rotary derivatives. The advantage of the whirling arm method of test is that the model is tested in curved flow in steady conditions and so needs no corrections to allow for the time lag in the downwash field over the tailplane. In addition the model can be tested with confidence both in and past the stall with the usual provisos of Reynolds number effects and flow oscillations at the stall.

In order to make these experiments an experimental rig had to be developed to support the model and measure the necessary forces and moments. It would appear that it was not possible to incorporate a suitable rig in the original whirling arm and so a new whirling arm was obtained.

The new whirling arm (Fig 2) differed

appreciably in design from the previous one in that it consisted of a largely symmetrical series of bays made from light tubing wire braced for extra rigidity. The model was located in the outer bay on one side at the same radius as the original arm and was pivoted about an axis through its centre of gravity by means of special fixtures (Fig 3). These fixtures were held rigidly in the centre of the bay by wires from the corners. The moments of the model about the various axes were measured by special balances incorporating spring suspensions which are fully described in references 7 & 8, together with the method of balancing out the centrifugal forces due to model weight.

Initial experience with the new whirling arm showed that the flow past the model was unsatifactory in that the circumferential swirl was of the order of 12%, rather higher than desirable. In addition there was also an outward radial component of swirl which resulted in the incoming flow to the model making an angle of about 3.5 degrees with the desired tangential direction.

Modifications were therefore made to improve the flow in the working bay. As much structure as possible was removed from the outer part of the balancing arm in an attempt to reduce the swirl in general and in particular to reduce the disturbances directly in the path of the model. Some of the structure at the tip of the balancing arm was left however apparently to support a measuring tube at approximately the radius of the model to measure either speed, swirl or static pressure at the model radius. Due to the removal of the structure, heavier balance weights had to be added and were positioned at the extremity of the remaining main structure. Secondly two large aerofoils were mounted vertically from the inner and outer leading vertical members of the end test bay to correct the radial swirl induced by the arm. As might be expected, the drag of these aerofoils was large and increased the swirl measured in the building to some 18%, but the aerofoils formed a slight contraction which accelerated the flow over the model so that tha swirl in the model region remained at 12%.

As the structure of the arm was very light, it was somewhat flexible. In addition, the aerofoils not only weighed 150 lb (68 kg) but were a considerable distance from the torsional axis of the arm with the result that a further 120 lb (54.5kg) balancing weight had to be added to balance the arm torsionally. In addition the original estimate of 50 lb (23 kg) for the weight of the model, support, balances and wind shield was seriously in error, with tha actual weight being some 160 lb (73 kg). The total load at the test bay was therefore some 400 lb (180 kg) against an original design load of 50 lb, resulting in a serious reduction in the factor of safety of the structure.

This gross overloading resulted in considerable difficulty in obtaining consistent, reliable results. Thus when it was decided that the models should be tested with driven propellers, the resultant increase in weight would have led to unacceptable flexibility of the structure as well as a further decrease in the safety factor.

After careful consideration of several alternatives (ref 1),it was decided that the only practical solution was to replace the arm with a completely redesigned structure in a specially designed building.

2.3 The third NPL whirling arm c1942

The operational requirements for the new facility were as follows:-

1) Initially it was required to measure yawing and rolling moments due to continuous yaw and pitching moment due to continuous pitch. Ultimately the measurements would be extended to measure lift, drag and sideforce as in a

measure lift, drag and sideforce as in a conventional windtunnel.

2) Rigidity and dynamic balance of the structure were essential.

3) The model radius should be 30 ft (9.14 m) as previously, but the maximum rotational speed would be 31.8 rpm to give a model speed of 100 fps (30.5 m/s).

4) The model speed should be controllable to within 0.15 fps (0.045 m/s) over the range of 8.5% to 100% of full speed.

5) The method of supporting the model should be the same as previously in concept but a much more rigid structure was essential.

6) It should be possible to mount flow correction aerofoils to adjust the flow over the model if necessary.

7) The model incidence should be variable over the range +/- 20 degrees.

8) The design loads are:-

weight of model and windshield	= 100 lb (45.5kg)
maximum model lift	= 100 lb (45.5kg)
maximum model drag	= 25 lb (11.4kg)

9) Provision should be made to dynamically balance the arm by means of counterweights.

10) The complete arm was to be housed inside a special circular building of 87ft (26.5m) in diameter and 18ft (5.5m) high. The main structure was to be positioned inside a circular screen wall extending from floor to ceiling with a continuous slot in it to allow the passage of the model support system. Eight sets of partial baffles from the floor and ceiling were to be provided in the test annulus to reduce the swirl in the annulus.

The facility is described in full in ref 1 and is illustrated in Fig 4. The drawing shows that the resultant design consists of a large braced-girder bridge type central structure which is symmetrical about the axis of rotation with a very substantial 'claw' structure at one end incorporating cantilevered booms or 'horns' from which the model was held in position by wires. Considering the lightness and flexibility of the previous structure, the new whirling arm went to the other extreme with a rotating mass of some 20,000lb (9,100kg) and needing a counterbalance weight of approximately 2,900lb (1,320kg) to dynamically balance the model and support system.

Calibration showed that the velocity was reasonably uniform over the area occupied by the model and that the swirl was 7.5% of the rotational speed. Some adjustment of the flow correction vanes was necessary to achieve an average yaw variation over the model region of about 1/4 degree.

2.4 The transfer of the whirling arm to C o A

When the arm was acquired by C o A, the only suitable building available to house it was not large enough to take the complete arm and model support claw. The design was therefore modified (Fig 5). The central arm structure with its motor and gearbox was installed unaltered. As the NPL had kept the motor-generator set providing variable voltage DC to the drive motor, another generator set was installed. Unfortunately this could only supply 600V DC maximum instead of the 720 V DC of the original set, resulting in a reduction of the maximum rotational speed of the arm to about 27 rpm instead of the original 31.8 rpm.

A new working section was built to fit inside the smaller building. It consisted of an annular test chamber of constant cross-section, 8.5 ft (2.6m) wide and 11.1 ft (3.38m high. This was much smaller than the orginal open section test area, but it was hoped that the vertical walls relatively close to the model would have the same effect in constraining any undesired radial flow as the guide aerofoils that had to be mounted at the end of the arm on the previous designs.Due to the building limitations the centreline radius was reduced to 27.25ft (8.3m). As the initial research programme was to be an investigation of wing characteristics in ground effect, it was decided to make the bottom wall of the test section adjustable in height. Because the wing would be rotating near the floor, it was not possible to install swirl dampers as had been done previously. The horizontal centreline of the arm was not central in the tunnel, being 7.0ft (2.56m) below the top wall; in addition it was not central in the 32 in. (0.81m) wide slot through which the model support system travelled, being approximately 1.5 in. (0.06m) above the centreline of the slot.

Calibration of the flow in the test section (ref 9) showed that the swirl was high (22.5% of the circumferential speed) and varied little with radius. The flow had an outward yaw of about 0.5 degrees in the neighbourhood of the vertical centreline of the test section, but this altered rapidly outside about 10in (0.25m) from the centreline. The yawmeter calibration also showed that the flow had a large downwards pitch of about 2 degrees which again varied appreciably across the section. It would seem likely that the erratic flow variations in both pitch and yaw across the section and the large downwash in the centre of the tunnel were due to a forward interference effect from the probe's support structure and should be disregarded except that the 1/2 degree yaw in the centre of the section may be a reasonable approximation to the yaw in undisturbed flow.

An earlier calibration (ref 10) had shown that the presence of the calibration rig and its support made relatively little difference to the measured swirl. In addition the swirl in the central volume containing the main arm structure was, if anything, greater than the swirl in the test annulus. These conclusions are qualitative rather than quantitive as there were some unresolved discrepancies in the measurements.

Later work by Andrews (ref 11) showed that the swirl could be reduced to about 17% by the installation of plates to both ends of the arm. However no details of the plate geometry are available.

In 1972 the facility was modified for the investigation of the dynamic characteristics of hovercraft in waves. As the object of the research was the behaviour of the cushion and skirt in the presence of waves, the airflow characteristics over the model were of minor importance which was fortunate as the test rig (Fig 5) was very bulky and as a result the swirl was probably very large. In order to scale properly the elastic forces in the skirt and air, it was found necessary to operate the model in an artificially enhanced gravity field. This was achieved by mounting the model on the end of the arm with its skirt vertical. The wave effect was achieved by running the model over a "wave board" mounted from the outer wall of the test section and extending 2ft (0.61m) on either side of the centreline of the arm. Although the hovercraft rig changed appreciably with time, the basic arm and test section remained unaltered until the hovercraft programme terminated in 1983.

3.0 MODIFICATION OF THE WHIRLING ARM FOR AERODYNAMIC TESTS

In the light of the evolution of the whirling arm, a critical appraisal was made of the desirable airflow qualities and how the models should be supported in the test section.

3.1 The importance of swirl

There is an instinctive feeling that the swirl should be kept as low as possible. The energy causing the swirl must come from the drag of the rotating structure, and the equilibrium value of the swirl will depend on the absorption of this energy in the test chamber and central volume. If the swirl is high, then the drag of the rotating structure must be high and thus the quality of the flow is likely to be poor because of the eddies shed by the inherently poor aerodynamic characteristics of the structure. In the present design, the absorption of energy in the test chamber is very small coming solely from the skin friction of the walls. In the installation at the NPL the absorption of energy in the working chamber was much greater due to the extensive system of baffles fitted. However these baffles must have resulted in considerable unsteadiness in the flow encountered by the model.

Another equally compelling reason for keeping the swirl as small as possible is that the test programmes will require the measurement of the overall forces on the model. The aerodynamic forces and moments on the model will be fairly small because the model speed will be approximately 72 fps (22m/s) maximum. These forces have to be measured in the presence of the centrifugal force in the horizontal plane due to the mass of the model, i.e. in a 6g environment. Thus in order to minimise the corrections that have to be applied for the centrifugal effects, it is essential to keep the aerodynamic forces as high as possible in relation to the centrifugal forces. Thus as the aerodynamic forces vary as the square of the air speed it is essential to keep the swirl as low as possible as the approach air speed equals the speed of rotation less the swirl speed and for every 1% reduction in air speed there is a 2% reduction in the forces to be measured. However there is no reduction in the centrifugal force thus leading to an even more unfavourable ratio of aerodynamic to centrifugal forces.

Similarly the pressures over the model vary with the square of the airspeed and thus the magnitude of the pressures to be measured by the pressure transducers falls appreciably with increase in swirl. As the pressures to be measured are already small so that the pressures and measuring equipment are only working in the lower part of their range, the discrimination of the system may be appreciably less if the swirl is high.

For these reasons it would appear that any redesign should tackle the problem fundamentally by reducing the drag of the rotating structure as much as possible regardless of whether it is in the test section or the central volume. If the resultant swirl is still considered to be too great then it may be necessary to fit baffles in the test section or other palliatives.

In the past it would seem that a swirl of about 7% was the lowest achieved and therefore this value should be accepted as the design target.

3.2 Requirements for a model support system

In any test it is essential that the model should be mounted so that the interference of the support system on the model should be as small as possible. It would therefore seem that the previous method of mounting the model to external balances by means of wires (refs 7 &

8 and Fig 3) should be abandoned in favour of the system generally used in transonic and supersonic tunnels where the model is mounted from a slender sting entering the model from the rear, and measuring the forces and moments on the model by means of an internal straingauge balance which is an integral part of the sting support. Although it may be necessary to distort the rear fuselage of some models to accommodate the support sting, the effects are likely to be small as compared with the effects of the wires etc. to external balances which generally have to be attached to models in aerodynamically sensitive regions where their presence may cause major changes in flow conditions, e.g. premature flow separations.

An additional disadvantage of the external balance is that it has to operate in a 6g environment. As the normal multi-component balance as used in subsonic wind tunnels is very large and heavy in order to minimise interaction between the various components, the design of a suitable general purpose balance will be difficult and it is likely that is will be necessary to design several balances capable of measuring only one or two components, as previously done at the NPL.

As there is considerable interest in measurements in the region of the stall, a large incidence range is desirable both in and normal to the plane in which the model is rotated. It was decided that the main continuously variable incidence range should be +/- 15 degrees in the plane of rotation. The actual range can be altered by the use of cranked support stings so as to vary the datum of the 30 degree total travel. Incidence in the plane at right angles to the plane of rotation will be achieved in one of the following ways:-

a) a series of cranked stings to give various fixed values of incidence
b) one sting of large crank which allows rotation at both the model and support end so that the wings can be kept in the same plane whilst the angular setting in the plane at right angles is altered

within the range determined by the crank angle and the offset in the plane of rotation is nulled by the main continuously variable incidence system

c) a continuously variable system based on either a pivot joint in the support sting or some form of virtual-centre mechanism attached to the main support

In the design of the support system it should be borne in mind that in order to minimise forward interference from downstream of the model, no large changes in sting cross-sectional area or sting direction should take place within approximately 2.5 body diameters behind the base of the model.

4.0 MODIFICATIONS TO REDUCE SWIRL

The main arm was a highly redundant structure fabricated from rolled steel angle sections with the exception of the outer frame which was a casting. The ratio of structural to total frontal area was relatively large. It is known that the aerodynamic drag of this type of structure is very high and therefore there was likely to be considerable drag and turbulence generated in the neighbourhood of the tip of the arm in the region of the slot between the central volume in which the arm structure rotates and the test section (ref 9). As has been noted in section 2.4, it had been found that the swirl had been reduced from 22% to 17% by the installation of plates at the end of the arm, but even so the swirl was still very high so it was likely that considerable energy was being transferred from the central volume to the test section via the slot. Accordingly it was decided to do limited lowspeed wind tunnel tests to investigate the drag of the structure and possible ways of reducing it so that any necessary modifications could be planned before the whirling arm tests on hovercraft were concluded.

4.1 Low speed wind tunnel tests on a partial model of the whirling arm structure

A 3/8 scale model of the outer two bays of the arm structure was made from commercially available aluminium angle which was available in approximately the correct scale sizes (Fig 6). The individual bracing members were bolted to the main corner members so that they could be removed if required. The outer bulkhead casting was represented by an angle section periphery mounted on an aluminium plate with the central hole represented and the web structure represented by wooden members. The inner bay was mounted on a 1/8 inch (3mm) thick aluminium plate which was attached to a centrally positioned 2.0 inch (50.8mm) diameter aluminium tube incorporating a strain gauge balance which measured the drag force on the structure and its line of action. The support tube was attached to the overhead balance of the CoA 3ft 6in (1.07m) diameter open-jet lowspeed windtunnel so that the whole of the structure was inside the jet. The model was aligned with the airstream to correspond with the conditions in the whirling-arm. Measurements were made of the drag of the structure both in its original condition and with the progressive removal or fairing of the members. It should be noted that the drag values quoted include the drag of the part of the support cylinder in the airstream; no attempt was made to measure this as a) it was common to all the measurements, b) it was small in comparison with the drag of the original structure and c) the tests were intended to be qualitative rather than quantitative.

The tests were made at a wind speed of 100fps (30.5m/sec). As the flow around the members is basically completely separated, it was Reynolds number insensitive and thus there was no need to fix transition.

The results are given in Table 1 and an analysis of them is shown in Fig 6. The analysis shows that the drag coefficient of the unfaired structure, based on the actual frontal area of the angle members,plates etc, does not vary greatly from 2.0 as successive members are removed. This agrees well with the drag coefficient of a two dimensional flat plate normal to the stream and not with the three dimensional value of 1.2 that is generally used (ref 12). As the structure tested consisted of several members in the wake of the leading member, either the wake was unaltered by the presence of the additional members, or the drag of the leading member was modified from the three dimensional value by the other members behind it.

However it was found possible to reduce the drag coefficient of the streamwise panels to 0.44 by adding an elliptical nose fairing to the front member,a similar fairing modified to have a 15 degree semi-angle trailing edge attached to the rear member, and a straight fairing between the front and rear members which covered the intermediate crossbracing. Thus by fairing the streamwise panels and removing the bracing in the vertical plane,it was found possible to reduce the drag of the model to less than 0.14 of its original value.

Oilflow patterns of the flow aroud the end of the arm were obtained by inserting a reflection plate on the model centreline (Fig 7). The patterns (Fig 8) showed conclusively that there was a considerable flow spillage around the unfaired arm resulting in large flow deviations extending a considerable distance from the tip. The revised faired structure reduced the flow spillage appreciably.

One possible method of reducing the spillage which must result in swirl in the test region is to reduce the width of the connecting slot between the central volume and the test region. An investigation of the effect of the slot width was made by using an additional plate mounted normal to the reflection plate to represent the inner wall of the test region (Fig 7). The changes of the flow patterns observed as the slot width was reduced were small (but favourable) in comparison with the large changes due to fairing the structure (Fig 8).

It was also attempted to represent a baffle system that would minimise flow through the slot (Fig 7). The flow patterns showed that the baffles had a small unfavourable effect as the the outflow as shown by the flow patterns on the reflection plate was slightly more marked.

4.2 Modifications to the arm structure

As the windtunnel tests showed that large reductions in the drag of the whirling-arm structure could be achieved by removing as much as possible of the bracing normal to the airstream and fairing the remaining members, an analysis of the stresses in the existing structure was made using the FINEL finite element analysis programme. At the time of doing the analysis the 3-D programme was experiencing some intermittent faults, and so the analysis was performed on a pseudo 2-D representation of the structure in which the reactions of the model and its support system were applied to representations of the vertical framework with the loadings due to the centrifugal force on the horizontal crossbracing applied at the appropriate nodes. For this analysis it was assumed that the weight of the claw, model,etc was 3000 lb (1364kg)acting on the centreline of the arm at a radius of 29 ft (8.84m). From this information the reactions at the corner nodes at the outer ends of the arm structure were calculated both with the arm at rest and with the arm rotating at 31.8 rpm. The results of the analysis are presented in Figs 9 & 10. They show that with the arm at rest (Fig 9), the compressive stress in the bottom beam is about 1600lb/sq.in giving a compressive load of about 4000lb compared with the 3700lb quoted in ref 1. The bracing,especially the vertical members are very lightly loaded. When the arm is rotating (Fig 10), both top and bottom main beams are in tension and the stress increases markedly towards the centre due to the centrifugal forces on the arm structure. The diagonal bracing is more highly stressed than when at rest, but nevertheless is still lightly stressed, while the vertical members are under a slight compressive loading. The stress at the outer extremity of the top member is approx 4600lb/sq.in., corresponding to a load of 11,400lb (5180kg) as compared with the 10,400lb (4730kg) estimated in ref 1. However the stress increases to 5600lb/sq.in. at the inner corner corresponding to a load of 14,000lb (6365kg)

It would appear that the calculated loads at the outer end of the arm both at rest and when rotating agree reasonably with the values given in ref 1 as the exact external loading used to determine the original loadings was not stated. However it would appear that the mass of the arm structure was not taken into consideration in the original calculations which therefore underestimated the maximum stress by some 23%. The stress levels, even so, are well within the safe level which is normally taken as about 18000lb/sq.in. for rolled steel sections.

Before proceeding further it was necessary to decide on a practical design for the revised structure. Consideration of the above stress analysis showed that the main corner members were all in tension when the arm was rotating and thus, as the structure was fundamentally stable, the crossbracing in the vertical plane was redundant and contributed unfavourably to the overall loading due to the centrifugal forces due to their mass. When the arm was at rest, the bottom corner beams were in compression, so some form of diagonal bracing was desirable to guard against buckling.

When the arm rotates there is a linear increase in circumferential speed (V) with radius. As the aerodynamic drag increases with the square of the speed, it is particularly important to minimise the frontal area of the structure and reduce the drag coefficient of the structural elements in the outer region. In the modified design it was decided to remove all the vertical and diagonal bracing in the two outer bays and to leave only a minimum of diagonal beams in the inner bays to form a rigid triangulated structure with two nodal points along the bottom beams to ensure that no buckling would occur under static loading. This could easily be done as all the vertical members were located by fitted bolts. It was also decided not to remove any of the horizontal interbeam bracing as it would be within a fairing similar to that tested in the lowspeed tunnel, and in any case the members were riveted together and so would have been more difficult to remove.

As the design of the model and its support system had not been decided in detail at this stage, the working loads for the revised arm structure were derived from the following assumptions :-

a) Although the present motor-generator set was only capable of driving the arm at about 26.5 rpm, it is possible that it may be replaced in the future by another capable of driving the arm at its original maximum speed of 31.8 rpm. Therefore all stressing should be done for the higher rpm.

b) The model weight was assumed to be 10 lb.(4.5kg) at a working radius of 27ft 3in (8.306m), and acted 76in. in front of the centreline of the arm. This weight may appear to be low, but past experience in the construction of dynamic models and calculations of the weight of a typical model using balsa shell construction showed that this weight is achievable.

c) The weight of the windshield which shields the model from the airstream so that the centrifugal effects on the measuring systems can be assessed, is included in the estimated weight of the sting. This wind shield need only be a light fabric-covered structure attached to the sting behind the model. Its weight should not exceed 5 lb.(2.5 Kg) maximum.

d) The maximum lift generated by the model was taken to be 100lb. Although it can act in either the vertical or horizontal plane, for stressing purposes ,it was considered to act vertically downwards at the same postion as the model weight. This was considered to be the most serious case as it applied torsion to the arm structure as a whole whilst loads in the horizontal plane would only alter the tension loads in the corner members where the previous calculations had shown that there was an adequate safety factor

e) The weight of the support sting was assumed to be 30lb (13.6kg) acting at a point 46in. (1.17m) ahead of the centreline of the arm structure. Again this weight estimate may appear to be low, but calculations have indicated that it is realistic given that the assumed model weights can be achieved. It will be shown in later discussions that it is essential for a variety of reasons to achieve the lowest pratical weight for the model and support sting as high weights degrade the accuracy of the experiments.

f) The initial model support system will allow the model to be pitched in the horizontal plane only. As it will be in the horizontal plane of the centreline of the arm and roughly symmetrically placed with respect to the end frame, its main effect will be on the tension in the corner members. However it is intended to provide a pitch facility in the vertical plane, and an allowance of 300lb was taken for a suitable system which was taken to act on the centreline of the arm at a radius of 28ft 9in. (8.76m) i.e. at the centre of the support system when the model os at zero incidence relative to the tangent to the working radius at the midpoint of its length.

The stresses in the revised structure with these applied loads and those due to the mass of the structure were then calculated using the same method as previously.

In addition the stresses in the redesigned structure were calculated for the original loads.

The results of these analyses are presented in Figs 11 - 14.

The analyses of the revised structure and model support system (Figs 11 & 12) show that due to the offset loading of the model and sting, the stresses in the front and back frameworks are slightly different, with the front frame being the more highly stressed. At rest, the diagonal members are now stressed more highly than the corner members, but even so,the maximum stresses (both compressive and tensile) are less than 500 lb/sq in. When the arm is rotating at maximum speed the stresses in the diagonal members are little altered while the stress in the top corner members increases to about 1600 lb/sq.in. maximum.

When the original loading conditions are applied to the revised structure (Figs 13 & 14), the stress levels are rather smaller than those calculated for the original structure primarily due to the reduced mass of the revised structure.

The FINEL package also has the facility to calculate the deflections of the structure. The calculated deflections in all cases was less than 0.02in. (0.5mm). the asymetric loading conditions imposed by the new support system caused negligible differential displacement of the front and back frames considered as independent frameworks. As the tip frame is a very rigid casting with extra bracing members welded to it and no allowance has been made for the effects of the extensive horizontal bracing on the torsional stiffness of the structure it would appear that in practice the structure will not twist under load.

The critical buckling lengths were calculated for the members under compression. In all cases they were considerably greater than the actual lengths of the compression members.

Thus the structure is lightly stressed for its proposed duty and considerable extra mass can be accommodated if required without endangering the main structure.

4.4 Fairing of the modified structure

The windtunnel tests on the 3/8 scale partial model had shown that considerable drag reductions could be made by fitting simple nose and tail fairings and filling in the space between the front and rear frames mith a flat fairing. The resultant faired strucrure had a drag coefficient of about 0.44 based on frontal area rather than approx 2.0 for the unfaired structure. The magnitude of the reduction can only be taken as approximate when applied to the whole whirling arm structure because, although the frontal area of the fairings remains constant, the chord of the fairing increase considerably towards the centre of the arm (the ratio of the tip/root chord being 0.39). In the case of the unfaired structure with totally separated flow, it is legitimate to base the drag coefficient on frontal area, but once the flow separations have been suppressed by the fairing most of the drag will come from the skin-friction drag and so depends more on wetted area rather than just frontal area. Thus based on frontal area, the sectional drag coefficient at the root will be approximately 2.5 times the sectional drag coefficient at the tip.

On the other hand the actual drag varies with the square of the approach velocity and the approach velocity varies with the radius, giving a 40:1 ratio in V^2 between the tip and the inner section.

In view of the amount of work necessary to fair the structure and the limited resources available to do it, an assessment was made of the amount of the arm structure that it was profitable to fair. Obviously all the remaining structure at the tip should be faired as the air velocities were highest in this region. The questions to be answered therefore were how much of the top and bottom frameworks should be faired and whether the vertical diagonal bracing should be faired.

The estimated variation of the sectional drag with radius of the faired and unfaired horizontal frameworks is shown in Fig 15. Although the faired structure shows an appreciable reduction in drag over the outer half of the arm, inboard of this the reduction is relatively small compared with that in the tip region. It was arbitrarily decided that once the sectional drag of the unfaired structure was less than that of the faired structure at the tip, then the effort in fairing the structure was unjustified. On this basis, the top and bottom fairings were only faired outboard of the first triangulation point.

The diagonal bracing presented rather a different problem. Any continuous fairing between the front and back members would have to take into account both the curved flow in which it would operate and the variation of flow curvature that occurs with change in radius. Thus not only would the fairing have to be cambered,but the camber would have to vary over the length of the fairing. In view of the large variation of camber required over the inner sections and their large chord it was considered that the most practical means of reducing the drag of the diagonal members was to replace the angle sections by tubular members.As the diagonal members were mainly in the inner half of the structure, it was decided that the reduction in drag that would be obtained was not sufficient to justify the effort needed to make the changes and so the members and their attachment plates were left unaltered. If ,at a later date, it could be shown that the separations from the diagonal bracings were causing unacceptable flow disturbances in the test section then it would be necessary to review this decision.

For reasons of lightness and ease of construction, the fairings over the top and bottom frameworks were made of thin plywood sheet over discrete wooden blocks attached to the metal structure. The shape of the fairing was the same as that used in the lowspeed tunnel tests, i.e a 2:1 elliptical nose, a straight constant thickness mid-section and a 2:1 elliptical tail section modified to have a 15 degree semi angle straight trailing edge extension.

Although the same section had been used for the fairing of the vertical tip bulkhead in the model tests, it was not considered that this was appropriate for the tip of the whirling arm where, because of the flow curvature, a symmetrical section would be working at a considerable incidence at its nose and so the crude section used might stall and leave some eddying in the test chamber from the separated flow. As the final fairing could not be designed until the model support and incidence systems had been designed, a temporary fairing was made, based on a possible design of the tip section,to enable the effect of a tip fairing on the transfer of energy from the rotation of the main structure in the central volume to the test chamber via the connecting slot. The fairing shape chosen (Fig 16) consisted of a circular arc of radius 265 inches (6.73m) on the outer side which provided a minimum fairing over the end bulkhead and a flat inner surface attached to the inner surface of the bulkhead. The nose and tail of the fairing incorporated a small radius. The fairing rotated just inside the connecting slot between the central volume and the test chamber and was slightly asymetric with respect to the arm, as was the slot.

4.5 Preliminary swirl measurements.

As has been noted previously, measurements of swirl at various positions in the test chamber (ref 10) had indicated that much of the swirl in the test chamber originated in the central volume in which the main structure rotated.

It was therefore decided to make a detailed evaluation of the swirl in the test chamber when only the arm structure was rotating, i.e with no structure projecting through the slot into the test chamber. This evaluation would obtain an assessment of the swirl characteristics in the test chamber when the original structure was rotating and enable the improvement in the swirl characteristics to be assessed as the structure was modified and faired.

Although it was known that the swirl would be high initially (> 10 fps (3m/sec)), it was hoped that the proposed modifications would reduce the swirl appreciably with a target of less than 3 fps (1m/sec). As any swirl in the test chamber would have to originate from the complex eddying flow in the neighbourhood of the rotating structure penetrating into the test chamber through the communicating slot, the swirl measured at a fixed position in the testchamber would be time dependent both in magnitude and direction. Because of the constraining effect of the slot, it is likely that the horizontal component of the flow would have the most effect on the flow in the path of the model. A suitable instrumentation system to measure the swirl would have to satisfy the following requirements:-

a) It should be capable of measuring airspeeds of 3fps (1m/sec) or less with a discrimination of 10% or less.

b) A bandwidth of at least 100 Hz was desired

c) The measuring device should either be capable of easily measuring the flow in three dimensions or alternatively be reasonably insensitive to the components of the swirl in the vertical plane.

The normal pitot-static/manometer system does not meet these requirements. Careful investigation of other systems such as anemometers and vortex shedding probes indicated that the constant temperature hotwire probe normally used for turbulence measurements best met the requirements. Although a 3-wire head would enable the flow direction to be determined in 3-dimensions, both the cost of the probe and the amount of analysis were not considered justifiable as the single wire with its axis vertical met the requirements being cheap, easy to operate, totally insensitive to flow direction in the horizantal plane and relatively insensitive to the flow in the vertical plane provided that it was fairly small compared with the velocity in the horizontal plane.

4.4.1 Calibration of the hotwire probes.

The principle of operation of the hotwire probe is that a servo amplifier maintains the temperature and therefore the resistance of the hotwire at a constant value as the airflow past it varies. Under normal operating conditions the heat losses from the wire are mainly due to conductive heat transfer to the passing air and so any change in airspeed past the wire causes a change in heat transfer and this requires a change in wire exitation voltage to maintain the wire temperature constant. If the ambient temperature does not alter, the calibration equation of the hotwire is :-

$$\sqrt{U} = k(V^2 - V_o^2)$$

where U= approach wind speed normal to the axis of the wire

k= calibration constant

V = Voltage applied to maintain the hotwire at a given constant temperature at the test wind speed

Vo= Voltage applied to the hot wire at zero wind speed to maintain the same constant temperature

As the heat transfer is also dependent on the difference between the hotwire and the ambient temperatures, the calibration constant obtained above also varies with temperature. The voltage required to keep a hotwire at a given temperature, T, is given by the equation :-

$$V^2 = A(T-To) + B(T-To)\sqrt{U}$$

where To = ambient temperature at the hotwire (ref 13) and A and B are calibration constants

Therefore Vo varies with (T-To) as does the calibration slope,B.

If the ambient temperature, To, varies from the datum ambient temperature, Td at which the calibration was made, the calibration slope will vary therefore with the ratio (Vo/Vod) where

Vo = voltage applied to the hotwire at zero speed under the present conditions

Vod = voltage applied to the hotwire at zero speed when the probe was calibrated

Thus the calibration equation becomes

$$U = (V^2 - Vo^2)/(k*(Vo/Vod)^2)$$

Although this method of calibration removes the necessity to measure the ambient temperature and simplifies the corrections for anbient temperature, it does require frequent measurement of Vo if the ambient conditions are varying.

Experimentally it is difficult to measure V0 accurately because of its great sensitivity to draughts and other slow air movements. This is particularly true of the whirling arm because of the persistence of swirl for a considerable time after the arm has ceased to rotate. The suppliers of the hotwire equipment, (DISA), suggested that steady, highly repeatable readings of Vo could be made by holding the tubular cover from the protective case in which the hotwires were supplied over the probe to act as a draught shield. This technique was found to be very satisfactory and was used throughout the swirl calibration tests.

Another point to be noted in the measurement of low speeds is that at speeds below about 1 fps (0.3m/s) the relationship derived previously gradually ceases to hold as the primary method of heat dissipation changes from forced convection to free convection until when $U = 0$ all the heat dissipation is by free convection. Thus the measured Vo is slightly higher than the true Vo required in the calibration formula. As the accuracy required at low speeds in the present tests is not high, the value of V0 was taken to be correct.

As will be described later, the calibration of the test chamber of the whirling arm was to be done using a 5-probe rake. The probe calibration was done in the CoA No 1B lowspeed wind tunnel which can be used for tests at low speeds up to 25 fps (7.5 m/s) by removing the tunnel contraction and mounting the model at the exit from the settling chamber. The 5-probe rake was mounted therefore at the settling chamber exit on the horizontal centre-line with the lefthand probe approximately on the tunnel centre-line. The tunnel speed was measured by a standard pitot-static tube mounted 3 inches (75mm) below the centre probe with the static holes in the same plane as the hotwires, th pressures being measured by a Betz manometer. The tunnel speed was then set in increments of 5 fps (1.5 m/s) between 5 and 25 fps (1.5 to 7.5 m/s) and at each speed the exitation voltage (V) was obtained from each probe. The zero-speed exitation voltage (Vo) was read at the beginning and end of each run as previously described. The calibration results were plotted in the form (V^2-Vo^2) v $\sqrt{U}$ and gave a good linear relationship. The best straight line was obtained that went through the origin and the experimental points. The calibration constants as defined in the equation were the zero-speed voltage (VoD) and the slope of the calibration line (Ks).

4.4.2 Measurement of swirl in the test chamber.

Once conditions had steadied, it was assumed that the flow was quasi-steady in character, i.e. the swirl at a fixed position in the test chamber varied as the arm rotated, but repeated itself during each hold as the primary method of heat dissipation changes from forced convection to free convection until when $U = 0$ all the heat dissipation is by free convection. Thus the measured Vo is slightly higher than the true Vo required in the calibration formula. As the accuracy required at low speeds in the present tests is not high, the value of V0 was taken to be correct.

As will be described later, the calibration of the test chamber of the whirling arm was to be done using a 5-probe rake. The probe calibration was done in the CoA No 1B lowspeed wind tunnel which can be used for tests at low speeds up to 25 fps (7.5 m/s) by removing the tunnel contraction and mounting the model at the exit from the settling chamber. The 5-probe rake was mounted therefore at the settling chamber exit on the horizontal centre-line with the lefthand probe approximately on the tunnel centre-line. The tunnel speed was measured by a standard pitot-static tube mounted 3 inches (75mm) below the centre probe with the static holes in the same plane as the hotwires, th pressures being measured by a Betz manometer. The tunnel speed was then set in increments of 5 fps (1.5 m/s) between 5 and 25 fps (1.5 to 7.5 m/s) and at each speed the exitation voltage (V) was obtained from each probe. The zero-speed exitation voltage (Vo) was read at the beginning and end of each run as previously described. The calibration results were plotted in the form (V^2-Vo^2) v $\sqrt{U}$ and gave a good linear relationship. The best straight line was obtained that went through the origin and the experimental points. The calibration constants as defined in the equation were the zero-speed voltage (VoD) and the slope of the calibration line (Ks).

4.4.2 Measurement of swirl in the test chamber.

Once conditions had steadied, it was assumed that the flow was quasi-steady in character, i.e. the swirl at a fixed position in the test chamber varied as the arm rotated, but repeated itself during each revolution of the arm. Thus it was hoped that a consistent overall pattern of the swirl flow could be built up from the readings taken during the different runs as the calibration rake was moved over the test section.

For the initial calibration with the original arm structure it was decided to measure the swirl over the greater part of the cross section of the test chamber to determine whether the offset position of the slot, the offset location of the arm structure in the slot and the "wave train" structure had any major effect. The flow calibration rake consisted of an aerofoil with the five hotwire probes spaced 7 inches (178 mm) apart along it and carried on 3 mm diameter holders projecting from the leading edge, the hot wires being 6.5 in (165 mm) in front of the leading edge. Two fixings were mounted at the ends of the aerofoil so that it could be held either by screwing one of the fixings to the inner wall or a vertical strut spanning the test chamber just clear of the "wave train" structure, or by clamping them to tensioned wires spanning the test section between the roof and floor. By this means the calibration probes could be located at points forming a square grid of 7inch (178mm) side based on the centreline if the slot, with the first column of holes 1 inch (25.4 mm) away from the inner wall (Fig 17). Because the end fixings differed in design and only one could be screwed to a support, the rake had to be reversed when it was fixed to the inner wall.

The hotwire servo amplifiers were connected to a Datalab multichannel event recorder which was set to sample the probe outputs simultaneously at a rate of 200Hz. At this rate of recording, the arm moved 4.34 inches (110 mm) along the centreline of the test section between readings at the standard test rpm of 25.34 rpm. This test speed was monitored by an extremely accurate rpm indicator which received one pulse per revolution from a combined source/ optical sensor operated by a mirror attachment on one end of the arm. The speed was adjusted until a steady reading was obtained which was within +/- 0.05 rpm of the nominal value. This accuracy was required to ensure that the number of samples obtained per revolution did not vary. The event recorder was triggered by the same pulse that operated the tachometer and which occurred when the centreline of the arm was 105.4 inches (2677 mm)in front of the measuring station measured along the centreline of the test chamber. This corresponded to triggering the recorder when the arm was 18.5 degrees in front of the plane of the measuring station. The event recorder took 4096 readings of each imput. After the data was recorded, the first 500-600 samples from each channel was transfered to an Intertec Superbrain microcomputer and stored on a disc file. The readings were then converted to speed by the method already described and scaled to the standard speed assuming that the swirl was directly proportional to the arm rotational speed. Unfortunately due to the early failure of one of the servo-amplifiers data was only taken from 4 of the 5 probes.

4.4.3 Analysis of the initial tests

In view of the large amount of data available, considerable thought was given as to how to present and analyse it both to understand the characteristics of the swirl flow in the whirling arm test chamber and how to assess changes in the flow quality as changes were made to the structure.

Although averaging the swirl measured at each station as the arm rotated through one revolution would give a good idea of the swirl distribution over the test section and meaning these values would give a single "figure of merit" value for assessing the effect of the structural changes, these values in themselves did not help greatly in understanding the details of the energy transfer from the central volume to the test chamber via the connecting slot.

It proved difficult to find a single method of presentation that adequately and simply showed the main characteristics of the flow in the test chamber. The variation with time of the swirl speed at 8 stations across the test chamber in the horizantal plane nearest the centre of the connecting slot is shown in Fig 18. The swirl speed at most of the stations varies between 9 and 15 fps (2.7-4.6m/s) but the swirl measured at stations 0700 and 0705 (i.e nearest the slot and about 1/3 the way across the test chamber) show considerably more variation with peak values approaching 30 fps (9 m/s) for a rotational speed of 72.3 fps (22 m/s) measured at the centre of the test chamber (station 0707). The readings began approximately 24 time intervals before the centre-line of the arm passed the calibration plane, the front of the arm being in the plane of the probes after approximately 20 time intervals.

At station 0700, which is at the centre of the slot and close to the inner wall of the test chamber, the swirl reaches a minimum value of c. 6fps (1.8 m/s) just as the front of the arm reaches the calibration plane presumably due to the acceleration of the air around the end of the arm. The swirl then increases rapidly to two closely spaced peaks of approximately 16 fps (4.9 m/s) which occur at 30 and 45 time intervals or just after the rear of the arm had passed the calibration plane. After the second peak, the swirl fell rapidly to about 8 fps (2.5 m/s) and then increased to a series of sharp peaks of about 27 fps (8.9 m/s) whih occured at between 130 to 180 time intervals after the commencement of recording. At this period the arm has rotated through some 90 degrees past the calibration plane. After these peaks the swirl then reduced back to the minimum value of 6 fps (1.8 m/s) at approximately 260 time intervals i.e just as the opposite end of the arm passes the calibration plane. A similar cycle then occured over the second half revolution. Whilst it was logical to expect peaks in the swirl speed as the two ends of the arm passed the calibration plane, it was surprising to find the additional peaks that occured when the ends of the arm were at about 90 degrees to the calibration plane and for the peaks to be considerably greater in magnitude than those that occured as the ends of the arm passed through the calibration plane.

Examination of the swirl variation at similar stations across plane 1 which is nearest the floor of the test chamber, (Fig 19) showed that the variation of swirl speed with time at a given horizontal station was much less than at plane nearest the centre of the communicating slot, plane 7, and that the marked peaks near the inner wall were no longer present. However the magnitude of the swirl speed over the calibration plane still varied between 8 and 18 fps (2.5 to 5.5 m/s) which was very little different to the speeds measured in plane 7 away from the immediate neighbourhood of the slot. However the swirl measured at stations 0103 and 0105 was considerably higher than those measured at the other stations at this height. The swirl measured at station 0111 was of approximately the same magnitude as at these stations over the first 120 time intervals, but reverts to the same magnitude as the other stations for the rest of the revolution.

The swirl variation with time is also plotted for plane 13 (Fig 20), which is the same distance from the central plane (7) as is plane 1. These show very similar characteristics to those described for plane 1 except that the swirl at the majority of stations is slightly less and that the swirl at station 1311 near the outer wall varies cyclically twice a revolution between the two levels of swirl mentioned previously, instead of there only one peak per revolution (473.6 time intervals).

This general pattern was repeated in plane 14 which is the highest plane at which a calibration was done but is still some distance from the roof of the test chamber (Fig 21). The cyclical variation of swirl at horizantal station 11 is still present, but is of reduced magnitude.

Although these graphs, and similar ones not presented, showed clearly the variation of swirl with time and demonstrated that the swirl distribution was symmetrical about the slot, it was still felt that some less confusing method of presenting the data was required to understand better the method of energy transfer from the central volume to the test chamber. It was therefore decided that a better appreciation of the swirl distribution over the calibration plane would be obtained if the swirl values at a given instant were plotted in the form of a three-dimensional isometric surface using the GINOSURF plotting programs. A sample isometric surface is presented in Fig 22. It should be noted that the marked peak at the rear centre position is false as swirl speeds of 40.0 and 0.0 fps were allocated to two adjacent stations there as the only easy way of forcing the program to present the results on a consistent scale. The diagram at the lower righthand corner shows the relationship if the (symmetrical) arm to the plane of the calibration rakes.

These isometric surfaces were plotted at 1/20 sec time intervals over one revolution of the arm i.e at every tenth set of calibration data. Examination showed that the main features of the flow were indeed quasi-steady in character although the detailed characteristics with respect to the two sequences of events examined as the ends of the arm passed the calibration plane. In view of this, the swirl distributions over the calibration plane are presented in Figs 23 - 30 for only just over 180 degrees rotation of the arm. The isometric drawings are presented 4 to a page on a reduced scale to enable the changes that occur as the arm rotates to be assessed more easily.

Examination of the figures showed that:-

a) The uneven "two-ridge" distribution across the calibration plane was a general characteristic of all the diagrams

b) The major changes in swirl as the arm rotates were confined to a relatively small region on the neighbourhood of the slot which extends between planes 5 and 9. These large swirl variations dissipated rapidly with radius and were much reduced in the region occupied by the model (Fig 17).

c) The existence of major disturbances at approximately 90 degree intervals of rotation of the arm was confirmed. As the probes were insensitive to flow direction in the horizontal plane, there was no means of ascertaining whether these large swirls were associated with large inflows or outflows through the slot.

d) Away from the influence of the slot, the swirl distributions in the vertical plane varied much less than those measured in the horizontal plane.

e) The swirl tended to decrease slightly with radius over the outer half of the chamber.

The periodic nature of the flow was demonstrated effectively by using the computer graphics facilities at the Computer Division, Rutherford and Appleton Laboratories, to draw the isometric surfaces of all the data on successive frames of a 16 mm film. Viewing the film confirmed the conclusions reached above and in particular showed very clearly that the major disturbances passing through the slot did not extend into the test chamber as far as the model radius.

The consistency of the "two ridge type of swirl distribution in the horizontal plane throughout all the data threw considerable doubt on the uniformity of the velocity distribution of the flow in the No 1B lowspeed windtunnel over the position occupied by the hot-wire rake when it was calibrated, especially as the ridges corresponded to a particular probe whose calibration gave a considerably higher calibration factor than the others. Later calibration of the individual probes in a common position in the tunnel showed that the original calibration factors were in error and that using the new calibration factors, the uniformity of the flow across the test chamber was much improved. As the recalibration of the probes was done immediately before the calibration of the test chamber after the model support system had been installed, it was decided that the work necessary to re-analyse the previous results was not justified as the general conclusions on the effect of the structural modifications was unlikly to be altered. The initial hot-wire calibration factors were used therefore to assess the improvements made by the intermediate modifications

4.4.4 Effect of the structural modifications on the swirl flow.

As it seemed that the flow was reasonably symmetrical about the horizontal centreline and so it was decided to assess the effects of the various modifications to the arm by measuring the flow across the channel at 3 grid heights only. These were chosen to be at height stations 00 (adjacent to the bottom wall), 04 (the maximum likely displacement of the model during test) and 07 (the slot centreline). The swirl in these three planes was averaged over one revolution of the arm and used as a "figure of merit" to assess the improvement made as the arm was progressively modified and faired. In addition the amount of energy needed to rotate the air in the test chamber at this mean swirl speed was calculated for each condition. These values are tabulated below for the four conditions tested before the model support system was installed. The four conditions were:-

a) The arm in its original form (Condition 0)

b) The arm with its structure minimised as described in section 4.2 and unfaired. (Condition 1)

c) As b) but with the vertical frame at the tip faired as described in section 4.4 . (Condition 2)

d) As c) but with the top and bottom frameworks faired as described in section 4.4 . (Condition 4)

Condition	arithmetic mean swirl (fps)	rms mean swirl (fps)	Energy (bhp)
0	12.6	13.1	0.500
1	9.7	10.4	0.375
2	4.2	4.7	0.065
3	3.7	3.9	0.045

These results show that the modifications reduced the swirl in the test chamber by approximately 70% and the energy transmitted into the test chamber by over 90%. As the power required to drive the arm was some 25 bhp it would appear that only a small proportion of this is transmitted into the test chamber through the connecting slot, but as there was only the skin friction of the walls to absorb the energy, the resultant swirl speed was high. The most effective modification was the fairing of the tip, followed by the minimisation of the structure.

It is instructive to look at the results in more detail. Firstly, the mean swirl at each of the test stations (Table 2) was divided by the mean swirl at the same station when the arm was in its original condition so as to make the results independent of the errors in the calibration factors of the probes as previously discussed.

These values are tabulated in Table 3 and plotted in Fig 31.

Looking at the results in the centre-line plane of the arm, (plane 07), it can be seen that the removal of a large portion of the structure in the vertical plane (Mod 1), had only a small effect (+/- 10%) on the mean swirl over the inner quarter of the test chamber. Outboard of this the comparative mean swirl fell rapidly to reach a minimum value of approximately 50% at the centre of the test chamber before increasing steadily to a value of 75% at about three-quarters way across the test chamber. Over the outer quarter, the comparative mean swirl fell rapidly to a value of about 25% at the station nearest the outer wall. This general pattern was repeated in the other two calibration planes (04 and 00) as shown in Figs 31 b) and c), although in plane 00 the variation over the inboard three-quarters of the test chamber was rather smaller. There was a marked reduction in swirl at the outboard station (station 14) in all the planes.

The fairing of the tip section (Mod 2) caused large reductions in the comparative swirl over nearly 80% of the test chamber with the greatest effect being apparent near the inner wall. Although the shape of the distribution was still uneven, the variation across the test chamber was less than previously. This modification however had little effect on the swirl near the outer wall which remained at the value previously measured.

The effect of fairing the top and bottom members (Mod 3) was to lessen the changes in swirl across the test chamber. Whilst the general effect was to reduce the swirl at most stations, the swirl over the outer 20% ot the chamber was slightly increased as compared with Mod 1.

So far we have only considered the effect of the various modifications on the mean swirl measured at various positions in the calibration planes and the mean of these values. The effect ot the modifications on the variation of swirl with time at the control stations 0700, 0704, 0707, 0710, 0404, 0407, 0410, and 0007 are presented in Figs 32 - 39. Before examining the results in detail, it should be noted that:-

a) no results are plotted for the final modification, Mod 3, owing to the accidental loss of both the raw and computed data after the results had been tabulated and meaned

b) owing to a timing error, the data recorded in the Modification 1 tests began 96 time intervals before the commencement of recording for the other cases.

The graphs show that at the two stations nearest the slot on the slot centre-line, the flow exhibits considerable variation with time in all cases, even though the average level drops as the arm is progressively modified. In all other cases the magnitude of the flow fluctuations diminishes as the arm is modified as does the general level of swirl.

As it is rather difficult to see easily the effects of the modifications on the swirl speeds near the slot owing to the large high-frequency variations in the curves and the difficulties in curve identification when they are continually crossing each other, the variations in swirl at the stations in plane 07 have been plotted against time for each of the modifications for which data was available (Figs 40 -42).

The graphs show that, compared with the datum case (Fig 40), the flow at station 0700 (nearest the wall in the plane of the slot) alters appreciably when the arm structure is minimised (Fig 41). As before, there is a large increase in swirl just after the arm has passed the calibration plane, but the peak that occured previously when the arm had rotated 90 degrees past the calibration plane is no longer present. On the other hand the peak swirl speeds recorded are considerably greater and die away more slowly, thus giving an average swirl speed at this station which shows little difference from the unmodified configuration. The reduction in swirl at the stations remote from the slot is very marked as is their greater uniformity.

When the tip of the arm was faired (Fig 42), the very large peaks in swirl measured near the slot as the arm rotates are supressed. The variation of swirl with time in this region is still greater than in the outer half of the test chamber, but is much improved as compared with the previous cases.

Summarising, the modification and fairing of the arm structure have resulted in a large reduction in the energy from the rotating structure that is transmitted into the test chamber to cause swirl. The considerable reduction made in the structural members in the vertical plane has not resulted in any significant reduction in the strength of the structure.

5.0 DESIGN OF THE MODEL SUPPORT SYSTEM

5.1 Design requirements

As mentioned previously, it had been decided to use a rear-sting to support the model in the test chamber. The design requirements for the support structure were as follows:-

a) the structure should be simple and therefore easy to manufacture,

b) it should be easy to alter the model incidence continuously in the horizontal plane over at least +/- 15 degrees relative to the tangent at the centre of the model.

c) the speed of changing the pitch should not be less than 2 degrees/sec, i.e full travel in approximately 15 secs. In addition, it would be an advantage to be able to add a "boost mode" to change pitch at up 15 degrees/sec if this is required at a later date.

d) provision should be made in the design so that at a later date the model incidence can be altered in the vertical plane over a similar range. Although continuous variation is desirable eventually, movement in fixed increments is acceptable initially.

e) the structure should be aerodynamically clean as it is in the test chamber which has little capacity to absorb the energy imparted to the air in the chamber by the drag of the structure.

f) as a considerable part of the structure will be in the test chamber where it will be subject to 'g' forces up to about 10g, it is important that the structure should be as light as possible to minimise both the structural loads and the balance weights necessary to balance the arm.

g) an additional reason for demanding a light structure is that access to the central volume and the test chamber is limited and most of the erection would have to be done by manhandling.

h) the length of a typical model should be taken as 60 in. (1520 mm). The centre of rotation is to be taken as being at the centre of the model and the rear sting is to extend 30 in. (750 mm) behind the model before there is any large discontinuous change in cross-sectional area, e.g. the leading edge of a support.

i) the loads imposed on the model support system by the model and its supporting sting are as previously specified, i.e the maximum aerodynamic load has components of 100 lb.(45 kg) acting simultaneously vertically downwards and horizantally outwards at the centre of the model, the maximum model weight is 10 lb.(4.5 kg.) also acting at the centre of the model, and the weight of the support sting and windshield is 30 lb. (13.5 kg.) acting 40 inches, (1016 mm) behind the centre of the model.

The two rates of changing incidence come from consideration of two completely different operating requirements. The lower rate of about 2 degrees/sec is specified as being appropriate to manual operation of the test as experience has shown that,from the operators point of view, it is desirable that the greatest alteration required should not take more than 10 to 15 seconds so as to avoid a falling off of his concentration when making large changes, while still permitting small changes of 0.1 degree to be made without undue trouble. The ability to operate at the higher rate could be of vital importance in some of the program of work proposed for the whirling arm in the future, e.g in the measurement of the rotational derivatives of an aircraft at and beyond the stall. In these tests the wing sheds large vortices which can persist for a considerable distance downstream of the model. Spillman (ref 14) has demonstrated by flight tests, that for wings of small sweep the effect of these vortices seems to be a maximum some 200 chord lengths behind the wing. These conclusions have been shown to be in broad agreement with other investigations on other aircraft of widely differing size and geometry. This distance, in terms of a typical model, unfortunately is approximately the circumference of the path of the model. This implies that in steady state testing, the model may experience appreciable unsteadiness in the oncoming flow due to its own wake. This in turn may make it difficult to measure the derivatives accurately and also raise doubts as to the validity of the experiment if the oncoming flow is very unsteady. This problem can be minimised by either breaking up the vortices in some way, or by increasing the model incidence rapidly from a low value so that the measurements at high incidence can be taken before the model encounters the large vortices shed at the higher incidences. If the latter method of test is adopted, then it will be required to traverse the total incidence range in approximately 2 secs thus giving the higher rate of change that must be a consideration for later incorporation.

5.2 Assessment of possible design solutions

An assessment was made of some of the designs that have been used to support models in wind tunnels in order to see which, if any, were most applicable to the special requirements of the whirling arm.

The type of model support often used in supersonic wind tunnels is the movable segment of a circle mounted on slides which enable it to rotate about its virtual centre (Fig 43a). the model support sting is mounted on the sector so that the centre of the model is at the virtual centre. This type of support system, while satisfactory in small sizes, becomes very heavy in large sizes and is also difficult to manufacture because of the lack of machines capable of machining the sector and its slides to the required accuracy. In our case the minimum radius of the segment would be 60 inches (1520 mm).

To overcome these difficulties in large sizes, an alternative model support system has been used in which the sting support is attached by two specially designed saddles to a pair of lead screws attached to the main structure, which can be rotated differentially to enable the model to be rotated whilst the centre of the model remains in approximately the same position (Fig 43b). Because of the linear movement of the saddles, the model moves backwards and vertically as the pitch is altered, but the movement is small and acceptable for angles up to 20 degrees or so. The design of the saddles is also complicated because although the attachment of the sting to one can be a simple pivot joint, the geometry of the system demands that the other must slide as well as pivot as pitch is altered. The lead screws and saddles are usually enclosed in a fairing with a wedge - shaped nose through which the support sting protrudes thus requiring a movable nose to the fairing. Even this type of system creates some difficulties in the large sizes due to the machining of the lead screws which become long and large in diameter especially if large loads are present on the plane at right angles to the plane of movement.

To avoid the difficulties inherent in tha accurate machining of large components, another design has been used which involves virtually no accurate machining of large components, but allows the model to be rotated about a virtual centre. The basic design is shown in Fig 43c. In essence, two bearings are located external to the tunnel by a rigid fabricated structure, one on each side of the tunnel, so that the bearings are in line with the centre of rotation. Each of the bearigs is the pivot point of a frame, these frames being connected together at the required radius by horizontal frames that span the tunnel. A segment of flame-cut commercial quality steel plate with wooden leading and trailing edge fairings is attached to the centre of the horizontal frames and passes through rectangular slots on the centre-line of the tunnel. The gap between the segment and the sides of the slot is sealed by a specially designed seal which makes allowance for the slight variation in gap that occurs as incidence is altered due to the normal commercial tolerances in the material and the manufacturing processes. Rotation of the model is achieved by raising and lowering the pivotted frames. In the original design by Sutton et al for the 3 ft transonic tunnel at RAE Bedford, incidence was altered by means of a motor-driven sprocket mounted from the tunnel shell which engaged in a commercial precision chain which was stretched over the rear of the upper part of the segment, thus completing a simple, easily constructed and effective design. Equally well a jack could have been used to alter incidence, the choice depending on the transducer chosen to measure incidence.

In some small intermittent supersonic tunnels operating at high Mach numbers and high pressures, it was found necessary to insert the model into the working section after the flow had been established so as to avoid the large loads on the model when the tunnel was started. In this type of tunnel, it was usual to use a smaller segment with the sting attached to the top, the segment being cantilevered from slides attached to the injection carriage, Fig 43 (d). These systems were relatively weak in torsion, but as the largest torsioal loads were expected to occur during the flow starting and breakdown processes (which were avoided), the torsional loads when measuring aerodynamic loads was adequate.

In all these designs angular movement was provided in one plane only, the pitch plane. Angular movement in the plane at right angles, the yaw plane, was obtained by rolling the model about its axis and pitching it, by mounting the model on a cranked sting or a combination of both methods. In general it was unusual to obtain large angles of pitch and yaw simultaneously. An exception to this was a special rig designed by the author for the 4ft x 3ft low speed auxiliary tunnel at RAE Bedford which could provide angle of pitch and yaw of 20 degrees simultaneously. It consisted of a half segment system mounted on a quadrant whose slides were below the bottom wall of the tunnel, both systems being operated by scissor jacks. The half segment system had to be made of steel in order to take the lateral loads without excessive angular deflection but the yaw mechanism was made from wood.

Before considering the final design of the model support system, general consideration was given to the problems of attaching it to the whirling arm. In order to ensure that the torsional and bending loads on the arm structure were kept to a minimum, it was decided that the centre of gravity of the support system should be as near the centre-line of the arm as possible. The tip frame to which the support system had to be attached consisted of a reinforced casting approximately 32 inches (810mm) square and 5 inches (127mm) deep, with a 23.5 inch (597mm) diameter central hole. The inner surface of this casting was machined flat as it had been designed so that the original model support system was inserted through the central hole and was held in position by a flange which was bolted to the machined face on the end casting. By this means, the centrifugal loads were transmitted directly to the end casting and the attachment bolts had only to take the static loads

This ruled out the designs based on segments as the segment, which was the heaviest part of the design, would have to be mounted on one side or other of the arm in order to achieve the necessary freedom of movement. Once these designs were eliminated, the only suitable design was that based on attaching the sting to the support structure by tho supports that could be moved differentially. As these supports had to take the aerodynamic and centrifugal loads on the model and its sting, it was required to locate them as far apart as was practical. It was therefore decided to locate them symmetrically on either side of the end casting at a distance apart of 40 inches (1016mm) which would give adequate clearance from the structure. As it had previously been decided that the centre of the model (and the centre of rotation) should be 60 inches (1524mm) in front of the support structure, an additional allowance o 6 inches (150mm) was made to allow for a nose fairing, resulting in the centre of the model being located 66 inches (1676mm) ahead of the front support.

In its datum position, the centre of the model was required to be in the centre of the test chamber with its axis aligned normal to the radius through the centre of the model. As long as the supports were parallel to each other, it was not necessary for them to be parallel to this radius for it to be possible to rotate the model approximately about its datum position. However as the movement of the model from the datum position was small and symmetrical with change in angle when the supports were parallel to the datum radius but became larger and asymmetrical as the alignment was inclined from this position, it was decided to align the supports parallel to the datum radius rather than with the axis of the arm. A second advantage of ths decision was that the model was located further ahead of the arm and therefore was less liable to be affected by any disturbed airflow caused by the arm.

It was rapidly realised that a design using screws to move the supports would not be satisfactory for the following reasons:-

i) The large movement required coupled with the large diameter of the rod required to minimise the deflection when the vertical loads were applied at maximum extension, resulted in a complicated, costly and heavy item.

ii) The rate of change of angle would be slow and was unlikely to meet the slower rate let alone the faster rate referred to above.

It was therefore decided to use plain tubes sliding in bearings with the differential movement obtained by attaching the ends to a control beam by a parallelogram linkage, the control beam being rotated about a fixed point by an hydraulic jack.

5.3 Description of the chosen design

The final design of the support system is shown in Fig 44. The model support sting, (1), was attached to a beam which in turn was attached to two parallel rods, (6), which were supported from a torsion box, (5), attached to the end frame of the arm. Each of these rods was located by two bearings so that they could move along their own axis, differential movement of the rods resulting in a change of model attitude.

Once the position and direction of the axis of the front rod had been fixed, further problems arise if a simple parallelogram linkage is used to connect the tubes to the control arm, (7), because:-

a) The ends of the tubes move along a straight line but the attachment points to the control beam move along an arc of a circle. Thus either the attachment points must be free to slide along the beam or some other form of flexibility must be incorporated in the attachment.

b) If the parallelogram linkage is pinjointed then the distance apart of the links will vary as the control beam is rotated. Thus either the rear tube constraints (bearings) must be able to move so that the tubes remain parallel or the attachment of the rear tube to the control beam and the sting support beam must slide.

In order to avoid the complication of sliding joints, simple pivots were used for the attachment of the tubes to the control beam, (7), and the beam to which the sting was attached. The necessary freedom of movement was achieved by incorporating an additional pivot in the main tubes,(6), to allow for the movement of the control beam attachment points relative to the axes of the main tubes, and by attaching the rear tube bearings to the torsion box,(5), by inclined pivotted links forming a second parallelogram linkage, (3), to allow for the displacement of the operating tubes as the pitch angle was altered.

The main loads on the linkage are in the horizontal plane and are due to the centrifugal loads on the arm linkage. These result in axial loading of the tubes as does the model loadings in the horizontal plane, the actual stresses being small. These loads, together with the loads imposed by the operating jack subject the control beam to considerable loads which have to be taken in bending, and therefore could result in appreciable bending of the beam resulting in a large correction due to centrifugal force having to be applied to the angular setting of the beam to obtain the true sting incidence. The magnitude of the loads applied to the support system is shown in Fig 45.

The aerodynamic loads acting in the vertical plane act 66 inches ahead of the front tube and when the rods are fully extended these, together with the weight of the model and sting, give rise to appreciable loads at the ends of the operating rods. Although it was originally hoped to keep the diameter of the rods to approximately 2 inches (50mm), the deflection of the rods under the worst loading was large and, in particular, resulted in an angular deflection of the sting carrier beam in the vertical plane of more than 2 degrees. In order to reduce this angular deflection to a more reasonable value of about 0.5 degrees, it was necessary to increase the external diameter of the rods to 3.5 inches (89 mm) even though the increase in weight (and therefore centrifugal load) was large.

The loadings in the vertical plane also determined the type of bearings used to support the tubes. Recirculating-ballbearings were not considered suitable as, although they had a low coefficient of friction, their outside diameter was large compared with their inside diameter, their load carrying capacity was limited and, in particular, there was some doubt as to their ability to absorb the large bending moments due to the vertical loads on the support tubes. In addition, a suitable size of bearing was expensive and heavy.

Ordinary plain bearings were rejected because of the likelihood of uneven wear due to absorbing the bending moments and their relatively large size and weight.

The chosen solution was to use two widely spaced, short length bearings on each tube so that the tube was simply supported rather than cantilevered, the extra deflection of the tube being partially compensated for by a relatively small increase in the tube diameter. For ease of manufacture and small frontal area, it was decided to use angular contact double cone rollers to allow axial movement of the tube. Although, in theory, the contact loads were very high as there was only point contact between the tube and roller, in practice the tube shape "flowed" or distorted to allow line contact with the resultant reduction in contact pressure. This solution would not be acceptable for prolonged continuous use, but was considered acceptable for the intermittent operation envisaged.

The torsion box (5) to which the rollers were attached passed through the hole in the end frame of the whirling-arm structure and was attached to it by a flange which was bolted to the machined face on the inside of the end frame.

The length of the main support tubes was such that when the rear tube was fully extended into the test chamber, the inner end was just clear of the inboard bearing. The main support tubes were connected to the control beam by lighter tubes with pivot joints at the ends to allow the necessary flexibility to absorb the geometric changes that occured as incidence was altered. These connecting tubes were considerably lighter than the main tubes as they did not have to take any bending moment and because ,when the arm was rotating, they are always in tension due to the centrifugal forces on the main support tubes and the outer connecting member being greater than the compressive loads due to the centrifugal and aerodynamic loads on the model and support sting.

The length of the connecting tubes was controlled by the following requirements:-

1) they should be sufficiently long so that their angular deflection from the axis of the main tubes should be small throughout the incidence range.

2) the pivot point of the control beam should be close to the point where the radius to the model centre crosses the front framework so as to find a good anchorage for the pivot point on the arm structure

3) a suitable anchorage position can be found for the operating jack

4) neither the front tube or the control arm should foul any part of the arm structure at any incidence

Coincidentally it happened that the intersection of the radius to the model centre with the plane of the front frame satisfied all these conditions especially condition 3) as the length and travel of the jack resulted in being able to locate its anchorage point on the very rigid central tower of the whirling arm.

In order to avoid undue stresses in the control beam pivot due to the weight of the beam, a number of plastic rollers were attached to the beam to provide support to the beam as they ran along a member (10) fixed between the diagonal bracing on the rear frame.

The attachment point of the operating jack to the control beam was chosen to minimise the angular deflection of the control beam due to the loads applied to it by the operating rods and the jack. It was important to do this as the angular deflection of the model due to centrifugal and aerodynamic loads in the horizantal plane cannot be measured directly while the arm is rotating except by a yawmeter on the model. As, initially at least, the variation of flow direction in the test chamber is unknown,it is advantageous for the angular deflection of the model support system to be as small as possible, so that any errors in the calculations of the support system are physically small (e.g if the possible inaccuracies in the deflection calculations are +/- 10%, it is obviously better to have an estimated deflection of 0.5 degree rather than 2 degrees). It should be pointed out that the deflections will vary not only with rotational speed but also with pitch and the weight of the model and its supporting sting, the centrifugal loads being of much greater significance than the aerodynamic loads.

The reactions imposed on the outer ends of the main support tubes by various combinations of model lift, model weight, sting weight and weight of the sting carrier are shown in Figs 45 and 46.

Of the various cases considered, case 1 corresponds to the design condition used for stressing the model support control beam. In this loading it was assumed that the pitch in the vertical plane would be provided by some simple system attached centrally to the operating tubes and which would weigh no more than 200 lb (90 kg) complete. Later work showed that while it might be possible to make a suitable system for that weight, there were very great difficulties in designing a low-drag fairing for it. This was because of the curvature necessary to conform to the airflow and the large range of pitch in the horizontal plane. In addition the solution eventually adopted for fairing the model support system in the horizontal plane made it impossible to use any arrangement which could not be completely contained within the fairing.

The other cases considered investigated varying the main parameters to cover variations in weight that seemed possible as additional design work was completed. The parameter changes were as follows:-

a) Model weight

It had been considered that it should be possible to make an aeroplane model that weighed about 10 lb (4.5 kg). If however it is desired to be able to remove the various aerofoil surfaces to find the effect of the various components, then not only does the model become more complicated, but metal rather than balsa or foam has to be used for the construction of the necessary joints, resulting in some increase in weight. Although it was thought that the model weight would not greatly exceed 10 lb, it was decided to investigate the effect of increasing the model weight to 20 lb (9 kg), case 2. If however a body is tested on its own, the weight of the model, even with pressure-plotting instrumentation, was expected to be considerably less than 10 lb. Thus the effect of reducing the model weight to 5 lb (2.25 kg) was also investigated, combined with reducing the model lift to the same value (case 6).

b) Sting weight

Originally it was considered that suitable stings would be made of either thick-walled aluminium tubing or much thinner steel tube which would give the same deflection for the same weight. However a sting was made of thick-walled steel tube which happened to be available with a resultant increase in weight to approximately 100 lb (45 kg), case 3.

When it appeared that it was not practical to design a vertical pitch mechanism located between the main support tubes, it was decided to vary the pitch in the vertical plane by incorporating a pivot in the sting in front of the model support fairing and to make the same weight allowance, 200 lb (90 kg) for the revised system but acting at the same position as the original sting, case 5.

c) Sting carrier weight

The original weight of 200 lb (90 kg) included an allowance for the system for altering pitch in the vertical plane. When it was decided to do this in another way, the sting carrier design was simplified to a single rectangular tube carrying sting attachment clamps, the whole weighing approximately 50 lb (22.5 kg), case 5.

From the results it can be seen that increase in weight forward of the front support tube increases the load on the front support tube and diminishes that on the rear tube. It would also appear that the item most likely to show large variations in weight is the sting and that this is mainly the result of using a steel sting of substantial dimensions, rather than designing a minimum weight but adequately stressed sting. The increased weight is not significant as far as the load-carrying capacity of the model support system is concerned, but it increases the load on the operating jack significantly and could cause it to be overloaded.

The last component of the model support system to be designed was the control beam and operating jack (Items 7-9, Fig 44) as its design depended on the weight of the other components.

As a parallelogram linkage system was used, the pivot point, length of beam and the attachment points of the connecting tubes was pre determined. The variables remaining to be analysed were the size of the beam and the position of the jack attachment point, which should be chosen to minimise the deflection of the beam due to the centrifugal force on the other members of the linkage.

The jack attachment point was located at 88.0 inches (2235 mm) from the forward pivot on the basis of weight estimates made in the design stage. These approximated to those shown in Table 4, which are the actual measured weights of the various components. A hollow box section of 4.72 in. by 2.36 in. with 0.194 in. thick walls (120 mm by 60 mm by 5mm thick) was used for the control beam with the major dimension in the plane of rotation. The deflections have been recalculated for the design cases specified in Fig 45 and are shown in Fig 47.

From these results, it appears that the original optimisation procedure was very satisfactory in that both the linear and angular deflections of ths beam were small in case 1, Fig 47, which approximated closely to the design conditions used to size the control beam. In the results, all the deflections were calculated relative to a base which was the line joining the beam pivot to the jack pivot point. The angular deflection of the beam at its pivot relative to this datum is that measured by the oitch indicator. The line joining the two support tube attachment points to the beam is parallel to the sting carrier and thus to the sting root. Thus compared with the "at rest" condition, the indicated pitch angle shows an apparent increase as the speed of the arm increases, whereas the line joining the support tube connections deflects so as to reduce its pitch. Therefore if the pitch angle is set while the arm is rotating, the model attitude is less than the indicated value by the sum of the unsigned angular deflections. Thus in case 1, the sting root incidence is approximately 1/4 degree less than the indicated value at the design speed of 31.8 rpm.

If the weight of the model is doubled (case 2), the jack and pivot loads alter very little, but the pitch correction increases by nearly 50%.

Increasing the sting weight from 30 lbs to 100 lbs (13.5 - 45.5 kg), case 3, increases both the jack and pivot loads by about 400 lbs (182 kg) and more than doubles the pitch correction, from 0.38 to 0.87 degrees.

Reducing the weight of the sting carrier to allow for the impossibility of incorporating a pitch-changing system into it, case 4, makes no difference to the angular deflections as would be expected, but reduces both the jack and pivot loads.

If, however, a pitch change mechanism is incorporated into the sting, increasing its weight to 200 lbs (91 kg), both the jack and pivot loads are increased (case 5) and the pitch correction is increased to 1.61 degrees or roughly double that of the previous case.

In contrast, if a body is tested which has a body weight and aerodynamic lift of 5 lb (2.3 kg) each, a sting weight of 30 lbs (13.6 kg) and the revised carrier shaft, weight 50 lbs (23 kg),case 6, then both the jack and pivot loads are reduced considerably as is the pitch correction which is now only 0.12 degrees.

These results show that the control beam can stand large changes in the weight allowances assumed for the model and sting without problem as far as the loads are concerned due to the parallelogram linkage being the major contributor to the loads. However increases in weight in the sting and model region have large effects on the pitch corrections that have to be applied in obtaining the true model attitude in the plane of rotation. In particular the sting weight is important and the design of the sting must be controlled closely as it is very easy to increase its weight greatly by increasing the wall thickness with no corresponding increase in stiffness or reduction in stress. If large sting weights are considered inevitable, then consideration should be given to increasing the stiffness of the control beam.

As the operating loads on the jack are high, the desired travel large and the required time of operation moderately small, at least in the unboosted case, either pneumatic or hydraulic piston type jacks were suitable. A hydraulic system was chosen because of the higher operating pressures available. Its control circuit is shown diagramatically in Fig 48. If it is required to reduce the time of operation to 2 seconds for full travel as discussed previously, it is proposed to achieve this by using a separate hydraulic reservoir instead of the hydraulic pump. This is regarded as satisfactory as it is assumed that data will be taken continuously as the model is moving from low to high incidence and it is not required to stop the model exactly at a required incidence.

The nominal incidence of the model in the horizontal plane is measured by means of a linear transducer mounted on the whirling arm structure and connected to the control beam 6 inches (150mm) from the pivot point so that the line of action of the transducer is perpendicular to the control beam when the model is at datum incidence.

The main features of the new model support system are shown photographically in Figs 49-50.

5.4 Fairing the pitch change linkage.

The swirl in the test chamber due to the arm structure had been reduced to approximately 4% of the arm speed by the modification and fairing of the main structure. When the model support system was installed, an appreciable part of it would be inside the test chamber thus creating additional drag leading to an increase in swirl. As the previous tests had shown that the energy needed to rotate the air in the test chamber at the swirl speed required could be provided by a structure at the end of the arm with an aerodynamic drag of about 0.36 lb. (0.16kg.) at 70 fps (21. m/sec), it was essential that the structure inside the test chamber should have as small an aerodynamic drag as possible. As the parts of the pitch change linkage in the central volume could affect the swirl, these members must be faired and/or shielded from the test chamber by a suitable fairing on the end of the arm.

5.4.1 Fairing the end frame of the whirling arm

The original end fairing, which had shown to have the greatest effect of all the modifications tested , had to be replaced when the new model support system was installed as it could not be easily modified to allow the new model support system to be installed. The old fairing had been designed as the minimum fairing to enclose the end frame, and as can be seen from Fig 16, did not completely prevent air from the central volume spilling into the test chamber as the outer surface of the fairing was inside the inner wall and the height of the fairing was less than the width of the slot in order to provide adequate clearance of the fairing from parts of the "Dexion" structure that projected into the slot.

The new end fairing was designed as before with a flat inner surface and a circular arc outer surface (Fig 51). As the outer surface of the fairing was inside the test chamber, the plywood skin of the circular arc surface was extended over the ends of the communicating slot to provide a baffle which would direct any air entering the test chamber from the central volume towards the floor or ceiling rather than allow it to travel radially towards the centre of the test chamber. This baffle is shown clearly in Figs 52 and 53. The clearance between the baffle and the inner wall may appear to be rather large, but this was necessary to provide adequate clearance when the fairing passed over a small local region where the wall profile varied appreciably.

The new fairing was made of wood, the construction and general dimensions being as shown in Fig 51. Because of the increased depth of the fairing and the stressed skin construction, the fairing was extremely rigid. The centre-section had a large cutaway on the flat surface to allow clearance for the attachment flange of the model support system torsion box and additional smaller cutaways for the operating rods. The design of the leading and trailing edges of the new fairing was rather different from that used previously as it was considered that less disturbance to the airflow would be obtained by extending the outer skin of the fairing some 9 inches (229mm) past the intersection of the inner and outer skins to form "thin-plate" leading and trailing edges similar to the curved-plate turning vanes often used in wind tunnel corners.

Similar fairings were made for both ends of the arm as the depth of the fairing allowed the necessary weights to balance the arm to be carried completely inside the fairing at the end of the arm remote from the model support system.

5.4.2 Fairing of the model support system

The parts of the model support system that were inside the test chamber were of poor aerodynamic shape and therefore would give rise to extensive flow separations and consequently high drag and swirl. In order to eliminate the flow separations, it was desirable to fair the sections as simply as possible.

The torsion box with the support tube rollers extended over the inner quarter of the chamber and was particularly bad aerodynamically, being a rectangular cross-section box with the rollers and their supports inclined to the oncoming flow. Some consideration was given to designing a minimum fairing to fit over the torsion box but including local bulges to fit over the rollers and supports. As the bulges considerably complicated the manufacture of the fairing and the largest bulges occurred over the rear half of the fairing where the airflow was most likely to separate, it was decided to install a constant chord, constant thickness fairing which would completely enclose the structure.

Outboard of the torsion box, the model support structure was relatively good aerodynamically as it consisted only of two tubes, one behind the other, connected at their extremities by a rectangular tube from which the support stings were mounted. Even so the drag of this configuration will be relatively high, especially at the extremes of its travel, as the airflow will separate from all the components. A minimum fairing attached to the outboard rectangular tube was considered but rejected a) because of the mechanical complication of dealing with the changes in planform as the pitch angle was altered and b) because the flow would separate from the tip section except over a small range when the tip was closely aligned to the local flow.

The chosen alternative, Fig 54 , was to provide a fixed, constant chord fairing cantilevered from the torsion box to within about 2 inches (50 mm) of the wave plates, and inside which the pitch change mechanism could move. However the sting would have to pass through the leading edge of the fairing and some means of sealing this gap had to be provided. The method adopted was to cover the gap with two sheets of thick, pliable rubber attached to the periphery of the gap with their free ends butting along the leading edge to form a seal. As the pitch was altered , the rubber was parted by the sting as it moved along the slot. The gap created in the neighbourhood ot the sting was sealed by a sheet aluminium fairing, 18 inches (457 mm) long formed to the shape of the nose. This seal had a hole in the leading edge through which the sting passed and was held in contact with the rubber by two springs attached to the sting holder. As the sting moved through its range of travel, it came into contact with the sides of the hole in the fairing and moved the fairing with it. As the seal was not rigidly attached to the sting, it could move and pivot as required to conform to the leading edge of the fairing.

The section shape chosen for both fairings was an ellipse blending into a 15 degree semi-angle wedge tail section.

Originally it was intended that the outer fairing would extend 6 inches (152 mm) ahead of the centre-line of the front support tube, thus giving some 30 inches (760 mm) of parallel sting between the base of a typical model and the nose of the model. If this was adhered to, the detail design of the sting carrier was such that the basic ellipse would have a thickness/chord ratio of 25%. This was considered excessive, so it was considered preferable to use a thinner section at the expense of allowing the nose of the fairing to move forward slightly. The resultant section was based in a ellipse with a major axis of 59 inches (1500 mm) and a minor axis of 9.41 inches (239 mm) located with its leading edge 9.5 inches (240 mm) ahead of the centre-line of the front support tube. The tail wedge gave the fairing an overall length of 70.94 inches (1802 mm) giving a thickness/chord ratio of 0.1326.

The fairing over the torsion box had to be of greater thickness as it had to contain the linkages that positioned the rollers through which the support tubes slid. The section shape again was elliptical with a 15 degree semi-angle wedge tail fairing. The ellipse had a major axis of 67.66 inches (1719 mm) and a minor axis of 13.53 inches (344 mm). The overall length of the fairing was 88.33 inches (2244 mm) resulting in a thickness/chord ratio of 0.1532. Because of the asymmetry of the roller linkages, the centre-line of the ellipse was designed to be 3.26 inches (63 mm) behind the centre-line of the torsion box, which resulted in the leading edge of the inner fairing being 3.26 inches (83 mm) ahead of the leading edge of the outer fairing.

It was decided not to fair the junction between the two fairings but to allow a vertical discontinuity allong a junction line which was a constant radius of 296.5 inches (7530 mm) from the centre of the arm. If any separations developed in this region, it would be simple to install a fence along the junction which would act in the same manner as a thin-plate turning vane to suppress any separations.

The fairings were largely prefabricated before assembly. When the inner fairing was being fitted, it was found that there was insufficient clearance between it and the rear roller linkage at extreme travel. It was found necessary to move the fairing backwards by approximately 5 inches (125 mm) in order to provide sufficient clearance.

Both fairings were of wooden construction with chordwise ribs attached to wooden spars which were fixed to the torsion box. The structure was then skinned with thin plywood. The complete weight of the wooden fairings over the torsion box and support tubes was approximately 63 lb. (28.6 kg).

It should be noted that by choosing to completely enclose the model support system in a fixed fairing, it was impossible to use a pitch change system centered on the support struts to change pitch in the vertical plane. However, investigations made before the fairing was designed had shown that the easiest method of changing pitch rapidly in the vertical plane was to pivot the front part of the sting about a point just in front of the fairing with the pitch being changed by means of an hydraulic jack reacting against a lever attached to the sting. The disadvantage of this type of attitude change was that the model moved appreciably vertically, but because of the asymmetrical positioning of the arm in the test chamber and the large height/width ratio of the cross-section, the model remains near the centre of the test chamber.

In view of the amount of work involved, no attempt was made to fair the rollers and support tubes in the central volume as it was hoped that the improved tip fairing would isolate the test chamber from the aerodynamic disturbances in the central volume. If it was found necessary at a later date to fair the tubes etc, a fairing could be installed similar to the inner fairing in the test chamber.

5.5 Balancing the rotating structure

Although the whirling arm is a substantial structure and the main framework and the fairings of the end frames are symmetrical, the installation of the model support structure on one end of the arm results in an unbalanced structure which it is necessary to counterbalance in order to minimise the out-of-balance loads on the main bearings when the arm is rotating. Because of the design of the model support system, the out-of-balance will vary as the pitch angle is changed, e.g. the rear support tube has an overall movement approaching 6 feet (1.8 m). It was considered that this variation in out-of-balance force was not large enough to justify the provision of an automatic counterbalancing device thus the arm was statically balanced with the model support system in its datum position, i.e. with the sting tangential to the radius from the centre of the arm to the nominal centre of rotation in pitch.

Initially the arm was to be rotated without the fairings for the model support system installed so that the operation of the system could be checked and any modifications made without the presence of the fairing impeding the commissioning. The details of the calculations for this case are shown in Fig 55. Once the support system was commissioned, the instrumentation platform and the fairings inside the test chamber were installed and the arm was rebalanced.

In subsequent operation, the balance weight must be adjusted if any other items are added to either the main structure or the support system

5.6 Design of the model support sting assembly

Although rear sting support systems have been in use for many years, additional factors have to be taken into account when their use in the Whirling Arm is considered. In a wind tunnel, the gravity forces on the model and sting are constant and independent of the test speed. Thus the deflection of the sting due to gravity loads and model weight is constant and can be zeroed out when the model is rigged prior to the test.

This is not the case in the Whirling Arm due to the centrifugal accelerations present when the arm is rotating which amount to some 6′g′ at the normal operating speed of 25.4 rpm. Although the deflection of the sting due to the aerodynamic and centrifugal loads on the model can be determined by static loading with weights, the deflection of the sting itself under centrifugal loading is not so easily determined as it is a function of the mass distribution of the sting and so is difficult to detemine experimentally by a representative loading except in the case of simple geometries. As the centrifugal loads due to the mass of the sting may be considerably greater than the combined centrifugal and aerodynamic loads due to the model, more attention than usual must be paid to the design of the sting, as the deflections in the plane of rotation have to be determined. The actual inclination of the model to the oncoming airstream can be determined experimentally if an yawmeter is incorporated into the model, but it is necessary to know the linear deflection of the model in order to apply corrections to the measured pressures and this may have to be determined theoretically. If a theoretical evaluation of the linear and angular displacement of the sting under load is required, then it is an advantage to keep the sting geometry as simple as possible in order to minimise the theoretical calculations.

The aerodynamic loads on models tested in the Whirling Arm are quite small due to the low wind speed of about 70 fps (22 m/sec) even though the models are quite large (a typical model length being about 60 inches (1.5 metres) with a wing span of the same order). The normal force generated by a model will vary between 1 lb (0.5kg) for a simple body and 60 lbs (27 kg) for an aircraft model. It would be an advantage therefore if the sting deflections under combined aerodynamic and centrifugal loadings were kept as small as possible both to keep the corrections small and also to minimise the effects of errors in determining them. In addition it would be an advantage to minimise the weight of the model and sting as they have to be rigged manually because of access restrictions.

In order to keep the aerodynamic interference from a rear sting support small, experience has shown that the ratio of sting diameter to model base diameter should be small, less than 0.5 if possible, and that the sting should either be parallel or have a very small constant divergence for not less than 2.5 - 3.0 base diameters behind the model base. After this, the sting/support cross-sectional area may increase more rapidly, but large discontinious increases in area should be avoided.

5.5 Choice of materials

Because of the effect of centrifugal force on the deflection of the sting, it was decided to examine the variation of material characteristics on the deflection of the sting under the test conditions present in the Whirling Arm.

Assuming that :-

a) the length of the sting is L

b) the sting is circular in cross-section with a constant outside diameter, D, and a constant internal diameter, d

c) the material of which the sting is made has a relative density of σ and a modulus of elasticity of E

d) the calculations apply to a sting which is cantilevered from a sting holder and do not take into account the deflections due to any weakened sections for strain measurement at the model end of the sting

Initially considering the sting alone rotating in an acceleration field of n"g".

$$\text{The moment of inertia of the sting, } I = \pi(D^4 - d^4)/64$$
$$= D^4(1-(d/D)^4)/64$$

$$\text{The mass/unit length, } w = \pi(D^2 - d^2)/4 \quad \text{under 1"g"}$$
$$= n\pi(D^2 - d^2)/4 \quad \text{under n"g"}$$

By beam theory the tip deflection of the sting (δ) is given by :-

$$\delta = nwL*L^3/8EI$$

and the angular deflection at the tip (θ) is given by:-

$$\theta = nwL*L^2/6EI$$

Substituting for I and w it is found that both deflections vary as the ratios σ/E, and $1/(1 + (d/D)^2)$

Support stings are usually made of steel, but if the stresses are sufficiently low and light weight is important, they can be made of aluminium or magnesium. It is found however that the ratio σ/E is exactly the same for these three materials and thus the unloaded sting will deflect the same amount under high "g" conditions regardless of whether it is made of steel, aluminium or magnesium. However the stings of the lightweight materials will be lighter and less highly stressed in absolute terms than the steel sting.

If a stiffer sting is desired, then it will have to be made of a material with a smaller ratio of σ/E. The readily available engineering plastics, both thermosetting and thermoplastic have larger values of σ/E than steel, and in many cases do not have a well defined elastic limit. The glassfibre reinforced plastics also have larger values of σ/E than the metals, but carbonfibre or Kelvar reinforced plastics whilst having approximately the same density as the glass-fibre reinforced plastics, can have E values approximately the same as steel if a high fibre/resin ratio is used and the fibre layup is largely unidirectional ratio as it could be for a tubular sting. As its density is approximately a quarter that of steel, a carbon fibre or Kelvar reinforced-plastic sting would be considerably lighter,stiffer and less highly stressed than a steel sting of the same dimensions. As no facilities were available for the manufacture of suitable reinforced-plastic tubes and they were not commercially available, it was decided to use conventional materials for the present.

When an end load, W, ia applied to the sting, the tip deflections under 1"g" conditions become:-

$$\delta = L^3 (3W + wL)/6EI$$
$$\theta = -L^2 (8W + 3wL)/24EI$$

As both W and wL will increase directly with centrifugal acceleration, the expressions are in fact the deflections/"g" and can therefore be scaled directly to give the deflections at any radius and/or rotational speed.

The end load on the sting will consist of a combination of the model weight and the aerodynamic lift both of which are dependent on the speed of rotation of the arm, the weight component varying with centrifugal acceleration and the aerodynamic forces varying with the dynamic pressure of the approaching airstream, both of which vary with the square of the rotational speed. In choosing the range of end loads to be investigated, it was decided to use values which would cover the design parameters of the first three models to be tested in the facility. The first was to be an isolated body which would have a maximum aerodynamic load of 1 lb (0.5 kg) and a design weight of about the same amount, this low weight being essential in order to be able to measure the aerodynamic forces accurately with a straingauged balance in the presence of the centrifugal loads. The second was a similar model designed to measure the pressure distribution over the model using Scanivalve pressure switches located in the model. Using lightweight materials but without using ultra-lightweight techniques, this model and instrumentation was estimated to weigh 5 lbs (2.3 kg). The third was a winged model which had a design weight of 10 lbs (4.5 kg) with an estimated maximum aerodynamic load of 60 lbs (27.25 kg). The corresponding maximum end loads, (6W + N), for these models were 7, 31 and 120 lbs (3.2, 14 and 54.5 kg). The range of end loads chosen for the calculations on sting deflections was 0, 60 and 120 lbs (0, 27.25 and 54.5 kg) which covered the estimated requirements.

The sting diameter was likely to be determined by aerodynamic rather than structural reasons due to the relatively low end loads. As stated previously it was thought that the maximum acceptable sting diameter would be 3.0 inches (76mm), but on models with small bases it might be necessary to use stings of smaller diameter without any reduction in the estimated end loads. It was thought that a range of sting dameters of 2.0, 2.5 and 3.0 inches (50.8, 63.5 and 76.2 mm) would cover most requirements.

As sting weight was also important in that it was an important contributor to the load on the jack used to alter the pitch of the model, it was unlikely that solid stings would be acceptable. The last design variable was therefore the ratio of inside to outside diameter of the sting (d/D). The range chosen was from d/D = 0 to 0.96 in steps of 0.24.

The tip deflection, tip inclination and root stress were determined for these ranges of conditions for both aluminium and steel stings which were 66,0 inches (1676 mm) long and encastered at one end. The results are presented in Figs 56 - 58. The weights of these stings were also calculated and are presented in Fig 59.

With no tip load, the deflections of the steel and aluminium tubes are virtually the same as would be expected as the values of σ/E are virtually the same. The deflections fall steadily as the inside diameter increases and at all the outside diameters considered, the deflections of the thinnest tubes are just over half that of the solid bar. The stresses exhibit the same variation but the stress levels in the steel tube are higher than those of a similar aluminium tube by the ratio of their densities.

When a tip load is present, the characteristics change somewhat. As the inside diameter increases, the deflections and root stresses fall slowly as before, but at the higher values of d/D, these quantities begin to increase, slowly at first and then very rapidly at values of d/D which are dependent on both the magnitude of the tip load and the outside diameter of the tube, but typically in the range of d/D of 0.6 to 0.9. For the tip loads considered this effect is much more pronounced at the smaller sting diameters.

The magnitude of the deflections for the aluminium tubes is also considerably greater than that of the corresponding steel tube as would be expected as the tip load is considerably greater than the weight of the tube in the case of the aluminium tubes.

If it is possible to use a 3.0 inch (76,2 mm) sting, then it is possible to keep the tip deflection at maximum load to about 0.3 inches (7.5 mm) and the angular deflection to less than 0.4 degree if a steel sting is used with a value of d/D less than 0.8. If an aluminium sting is used then the deflection will increase to 0.5 inch (12 mm) at the heaviest load with an angular deflection of 0.7 degree as long as the value of d/D does not exceed 0.65. Taking the largest values of d/D that it is practical to use for the heaviest load, the comparative sting weights are 55 lbs for the steel sting and 35 lb for the aluminium one.

For the 2.0 inch (50.8 mm) stings, The tip deflection increases dramatically, being approximately 1.0 inches (25 mm) for the steel sting and 2.0 inches (50 mm) for the aluminium sting with corresponding angular deflections of 1.3 and 2.6 degrees provided that the d/D ratio is less tha 0.6 for the steel sting or 0.5 for the aluminium one. The corresponding sting weights are 35 lbs (16 kg) and 15 lbs (7kg), i.e. approximately half the weight of the 3.0 inch (76.2 mm) diameter stings but at the expense of approximately four times the deflection.

It would therefore appear that if it is possible to use the larger diameter sting then either the steel or the aluminium stings will give satisfactorily small deflections, but with considerable weight savings if aluminium is used. If smaller stings have to be used subject to the same loads, then there is an increasing advantage in using steel as the outside diameter is reduced and at the same time the weight disadvantage compared with the 3 inch diameter aluminium sting is reduced.

The attachment of the sting to the model support linkage must also be examined. Although flat-plate joints have been used, the most compact type of joint in commom use is the circular section parallel or taper plug and socket joint. The desirable characteristics are :-

1) there should be minimal or no increase in diameter at the joint
2) There should be a positive axial location
3) It should be possible to rotate the model accurately to predetermined roll angles within +/- 180 degrees of the datum position and lock it in that position
4) The joint must be capable of being separated easily without applying force via the model and/or balance
5) The manufacture should be as simple as possible

The design features that are common to the plug and socket joints are a) the length of the joint is usually not less than 3 joint diameters, b) for stressing purposes it is usually assumed that the load is transfered at two planes at the beginning and end of the joint and c) the moment of inertia of the socket at either plane should not be less than that of the plug in the same plane.

Some of the types of joint used are shown in Fig 60. The plug is usually recessed relative to the outside diameter of the sting so there is no increase in diameter at the joint and to enable the resultant joint face to be used as an axial location in the case of parallel joints. The joint surface on the plug is usually recessed along part of its length to make the fitting of the load transfer surfaces easier. This is done by "blueing" the joint surfaces and scraping down the high spots to ensure good contact and therefore efficient load transference. It is usual to specify that intimate contact should exist over at least 80% of the joint surface. Whether or not this high standard is justified is dubious as experience has shown that however good the standard of the initial fit, the standard deteriorates rapidly with use. As the efficiency of the joint does not seem to be impaired by the deterioration in fit, it seems likely that the initial standard was unnecessarily high and that a lower standard, and therefore cheaper, fit would be acceptable.

In general there seems little to chose between the parallel and taper joints except that in many cases quite small taper angles are used, 5 degree semi-angle or less. This has disadvantages in that the resultant joint tends to "grow" together with the result that some form of mechanical joint separation is required often with additional complication and therefore cost. This can be avoided by increasing the taper to about 15 degrees semi-angle (depending on material) when the joint will separate naturally. In practice this large taper angle is combined with a parallel section to give the desired length of joint.

The joint surfaces are generally brought into contact and maintained thus by some system of keys or screws whose action can be reversed to "part" the joint. When it is required to rotate the joint, the most usual system is to machine a "Vee" groove in the rear of the plug using suitably positioned screws to engage in the relative side of the groove to provide the necessary closing or openining action.

When considering the type of joint to be used on the Whirling Arm, it became apparent that considerable departures could be made from the conventional designs which would result in an equally satisfactory joint, but one that was both lighter and easier to manufacture.

As the sting attachment to the linkage would be completely inside the model support fairing there could be a discontinuity in diameter at the front of the joint. This was advantageous as reducing the diameter of the sting for a joint would greatly increase the stress level in the proposed thin-walled tubular stings. The use of this type of sting in turn dictated a parallel joint which would be at least 9 inches (230 mm) long. If the socket was made of steel, then the minimum weight would be about 30 lb (14 kg) which seemed rather heavy.

The convential stressing assumption was that the loads were transferred via the mating surfaces at the ends of the joint. It therefore seemed logical to reduce weight by using the sting carrier member of the parallel linkage as the load carrying member and transfer the load to it by relatively thin pedestals made from plate material, Fig 60. Rather than machine the sting and bore the pedestals to provide the required mating surfaces, it was decided to use split-clamp joints on the pedestal to secure the sting, which could therefore be left unmachined. This would provide good load transference and a positive means of preventing axial movement of the sting while at the same time allowing axial movement of the model within the limits of the length of the sting.

The pedestals were bolted to machined pads on the sting carrier. As it was required to be able to align the model to the flow in the vertical plane, adjustment of the sting inclination was proveded by using a pivot joint on the front pedestal and attaching the rear pedestal to the carrier by two bolts passing through slotted holes in the pedestal base.

6.0 INSTRUMENTATION

The existing instrumentation system took amplified signals from transducers on the arm via sliprings and recorded them on a multi-channel ultra-violet recorder. As most of the work done consisted of studying dynamic responses, this method of recording was quite satisfactory. Much of the work proposed for the reconditioned Whirling Arm required accurate quasi-steady measurements for which the U/V recorder system was ill-suited as the discrimination of the system was poor and the analysis of results laborious. To improve the accuracy of the results, it was proposed to measure the output voltages by modern analogue-digital (A-D) converters which were capable of sampling analogue signals at a rapid rate. When data is taken at a rapid rate, it is important to avoid unsteadiness in the transmission lines such as might be caused by faulty slip-rings. As the existing slip-rings were nearly 40 years old and had several known faulty channels, it was considered best to mount a self-contained recording system on the arm which would control the test and store the data taken. The data would then be transferred to another computer when the arm was at rest either by a plug-in line or alternatively through the slip-rings if these proved to be satisfactory under static conditions. It was required to measure the outputs of not less than 16 transducers as well as control the operation of various items of equipment such as pressure switches and model attitude control systems.

Although a hard-wired controller could be developed to perform the task, it was considered advantageous to use a computer-based system if possible. Initially the possibility of mounting a standard microcomputer on the arm was examined, but the advice of the manufacturers was that they were unhappy about mounting disc units and the display screen on the arm due to possible unreliability due to the centrifugal force and vibration. Although it might be possible to disable or remove these units before the arm was started,it was thought better not to incorporate them into the controller but to use a separate compatible computer in the control room on which the control programs could be developed and the preliminary analysis of results could be done prior to transferring the results to a larger computer to do the final analyses and graphs.

6.1 Description of the control system

As it was desirable to make the system as versatile as possible, it was considered that a "board-type" unit should be used on the arm to control the data-gathering system. These units are built around a common "bus" incorporated into a printed circuit board, known as a "back-plane" or "mother-board", into which it is possible to plug other boards, each of which performs a desired function. Of the several board systems available the one known as the "S 100" system seemed the most attractive as it had the largest selection of function boards and the board size was smaller than most comparable systems. This latter point was of significance because experience had shown that if large boards with many components on them were operated in vibratory conditions or under "g", then there was a long term tendency for the etched tracks to crack resulting in unreliable operation. As boards incorporating many different computers (8, 16, or 32-bit) were available, the choice of system depended on compatibility with the microcomputer to be used in conjunction with the data-gathering system. The choice of this in turn, depended on the software available, operating system, languages etc. In particular, it was important that "off-the-shelf" driver programs for the data-acquisition units should be available so as to minimise development work.

6.1.1 Choice of microcomputer

Besides working in conjunction with the data-acquisition unit on the Whirling Arm, the microcomputer was required to be further processing of the results and be capable of plotting them both on the display screen and also on a printer/plotter. Besides the printer/plotter interface, an RS 232C interface and file transfer program was required so that the microcomputer could be used as a terminal to larger computers and also could interchange data or program files. It was found that at the time that a decision had to be made, the most satisfactory low-cost systems that met the requirements were those based on the CP/M operating system with BASIC as the main language.

An Intellec Superbrain II with two disc drives was chosen as it met all the requirements and in addition, it was available from a local agent who offered software support and servicing facilities. Additional advantages were that all the equipment was contained in two cases, the computer case incorporating the computer, display, disk drives, graphics hardware and interfaces, and the printer/plotter. In addition it was found that the computational speed was very fast as the computer used two Z-80 microprocessors, one servicing the keyboard, screen and input/output ports while the other was solely concerned with computing.

The complete system consisted of the following:-

Superbrain II microcomputer with

64Kbyte store

2 350Kbyte disc drives

2 RS232C interface ports

graphics (hardware and software)

Epson FX80 printer/plotter

Software consisting of:-

CP/M operating system

MBASIC interpreter

FORTRAN IV compiler

WORDSTAR wordprocessing package

CDTERM terminal emulator and file transfer package

6.1.2 Choice of data-acquisition computer

The requirements for this computer were that it should consist of a basic unit containing the power supplies etc and a S 100 motherboard with at least 10 slots for S 100 boards. The boards required should include a multichannel A/D converter, an RS232C interface, an IEEE 488 instrumentation interface and interfaces for the operation of relays and the reception of "control status" signals. Software should be available to drive all the interfaces, preferably from a BASIC program. The computer was to control the test with a program loaded into it from the Superbrain microcomputer, but working completely independently of it when the Whirling Arm was in operation. The programming language should be BASIC (MBASIC if possible).

A Sirton MIDAS system was chosen because all the software and hardware was available from the one supplier together with good software and hardware back-up and maintenance. In addition the firm showed the best appreciation of our requirements and therefore were in a good position to help and advise in the event of any problems occurring.

The system consisted of the following hardware:-

Sirton MIDAS unit with power supplies and a 15-slot S 100 motherboard
Godbout CPU-Z Z-80 computer board
two 32Kbyte ROM boards
communications board (3 parallel and 1 RS232C serial interface)
16/32 channel multiplexed 12 bit A/D converter
8 channel reed relay output and 8 channel opto-isolated input board
IEEE 488 instrumentation interface

the following software was provided:-

LINKCOM

This is a basis for communication software between a master CP/M system and a non CP/M slave system.

The slave portion of LINKCOM is PROM based and provides a very primitive operating system used to manage the slave unit and its execution of programs.

The master portion of LINKCOM resides in the CP/M computer and uses normal CP/M calls for all interchange of instructions between the user and the programs that are necessary to exchange programs and data between the master and slave systems. It also can be used to command the slave to start or stop the operation of the process control program.

XYBASIC

This is a form of BASIC designed to be particularly easy to use to write control programs. The version used is designed for operation in a "stand-alone" system, while at the same time allowing the operating programs to be developed on a CP/M system.

IEEE 488 instrument interface controller.

6.2 The data recording system

The design of the system was determined by:-

a) the type of sensors to be used to measure the quantities to be recorded, the magnitude of their output and the number of channels necessary

b) the amplification needed to convert the level of the output signals to that required by the measuring component of the recording system

c) any filtering of the output signals necessary to give an acceptably steady signal for the recording of the nominally "steady-state" signals in the presence of vibration and electrical noise

d) the discrimination and speed of measurement of the measuring component together with the required rate of sampling data.

6.2.1 Requirements for the analogue-to-digital converter

In aerodynamic experimental work it is usual to have a discrimination of not more than 0.1% of the maximum value to be measured. As an analogue-to-digital converter is to be the measuring component, a 10 bit converter is the minimum that should be used (discrimination 1 in 1024). In practice, many of the forces and moments to be measured can have both positive and negative values and it may not be possible for the output voltage to be measured to be conditioned to the full range of the converter. As each of these restrictions could impose a factor of 2 on the discrimination available, it is desirable to use a 12 bit analogue-to-digital converter which has a discrimination of 1 in 4096 of its range.

It is difficult to give a precise figure as to the desired sampling time of the converter. The overall data sampling rate depends critically on the complexity and efficiency of the control program as well as the number of data channels to be read. If a high level language such as BASIC is used, then it is unlikely that data rates of more than a few hundred channels/sec will be achieved. However, by using assembly language and sampling only one channel, considerably faster sampling rates may be achieved, but probably still less than 10K Hz. It was decided to specify a medium speed analogue-to-digital converter with a conversion time of about 25 µsec as faster units were considerably more expensive and slower units, though probably satisfactory, were little cheaper.

6.2.2 Sensors

The two main types of sensors to be used were resistance strain-gauge bridges incorporated in specially designed strain-gauged balances for the measurement of the forces and moments acting on a model and commercially available pressure transducers for the measurement of pressures.

Straingauged balances are often designed for each facility so that they give maximum output for the maximum forces and moments on a typical model tested in that facility. The usual 4-gauge resistance strain gauge bridge gives a maximum output of about 30 mV when used for high accuracy, low drift measurements although difficulties in the design of multi-component balances may restrict the output of some of the components to considerably less. As one side of the power supply to the straingauge bridge is usually connected to the system earth, the signal output is floating relative to the system earth.

The choice of pressure transducers for use in the Whirling Arm is restricted because of the low pressures to be measured. If we assume that the present Whirling Arm can only be rotated at a speed of 27 rpm and there is no swirl present, then the maximum approach speed of the air to the model will be 77 fps (23.5 m/sec), giving a maximum value for the dynamic head (q) of 34.3 mm H_2O. The pressures to be measured will therefore fall in the range $\pm$ 35mm H_2O relative to the static pressure in the test chamber of the Whirling Arm, with most of the pressures over a typical wing-body configuration being well within the range +/- 20 mm H_2O. If the motor driving the arm was replaced so that the full design speed of 31.8 rpm was obtainable, then the maximum approach speed would increase to 90.7 fps (27.6 m/sec) with a corresponding value of q of 47.7 mm H_2O.

If the pressure readings have to be taken at many positions over the model, it is usual to use one or more Scanivalve pressure switches to connect the pressure leads from several pressure tappings sequentially to one transducer which is housed in the pressure switch. This restricts the choice of transducer that can be used because of the need to fit into the housing and the limited space around it. However other larger transducers can be used if they are mounted externally to the pressure switch and connected to a dummy transducer in the switch by a length of pressure tubing. The disadvantages of this are the additional space requirements in the model and the increased settling time that has to be allowed for the pressure to settle after switching because of the additional lag due to the extra volume of the connecting lead.

Most of the transducers that fitted the available pressure switches (Scanivalves) were of the resistance straingauge type of which the lowest range nominally available was +/- 1.0 psi (+/- 700 mm H_2O) which was some 20 times the required range. The output of these transducers was about 30 mV fullscale reading. However one manufacturer, Setra, made a series of compatible transducers based on an inductance bridge, one of which had a range of +/- 0.1 psi (+/- 70 mm H_2O) which was only twice the range required. The transducer had an internal signal conditioning unit which provided a fully-floating output of approximately +/- 3V fullscale deflection (fsd). As these transducers would still provide an adequate output over the required working range, it was decided to use them for the tests in which Scanivalves had to be used.

Low-range pressure transducers were available to measure pressures as low as +/- 1 mm H_2O, but these mainly had large diaphragms and large internal volumes in order to get the required sensitivity. As a result they had a slow response to pressure changes and, in many cases, the output stability with temperature and time was rather large. Investigation showed that one manufacturer, Celesco, had developed a relatively small, low cost variable reluctance differential pressure transducer which was available in ranges from +/- 20 mm H_2O upwards. The required excitation was 15V at 4kHz which resulted in an output of +/- 35mV. As modern instrumentation works from DC supplies, a small carrier demodulator circuit board was available which worked from a DC supply and on which the transducer was mounted. The maximum output of the combined unit was then +/- 10V DC with one of the signal output leads earthed to the system earth (ie a single ended output). In addition the circuit board made it possible to adjust the sensitivity by a factor of approximately two from the nominal sensitivity and also the output zero could be adjusted by +/- 6V at nominal transducer sensitivity. As the pressure cavity volume was small and the lineararity,hysteresis and temperature characteristics were good, it was decided to provide transducers with ranges of +/- 20 mm and +/-50 mm H_2O to be used either as back-up for the Scanivalve transducers or for the measurement of individual pressures.

One additional problem that was investigated was the behaviour of the transducers under the centrifugal force that exists under operational conditions. The normal method for minimising the effect of centrifugal acceleration is to mount the transducer so that its diaphragm is in the plane of the acceleration. If however the transducer is mounted in a model so that its diaphragm is in the plane of acceleration when the model is at its datum attitude, this will no longer be the case when the model attitude is altered. At an attitude of 20 degrees, for instance, there will be a component of 2g normal to the diaphragm which must have negligible effect on the transducer. The Setra transducer specification gives a correction of 0.0002 psi/g for accelerations normal to the diaphragm which translates into a centrifugal correction of 0.0004 psi maximum for a model on the Whirling Arm. As this is less than ½% of the transducer range, the correction is negligible in most cases. No acceleration corrections were quoted for the Celesco transducers, but several of these transducers have been in use for some time on the centrifuge at the Institute of Aviation Medicine, Farnborough, Hants. Although the acceleration loads imposed on the transducers were greater than those present on the Whirling Arm, their experience indicated that the acceleration corrections were very small.

The magnitude of the main sensor outputs under the conditions present in the Whirling Arm are summarised below:-

sensor	max output	output type
resistance straingauge	+/- 30mV	floating
0.1psi Setra transducer	+/- 1.5V	floating
20 mm H_2O Celesco	+/- 10V	single ended
50 mm H_2O Celesco	+/- 5V	single ended

6.2.3 Signal conditioning

The multiplexed A-D conversion board selected for the MIDAS data acquisition system determined the output requirements of the signal conditioning units.

The board could accept either 32 single-ended or 16 floating inputs, but not a mixture. (A single-ended input is one in which one of the pair of signal leads from the sensor is connected to the system earth. In the case of a floating input, one of the power supply leads is connected to the system earth and the signal leads are therefore floating with respect to the earth potential.) As it is easy to change a floating input to a single-ended input but not vice-versa, it was decided that all inputs to the multiplexer should be single ended.

The fullscale range of the A-D converter can be set to a variety of values by physically altering jumper leads. Thus one of the ranges had to be selected as standard. The ranges available are 0→10V,-10→+10V and -5→+5V. The maximum sensor output is -10→+10V from the +/- 20 mm H_2O Celesco pressure transducer which results in the choice of the -10→+10V range of the A-D converter as the standard. The signal conditioning units must therefore be designed to provide a single ended 10V output for the maximum signal expected from the sensor.

The most complex signal conditioning unit is that to be used with the outputs of the straingauged balances. The main reasons for this are:-

a) A straingauged balance is designed to resolve the overall force on the model into its components about a standard axis system with the minimum interaction between components. Unfortunately the components generally differ greatly in magnitude and, for design and manufacturing reasons, the output of the straingauge bridges can also vary greatly, with maximum outputs of the various components being anywhere in the range of 1 → 30mV. This means that the gain of the signal conditioner should vary between about 300 and 10,000 either continuously or in discrete steps so that the maximum output of any component can be set to between 5 and 10V.

b) Although the aerodynamic forces and moments are to be measured at a series of fixed attitudes and therefore should be at a constant value at each attitude,in practice the output signal has unsteadiness superimposed on it due to unsteadiness in the test conditions, vibration, electrical noise, etc. As the A-D converter samples data very rapidly, successive readings of the same quantity may vary greatly making some system for obtaining the mean value of the output essential. This can be done numerically by taking a large number of nominally identical readings and averaging them or, alternatively, by passing the analogue output signal through a low-pass active filter with a suitable cut-off frequency before sampling the signal with the A-D converter. The model excitation generally seems to be "white noise" and so the maximum signal response will tend to occur at the natural frequencies of the balance. For the model-balance combinations likely to be used in the Whirling Arm, the natural frequencies are likely to be greater than 10 Hz so the filter cut-off frequency should be about 1 Hz to ensure adequate attenuation of the unsteadiness at the required frequencies. Other cut-off frequencies may be desirable if it is required to take data while the model is being pitched.

The normal instrumentation amplifier that would be the basis of the signal conditioner is designed to accept a floating input signal and produce a single ended output signal as desired.

Because the balance output signals are low-level with a required resolution of a few μV, it is usual to provide a signal conditioner for every input signal so that the multiplexing can be done at a high-level where the switching characteristics of the multiplexer are less important.

As signal conditioning units with the required characteristics were not available, a unit was designed based on the Analogue Devices AD 2B30 to provide 7 switchable gains of approximately 30, 60, 120, 240, 480, 960 and 1920 and a 3-pole (attenuation 18 db/octave) low-pass active filter with switchable cut-off frequencies of 2 and 10 Hz. Besides the main (filtered) output, the AD 2B30 also provided an auxiliary unfiltered output for monitoring purposes to ensure that the incoming signal to the filter is not "cut-off" by the amplifying stage. If required, both the amplifier gains and the filter cut-off frequencies can be changed by altering the setting resistors and capacitors.

Initially 8 signal conditioning units were built in two cases of 4 units, with another 2 units as spares.

The Setra scanivalve transducers required an amplifier gain of approximately 8 to convert the maximum expected (floating) input signal to the required +/- 10V single ended output. The signal conditioning unit was based on an Analogue Devices AD521 instrumentation amplifier whose gain could be varied by a simple potentiometer to allow for the variation of the transducer calibrations in producing the required 10V maximum output. In the measurement of pressures the volumes of the connecting tubing and the transducer cavity act as a low-pass filter so filtering of the output signal was not required.

As it was not expected that more than two 48-port scanivalves would be used at the same time, two Setra signal conditioning units were built in a common case.

As the output of the Celesco pressure transducers already meets the requirements of the A-D converter and does not require filtering for the reason mentioned above, the transducers did not require signal conditioning units

6.2.4 IEEE 488 instrumentation interface

The need to connect instruments easily into digital data acquisition systems has long been recognised resulting in the adoption of a standard interface for both computers and instruments known as the IEEE 488 interface. This allows the interconnection of up to 15 units in any one system provided that the total length of the connecting cable between the units is less than 30 feet.

In order to be able to connect instruments conforming to this standard into the Whirling Arm data acquisition system to supplement the instrumentation previously described, the MIDAS controller has been provided wit an IEEE 488 interface port. At present its control program has to be written in assembly language as a subroutine in the main XYBASIC control program.

6.2.5 Measurement of the rotational speed of the arm

Originally the rotational speed of the arm was measured by an analogue instrument which not only was relatively inaccurate but also had inadequate discrimination to enable centrifugal corrections to be applied to the measurements so as to obtain the required accuracy of results. In the swirl investigations, the rotational speed was read by a highly accurate universal timer which was triggered once a revolution by an optical switch and gave a direct digital reading of the rpm to 6 decimal places. The tests showed that the speed of the arm remained constant within +/- 0.02 rpm of the set speed for long periods of time due to the high inertia of the rotating structure. It was also found possible to set the initial speed to within the same limits without undue trouble. Thus the rotational speed of the arm could be set and maintained within about +/- 0.1% at the normal operating speed of the arm, 25.4 rpm.

This performance was sufficiently good so that the tests could be considered to be made at a constant speed and it was not required to record the test rpm with each data point to achieve the required accuracy.

As the timer was a highly accurate general purpose instrument, it was considered uneconomic to use it for routine measurements of the speed of the Whirling Arm, thus a COMPACT single purpose digital rpm indicator triggered by a magnetic proximity switch, was installed above the control desk so as to set and monitor the rotational speed, the rpm being displayed to 3 decimal places.

6.3 Installation of the instrumentation

In order to provide good ease of access to the instrumentation and to subject it to as little centrifugal force as possible in the interests of reliability, the MIDAS micro-computer, signal conditioning units, instrumentation power supplies, the Scanivalve controller and the Celesco transducer measuring the dynamic head were located on an instrumentation platform mounted on the bottom frame of the arm structure just outboard of the central tower (Fig 61). All items of equipment, cables etc on this platform had to be positively secured as they would be subjected to centrifugal accelerations of up to 2"g".

The sensors(apart from the Celesco transducer measuring the dynamic head), the Scanivalve pressure switches and any remote-control drive systems to alter the model configuration were normally mounted inside the model or close to it, and thus had to be connected to the signal conditioning units and/or the MIDAS control and recording system on the instrumentation platform. The connecting cables installed consisted of two 32-core instrumentation cables and one 8-core heavier duty cable to be used for those leads which have to carry the larger currents necessary to operate solenoids, motors etc or the power supply leads for multi-channel straingauge bridges using a common stabilised power supply. Each of the 32-

core cables was terminated in a 37-way "D" connector mounted on the front sting support clamp. The cables the ran via the interior of the support tubes to the instrumentation platform where they were terminated in a box by twenty 9-way "D" sockets. Only four ways of each socket (numbers 1, 5, 6 and 9) were used and as each sensor or straingauge bridge requires 2 power and 2 signal leads, any sensor can thus be quickly connected to any signal conditioning unit. Sockets number 10 and 15 are connected to the heavier duty 8-core cable using the same ways as used by the instrumentation wiring.

7.0 MEASUREMENT OF SWIRL WITH FAIRED MODEL SUPPORT SYSTEM

As previously, hotwire anemometers were used to assess the distribution of swirl in the test chamber. Because the fairing extended almost completely across the channel, the previous method of supporting the rake from vertical wires could not be used. Instead the rake was supported from wooden stands attached to the floor of the test chamber. It had not been possible to repair the fifth servo amplifier so only four hot-wire probes could be used. These were repositioned to avoid the gap that was previously present in the calibration grid and the stands fixed so that the probes could be positioned at the lateral stations 00 to 11 inclusive (Fig 17). In order to avoid the model support system fairing it was only possible to position the rakes vertically at stations 00 to 05 inclusive.

The probes were recalibrated in the CoA No. 1B lowspeed wind tunnel, but as analysis of the previous swirl measurements had raised doubts on the accuracy of the previous calibrations due to flow variations over the length of the rake (section 4.4.3), the probes were calibrated singly at an identical position in the tunnel.

The measurements of swirl were made using the Datalab multichannel recorder as previously. As before the arm speed was set to 25.34 rpm and the first 480 readings after the event recorder was triggered were analysed. Table 5 lists the variation at all the stations of the mean swirl (arithmetic and rms) together with the maximum and minimum values recorded in these 480 readings which covered slightly more than one revolution of the arm. Also shown is the arithmetic mean of all the readings in each horizontal plane

Examination of these results shows the following main features of the swirl:-

a) The mean swirl velocity in each horizontal plane varies surprisingly little, varying between 13.07 to 14.24 fps (3.98 to 4.34 m/sec). The largest values occurred nearest the floor (plane 00) and in the plane nearest the rotating fairing (plane 05).

b) The swirl decreases slightly with increase in radius, the effect being most noticeable in plane 05 mainly because of the higher swirl measured in the junction of the fairings.

c) The maximum value of the swirl measured at each station is closer to the mean value than the minimum value by a factor of about 2 except near the inner wall in plane 05 where the difference between the maximum and minimum swirl speed is much greater and their difference from the mean swirl is about equal.

In order to examine the swirl characteristics in more detail the variation of the swirl with time was plotted. Because of the difficulty in identifying the various stations when the distributions at many stations were plotted on the same graph, only selected distributions are plotted here (Figs 62- 64).

Initially the swirl distributions were examined over the boundary of the area that might be occupied by a model, i.e by stations 0303, 0503,0511 and 0311, Fig 17.

The main feature of all the distributions is the large local reduction in swirl that occurs at about time interval 90, Figs 62 & 63. This local reduction in the swirl is the result of the superposition of the velocity field around the fairing on the swirl as the fairing passes through the calibration plane and accounts for the greater displacement of the minimum value of the swirl from the mean value as noted in c) above. The resultant pressure distribution therefore will be "carried around" the test chamber by the fairing and is the means by which energy is transferred from the fairing to the air mass in the test chamber to cause swirl. As the model travels around the test chamber ahead of the fairing, it will not be affected by the peaks in swirl due to the fairing as if will only "see" the smaller perturbations in the swirl present in the oncoming flow as defined by the flow perturbations ahead of the fairing at time intervals between 55 and 70.

If the distributions at the various stations are examined, it can be seen that at the outer stations, the minimum swirl occurs earlier which corresponds to the fairing crossing the calibration plane earlier due to its forward sweep, Fig 62. In addition, the peak in the distribution becomes less pronounced as the measuring stations get further away from the fairing, see Fig 63 which also includes swirl variations measured in the plane nearest the floor. The distributions show the slight reduction in swirl with increase in radius as mentioned above. In the early whirling arms, swirl measurements were made at only one radius and it was assumed that the swirl increased with radius as it was usual to define the swirl as a % of the speed of the arm over the ground rather than as an absolute value. However the present results confirm the measurements made by Kumar and Ashill, refs 9 & 10, which also showed that the swirl varied little with radius in the CoA Whirling Arm. This indicates that general physical nature of the generation of the swirl flow is different when a small enclosed test chamber is used rather than rotating the model in a much less confined space. The distributions also show that the swirl measured at the station nearest the slot between the central volume and the test chamber, station 0503,is much more unsteady than at the other stations.

The initial investigation into the flow in the test chamber due to the rotation of the arm structure in the central volume had shown clearly that the flow round the end of the structure caused considerable local swirl variations as the arm passed the measuring plane but these did not extend radially very far into the test chamber. In view of the greater unsteadiness in swirl present at station 0503, it was decided to look at the time histories of the swirl at stations near the inner wall of the test chamber.

The distribution measured at station 0500, the station nearest to the communicating slot, Fig 64, shows much greater unsteadiness in the swirl measurements. In particular there are very large local peaks about time intervals 120 and 360 . The first time interval corresponds to the rear of the model support fairing passing the measuring plane and indicates that a disturbance from the central volume has penetrated into the test chamber. This is probably the disturbance due to the unfaired roller supports for the main support tubes. The disturbances near time interval 360 are rather less in magnitude and it is significant that the difference in time corresponds to 180 degree rotation of the arm, so that these disturbances occur after the passage of the other end of the arm, i.e. the end without the model support. The distributions also show that the flow is much steadier immediately ahead of these large disturbances indicating that the fairing is effective in preventing disturbances penetrating into the test chamber. Fig 64 also shows the swirl distributions at stations close to station 0500. It can be seen that the major disturbances at the rear of the fairings do not penetrate very far radially into the test chamber although the general level of unsteadiness is still high.

The measurements made near the inner wall in the horizontal plane just below the slot (plane 03), show that the level of unsteadiness is much less and that the large peaks near time intervals 120 and 360 are not present. This demonstrates that the disturbances generated in the central volume and which pass into the test chamber through the slot, are confined to the plane of the slot.

The swirl variations in the vertical plane nearest the inner wall, Fig 64c, show that the swirl distributions away from the slot are very similar and do not differ greatly from the measurements made in vertical plane 03, Fig 63a. It is therefore concluded that any disturbances that penetrate into the test chamber via the labyrinth baffle on the end fairings of the arm, do not cause any appreciable unsteadiness in the test chamber.

8.0 FURTHER MODIFICATIONS TO REDUCE SWIRL

As the general level of swirl was much higher than had been hoped, some thought was given as to whether it could be reduced easily. Although some of the disturbances in the central volume were transmitted through the connecting slot, it was considered that the major contribution to the swirl was the drag of the model support system. As it appeared unlikely that this could be substantially reduced, some method of increasing the energy absorption characteristics of the channel had to be found. The simplest method was by installing baffles in the test chamber as had been done when the facility was installed at NPL. It was considered that the solid baffles used previously, while efficient in producing drag and therefore absorbing energy, produced an eddying flow behind them which must have resulted in the model encountering unsteady conditions as it traversed the test chamber. If the solid baffles were replaced by baffles made from fine mesh net as used for turbulence reducing screens in wind tunnels, then the drag of the baffles would not be reduced appreciably but the flow behind them would be less unsteady because with some air passing through the screens, the mixing process would be less violent.

8.1 Initial investigation of porous baffles

Two sets of porous baffles were made from fine-mesh nylon net curtain material. Each set consisted of two screens which spanned the test chamber. One screen extended 50 inches (1270 mm) down from the ceiling and the other extended 36 inches (915 mm) up from the floor of the test chamber leaving a central gap through which the model and its support could pass (Fig 65). The edges of the material were turned over and sewn to form a tube through which spring curtain rod was threaded. The curtain rod was then stretched and secured to hooks fixed to the walls of the test chamber. In addition the edges of the top baffles were stapled to the walls. This was not done on the lower baffles as it was decided that they should be easily removable to afford free access to all of the test chamber. The two sets of baffles were installed diametrically opposite each other, with one pair approximately 6 ft (2 m) behind the calibration plane to avoid any large scale turbulence immediately behind the baffle. Tests showed that the edges of the top net kept reasonably rigid when the arm was rotating. The bottom net however tended to billow out as the model passed and the edge near the floor lifted appreciably. As this was considered detrimental, this edge was anchored to the floor in order to stabilise the baffle.

In order to assess rapidly whether the porous baffles were effective in reducing swirl the output of a single hotwire probe was installed at station 0506. The output of the servo-amplifier was read manually by a digital voltmeter which sampled data at a rate of 2 readings per second. The numerical value of the swirl obtained from these readings was of no particular significance because of the limitations of the instrument and the unsteadiness of the readings. As approximately the same results were obtained by two operators, it was considered that the swirl thus obtained could be used to assess any improvement due to the installation of the baffles. A swirl of 7.9 fps (2.42 m/sec) was obtained without the baffles which was reduced to 3.4 fps (1.04 m/sec) when the baffles were installed, a reduction in swirl of more than 50%.

Qualitative confirmation that the baffles had a noticeable effect came from impressions obtained on entering the test chamber immediately after the arm had come to rest. Without the baffles a noticeable swirl could be felt which persisted for a considerable time. With the baffles installed, no swirl could be felt on entry.

8.2 The final baffle configuration

For the final configuration it was decided to use six sets of porous baffles spaced equally around the circumference of the test chamber. The bottom baffles were the same as previously used, but a different shape was used for the top baffles.

As it was now intended to alter the attitude of the model in the vertical plane by rotating the sting about a pivot just in front of the model support fairing, the nose of the model would move appreciably upwards as the attitude was increased. Estimates of the nose position of possible models at an attitude of 35 degrees were made to determine the maximum depth of the top baffle. The maximum estimated depth was only 12 inches (305 mm) which was an unacceptable reduction from the previously tested configuration. In order to increase the baffle area, it was decided to keep the original depth at the walls but to use a Vee-shaped bottom edge, stabilised as before by spring rod, to allow passage of the model (Fig 65).

It was not considered desirable to measure the swirl in the same way as previously because most of the measuring stations would be in the lee of the bottom baffles. It was therefore decided that the swirl speed should be determined from the measurements of the speed of the air approaching a probe attached to the arm at the radius of the centre of the test chamber. A pitot-static had been attached in this position from the end of the arm remote from the model, (Fig 66), as part of the standard instrumentation whose purpose was to measure the approach velocity of the air to the model and provide a static-pressure datum for pressure transducers (see section 9). As the response of the pitot-static tube would be inadequate for investigating the steadiness of the approach flow in any detail, a hot-wire probe was attached to the pitot-static tube with its servo-amplifier in the adjacent tip fairing. The output of the amplifier was transmitted to the control room via the sliprings on the arm. Several attempts were made to determine the flow fluctuations by both analogue and digital recorders but with inconclusive results.

The mean speed recorded at constant rpm varied with each recording varying between 56 and 72 fps (17 to 22.8 m/sec) for a rotational speed of 72.3 fps (22.0 m/sec). A possible explanation of this was that the low overheat ratio used by the hotwire probe resulted in poor accuracy when used to measure speeds much higher than the 10 fps (3 m/sec) for which the overheat ratio had been optimised.

The results initially looked promising in that regular excursions from a relatively constant base were present. Further analysis revealed that there were many discrepancies. Firstly the excursions although at regular intervals never seemed to persist for more than 3 or 4 cycles before missing a few cycles. It was felt that if the sensitivity of the system was sufficient to record the effect of one baffle then there should be no difficulty in detecting the presence of all similar baffles. Secondly the frequency of the excursions differed appreciably from that expected from the number of baffle positions and the speed of the arm. Thirdly the peak speeds recorded were often in the range 80 - 85 fps (24 - 26 m/sec) i.e. up to 20% above the rotational speed of the arm. The most likely explanation of the second and third features was that they were due to electrical noise in the system possibly due to bad contacts in the particular sliprings used.

As time did not allow any further modifications to be done to the Whirling Arm, no further attempts were made to investigate the detailed characteristics of the approach flow in the model position.

9.0 ASSESSMENT OF THE ACCURACY OF MEASUREMENT OF AERODYNAMIC COEFFICIENTS IN THE WHIRLING ARM

As it is likely that the unsteadinesss in the approach flow to the model in the Whirling Arm is significantly greater than that in a windtunnel because of the effects of swirl and the swirl-damping baffles, some brief tests were made to assess the effects of this unsteadiness on the accuracy of measurement.

The dynamic head (q_∞) of the airstream approaching the model is used in the conversion of the measurements to non-dimensional form. It is defined by the equations

$$
\begin{aligned}
q_\infty &= \tfrac{1}{2}\rho V_\infty^2 \\
&= \tfrac{1}{2}\rho(V_r - V_\infty)^2 \\
&= H_\infty - p_\infty
\end{aligned}
$$

where V_∞ = approach speed

V_r = tangential speed

V_s = swirl speed

H_∞ = approach total pressure

p_∞ = static pressure

Thus the dynamic head can be obtained from a knowledge of the rotational speed of the arm and the swirl velocity, or measured directly by a pitot-static probe on the datum radius at an interference-free position near the model. It was considered that whilst the measurement of the tangential speed was both easy and accurate,the measurement of a mean swirl speed was difficult experimentally and thus the best and most reliable solution was to measure the dynamic head by a pitot-static probe.

The positioning of the pitot-static probe presented some difficulties. Because of the design of the tip fairing of the arm structure, the positioning of the model relative to the tip fairing and the presence of the baffles, it was found impossible to find a suitable probe position in the neighbourhood of the model. The probe was mounted therefore from the tip fairing remote from the model so that it was at the model radius and height, (Fig 66). There are two main criticisms of this solution. Firstly the damping of the wake from the model and the support fairing will not be fully attenuated with the result that the readings may be somewhat more unsteady than if they had been made near the model. Secondly the additional drag from the probe installation will result in additional swirl at the position of the model. It has always been assumed that the swirl generated by the rotation of the arm rapidly assumed a quasi-steady state when the arm stopped accelerating. This is probably true at a particular position relative to the arm, but the swirl investigations have shown that circumferential variations in swirl exist and therefore the approach speed at the model may not be the same as that at the probe. The relationship between the approach velocities at the two positions can be determined when a model with a pitot-static probe is tested.

As the dynamic head needs to be recorded as part of each data scan, the pitot and static pressures were connected to the ports of the +/-50mm H_2O Celesco differential pressure transducer and became part of the permanent instrumentation system.

When pressure measurements are made on a model, the results are generally presented in the form of the non-dimensional coefficient, C_p, defined as

$$C_p = (p - p_o)/q_a$$

where p = pressure measured

p_o = static pressure

q_a = dynamic head

As differential pressure transducers are used, $(p - p_o)$ can be measured directly by connecting the static pressure to one side of the transducer diaphragm as a reference pressure and connecting the other pressures to be measured to the other side of the transducer diaphragm by a Scanivalve pressure switch. As has been noted, there is a correction to be made for the effect of centrifugal force when measuring pressures at two different radii, thus for this pressure correction to be zero, the static pressure tapping should be on the rotating structure at the datum radius. It should be pointed out that the centrifugal pressure correction depends solely on the relative radii of the pressure orifices and is independent of the location of the differential pressure transducers. This is because the correction between the datum radius and that of the transducer is the same for both pressures and thus the pressure difference seen by the transducer is unaltered by its position. The pitot-static probe already provided for the measurement of total pressure is therefore a suitable source for the static pressure.

9.1 Measurements of swirl with an aircraft model installed

After the baffles were installed, some brief tests were made with an aircraft model to test the efficiency of the centrifugal load cancellation system used in the design of its strain-gauged balance. After these tests were completed some additional tests were made to measure the swirl at different test conditions.

In the tests to assess the strain-gauged balance, multiple samples of the balance outputs had been made and the results analysed to obtain both the mean value and the standard deviation over a range of conditions. The results had shown that the standard deviation of the balance outputs had increased appreciably as the rotational speed increased presumably because of the increasing unsteadiness of the flow approaching the model.

For the present tests the model was mounted with its wings vertical and their upper surfaces facing towards the outside of the test chamber. As the balance calibration tests had not been concerned with obtaining good aerodynamic results, the gap in the model support fairing through which the sting protruded was not faired as it would normally have been. A BASIC program was written to sample sequentially the output of the pitot-static probe described above and a channel of the straingauged balance whose output had been shown to have large standard deviations, obtaining 500 pairs of readings in approximately 10 seconds. The program converted the outputs to approach speed and volts respectively and obtained the mean value and standard deviation of the 500 values of each quantity.

Initially the variation of approach speed with rpm was investigated and it was shown that a very linear relationship existed between them with relatively small progressive changes in slope as the lift was varied from negative to positive. The table below shows the effect of the model attitude on the approach speed at a rotational speed of 25.00 rpm, corresponding to a tangential speed of 71.34 fps (21.74 m/sec) at the test radius.

condition	V_∞ @ 25.00 rpm fps	m/sec	% swirl
1. Zero lift -L.E unfaired	61.57	18.77	13.69
2. max +ve lift - L.E unfaired	60.76	18.52	14.83
3. max -ve lift - L.E unfaired	62.54	19.06	12.34
4. Zero lift - L.E faired	63.22	19.27	11.38
5, max -ve lift - L.E faired	63.69	19.41	10.72

The results show that with the model at approximately its no-lift angle a mean swirl of 13.7% was present. When the model attitude was changed by approximately 10 degrees nose outwards (+ve lift) the swirl was increased to 14.8% as a result of the increased model drag at high lift conditions. However when the attitude was altered to approximately -10 degrees (nose inwards) the swirl was reduced below that at zero lift by approximately the same amount. Although the wing had a certain amount of camber, it would have generated a substantial amount of negative lift at -10 degrees attitude. It is therefore surprising that the effect of the resulting increase in drag is to reduce the swirl. The most probable explanation of this is that the wing trailing vortices at -ve attitude pass closer to the junction between the two sections of the fairing over the model support system and somehow improve the flow and reduce its drag.

As the swirl was rather greater than expected, it was thought that the unfaired section of the leading edge could be the cause of additional drag and therefore increased swirl. The gap was temporarily faired and sealed and some of the tests repeated. These showed that the swirl was reduced by nearly 2% in comparable conditions and that negative lift again resulted in a decrease in swirl but only by about half the previous amount.

9.2 Investigation into the steadiness of measurements

As it had been found that the standard deviations of the balance outputs increased with increasing rpm, the variation of the standard deviation of both speed and balance output were examined. The variation of the standard deviations with rpm could still be taken as linear though with greater scatter than previously. The table below shows the effect of the configuration changes on the standard deviations of the approach speed and balance output at a rotational speed of 25.00 rpm.

Condition	standard deviation		
	approach speed		balance output (V)
	fps	m/sec	
1.Zero lift -L.E unfaired	3.09	0.94	0.0199
2. max +ve lift -L.E unfaired	2.62	0.80	0.0248
3. max -ve lift -L.E unfaired	2.98	0.91	0.0183
4. zero lift - L.E faired	2.83	0.86	0.0183
5. max -ve lift -L.E faired	2.84	0.87	0.0178

Considering first the approach speed, the standard deviation is about 5% of the actual approach speed and does not vary greatly with the test conditions although there are small trends that are configuration dependent. Firstly, fairing the leading edge slot reduces the standard deviation slightly (compare conditions 1 and 4, 3 and 5). Secondly, the standard deviations at zero and -ve lift are similar and noticeably greater than that at high +ve lift. The first result is consistent with the fairing of the leading edge gap cleaning up the flow over the fairing and thus reducing its drag and the swirl. The second result implies that the vortices present in the high +ve lift case somehow improve the steadiness of the flow which seems inconsistent with the increase in swirl speed caused by the increased drag in this condition.

Considering the standard deviations of the balance output, it can be seen that fairing the leading edge gap reduces the standard deviation slightly, but the standard deviation is markedly increased at high +ve lift which is the direct opposite to the effect of lift on the standard deviation of the approach speed.

Although the detailed results are inconsistent as far as the effect of lift is concerned, they do give a good indication of the general level of unsteadiness to be expected in measurements made in the facility.

9.3 Comparison of approach speeds at the model and pitot-static probe

The installation of a pressure plotted body in the Whirling Arm allowed a comparison to be made of the approach velocities measured by a pitot in the nose of the model and the pitot-static probe mounted from the tip fairing remote from the model. The pitot pressure at the nose of the model was measured by the Scanivalve system whose pressure transducer was referenced to static pressure measured by the pitot-static probe, thus giving a measurement of the dynamic head.

9.3.1 Experimental details

The previous tests had shown that there was considerable unsteadiness in the approach speeds measured by the pitot-static probe. As this may have been partly due to fluctuations in the static-pressure measurements made by the probe in the presence of eddying flow produced by the baffles, it was decided to attenuate any fluctuations by inserting a constriction in the connecting tubing. Accordingly a short length of 1.5 mm i.d. tubing about 18 inches (500 mm) long, was inserted into the normal 5mm i.d. pressure leads close to the probe. As there was some 30 ft (9 metres) of the larger tubing between the constriction and the Celesco transducer and an additional 40 ft (12 metres) to the Scanivalve transducer, any pressure fluctuations in pressure at the probe should be considerably attenuated. The lag induced in the system by the constriction is not important as the static pressure should be invariant in the time scale of the test.

The previous data acquisition program was re-written so that the recording rate was approximately doubled and the data was analysed in a slightly different way. As before 500 readings from each transducer were sampled and the mean value and its standard deviation were obtained. In an actual test on an extensively pressure-plotted model, the time taken to do this for every pressure measured would be prohibitive, but some meaning of the measurements was obviously required in view of the large standard deviations occurring in the previous test. It was therefore decided to re-analyse the data to obtain the mean value and standard deviation of successive smaller groups of data to see how closely they approximated to the "500 reading" values. The minimum size of group was 25 readings as the time to record this amount of data approximated to the time the model took to traverse the distance between two baffles at the normal test speed of about 25 rpm. The analysis was then repeated for group sizes of 50 and 100 readings, the latter being the largest considered practical in an actual test.

9.3.2 Test program

The dynamic heads at the pitot-static probe and the model nose were measured at rotational speeds of approximately 18.4 and 25.6 rpm with the model at an incidence of 5 degrees from datum so that the nose was at the datum radius and aligned closely to the approach flow.

In addition tests were made with the arm at rest and a suction approximately equal to the dynamic head applied to the reference side of the pressure transducers.

9.3.3 Analysis of results

The static tests showed that, when the mean equivalent speed measured at the model nose was 64.15 fps (19.56 m/sec), the mean speed measured by the probe was about 0.3 fps (0.09 m/sec) greater giving a ratio of nose/probe speed of 0.996. The standard deviation of the nose speed was 0.07 fps (0.02 m/sec) as compared with 0.04 fps (0.012 m/sec) for the probe.

The test results for the tests at 18.42 and 25.59 rpm are plotted in Figs 67 & 68.

At a rotational speed of 25.59 rpm analysis of all 500 readings gave a mean "nose" speed of 66.49 fps (20.27 m/sec) with a standard deviation of 1.76 fps (0.54 m/sec). The ratio of "nose" speed to tangential speed was 66.49/73.02 (0.9105) giving a swirl of 8.95%.

When the readings were re-analysed in successive groups of 25, the mean speed varied between 65.6 and 67.3 fps (19.99 and 20.51 m/sec) with standard deviations varying between 1.34 and 2.02 fps (0.41 and 0.62 m/sec). Analysis in successive groups of 50 gave mean speeds varying between 65.45 and 66.89 fps (19.95 and 20.39 m/sec) and standard deviations varying between 1.45 and 1.94 fps (0.44 to 0.59 m/sec). Analysis of the results in successive groups of 100 readings gave mean speeds varying between 66.04 and 66.85 fps (20.13 and 20.38 m/sec)/sec and standard deviations varying between 1.65 and 1.83 fps (0.50 and 0.56 m/sec). Thus the variations in mean speed and standard deviation decreased steadily with increase in sample size. If, however, the results are plotted against time (or number of samples) with the values plotted at the midpoint of the sample (Fig 68) it can be seen that all the points lie on a well-defined if irregular curve which presumably defines the variation of the quantities with time and demonstrates the smoothing effect of taking a larger sample. This characteristic is common to all the quantities plotted in Figs 67 and 68.

At a rotational speed of 18.42 rpm, the mean speed measured over 500 readings was 47.73 fps (14.55 m/sec) with a standard deviation of 1.18 fps (0.36 m/sec). The ratio of "nose" speed to tangential speed was 47.73/52.56 (0.908) giving a swirl of 9.2% which compares well with the 8.95% measured at the higher speed. The standard deviation scales fairly well with rpm being slightly less than the predicted value.

The effect of varying the size of the group used in averaging the results was slightly different in that there now was little difference in the scatter in both velocity and standard deviation between the 25 and 50 reading groups, but the 100 reading groups approximated closely to the control 500 reading group (Fig 67).

Turning now to the analysis of the pitot-static probe readings, at 25.59 rpm analysis of all 500 readings gave a mean speed of 66.08 fps (20.14 m/sec) and a standard deviation of 3.09 fps (0.94 m/sec), the ratio of probe speed to tangential speed was therefore 0.905 giving a swirl of 9.5%.

Repeating the analysis using successive groups of 25 readings, the probe speed varied between 65.3 and 67.1 fps (19.90 and 20.45m/sec) with the standard deviations varying between 2.2 and 3.9 fps (0.67 and 1.19 m/sec). Analysis in groups of 50 readings showed the approach speed varied between 65.33 and 66.85 fps (19.91 to 20.38 m/sec) with its standard deviation varying between 2.81 and 3.63 fps (0.86 to 1.11 m/sec). Increasing the group size to 100 readings resulted in the approach speed varying between 65.35 and 66.69 fps (19.92 and 20.32 m/sec) with its standard deviation in the range 2.71 to 3.25 fps (0.83 to 0.99 m/sec). The scatter in the speed and standard deviation results is smaller for the groups of 100 readings than for the groups of 50 and 25 readings which have appreciably larger scatters (Fig 68).

When the arm speed was reduced to 18.42 rpm, the mean approach speed to the probe averaged over 500 samples was 47.79 fps (14.57 m/sec) with a standard deviation of 2.04 fps (0.62 m/sec). The ratio of approach speed to tangential speed was 0.909 giving a swirl of 9.1%. As before the standard deviation scaled fairly well with the reduction in rpm, but as the measured values in both cases were slightly below the expected values, it is likely that the variation with rpm is parabolic as would be expected, but the differences between the linear and parabolic predictions are small over the range considered. As before the groups of 100 readings show the least scatter,

Comparing the results from the "nose" pitot and the probe, two main conclusions can be arrived at:-

a) There is very little difference in the approach speeds measured at the nose of the model and the pitot-static probe mounted from the other end of the arm at either test speed. Taken over the analysis of all the groups of readings the ratio of approach speed at the model nose to the speed at the probe varies between 0.97 to 1.03, with the main part very close to 1.00.

For general use, it can therefore be assumed that the approach speed at the probe is equal to that at the model.

b) The standard deviation of the approach speed readings is nearly twice as great for the probe as those for the nose pitot, reversing the results of the "static" test which however showed much smaller standard deviations. As the standard deviation of the probe speed for these tests is very close to those obtained when the winged model was installed, it would appear that putting the constriction into the static pressure line has had little effect, and that the probe static pressure was not unsteady. If follows then that the fluctuations in the approach velocity result from the fluctuations in pitot pressure and that although the swirl has stabilised at the probe position, considerable damping of the eddies in the wake takes place between the probe and the model.

9.4 Repeatability of pressure coefficient (C_p) measurements

The conclusions drawn from the above tests was that the static pressure used as the Scanivalve reference pressure was adequately steady and that the effect of the flow fluctuations at the model position would be minimised if the average of 100 readings could be taken. However in a typical test over 2500 pressure values may be required at one pitch condition, making it essential to average the smallest number of readings that would give an acceptable accuracy. An additional point to be borne in mind is that the measured pressures have to be divided by the velocity head as measured by the pitot-static probe that has to operate in considerably less steady conditions than the model. It was therefore decided to extend the previous test program to investigate the effect of sample size on the scatter to be expected in measuring pressure coefficients.

9.4.1 Effect of sample size.

The test procedure was exactly the same as previously except that the Scanivalve was cycled until a pressure tapping on the parallel afterbody of the model was connected to the transducer. As before 500 readings were taken in rapid succession and analysed as a whole and as a series of groups of different sizes. The data acquisition program was altered to present the both the pitot-static and model pressure tapping pressures in mm H_2O and to divide the group values of these pressures to obtain the corresponding C_p values.

The results are plotted against time in the same manner as previously. The variation of the mean values of static pressure, velocity head and pressure coefficient are presented in Fig 69 and their standard deviations on Fig 70.

Examination of the body pressure groups shows that there was a consistent variation shown in all the groups which was not shown in the pitot-static readings, Fig 69. The most likely explanation of this was that a slow leak of about 0.1 mm H_2O/sec was present in the scanivalve seals to this particular port. In both cases however the standard deviations were large compared with the pressures being measured, Fig 70. For the body pressure, the mean pressure from all 500 readings was 0.601 mm H_2O with a standard deviation of 0.09 mm H_2O while the corresponding values for the probe were a mean value of 24.80 mm H_2O with a standard deviation of 2.09 mm H_2O. which gave a mean value of C_p of 0.0242

A slightly different method was used to assess the effect of size of the group in the evaluation of the pressure coefficient as the data acquisition program only worked out the mean C_p for each group and did not store the individual results. Thus the C_p values for each set of groups was averaged and their standard deviation obtained. As would be expected, all sizes of group gave the same average value of $C_p = 0.0242$ but the standard deviations varied slightly with group size. Both the "25" and "50" groups had a standard deviation of 0.0015, but increasing the group size to 100 measurements resulted in a slight decrease in the standard deviation to 0.0013.

Thus for all practical purposes, little was to be gained in averaging groups of more than 25 readings. If higher accuracy and consistency is desired, it is considered that the dynamic head should be measured near the model where the pressure fluctuations are less.

9.4.2 Repeatability of C_p measurements

After this assessment of the number of readings that it was necessary to average to get acceptable results, a full program of tests was made on the pressure plotted body taking and averaging 25 readings to obtain the mean pressure at each Scanivalve port. The normal test procedure at each attitude was to take pressure readings from 70 tappings along a body generator, roll the body through 10 degrees , scan the pressures in the new roll position and continue until the body had been rotated through 360 degrees. At the completion of the tests it was decided to do a complete attitude scan without rolling the model. In this way 37 readings of the pressures at each station would be obtained under normal running conditions so that the repeatability of the readings could be assessed.

A suitable test attitude was chosen so that the pressures to be measured varied between $C_p = 0.6$ and $- 0.4$. The Cp values at each port were then meaned, and their standard deviation and maximum and minimum values found, Table 6. The standard deviation of the C_p values at each station were plotted against $|C_p|$ in Fig 71. Most of the results are at low values of C_p, but there are sufficient at the higher values to show that, although there is considerable scatter, a reasonable straight line can be drawn through the points. Thus it would appear that the standard deviation increases with the magnitude of the pressure being measured. This feature is probably due to the large variations in total head. If the pressure measured is small and it is divided by a relatively large value (the dynamic head) which can vary appreciably, then the quotient does not vary greatly. If the pressure measured is large and is then divided by the dynamic head, then the pressure coefficient will exhibit a variation which is proportional to the pressure measured and the percentage standard deviations of the dynamic head and the measured pressure.

The equation of the mean line drawn is:-

$$C_{pSTD} = 0.0025 + 0.0166|C_p|$$

Although this enables a good estimate to be made of the overall accuracy to be expected in measuring pressure coefficients, it gives no idea of the magnitude of the occasional "rogue" value. As the maximum and minimum values recorded at each station in the repeatability tests are listed in Table 6, the variation of these from the mean values was obtained and is plotted in Fig 71b. As in the case of the standard deviations, there is a considerable scatter in the values, but there still is the trend for the variation to increase with $|C_p|$. At low values of $|C_p|$, the maximum variation is generally within +/- 0.0075 or about three times the standard deviation. This ratio also appears to hold approximately throughout the range of the tests.

At each data point in the above tests, the dynamic head was measured along with the pressures measured at corresponding ports of the two Scanivalves and the C_p values were obtained by dividing the "port" pressures by the dynamic head measured at the same time. Originally this method of recording data had been adopted as the swirl speed, and therefore the approach speed was not known, neither was its variation with pitch angle. Thus by measuring the dynamic head at every data point, a data bank would be created which defined the swirl characteristics of the arm and model.

As the previous analysis suggested that the reason for the increase in the standard deviation of C_p with C_p was the unsteadiness of the total head readings, the basic pressure measurements were analysed to see if they confirmed this conclusion. If they did so, greater accuracy could be obtained by dividing the pressures by the mean dynamic head rather than the actual measured value.

Analysis of the dynamic head measurements, Table 7, showed that the mean value of the approach speed for the measurements at the different ports varied by only +/- 0.5% during the test. The standard deviation of the dynamic head measured at a particular port varied between 0.26 and 0.46 mm H_2O, i.e. between 1.03 and 1.86% of the mean dynamic head. Taking an average value of 1.44%, this compares favourably with the value of 1.66% deduced previously. Unfortunately however, the maximum values of the standard deviations of C_p and dynamic head do not occur at corresponding locations.

The average value of the approach speed for the whole set of readings was 66.21 fps (20.18 m/sec) which represents a swirl speed of 6.44 fps (1.96 m/sec) or 8.8% of the translational speed at the test radius.

Examination of the pressures measured at the various pressure tappings, Table 8, showed that most of the standard deviations had values of about 0.06 to 0.08 mm H_2O, but some ports had appreciably greater values which exceeded 0.15 mm H_2O. Although some of these ports were measuring larger (unsigned) pressures, there did not seem to be a consistent relationship between the magnitude of the standard deviation and the measured pressure. It was noticed however it was noticed that the pressure points on the forebody of the model (ports 1 - 15, 51-2 and 65 - 68) had larger standard deviations than the remainder. In addition, it seemed that the pressure points nearest the nose (ports 1, 2, 51, 52, and 65 - 68) had the largest standard deviations of pressure and that the magnitude of the standard deviation decreased as the distance of the pressure point from the nose increased. This was not completely true as the standard deviation of the pressures on the suction surface of the body (ports 51 - 64) decreased more rapidly with distance than those on the under surface. If the local angle of the body surface to the oncoming flow is used as a criterion rather than the distance from the nose, then the results become consistent.

It would therefore appear that the larger standard deviations of the pressure occur on the forward facing surfaces of the body and depend on the local inclination of the surface of the body to the oncoming airstream.

The pressure coefficients were then recalculated using the mean dynamic head for the whole data set, Table 9, rather than the instantaneous values previously used, Table 6. Comparison of the two sets of values show that there is little significant difference between them except for the first few ports where there are some significant changes in the maximum and minimum values recorded and the standard deviations but these do not lead to comparable changes in the average pressures

10.0 INITIAL OPERATING EXPERIENCE

Initial use of the Whirling Arm to pressure-plot a body and to measure the rotary derivatives of an aircraft model showed up some instrumentation problems which are briefly mentioned here. They will be discussed in more detail in future reports

10.1 Measurement of pitch angle

The pitch angle was measured by a linear potentiometer attached to the control beam near its pivot point and to an angle beam which ran between the inboard vertical diagonal bracing on the sides of the arm. It was found that the pitch reading changed about 0.6 degree when the arm was accelerated from rest to full speed and returned to the initial reading when the arm was stopped. As this was much greater than expected from the calculations on the deflection of the control beam, it was thought that the cause was air in the hydraulic circuit operating the jack. Some small improvement was made by bleeding the system and it was assumed that the problem was due to an airpocket in the jack itself which could only be cured by removing the jack from the arm. This was not considered to be justified as the pitch angle could be set when the arm was rotating at the test speed.

Initially the usable pitch range was +/- 10 degrees due to the fouling of the sting with the internal structure of the fairing. This was later increased to nearer the full design range to enable measurements to be made at incidences past the stall incidence of the aircraft model. When this was done the fixings of the pitch potentiometer had to be altered as the travel required was greater than that available. In the new position the apparent change of angle between rest and normal operating speed was almost doubled leading to the conclusion that undue deflection of the structure was occurring in the neighbourhood of the pivot. Ormerod found by measuring the movement of the support tubes relative to the end frame of the arm that the movement of the tubes between at rest and the normal operating speed was consistent with the calculated value, but that the structure locating the control-beam pivot deflected due to the component of the jack load acting along the beam. The support structure was stiffened by a diagonal member welded between the pivot mounting beam and the central tower, (Fig 70). This was successful in almost completely eliminating the apparent deflection due to centrifugal effects.

10.2 Electrical connectors

Ooriginally the electrical connectors used inside the pressure plotting model to connect the transducers, Scanivalves etc. to the wiring harness inside the model were the standard DIN connectors used throughout the department in which the two halves of the connector were positively locked together by a locking nut. Considerable problems occurred with the panel-mounted half of these connectors due to the output tags breaking due to the centrifugal loads imposed on them by short unsupported lengths of cable. These sockets were replaced by ones with more robust tags but at the expense of losing the positive locking system and relying on taping together the two halves of the connector. This solution proved satisfactory although not ideal. The best solution would have been to use DIN connectors with a different pin arrangement which had both the more robust tags and a positive lock between the two halves of the connector, but this solution was not adopted as it would have required the replacement of all the DIN connectors in use in the department.

10.3 Scanivalve operation

The Scanivalve pressure switches used in the pressure-plotting tests were cantilevered from a bulkhead in the model by the normal mounting flange on the rotary solenoid which is used to rotate the switch between successive pressure ports. The Setra pressure transducer, which was both long and relatively heavy because of the signal conditioning unit incorporated in it, was mounted at the end remote from the mounting flange as was the pneumatic connector with the attached pressure leads which were unavoidably unsupported for a short distance to allow for assembly etc. Although the initial commissioning tests, which did not involve rolling the model, were satisfactory, once the tests began which involved rolling the body considerable problems were encountered.

At certain roll angles the operation of the Scanivalves became erratic as the Scanivalves went out of synchronisation causing the run to be abandoned. The reason for this was eventually traced to two independent faults.

a) The rotary solenoid and its ratchet system were attached to the body of the solenoid by two diagonally opposite pillars with the result that the stiffness of the unit to imposed forces was markedly reduced when the imposed force was applied in planes at large angles to the plane of the pillars. When the model was rotated so that this was so, the 6"g"centrifugal acceleration on the body of the scanivalve, the transducer and pressure leads caused sufficient mis-alignment to jam the Scanivalve. This was cured by using an external stiffening frame between the rotary solenoid and the body of the Scanivalve.

b) When using the Scanivalve controller to operate the Scanivalves, a contact was opened momentarily as part of the control system controlling the stepping of the Scanivalve. One half of the contact consisted of a contact block mounted at the end of a spring steel arm. After prolonged use the closing force due to the spring diminished and at certain roll angles the force due to the centrifugal acceleration on the contact mass was greater than the restoring force due to the spring and so the contact remained open and the Scanivalve solenoid remained energised but did not step further. Once the Scanivalves were out of step or one was inoperative, any attempt to "home" the Scanivalves resulted in complete loss of control and the Scanivalves operate continuously. This problem was overcome by only using the controller for manual operation of the scanivalves to check their operation and to synchronise them when the arm was at rest. Once the arm was in motion, the scanivalve controller was by-passed and the Scanivalves were controlled by the MIDAS microcomputer through relays with only stepping operations allowed.

10.4 Operation of the COMPACT rpm indicator

Although this instrument worked satisfactorily in the initial tests, when the pressure-plotting model was being tested considerable electrical interference was present so that the indicator only gave sensible readings at infrequent intervals during the test, but luckily sufficiently frequently to monitor the test speed adequately as the arm speed was naturally steady. Eventually the interference was traced to the cable between the MIDAS and Superbrain microcomputers and the cable between the rpm indicator and its pickup running adjacent to each other over a short distance. The interference only became noticeable during the pressure plotting tests because the MIDAS was transmitting information to the Superbrain almost continually to check the progress of the test. As the cables were only in close proximity for a short distance, it is hoped that a minor re-routing of the cables and the installation of additional screening will cure the interference.

10.5 Reed relays in the MIDAS controller

The relays in the MIDAS controller were used to control the rotary solenoids used in the Scanivalve pressure switches and a similar one used to roll the model. As these solenoids operated of 40 and 50 V DC respectively and the reed relays were only rated at 5 - 9 V DC, the reed relays were used to control the operation of heavy duty transistorised relays that did the actual switching.

After some time, the operation of the reed relays became unreliable as they tended to stick in the closed position although they operated normally again after the power supply to the transistorised relays was switched off for a period. This was very unsatisfactory as it was not always obvious that the relays were stuck especially as the solenoids were only rated for intermittent operation. As a result the solenoids got extremely hot even if the fault was detected immediately as there was no means of switching off their power supply until the arm was brought to rest.

As the transistorised relays required only a very small current to operate them, the supplier was consulted as to the likely cause of the problem. It appeared that reed relays can become unreliable if they are only passing a very small current and the cure proposed was to provide an alternative path to earth via a resistor chosen so that a current of about 50% of the rated current passes through the relay when it is closed.

11.0 FUTURE DEVELOPMENTS

Although the swirl in the test chamber has been approximately halved by the modifications made to date, it is felt that it would be a great advantage if the approach flow to the model could be made steadier and if some means could be found of breaking up the wing vortices at a safe distance behind the model to prevent them persisting until they encounter the model.

The work so far has concentrated firstly in minimising the swirl in the central volume and preventing energy transfer into the test chamber and secondly in increasing the energy absorption capacity of the test chamber by the installation of baffles which reduced the swirl at the expense of introducing large scale eddies.

As the energy needed to produce the swirl flow is very small, less than 0.1 KW, it would seem that the best approach might be to put energy into the test chamber to counteract the swirl, especially if it could be done in such a way as to break up the wing vortices. One possible method that could be used is to install a small tube near the trailing edge of the model support fairing with rows of small holes inclined to the plane of rotation through which compressed air could expand to form a jet curtain. This would be capable of breaking up the wing vortices and also providing enough energy in the plane of rotation to eliminate the swirl. Alternatively a large multi-bladed pusher propeller could be installed behind the trailing edge of the support fairing to perform the same task. This would probably more efficient in reducing the swirl but possibly less efficient in breaking up the vortices.

The compressed air curtain would be the easiest to install but would need more development work.

12.0 ACKNOWLEDGMENTS

The author would like to thank Attack Weapons and Aerodynamics Departments, Royal Aircraft Establishment, Farnborough Hants for their financial support of this work which formed part of the work done under Agreement No 2028/131-XRAW

The author would like to acknowlege the help given to him by the following:-

E.W.Osbourn for the supervision of all the work involved in the modification of the Whirling Arm, the assembly and commissioning of the model support system and its fairings, the installation of the instrumentation and his invaluable help in all aspects of the operation of the Whirling Arm.

M. Watts and B. Neal for the building and installation of all the fairings and the installation of the model support system.

D. Clenton of the Design Drawing Office CoA for the detail design of the model support system and the supevision of its manufacture in the Design Workshop

L.C. Moon of Sirton Computers Ltd for his help and advice in blending the Midas and Superbrain computers into an integrated system.

Dr J.M. Shanks formerly of Off-shore Structures Dept, College of Aeronautics, for introducing me to the intricacies of FINEL

R. Watson formerly of the Computer Centre CIT for assistance in transfering data to the VAX computers and organising the conversion of the computer graphics presentation of the flow in the test chamber into a film.

A.O. Ormerod of Aerodynamics Dept, College of Aeronautics, for organising the installation of the porous screens, making his aircraft model available for the initial assessment of the characteristics of the Whirling Arm and discussions on general problems that arose in the commissioning.

REFERENCES

1	Halliday, A.S Allwood, P.H Caborn, N.H	The new Whirling Arm at the National Physical Laboratory R&M 2286, August 1946
2	Benjamin Robins	Mathematical tracts of the late Benjamin Robins Volume 1. James Wilson, London
3	Advisory Committee for Aeronautics	Report for the year 1909 - 10
4	Bairstow, L Bramwell, F.H Sillick,W,E.G	Determination of the movement of air in the Whirling Table Shed due to the motion of the Whirling Arm with and without propellers. R&M 34 March 1911
5	Bramwell,F.H Relf, E.F Fage, A	On the determination on the Whirling Arm of the pressure velocity constant for a pitot (velocity head and static pressure) tube; and on the absolute measurement of velocity in Aeronautical work. R&M 71, December 1912
6	Jones, R	The distribution of normal pressure on a prolate spheroid. R&M 1061, December 1925
7	Halliday, A.S Bryant, L,W Burge, C.H	The experimental deternination of pitching moment on an aeroplane due to rotation in pitch R&M 1556, March 1933

REFERENCES (CONTINUED)

8	Halliday, A.S Burge, C.H	Experiments on the Whirling Arm. Yawing and rolling moments on the Hornbill and various aerofoils, also pressure distribution and flow tests on R.A.F. 15 R&M 1642 August 1934
9	Ashill, P.R Osbourn, E.W	Calibration of the flow in the channel of the Whirling Arm. CoA Note 177, October 1969
10	Kumar, P.E	The College of Aeronautics Whirling Arm. Initial development tests. CoA Note 174, May 1967
11	Andrews, E.J	The Whirling Arm and related research CoA Aero/46/EJA July 1971
12	Hoerner, S.F	Fluid dynamic drag. Hoerner 1965
13	Bearman, P.W	Corrections for the effect of ambient temperature drifts on hot-wire measurements in incompressible flow. DISA Information No 11, May 1971
14	Spillman, J.J	Aerodynamics of vortical type flows in three dimensions. Paper 31 B. AGARD Conference Procedings No. 342

Configuration	Approximate structural frontal area (sq in)	Measured Drag (D) (lb @ 100 fps)	C_D	D/D_1	C_D/C_{D_1}
1	140.8	24.01	2.07	-	-
2	123.2	21.00	2.07	0.875	1.00
3	99.2	15.45	1.89	0.643	0.913
4	90.4	14.14	1.90	0.589	0.918
5	90.4	14.19	1.91	0.591	0.923
6	112.3	18.21	1.97	0.758	0.952
7	90.4	3.27	0.44	0.136	0.213
8	90.4	5.18	0.70	0.216	0.338
9	90.4	8.99	1.21	0.374	0.584
10	90.4	9.47	1.27	0.394	0.614
11	90.4	10.41	1.40	0.434	0.676
12	90.4	15.06	2.02	0.627	0.976

Description of Configurations

1	As whirling arm
2	Out diagonals removed (front and back)
3	As 2, but inner diagonals removed
4	As 3, but centre struts removed
5	As 4, but centre strut attachments replaced
6	As 4, but single diagonal strut in each panel
7	As 4, but side bottom and top panels faired
8	As 7, but tail fairings removed
9	As 8, but nose fairings removed
10	As 9, but outer panel fills removed
11	As 10, but inner panel fills removed
12	As 11, but side panel fills removed

TABLE 1 Analysis of the effect of modifications on the aerodynamic drag of a 3/8 scale model of the two tip bays of the 3rd NPL Whirling Arm.

Station	Mean Swirl speed fps			
	Original Structure	Mod 1	Mod 2	Mod 3
0000	9.99	8.79	2.93	1.98
0400	9.37	8.32	2.91	2.41
0700	15.72	15.47	7.50	5.59
0002	10.40	9.67	2.60	2.66
0402	10.21	10.33	2.76	3.03
0702	10.43	11.48	4.07	3.43
0003	13.43	11.76	5.19	3.33
0403	13.60	12.56	5.31	4.11
0703	14.12	12.61	7.44	3.91
0004	16.28	15.11	5.79	4.06
0404	17.18	15.10	5.74	5.60
0704	17.53	16.58	8.87	6.08
0005	15.08	12.73	5.52	4.57
0405	16.69	11.73	6.30	4.98
0705	18.47	13.04	6.56	5.63
0006	12.34	10.17	4.79	3.61
0406	13.86	9.54	5.34	3.84
0706	13.89	9.75	5.43	3.75
0007	7.89	5.95	1.57	2.55
0407	10.30	5.22	2.34	2.68
0707	10.83	5.08	2.47	2.61
0009	10.20	8.16	3.28	3.15
0409	11.67	7.67	4.14	3.22
0709	11.91	7.57	4.18	3.16
0010	14.96	12.62	4.47	4.00
0410	15.50	11.89	5.51	4.49
0710	18.16	12.30	4.91	5.87
0011	11.82	9.88	3.84	3.17
0411	12.16	9.94	4.90	3.70
0711	13.77	10.07	3.87	4.04
0012	7.88	6.37	1.04	2.18
0412	8.61	6.56	1.64	2.82
0712	10.87	6.31	0.90	3.52
0014	9.47	3.31	2.79	2.41
0414	9.49	3.04	3.13	3.53
0714	11.18	3.10	2.60	4.58

TABLE 2 Variation of mean swirl speed with station for a rotational speed of 25.34 rpm corresponding to a speed of 72.32 fps at 27.25 ft radius i.e. at the centre of the test chamber.

Station	Mod 1	v/v_o Mod 2	Mod 3
0000	0.879	0.293	0.198
0002	0.930	0.250	0.258
0003	0.876	0.386	0.248
0004	0.928	0.356	0.302
0005	0.844	0.366	0.303
0006	0.824	0.388	0.292
0007	0.754	0.199	0.323
0009	0.800	0.322	0.309
0010	0.844	0.299	0.267
0011	0.836	0.325	0.268
0012	0.808	0.132	0.277
0014	0.350	0.295	0.254

a) Plane 00

0400	0.888	0.311	0.257
0402	1.011	0.270	0.297
0403	0.924	0.398	0.302
0404	0.879	0.334	0.325
0405	0.703	0.377	0.298
0406	0.688	0.385	0.277
0407	0.507	0.227	0.260
0409	0.657	0.354	0.276
0410	0.767	0.355	0.289
0411	0.817	0.402	0.304
0412	0.762	0.190	0.330
0414	0.320	0.330	0.372

b) Plane 04

0700	0.984	0.477	0.356
0702	1.095	0.388	0.327
0703	0.893	0.526	0.277
0704	0.946	0.506	0.347
0705	0.708	0.355	0.305
0706	0.702	0.391	0.267
0707	0.460	0.288	0.241
0709	0.636	0.351	0.265
0710	0.677	0.270	0.323
0711	0.782	0.281	0.293
0712	0.580	0.083	0.323
0714	0.277	0.233	0.410

c) Plane 07

TABLE 3 The relative improvement in swirl speed at each measurement station as the arm structure is modified.

Component	Weight (lb)	Mean radius (ft)	Mean 'g'	Centrifugal load (lb)
Sting (design)	30	28.1	9.68	290.0
Sting carrier	52	30.0	10.35	538.25
Front support tube	120	23.6	8.12	974.4
Rear support tube	120	26.15	9.0	1079.4
Front connecting tube	40	14.40	4.96	198.3
Rear connecting tube	40	16.72	5.76	230.4
Control beam	80	8.79	3.02	241.95

TABLE 4 Weights and centrifugal loadings of the moving components when rotating at 31.8 rpm with linkage fully extended.

Station	V_{mean}(fps)	V_{RMS}(fps)	V_{max}(fps)	V_{min}(fps)
0000	15.13	15.15	17.53	10.99
0001	14.45	14.46	16.15	10.89
0002	14.44	14.46	16.54	10.20
0003	14.12	14.15	16.44	9.45
0004	13.87	13.91	16.46	9.44
0005	13.70	13.72	16.42	9.70
0006	13.72	13.75	15.53	8.02
0007	13.86	13.88	16.42	9.70
0008	13.87	13.91	16.49	10.37
0009	13.44	13.46	15.72	9.33
0010	13.48	13.49	15.87	9.89
0011	13.39	13.42	15.71	9.19

1) Mean swirl velocity over plane x = 00 is 13.94 fps (4.24 m/sec)

0100	14.72	14.78	17.34	9.55
0101	14.15	14.22	17.02	9.26
0102	14.64	14.67	17.20	9.83
0103	14.02	14.05	16.97	9.27
0104	13.56	13.61	16.72	9.50
0105	13.20	13.22	15.23	8.99
0106	12.81	12.83	14.81	8.99
0107	13.46	13.48	15.42	9.25
0108	13.89	13.93	15.67	9.78
0109	13.70	13.71	15.61	9.69
0110	13.85	13.86	15.54	9.84
0111	14.09	14.11	16.07	9.94

2) Mean swirl velocity over plane x = 01 is 13.83 fps (4.22 m/sec)

0200	13.68	13.73	15.91	8.13
0201	13.27	13.30	16.08	8.30
0202	12.54	12.55	14.71	8.44
0203	13.51	13.55	15.74	8.46
0204	13.83	13.86	15.76	9.16
0205	13.63	13.65	15.55	9.09
0206	13.34	13.35	14.91	8.76
0207	13.88	13.90	16.01	8.79
0208	12.69	12.71	15.29	8.25
0209	12.41	12.43	14.61	8.43
0210	11.73	11.74	13.35	8.49
0211	12.40	12.43	14.54	7.66

3) Mean swirl velocity over plane x = 02 is 13.07 fps (3.98 m/sec)

Table 5A Swirl Velocities measured in the calibration plane (x = 00 to 02)

Fully faired whirling arm with revised tip fairing and faired model support system [MOD4]

Station	V_{mean}(fps)	V_{RMS}(fps)	V_{max}(fps)	V_{min}(fps)
0300	14.41	14.46	17.12	8.95
0301	13.77	13.82	16.52	7.69
0302	13.35	13.38	15.68	8.51
0303	14.28	14.30	16.34	8.30
0304	14.33	14.38	16.95	8.42
0305	14.41	14.44	16.64	8.84
0306	14.27	14.29	16.48	9.02
0307	13.76	13.79	16.07	7.12
0308	13.13	13.17	14.88	7.42
0309	12.84	12.86	14.57	8.52
0310	12.00	12.02	14.19	7.64
0311	12.71	12.73	14.74	7.82

4) Mean swirl velocity over plane x = 03 is 13.61 fps (4.15 m/sec)

0400	13.49	13.49	15.73	9.28
0401	13.26	13.30	16.59	7.33
0402	12.11	12.17	15.72	7.61
0403	13.46	13.50	16.46	9.67
0404	14.59	14.66	16.89	6.66
0405	14.53	14.57	17.05	8.51
0406	14.58	14.61	16.51	8.68
0407	14.38	14.42	16.23	7.33
0408	12.61	12.68	15.18	6.02
0409	12.32	12.35	14.21	6.09
0410	11.38	11.41	13.28	6.03
0411	12.37	12.40	14.47	8.03

5) Mean swirl velocity over plane x = 04 is 13.25 fps (4.04 m/sec)

0500	16.07	16.31	25.77	3.73
0501	15.83	15.98	22.30	5.02
0502	16.23	16.46	21.68	5.12
0503	14.47	14.61	20.05	0.93
0504	14.76	14.86	18.40	5.89
0505	14.15	14.20	16.94	6.49
0506	13.52	13.56	16.39	6.54
0507	13.92	13.99	16.36	4.76
0508	13.84	13.92	17.82	5.59
0509	12.99	13.07	17.39	4.82
0510	12.21	12.27	14.70	5.09
0511	12.90	12.95	15.22	5.28

6) Mean swirl velocity over plane x = 05 is 14.24 fps (4.34 m/sec)

Table 5B Swirl Velocities measured inthe calibration plane (x = 03 to 05)

Fully faired whirling arm with revised tip fairing and faired model support system [MOD4]

PORT	MEAN	ST DEV	MAX	MIN
1	0.5076	0.0109	0.5306	0.4839
2	0.5422	0.0117	0.5648	0.5154
3	0.4247	0.0086	0.4431	0.4105
4	0.3463	0.0077	0.3609	0.3329
5	0.2564	0.0079	0.2778	0.2390
6	0.1857	0.0050	0.1941	0.1751
7	0.1259	0.0059	0.1383	0.1147
8	0.0694	0.0053	0.0825	0.0595
9	0.0288	0.0049	0.0386	0.0186
10	-0.0152	0.0039	-0.0077	-0.0258
11	-0.0596	0.0050	-0.0516	-0.0748
12	-0.0964	0.0053	-0.0814	-0.1097
13	-0.1115	0.0043	-0.1016	-0.1212
14	-0.1556	0.0044	-0.1455	-0.1656
15	-0.1438	0.0040	-0.1357	-0.1526
16	-0.1546	0.0044	-0.1445	-0.1636
17	-0.1252	0.0032	-0.1193	-0.1322
18	-0.0953	0.0031	-0.0880	-0.1017
19	-0.0818	0.0032	-0.0747	-0.0885
20	-0.0733	0.0031	-0.0639	-0.0795
21	-0.0608	0.0021	-0.0562	-0.0657
22	-0.0561	0.0028	-0.0467	-0.0609
23	-0.0480	0.0023	-0.0431	-0.0528
24	-0.0466	0.0025	-0.0375	-0.0510
25	-0.0406	0.0025	-0.0356	-0.0471
26	-0.0407	0.0032	-0.0342	-0.0472
27	-0.0330	0.0026	-0.0267	-0.0391
28	-0.0332	0.0032	-0.0244	-0.0408
29	-0.0281	0.0026	-0.0216	-0.0331
30	-0.0291	0.0028	-0.0196	-0.0351
31	-0.0243	0.0043	-0.0059	-0.0316
32	-0.0262	0.0024	-0.0217	-0.0323
33	0.0017	0.0016	0.0052	-0.0014
34	-0.0224	0.0023	-0.0174	-0.0280
35	0.0129	0.0020	0.0167	0.0074
36	-0.0217	0.0024	-0.0121	-0.0260
37	0.0033	0.0018	0.0069	0.0000
38	-0.0089	0.0033	0.0010	-0.0144
39	0.0131	0.0017	0.0164	0.0092
40	-0.0157	0.0030	-0.0083	-0.0225
41	0.0042	0.0015	0.0080	0.0003
42	-0.0088	0.0027	-0.0026	-0.0136
43	0.0131	0.0019	0.0173	0.0088
44	-0.0059	0.0028	0.0045	-0.0114
45	-0.0021	0.0023	0.0032	-0.0059
46	-0.0049	0.0030	0.0059	-0.0129
47	-0.0116	0.0021	-0.0063	-0.0149
48	-0.0136	0.0023	-0.0052	-0.0175
49	-0.0176	0.0018	-0.0136	-0.0212
50	-0.0410	0.0023	-0.0359	-0.0459
51	0.1692	0.0077	0.1813	0.1479
52	-0.2111	0.0050	-0.2017	-0.2217
53	-0.2902	0.0050	-0.2782	-0.3030
54	-0.2448	0.0048	-0.2326	-0.2537
55	-0.1856	0.0043	-0.1774	-0.1958
56	-0.1768	0.0053	-0.1663	-0.1872
57	-0.1530	0.0043	-0.1431	-0.1632
58	-0.1348	0.0050	-0.1251	-0.1468
59	-0.1027	0.0030	-0.0967	-0.1083
60	-0.0629	0.0031	-0.0546	-0.0693
61	-0.0409	0.0023	-0.0357	-0.0453
62	-0.0355	0.0025	-0.0282	-0.0417
63	-0.0209	0.0024	-0.0165	-0.0267
64	-0.0196	0.0026	-0.0130	-0.0258
65	0.5070	0.0111	0.5339	0.4845
66	0.1711	0.0099	0.1933	0.1495
67	0.1703	0.0072	0.1861	0.1528
68	0.4624	0.0125	0.4927	0.4440

Rotational speed = 25.46 rpm approx

Table 6. Repeatability of Cp measurements, pitch = -4 degrees

PORT	MEAN	ST DEV	MAX	MIN
0	25.307	0.365	25.929	24.420
1	25.487	0.349	26.367	24.832
2	25.520	0.319	26.093	24.869
3	25.426	0.381	26.158	24.379
4	25.368	0.276	25.977	24.887
5	25.384	0.384	26.214	24.419
6	25.407	0.291	26.042	24.920
7	25.418	0.338	26.109	24.551
8	25.437	0.263	26.128	24.968
9	25.417	0.382	26.222	24.641
10	25.421	0.360	26.412	24.776
11	25.377	0.379	26.266	24.521
12	25.396	0.376	26.170	24.610
13	25.372	0.345	26.511	24.735
14	25.403	0.287	25.920	24.964
15	25.462	0.360	26.294	24.829
16	25.465	0.268	25.891	24.868
17	25.332	0.310	26.034	24.578
18	25.443	0.339	26.262	24.887
19	25.432	0.383	25.999	24.388
20	25.350	0.383	26.342	24.569
21	25.418	0.316	26.184	24.870
22	25.294	0.421	26.341	24.148
23	25.444	0.381	26.275	24.452
24	25.308	0.407	26.394	24.556
25	25.350	0.341	26.216	24.570
26	25.463	0.311	26.358	24.874
27	25.267	0.432	26.301	24.468
28	25.366	0.377	26.098	24.422
29	25.287	0.334	26.067	24.604
30	25.452	0.364	26.241	24.857
31	25.347	0.464	26.347	24.333
32	25.458	0.433	26.115	24.646
33	25.435	0.363	26.380	24.684
34	25.407	0.382	26.266	24.623
35	25.307	0.343	26.076	24.551
36	25.399	0.416	25.999	24.349

Rotational speed = 25.45 rpm approx

Translational speed at 25.46 rpm = 72.653 fps

Mean dynamic head for complete data set = 25.3953 mm H2O

Mean approach speed = 66.2119 fps

Approach speed/translational speed = .911345

Table 7. Repeatability of dynamic head measurements, theta = -4 degrees

PORT	MEAN	ST DEV	MAX	MIN
1	12.934	0.188	13.359	12.606
2	13.817	0.209	14.336	13.396
3	10.837	0.182	11.202	10.472
4	8.836	0.186	9.233	8.434
5	6.517	0.171	6.884	6.152
6	4.721	0.130	4.974	4.437
7	3.194	0.153	3.555	2.908
8	1.760	0.135	2.107	1.504
9	0.731	0.125	0.982	0.480
10	-0.387	0.097	-0.198	-0.644
11	-1.514	0.120	-1.317	-1.865
12	-2.448	0.122	-2.120	-2.735
13	-2.834	0.098	-2.561	-3.027
14	-3.956	0.104	-3.767	-4.148
15	-3.657	0.093	-3.473	-3.839
16	-3.932	0.104	-3.695	-4.128
17	-3.183	0.076	-3.051	-3.341
18	-2.422	0.077	-2.189	-2.582
19	-2.079	0.079	-1.941	-2.258
20	-1.864	0.077	-1.643	-2.028
21	-1.543	0.055	-1.421	-1.676
22	-1.423	0.075	-1.158	-1.550
23	-1.220	0.063	-1.076	-1.340
24	-1.183	0.066	-0.963	-1.309
25	-1.029	0.059	-0.901	-1.197
26	-1.033	0.079	-0.878	-1.199
27	-0.839	0.068	-0.692	-1.006
28	-0.843	0.082	-0.629	-1.054
29	-0.715	0.062	-0.564	-0.838
30	-0.741	0.069	-0.505	-0.871
31	-0.618	0.109	-0.151	-0.792
32	-0.667	0.060	-0.554	-0.811
33	0.043	0.041	0.132	-0.036
34	-0.566	0.058	-0.445	-0.700
35	0.327	0.051	0.433	0.193
36	-0.553	0.062	-0.313	-0.651
37	0.085	0.047	0.179	0.001
38	-0.227	0.084	0.024	-0.361
39	0.331	0.043	0.413	0.234
40	-0.398	0.076	-0.213	-0.575
41	0.107	0.037	0.201	0.006
42	-0.223	0.067	-0.066	-0.341
43	0.333	0.051	0.456	0.221
44	-0.150	0.072	0.113	-0.288
45	-0.054	0.058	0.080	-0.149
46	-0.124	0.077	0.150	-0.330
47	-0.293	0.051	-0.167	-0.382
48	-0.344	0.057	-0.131	-0.443
49	-0.447	0.046	-0.352	-0.540
50	-1.040	0.055	-0.925	-1.145
51	4.310	0.199	4.624	3.734
52	-5.374	0.104	-5.157	-5.615
53	-7.330	0.080	-7.120	-7.490
54	-6.184	0.080	-5.915	-6.388
55	-4.706	0.081	-4.556	-4.901
56	-4.483	0.103	-4.248	-4.685
57	-3.869	0.096	-3.631	-4.125
58	-3.408	0.128	-3.175	-3.768
59	-2.614	0.070	-2.446	-2.764
60	-1.600	0.075	-1.357	-1.727
61	-1.036	0.055	-0.928	-1.162
62	-0.899	0.059	-0.723	-1.042
63	-0.532	0.060	-0.417	-0.680
64	-0.499	0.066	-0.339	-0.659
65	12.893	0.179	13.179	12.548
66	4.351	0.253	5.011	3.789
67	4.326	0.185	4.765	3.923
68	11.746	0.280	12.312	11.105

Rotational speed = 25.46 rpm approx

Table 8. Repeatability of pressure measurements, pitch = -4 degrees

PORT	MEAN	ST DEV	MAX	MIN
1	0.5094	0.0074	0.5262	0.4965
2	0.5442	0.0083	0.5646	0.5276
3	0.4268	0.0072	0.4412	0.4125
4	0.3480	0.0073	0.3636	0.3322
5	0.2567	0.0067	0.2711	0.2423
6	0.1859	0.0051	0.1959	0.1747
7	0.1258	0.0060	0.1400	0.1145
8	0.0693	0.0053	0.0830	0.0592
9	0.0288	0.0049	0.0387	0.0189
10	-0.0152	0.0038	-0.0078	-0.0254
11	-0.0596	0.0047	-0.0519	-0.0735
12	-0.0964	0.0048	-0.0835	-0.1077
13	-0.1116	0.0038	-0.1009	-0.1192
14	-0.1558	0.0041	-0.1484	-0.1634
15	-0.1440	0.0037	-0.1368	-0.1512
16	-0.1548	0.0041	-0.1455	-0.1626
17	-0.1254	0.0030	-0.1202	-0.1316
18	-0.0954	0.0030	-0.0862	-0.1017
19	-0.0819	0.0031	-0.0765	-0.0889
20	-0.0734	0.0030	-0.0647	-0.0799
21	-0.0608	0.0022	-0.0560	-0.0660
22	-0.0560	0.0030	-0.0456	-0.0610
23	-0.0480	0.0025	-0.0424	-0.0528
24	-0.0466	0.0026	-0.0379	-0.0516
25	-0.0405	0.0023	-0.0355	-0.0471
26	-0.0407	0.0031	-0.0346	-0.0472
27	-0.0330	0.0027	-0.0273	-0.0396
28	-0.0332	0.0032	-0.0248	-0.0415
29	-0.0282	0.0025	-0.0222	-0.0330
30	-0.0292	0.0027	-0.0199	-0.0343
31	-0.0243	0.0043	-0.0059	-0.0312
32	-0.0263	0.0024	-0.0218	-0.0320
33	0.0017	0.0016	0.0052	-0.0014
34	-0.0223	0.0023	-0.0175	-0.0276
35	0.0129	0.0020	0.0171	0.0076
36	-0.0218	0.0024	-0.0123	-0.0256
37	0.0033	0.0018	0.0070	0.0000
38	-0.0089	0.0033	0.0010	-0.0142
39	0.0130	0.0017	0.0163	0.0092
40	-0.0157	0.0030	-0.0084	-0.0226
41	0.0042	0.0015	0.0079	0.0003
42	-0.0088	0.0026	-0.0026	-0.0134
43	0.0131	0.0020	0.0180	0.0087
44	-0.0059	0.0028	0.0045	-0.0114
45	-0.0021	0.0023	0.0032	-0.0059
46	-0.0049	0.0030	0.0059	-0.0130
47	-0.0115	0.0020	-0.0066	-0.0150
48	-0.0136	0.0023	-0.0051	-0.0174
49	-0.0176	0.0018	-0.0139	-0.0213
50	-0.0409	0.0022	-0.0364	-0.0451
51	0.1697	0.0078	0.1821	0.1471
52	-0.2116	0.0041	-0.2031	-0.2211
53	-0.2887	0.0031	-0.2804	-0.2950
54	-0.2436	0.0031	-0.2330	-0.2516
55	-0.1853	0.0032	-0.1794	-0.1930
56	-0.1766	0.0041	-0.1673	-0.1845
57	-0.1524	0.0038	-0.1430	-0.1625
58	-0.1342	0.0050	-0.1250	-0.1484
59	-0.1029	0.0027	-0.0963	-0.1089
60	-0.0630	0.0029	-0.0535	-0.0680
61	-0.0408	0.0022	-0.0366	-0.0458
62	-0.0354	0.0023	-0.0285	-0.0410
63	-0.0210	0.0024	-0.0164	-0.0268
64	-0.0197	0.0026	-0.0134	-0.0260
65	0.5078	0.0070	0.5190	0.4942
66	0.1714	0.0100	0.1974	0.1492
67	0.1704	0.0073	0.1877	0.1545
68	0.4626	0.0110	0.4849	0.4374

Rotational speed = 25.46 rpm approx

Table 9. Repeatability of Cp measurements, pitch = -4 degrees
(using mean dynamic head)

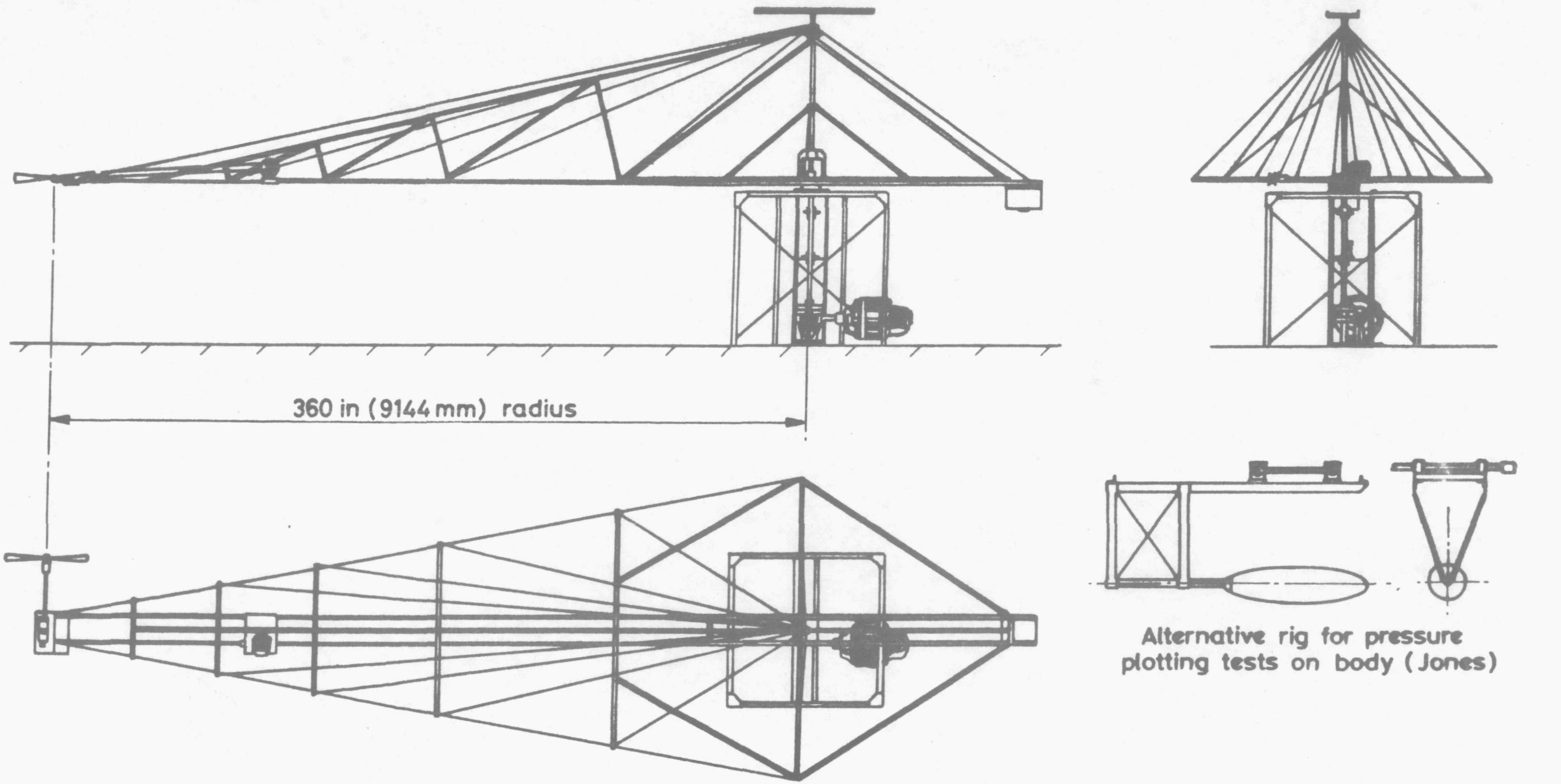

Figure 1. First NPL whirling arm.

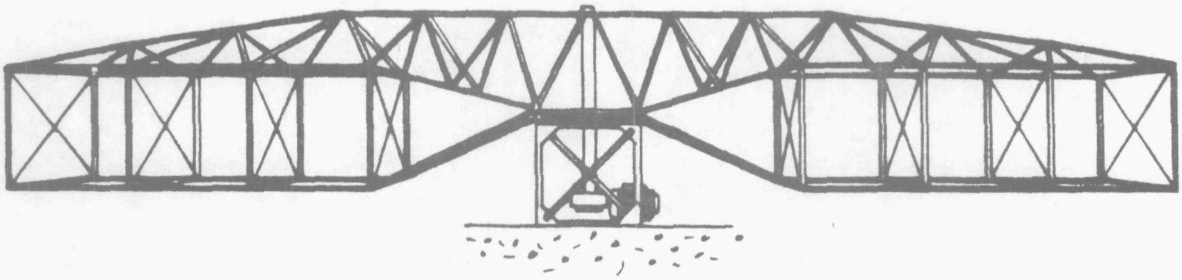

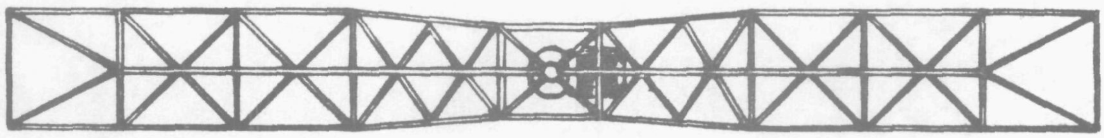

a) As designed.

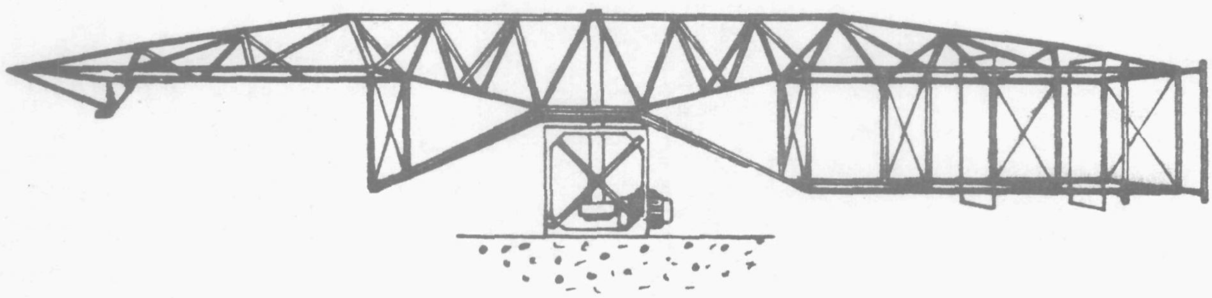

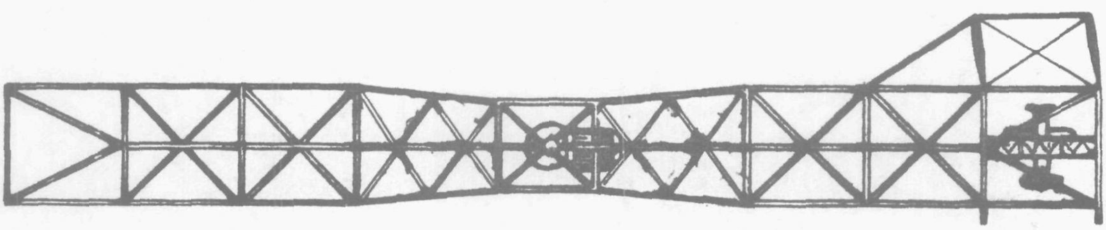

b) After modification.

Figure 2. Second NPL Whirling arm.

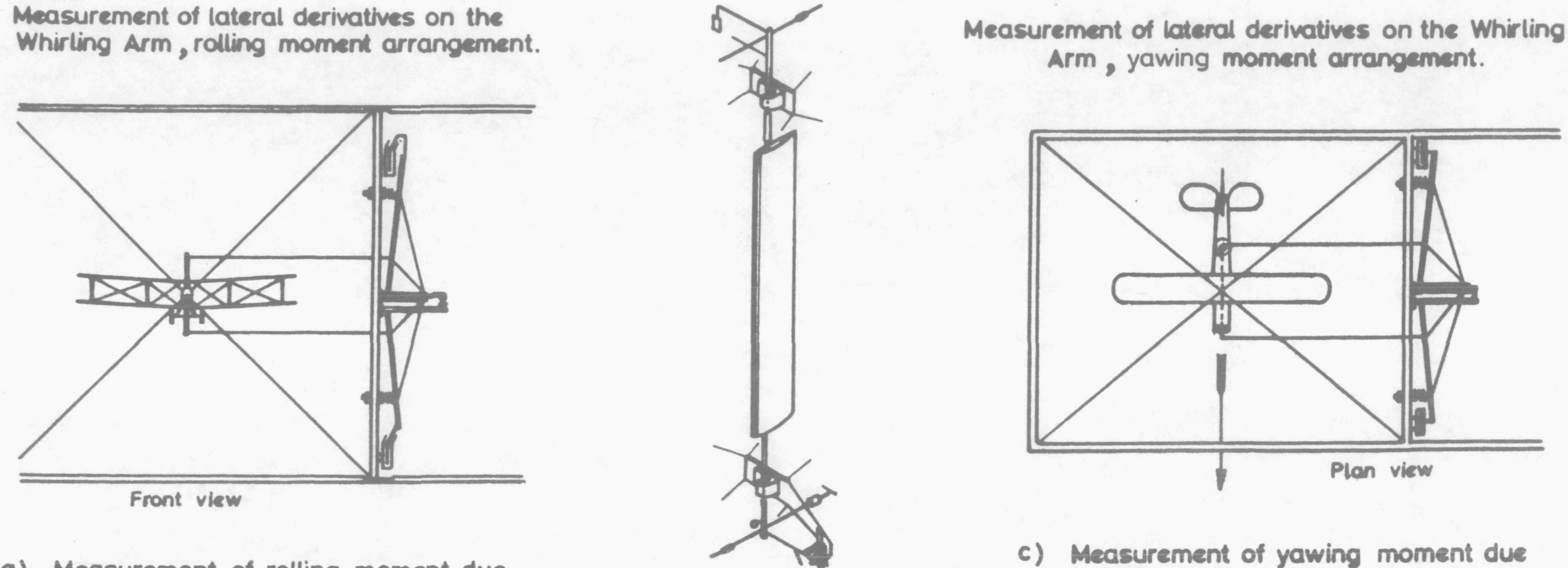

a) Measurement of rolling moment due to rotation in yaw (ℓ_r).

b) Measurement of pitching moment due to rotation in pitch (m_q).

c) Measurement of yawing moment due to a rotation in yaw (n_r).

Figure 3. Special purpose balances for the measurement of the rotary derivatives using the second NPL Whirling Arm.

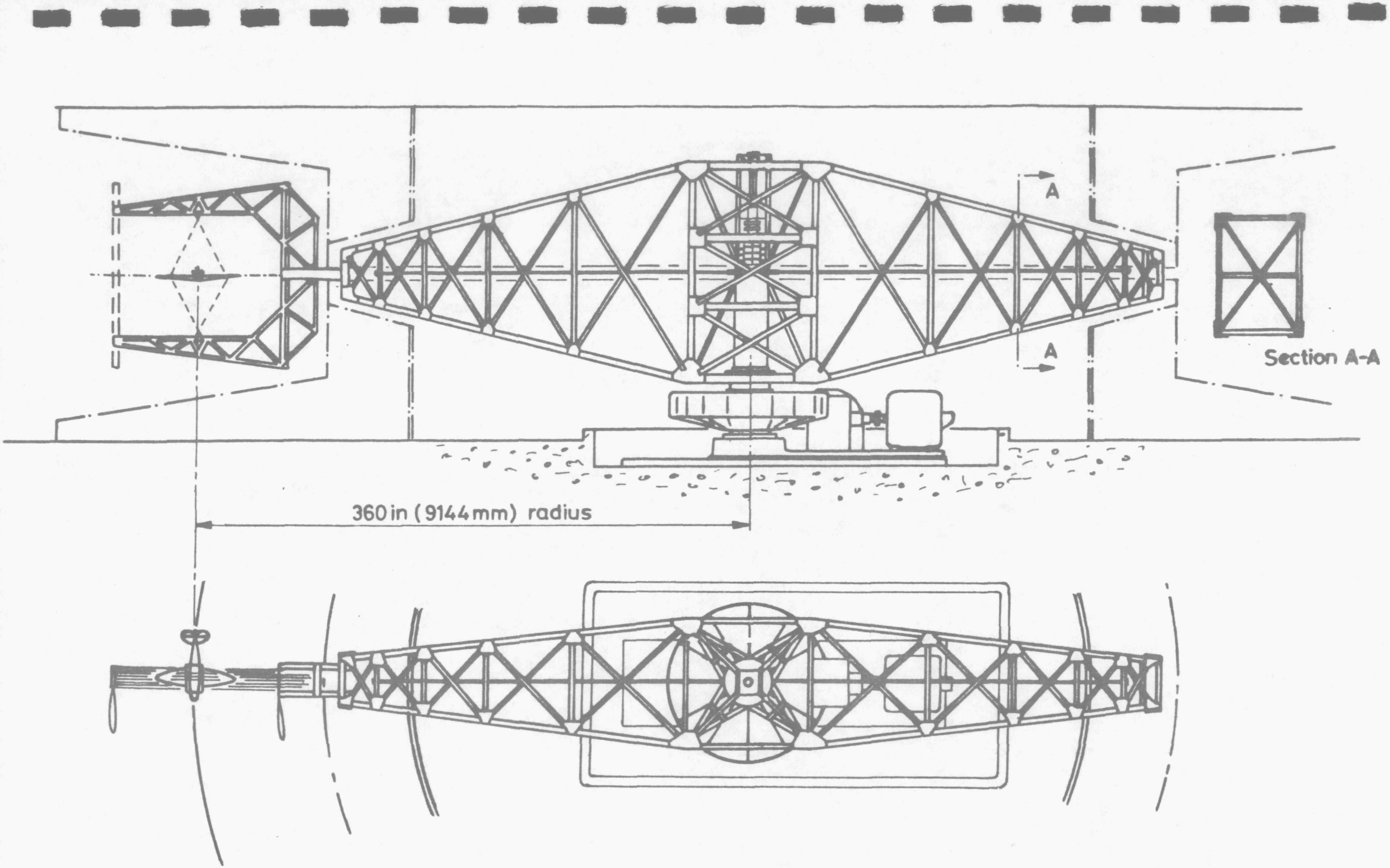

Figure 4. Third NPL whirling arm in it's original form.

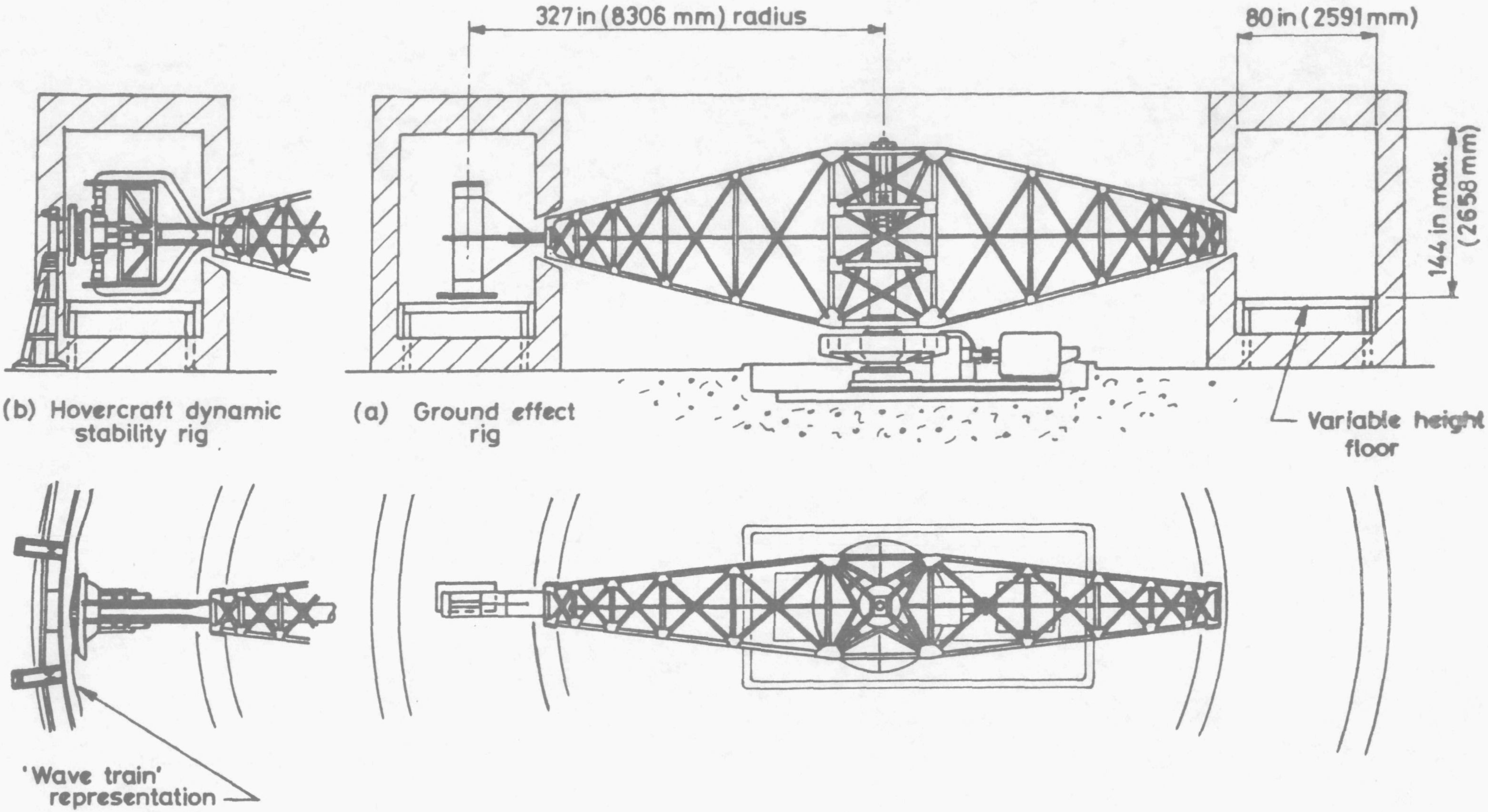

Figure 5. Third NPL whirling arm as re-erected at the College of Aeronautics.

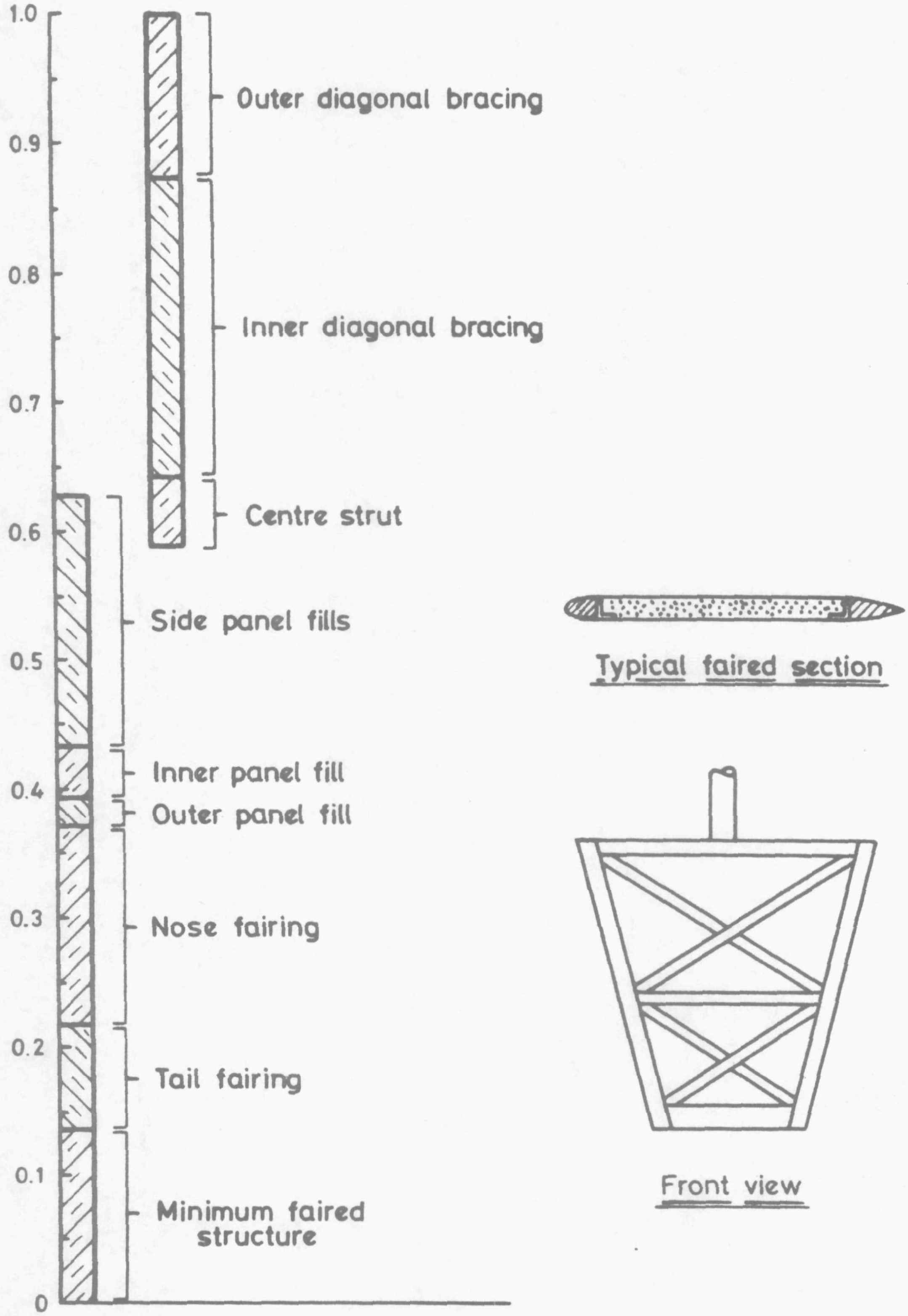

Figure 6. Experimental drag analysis of outer two panels of whirling arm structure.

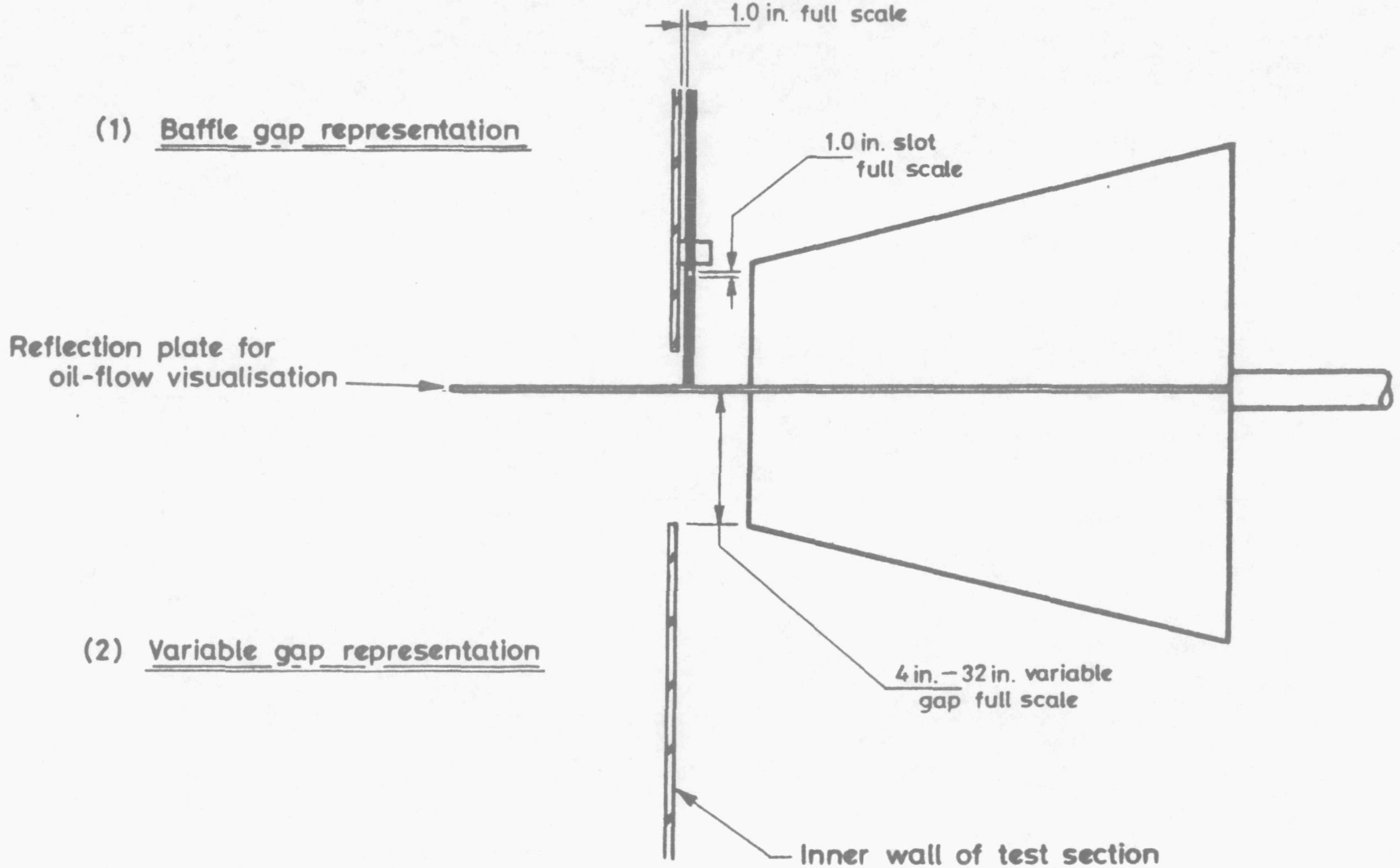

Figure 7. Flow visualisuation tests, experimental details.

ORIGINAL STRUCTURE — FAIRED MINIMISED STRUCTURE

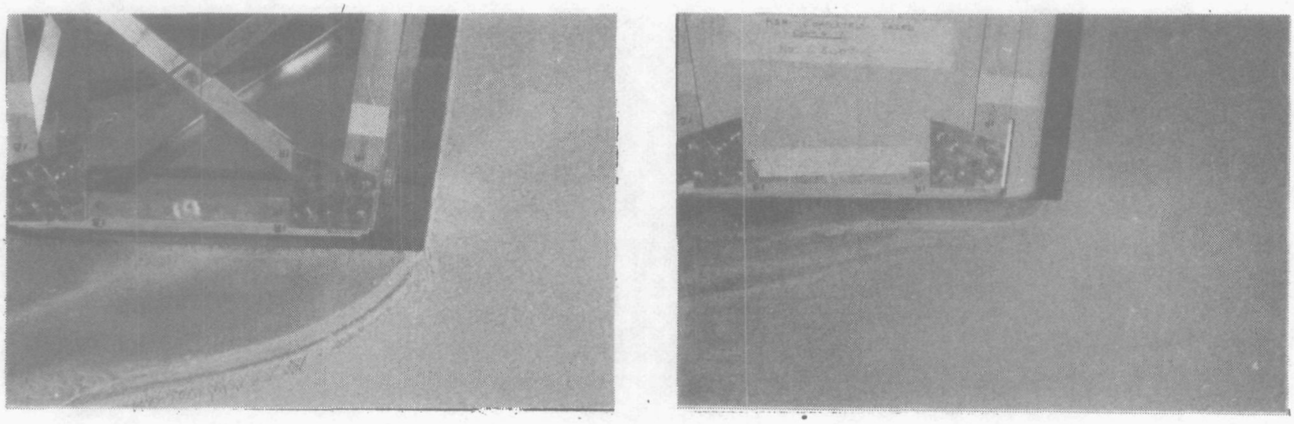

Unconstrained flow.

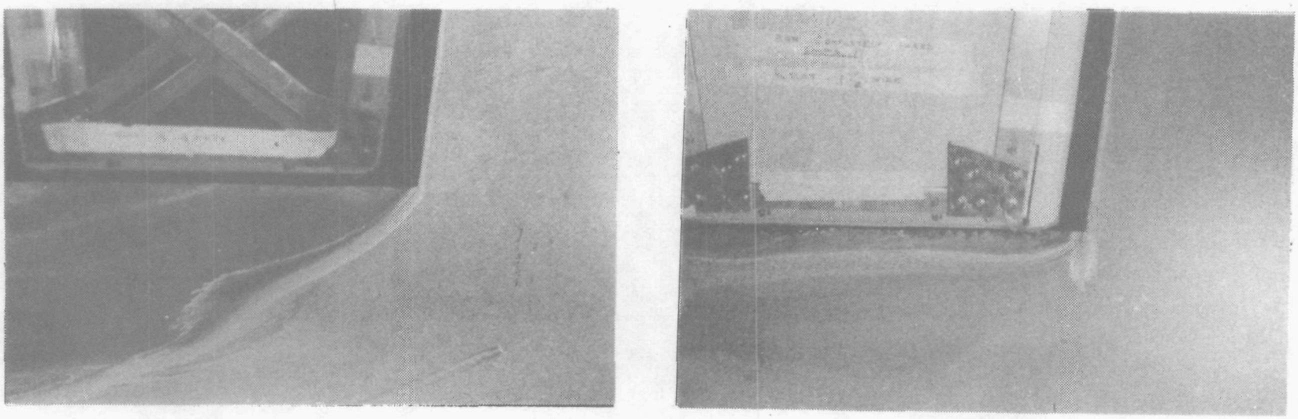

4 inch. wide (full scale) slot represented

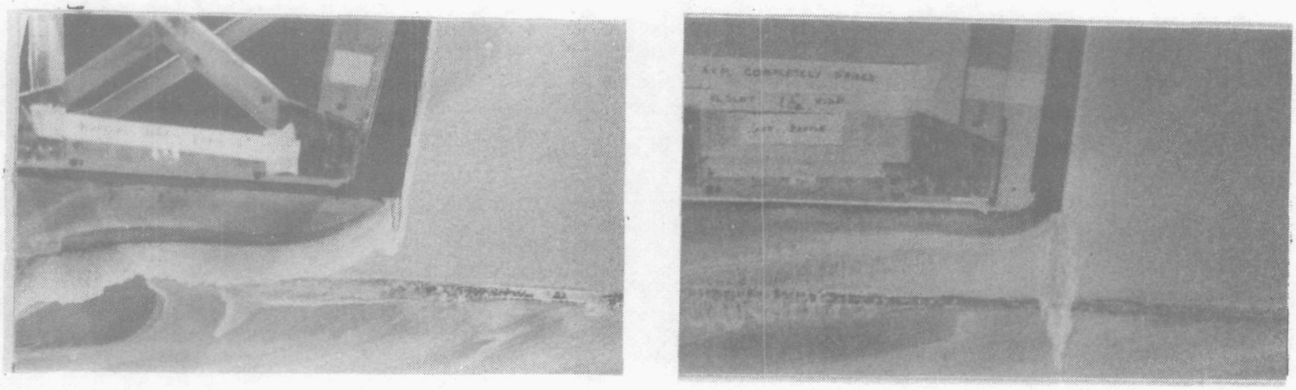

4 inch wide slot with baffle

Figure 8. Oil flow patterns of flow on centre-line of the structure.

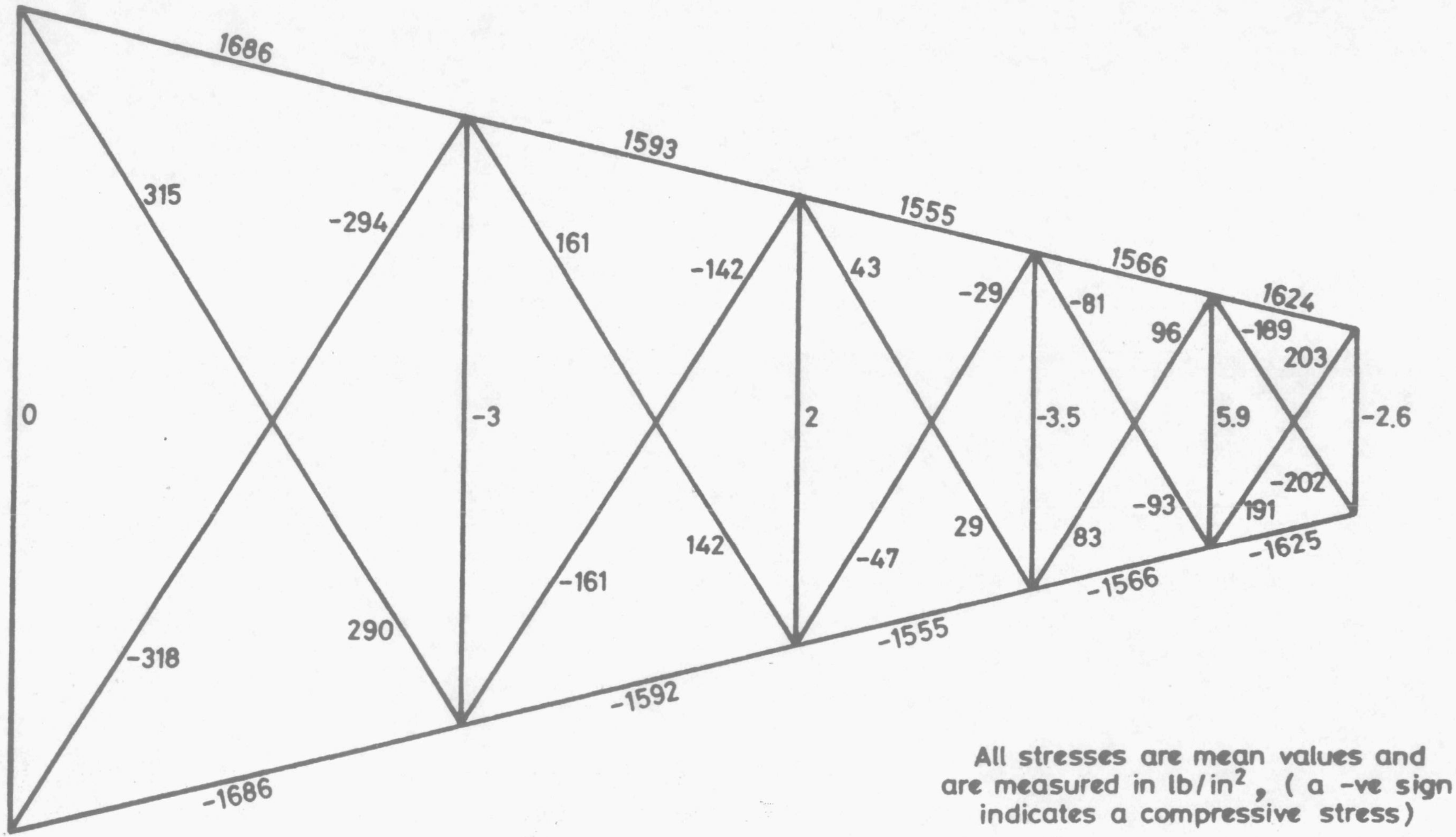

Figure 9. Static stress distribution in the original structure with external load of 3000 lb centrally applied at 29 ft radius.

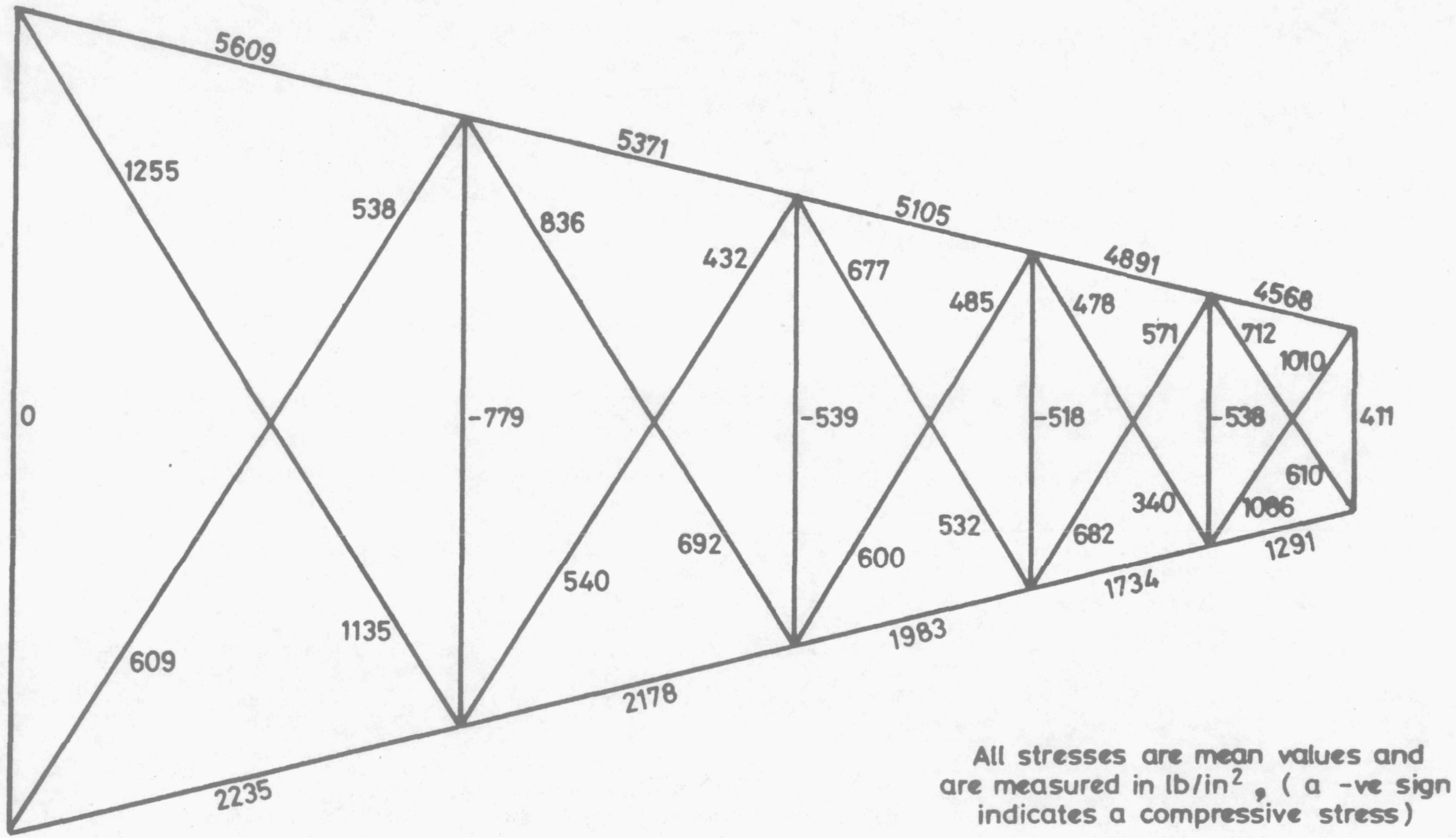

Figure 10. Stress distribution in the original structure when rotating at 31.8 rpm with an external load of 3000lb centrally applied at 29ft radius.

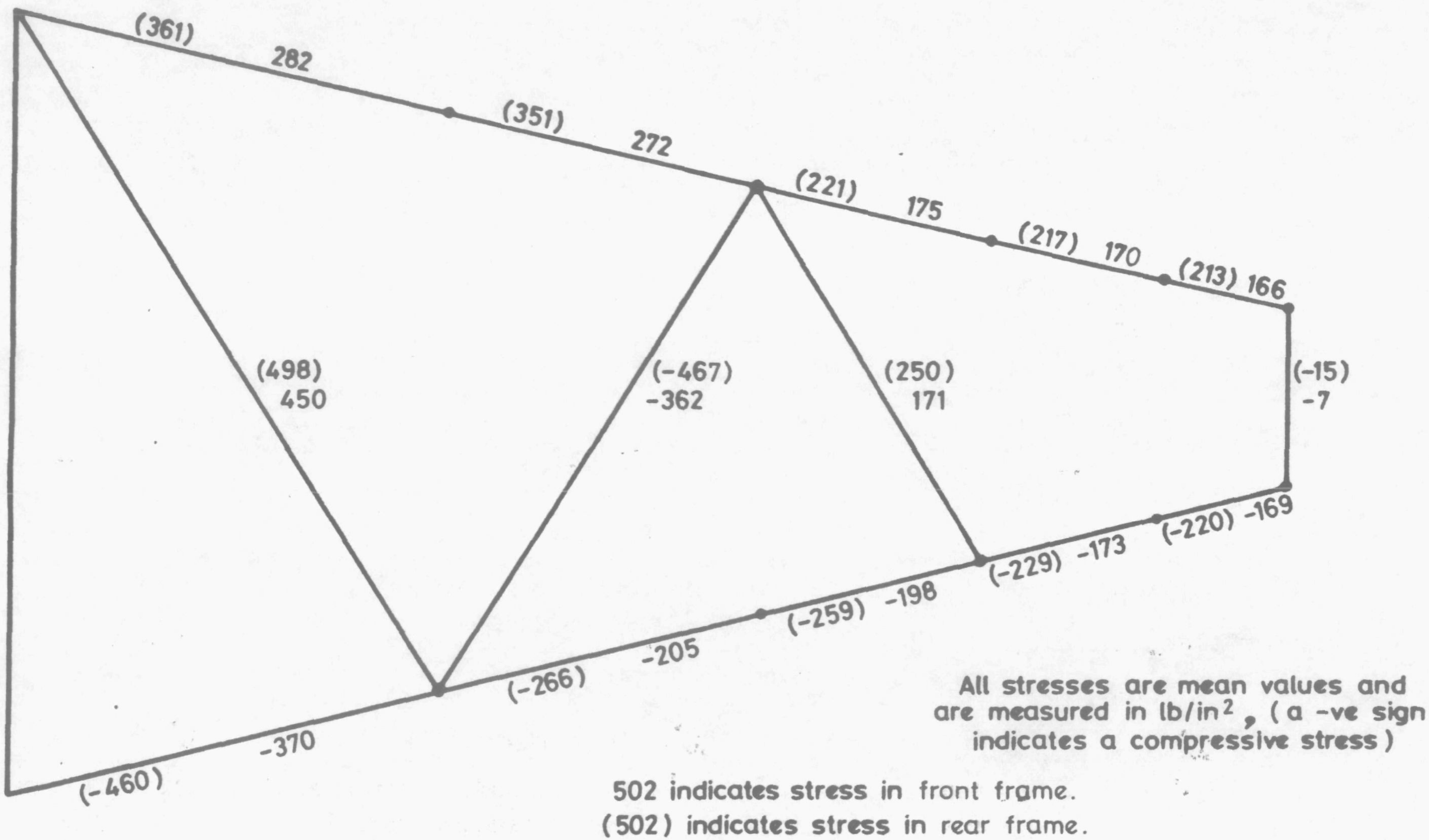

Figure 11. Static stress distribution in the revised structure with design external loading.

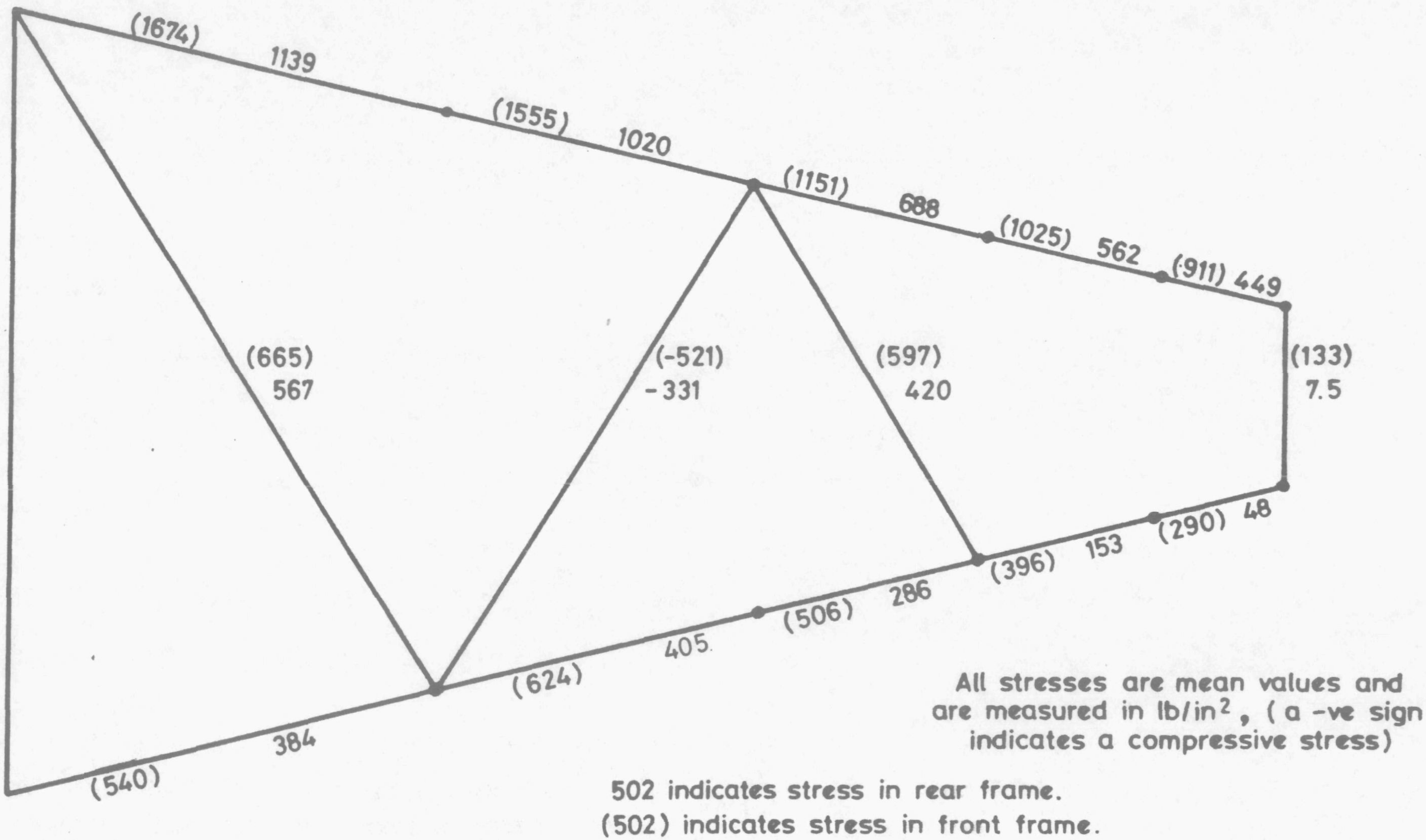

Figure 12. Stress distribution in the revised structure when rotating at 31.8 rpm with design external load.

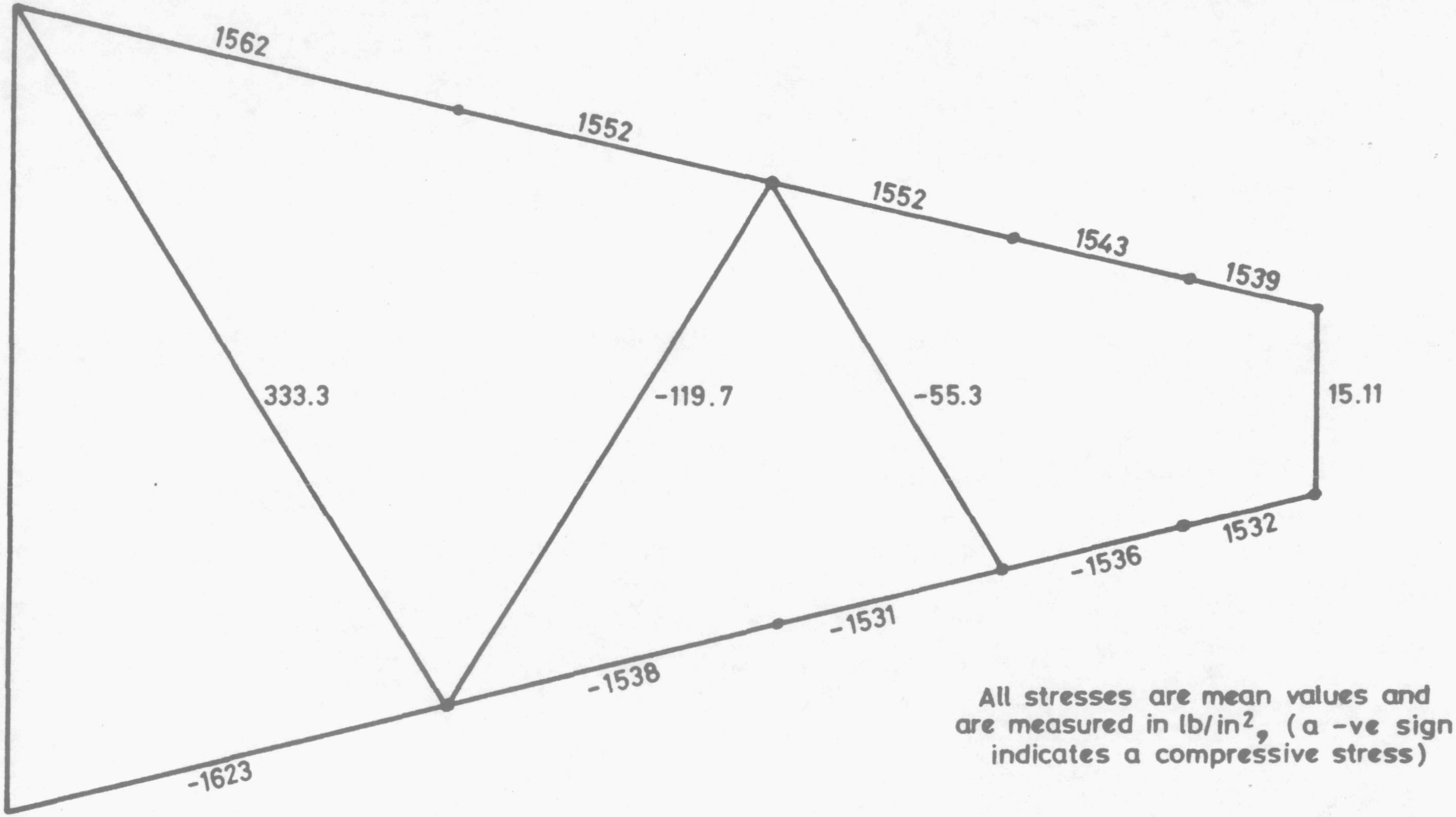

Figure 13. Static stress distribution in the revised structure with external load of 3000 lb centrally applied at 29 ft radius.

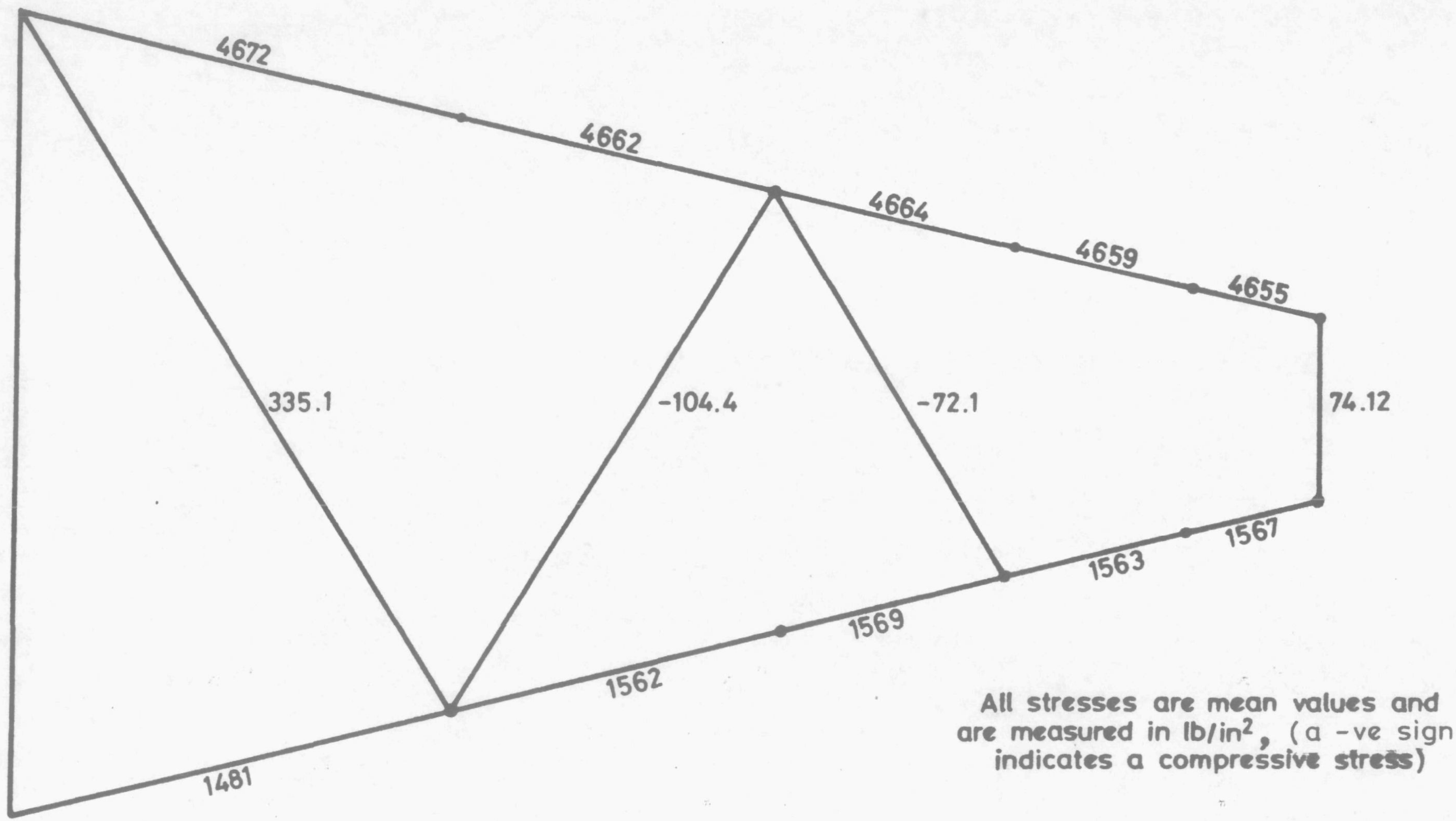

Figure 14. Stress distribution in the revised structure when rotating at 31.8 rpm with an external load of 3000 lb centrally applied at 29 ft radius.

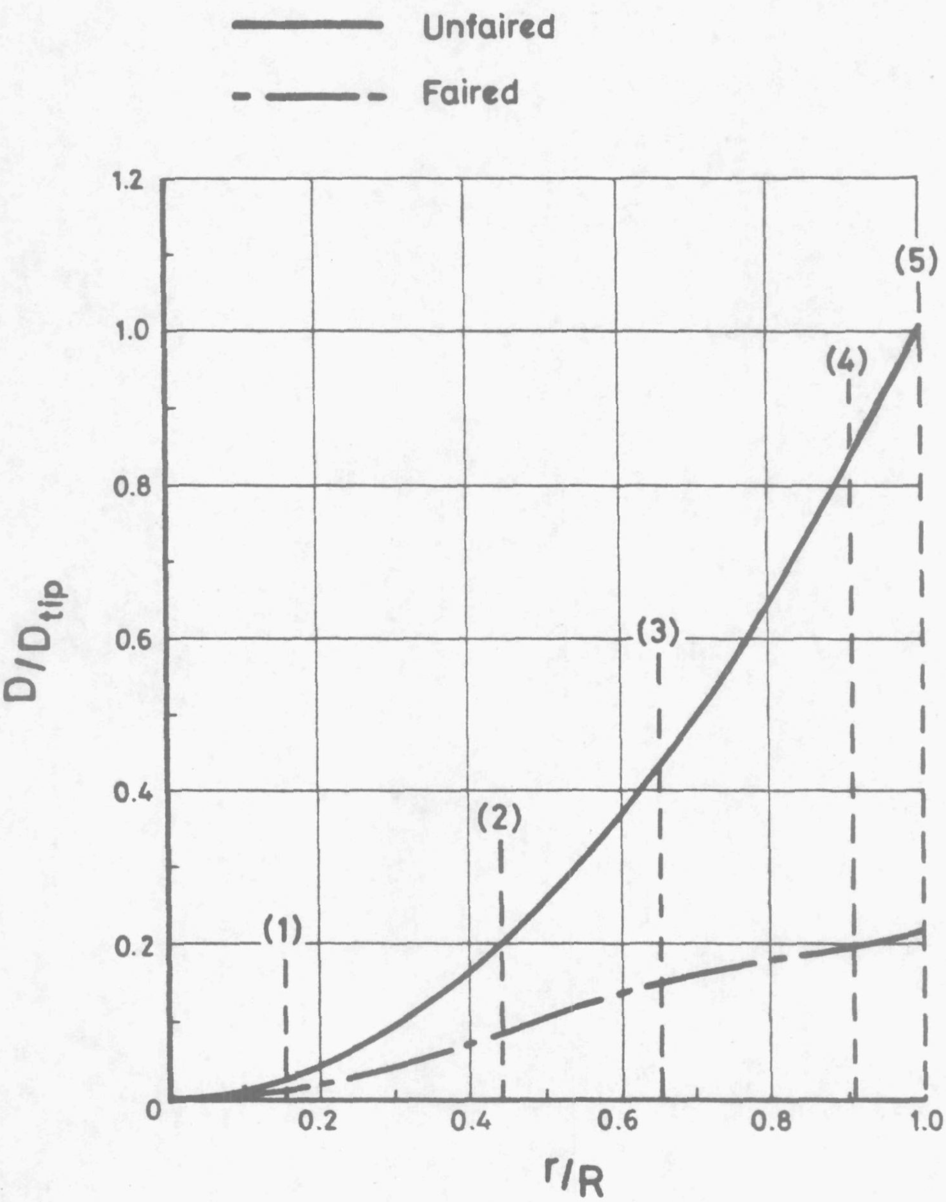

Figure 15. Effect of fairings on the variation of the relative sectional drag of the whirling arm with radius.

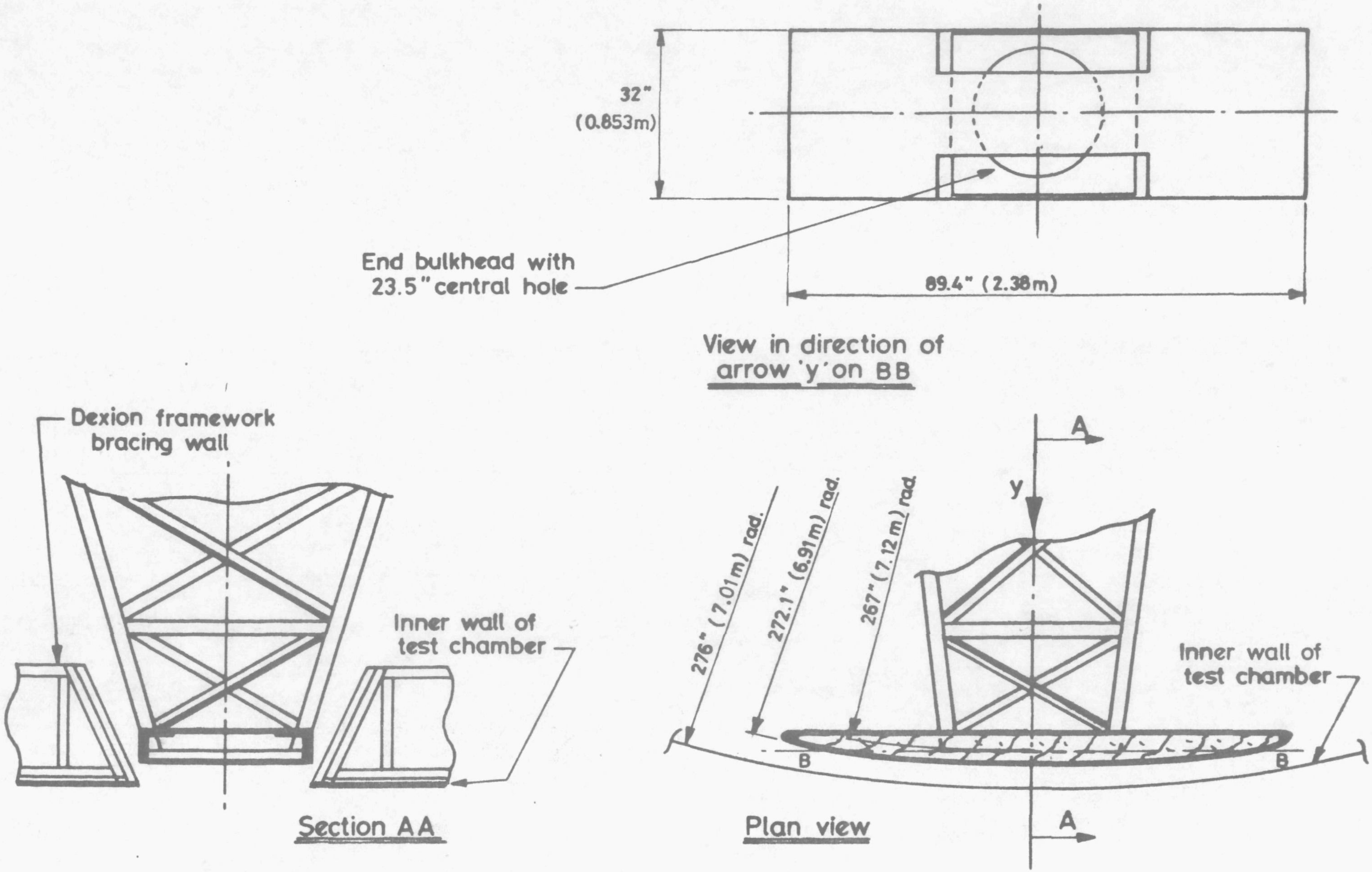

Figure 16. First tip fairing.

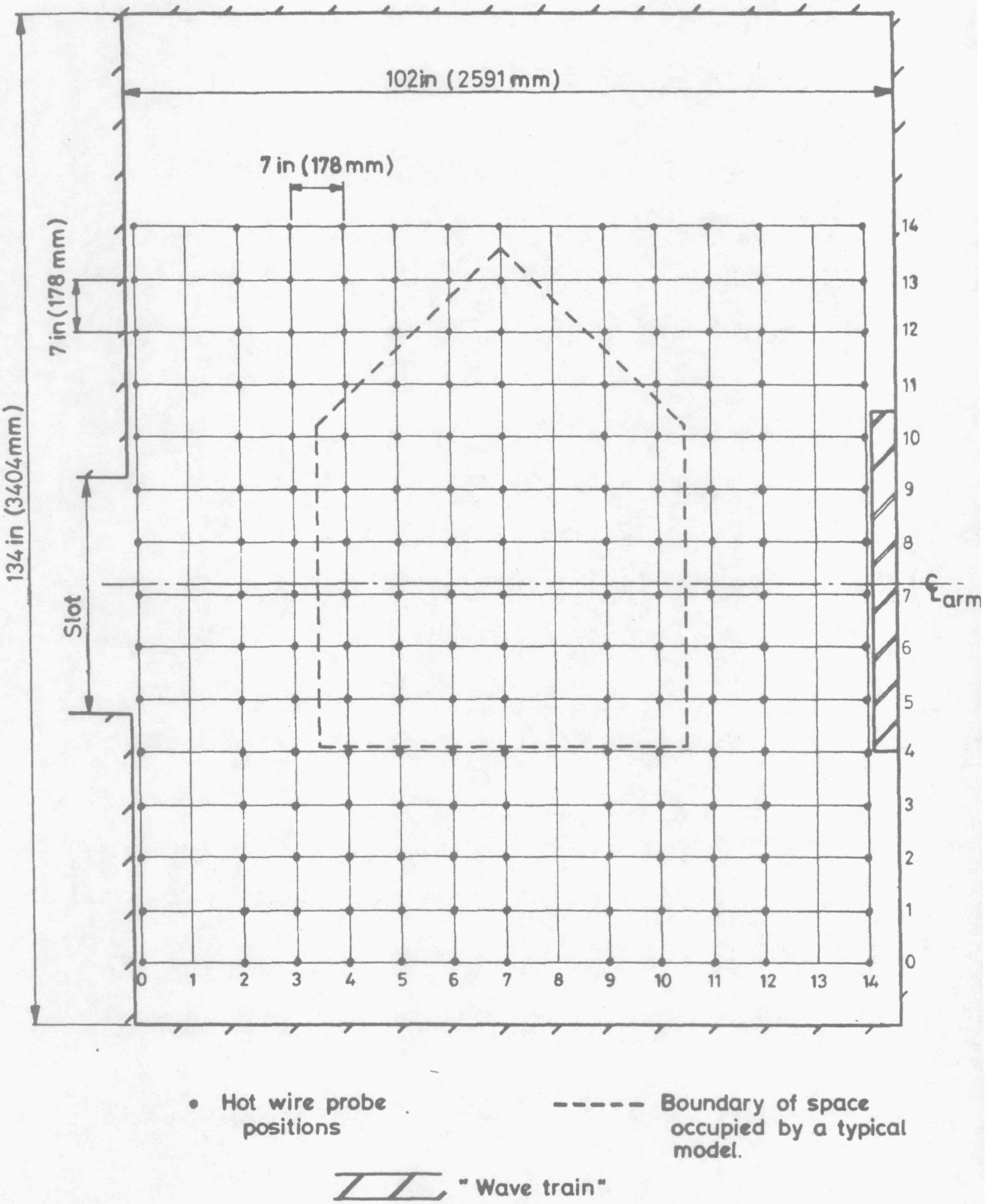

Figure 17. Swirl calibration rig.

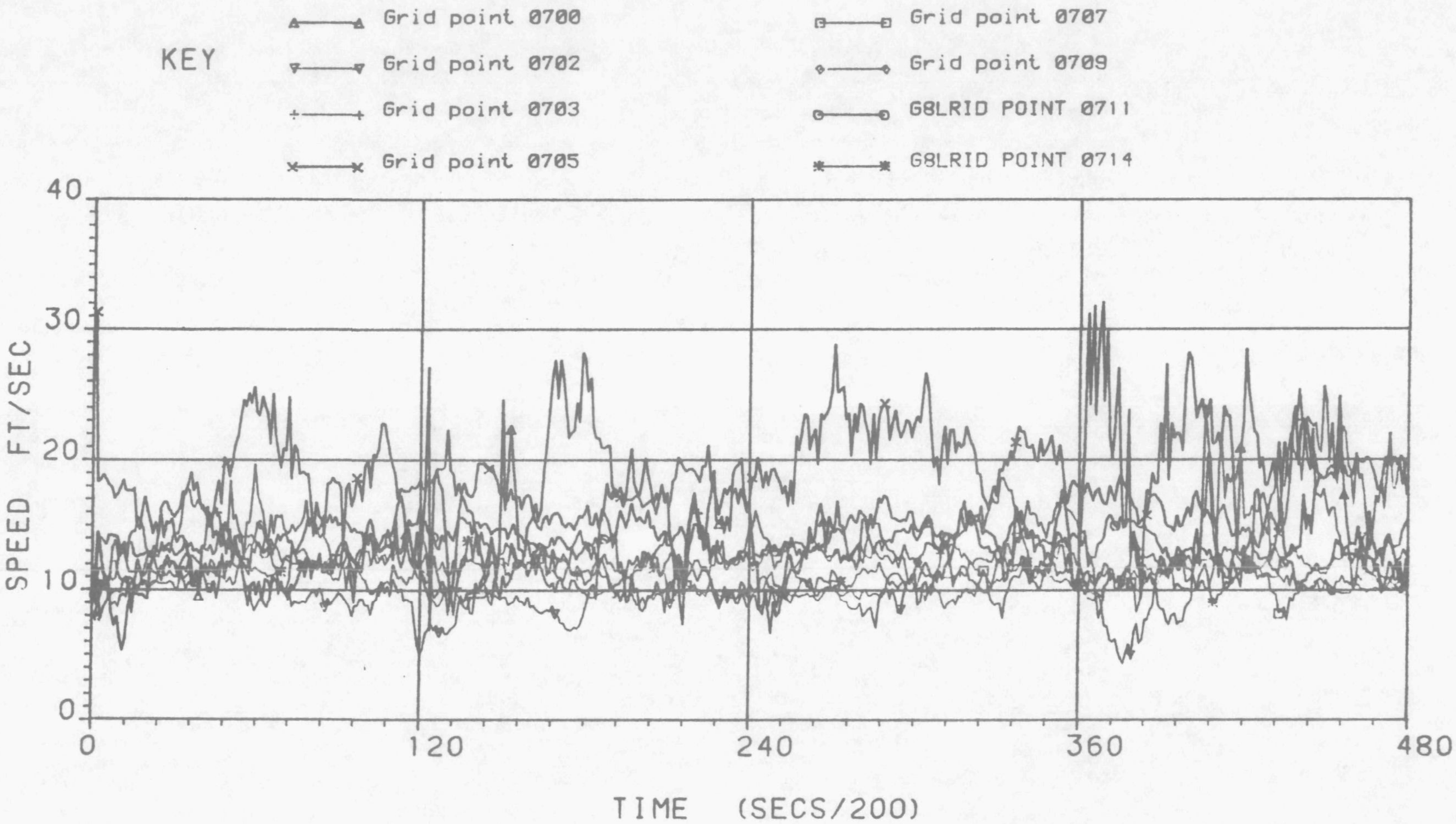

FIG **18**. VARIATION OF SWIRL SPEED WITH TIME AT STATIONS 0700, 0702, 0703, 0705, 0707, 0709, 0711, 0714 WHIRLING ARM IN ORIGINAL CONDITION

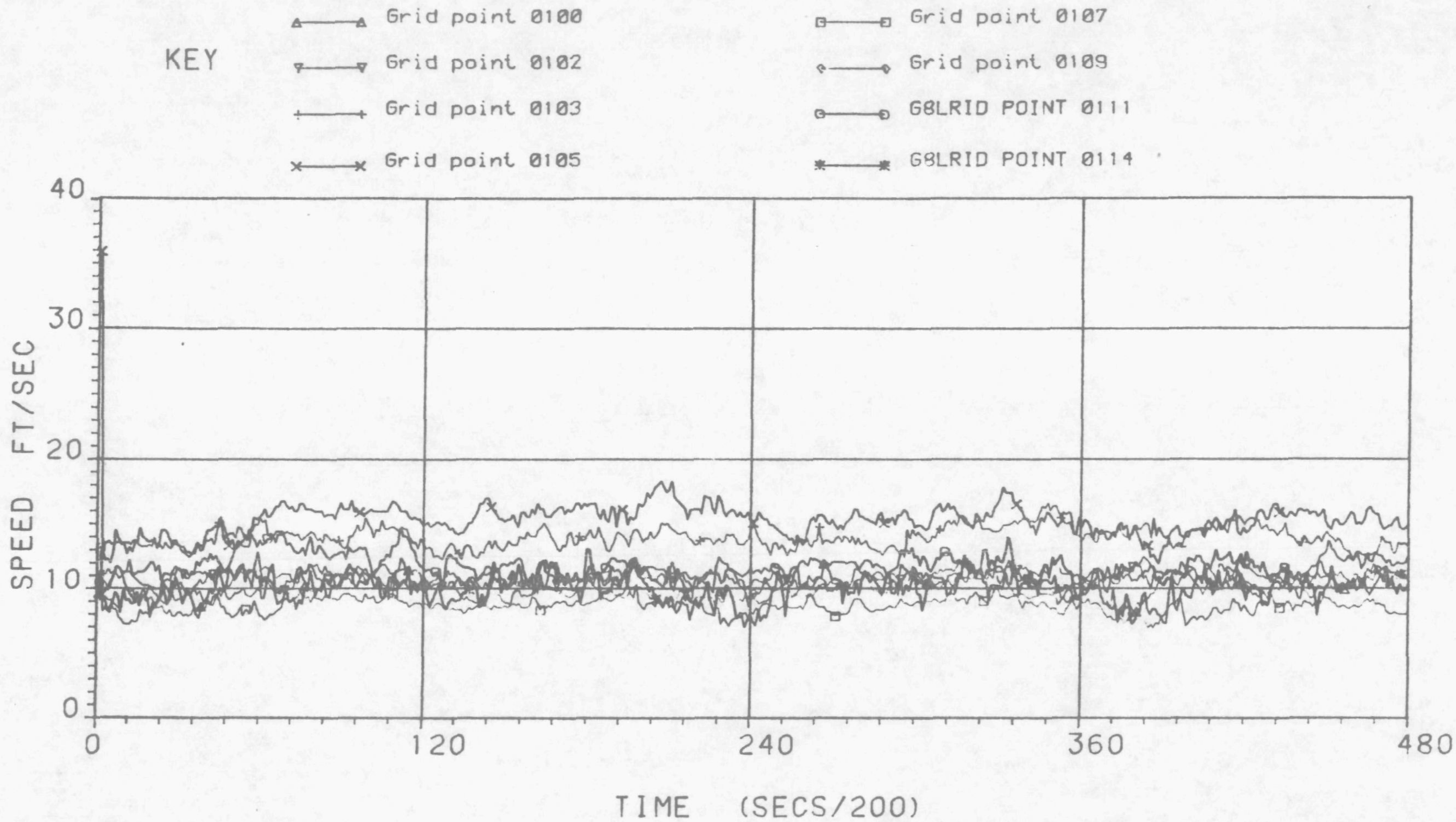

FIG 19. VARIATION OF SWIRL SPEED WITH TIME AT STATIONS 0100, 0102, 0103, 0105, 0107, 0109, 0111, 0114 WHIRLING ARM IN ORIGINAL CONDITION

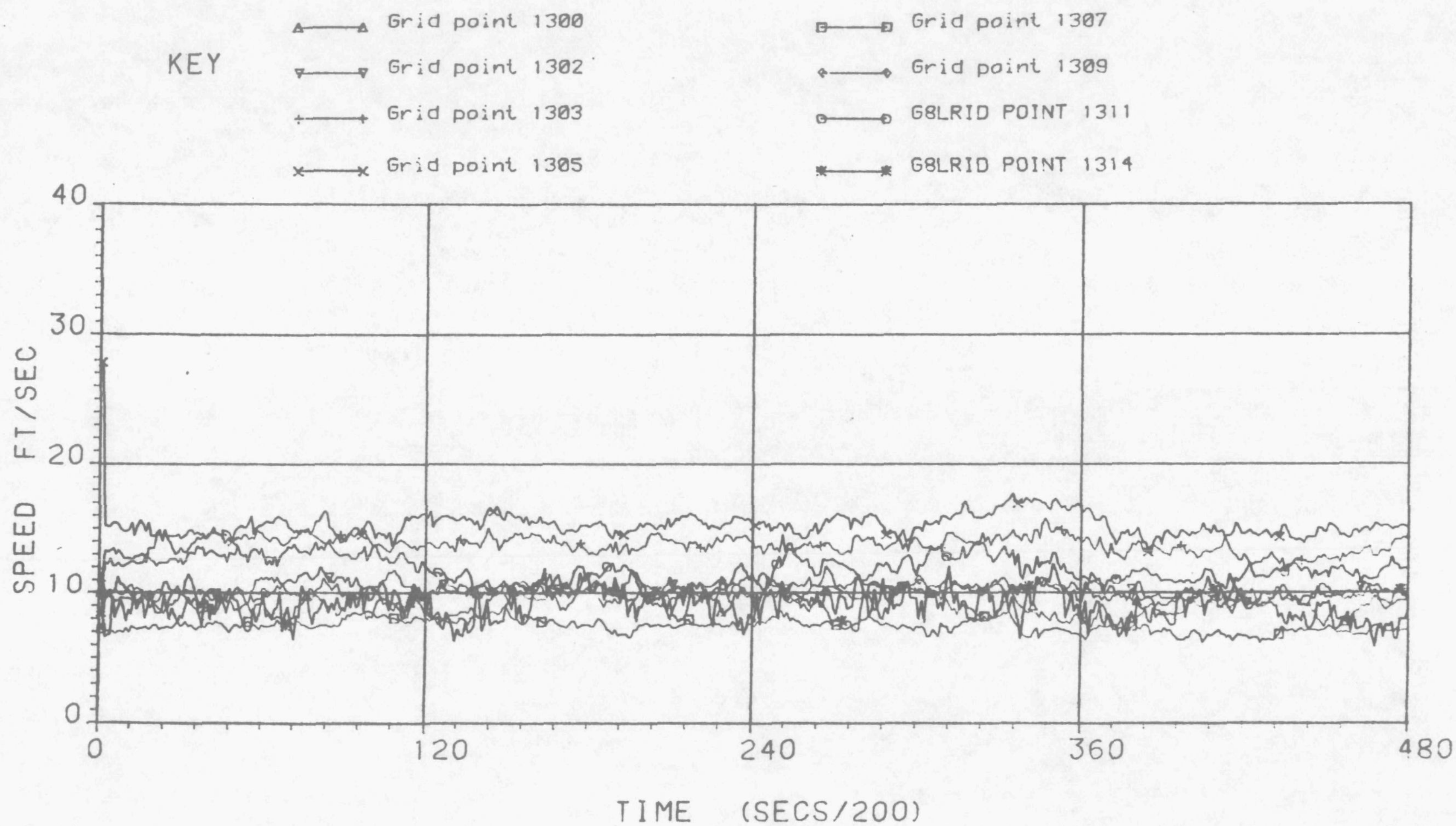

FIG 20. VARIATION OF SWIRL SPEED WITH TIME AT STATIONS
1300, 1302, 1303, 1305, 1307, 1309, 1311, 1314
WHIRLING ARM IN ORIGINAL CONDITION

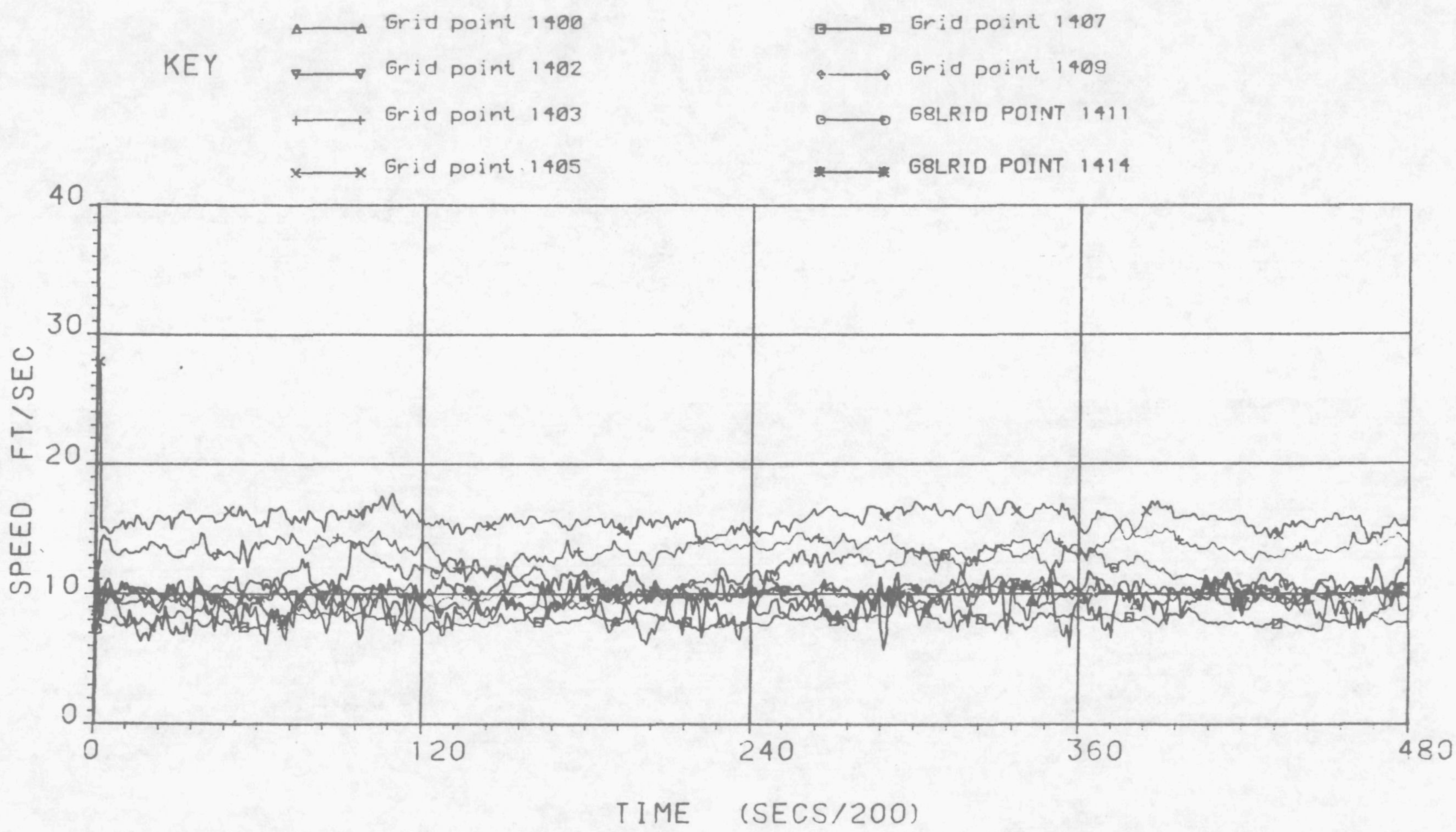

FIG 21. VARIATION OF SWIRL SPEED WITH TIME AT STATIONS 1400, 1402, 1403, 1405, 1407, 1409, 1411, 1414 WHIRLING ARM IN ORIGINAL CONDITION

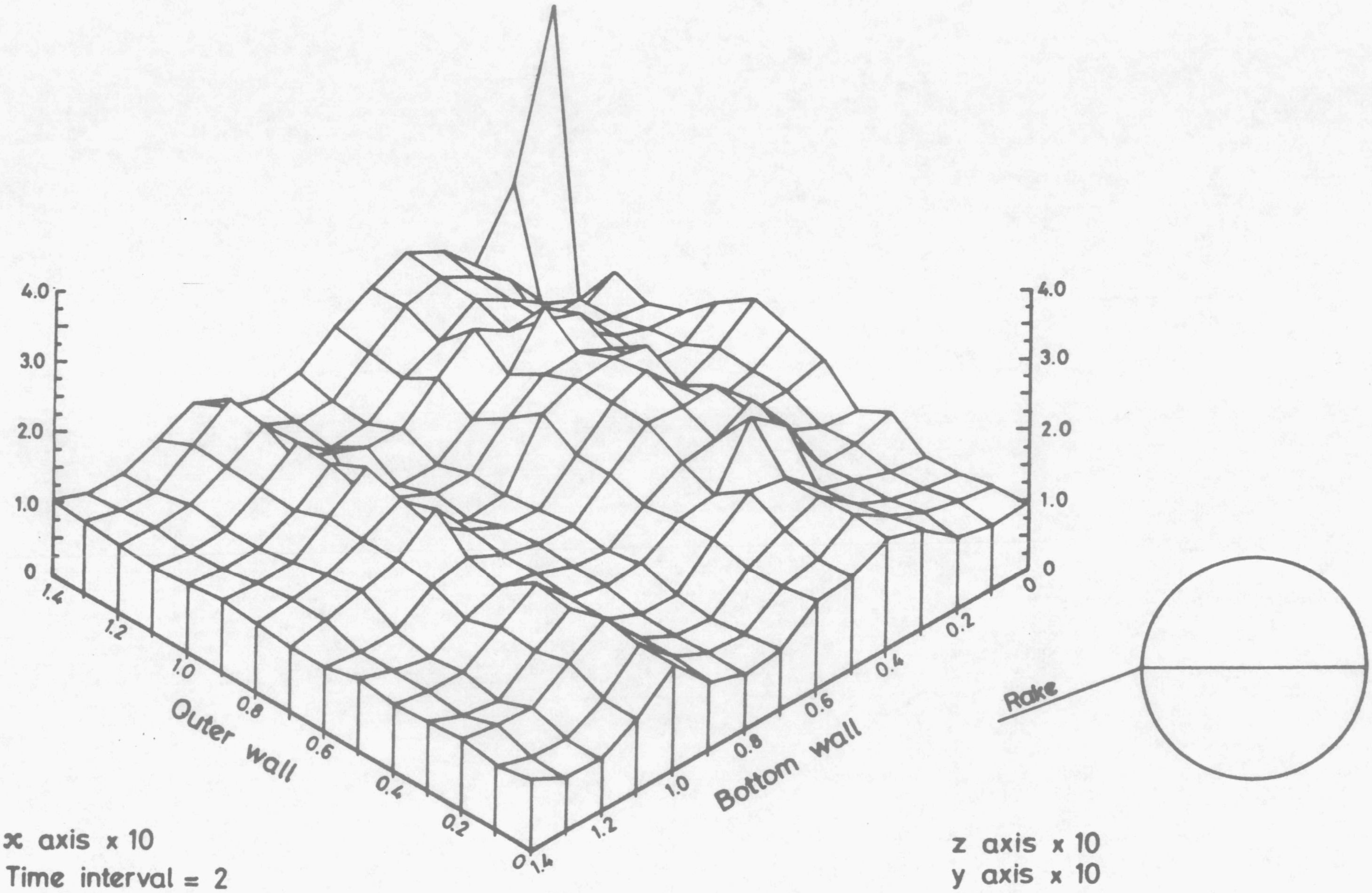

Figure 22. Original whirling arm. Variation of swirl in calibration plane.

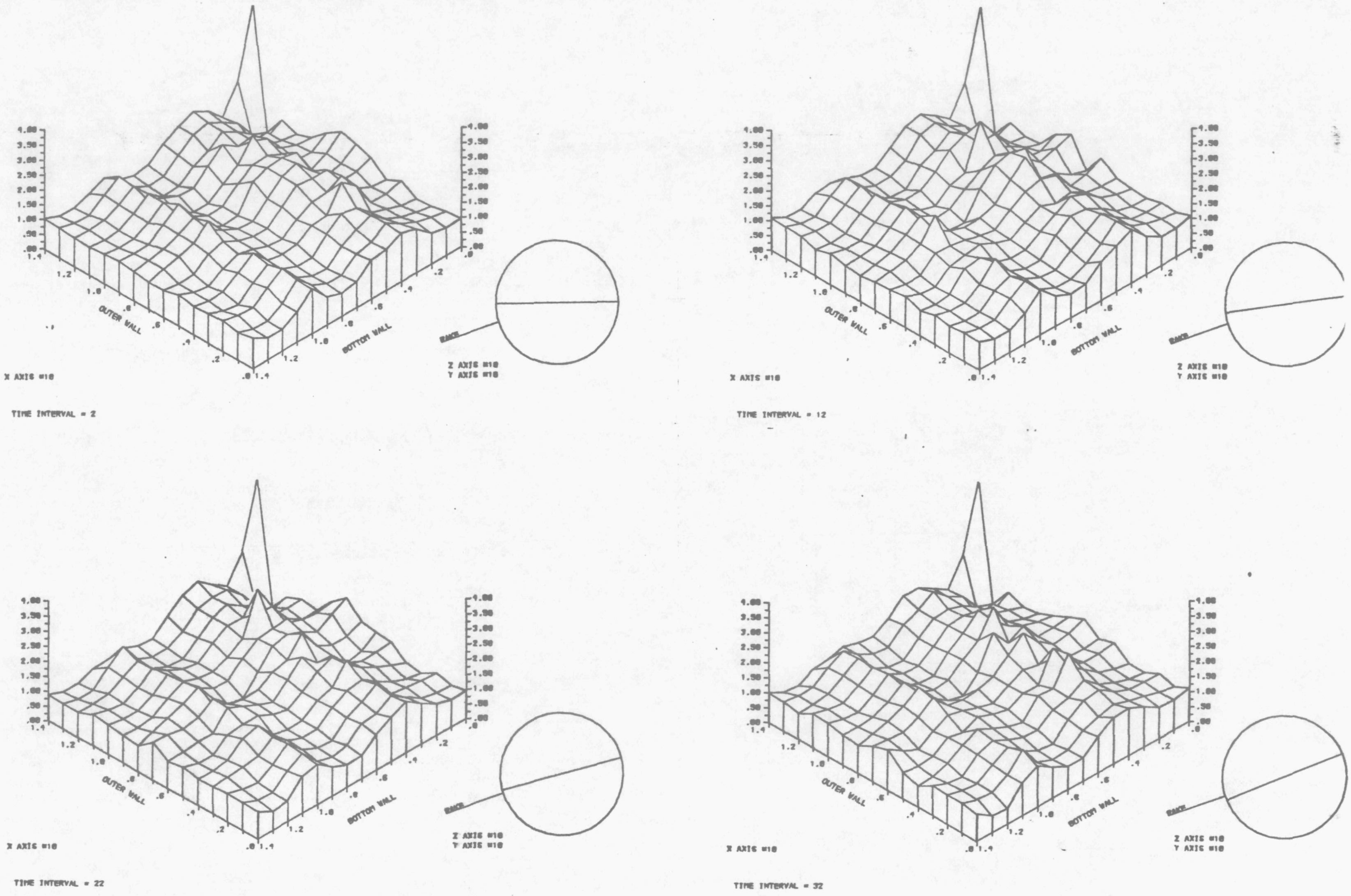

Figure 23. Variation of swirl speed over the calibration plane (1).

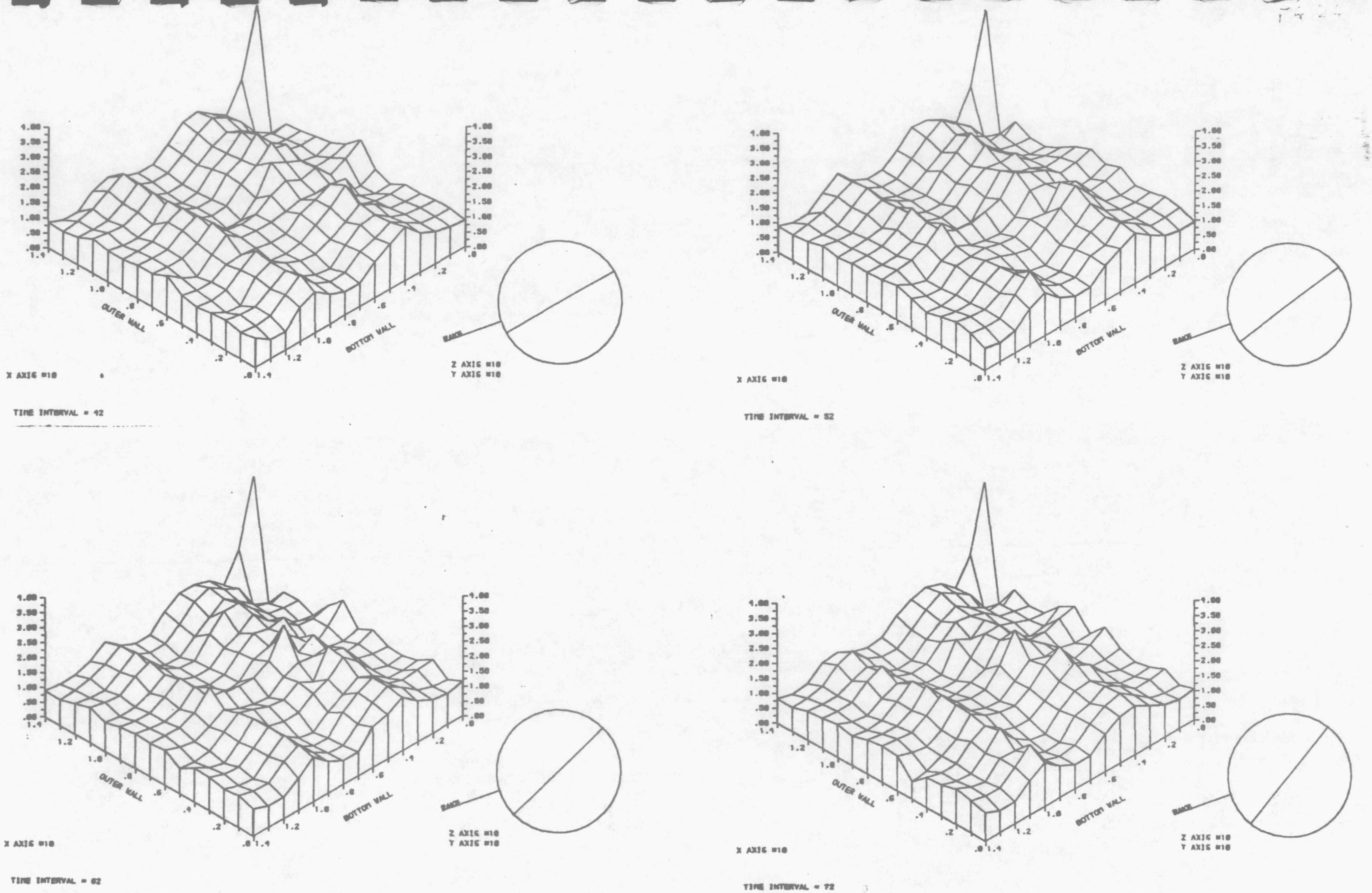

Figure 24. Variation of swirl speed over the calibration plane (2).

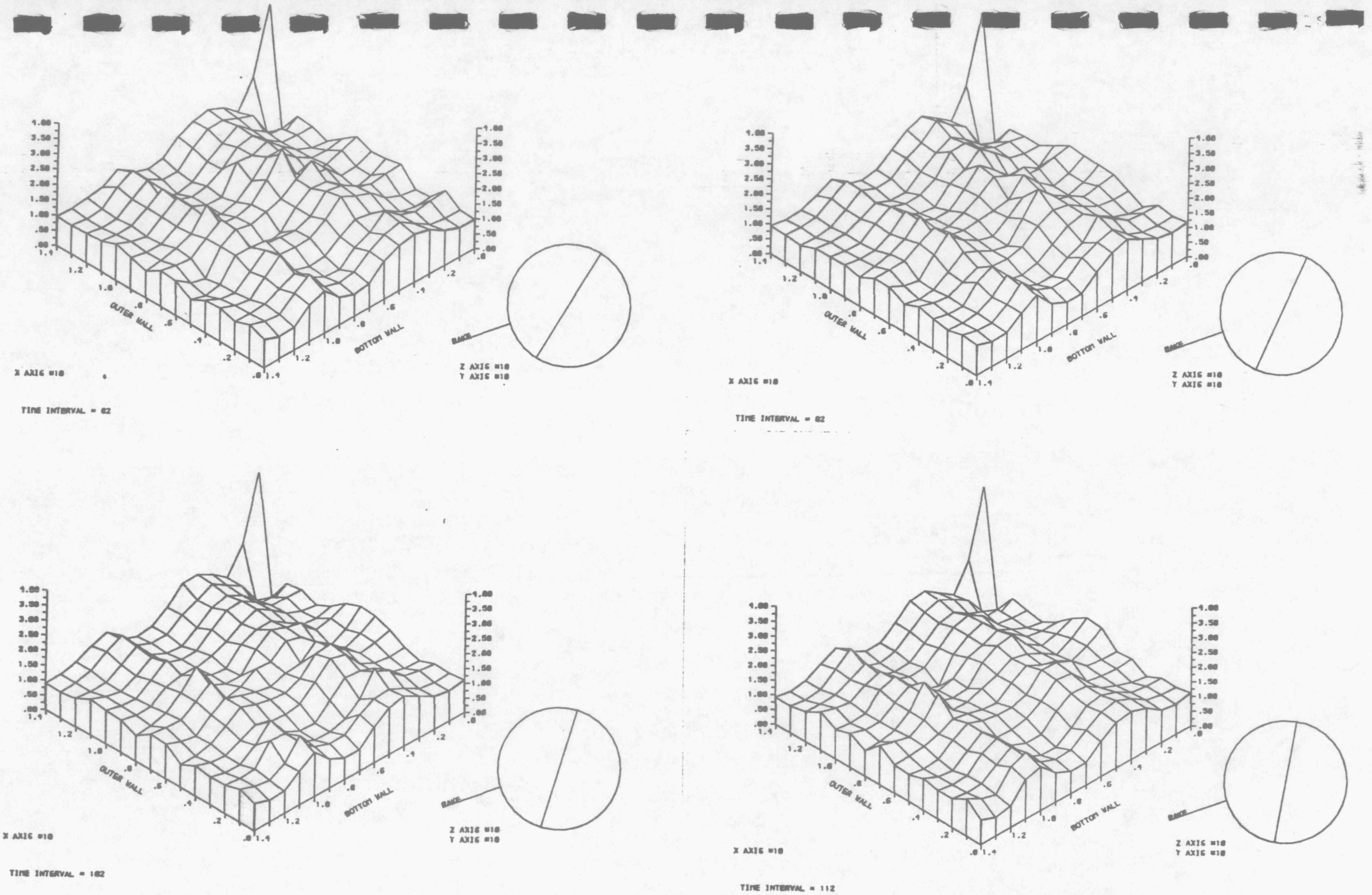

Figure 25. Variation of swirl speed over the calibration plane (3).

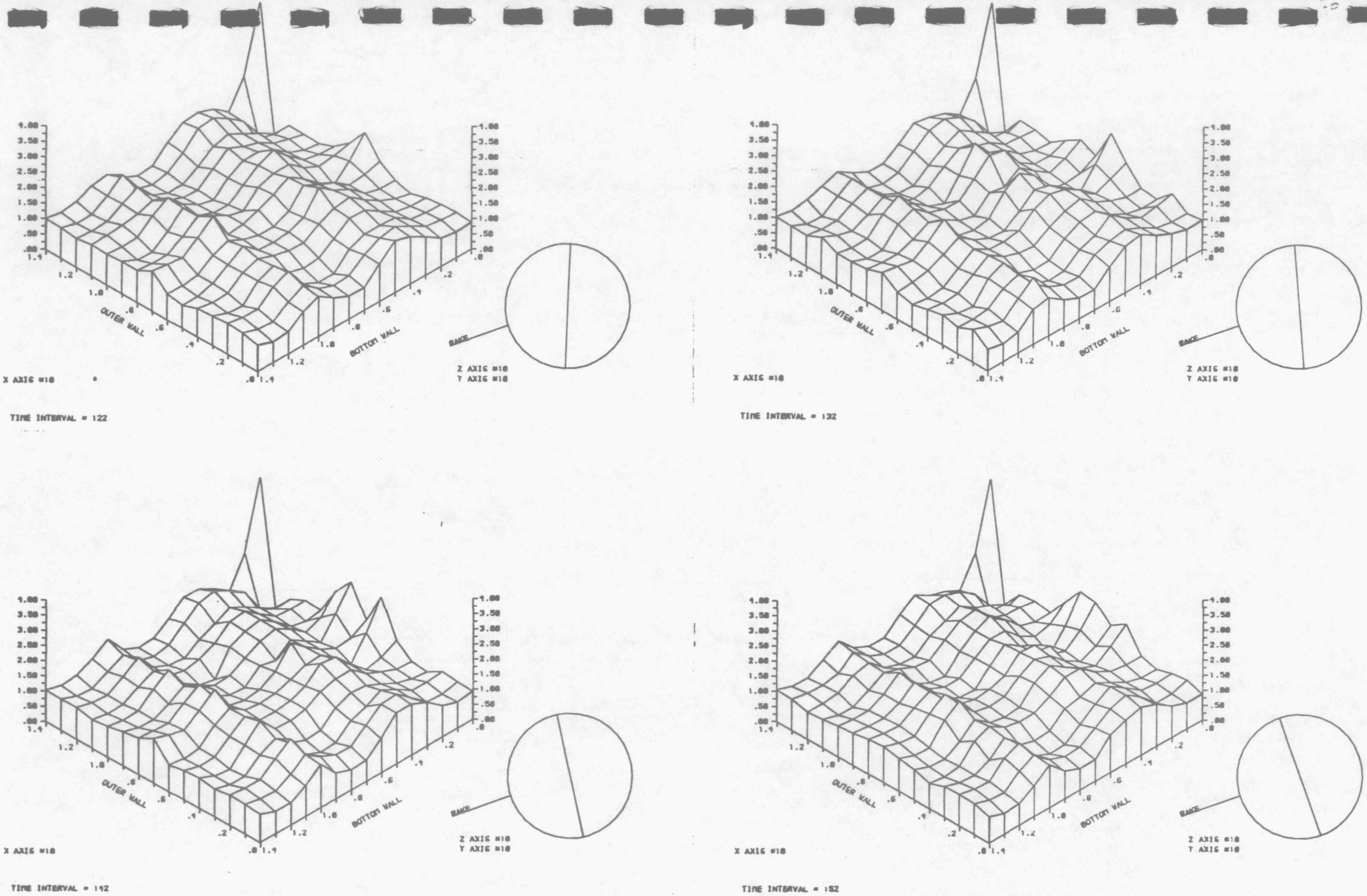

Figure 26. Variation of swirl speed over the calibration plane (4).

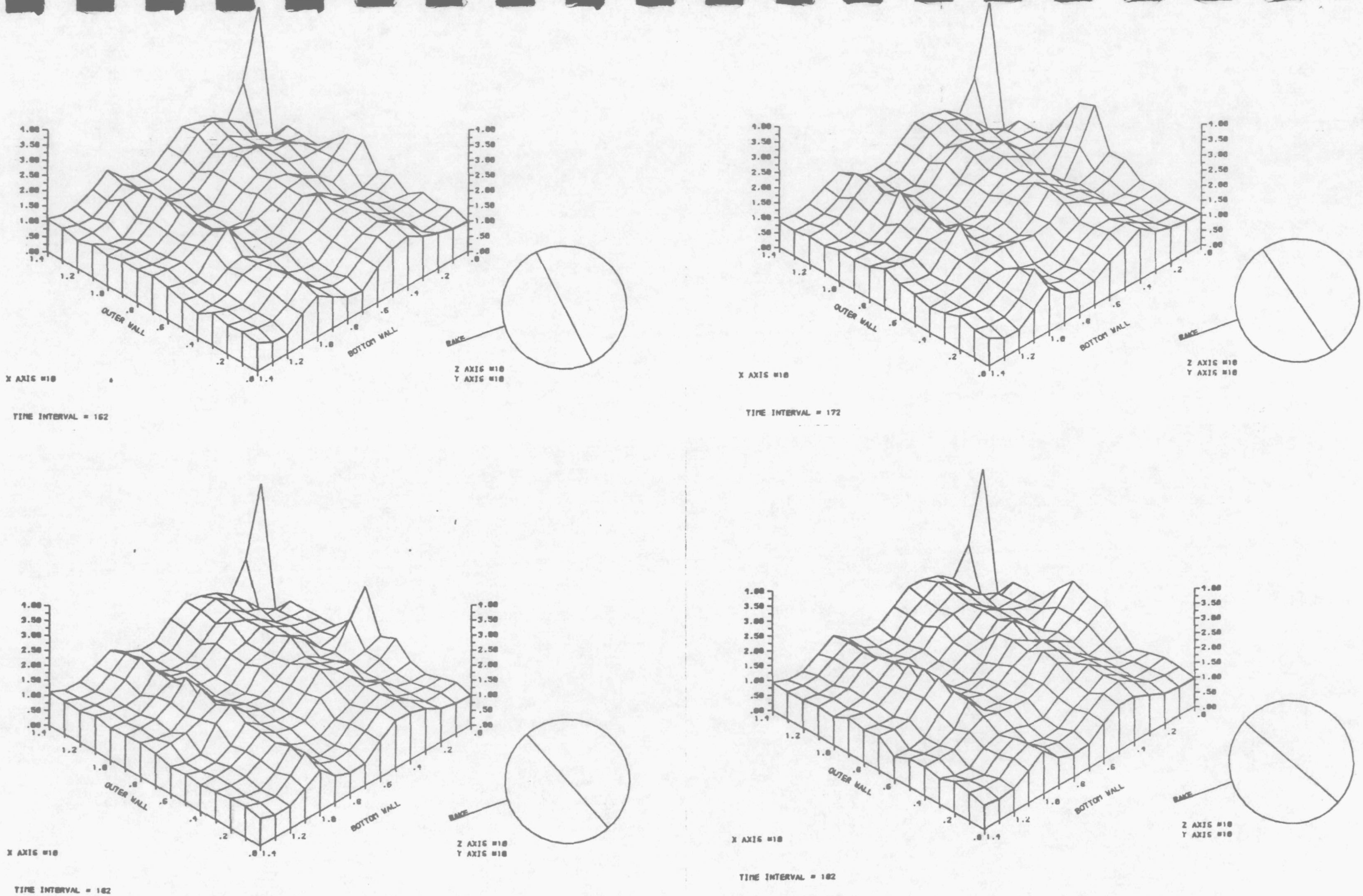

Figure 27. Variation of swirl speed over the calibration plane (5).

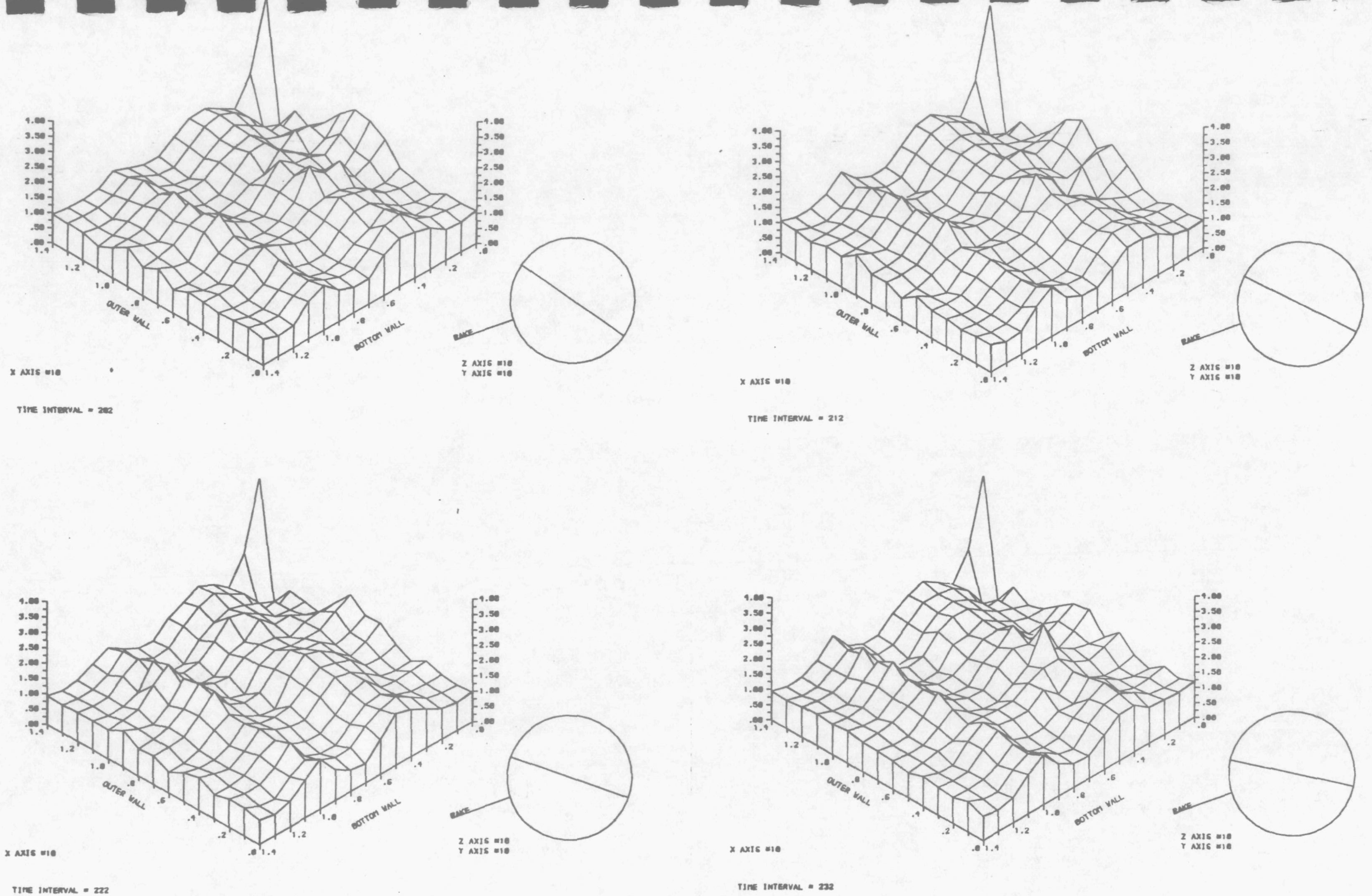

Figure 28. Variation of swirl speed over the calibration plane (6).

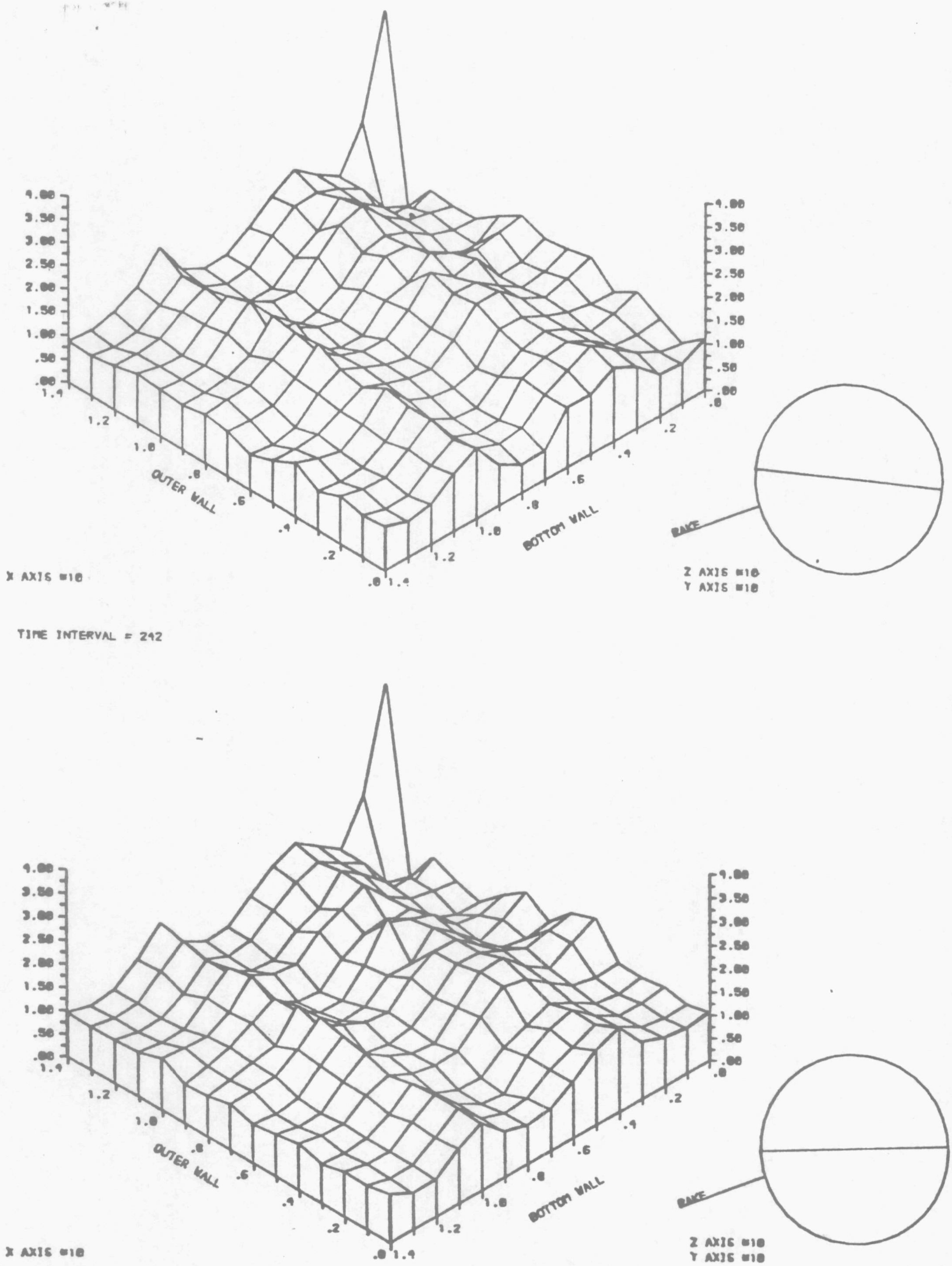

Figure 29. Variation of swirl speed over the calibration plane (7).

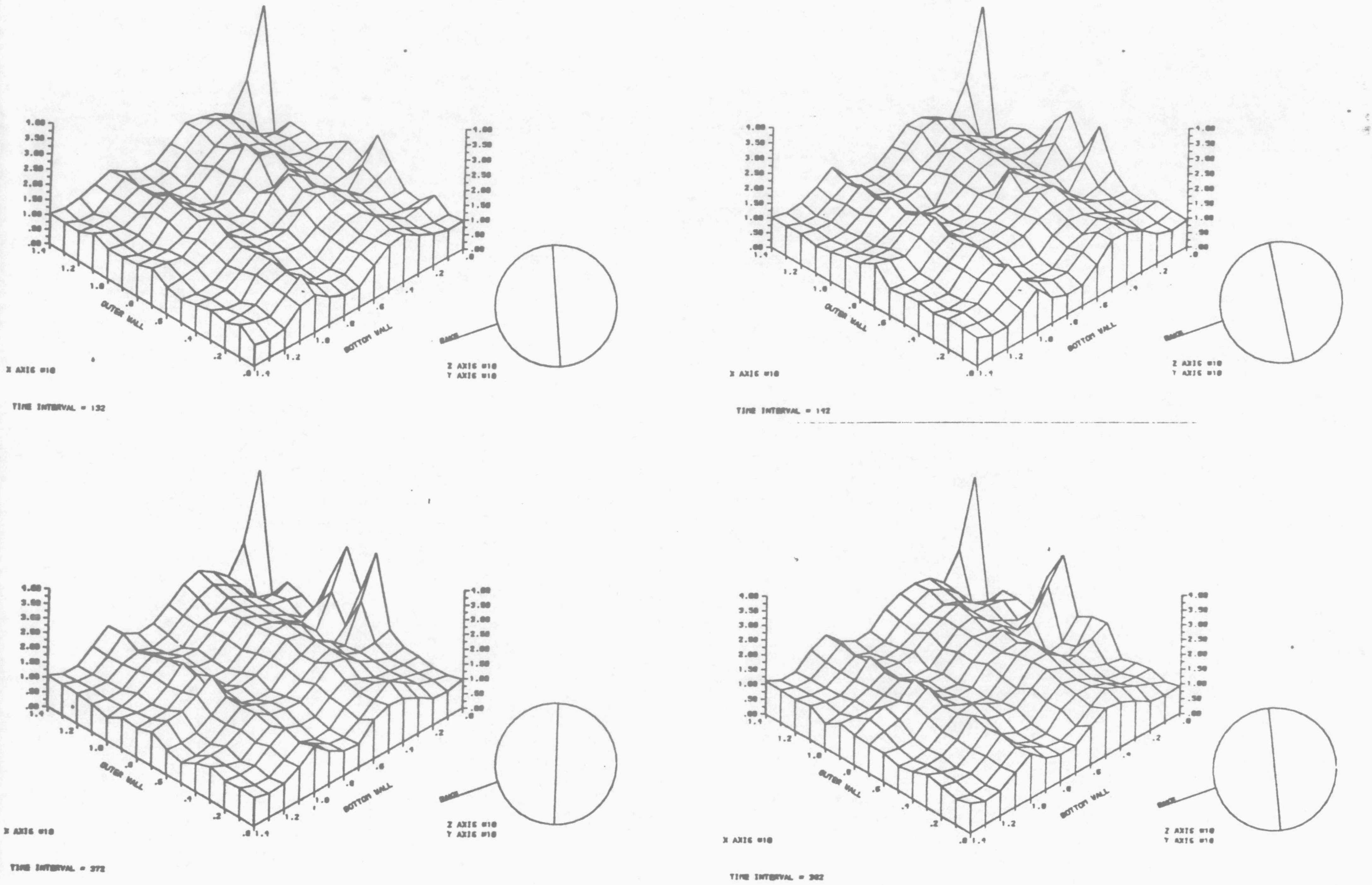

Figure 30. Symmetry of swirl in relation to the arm.

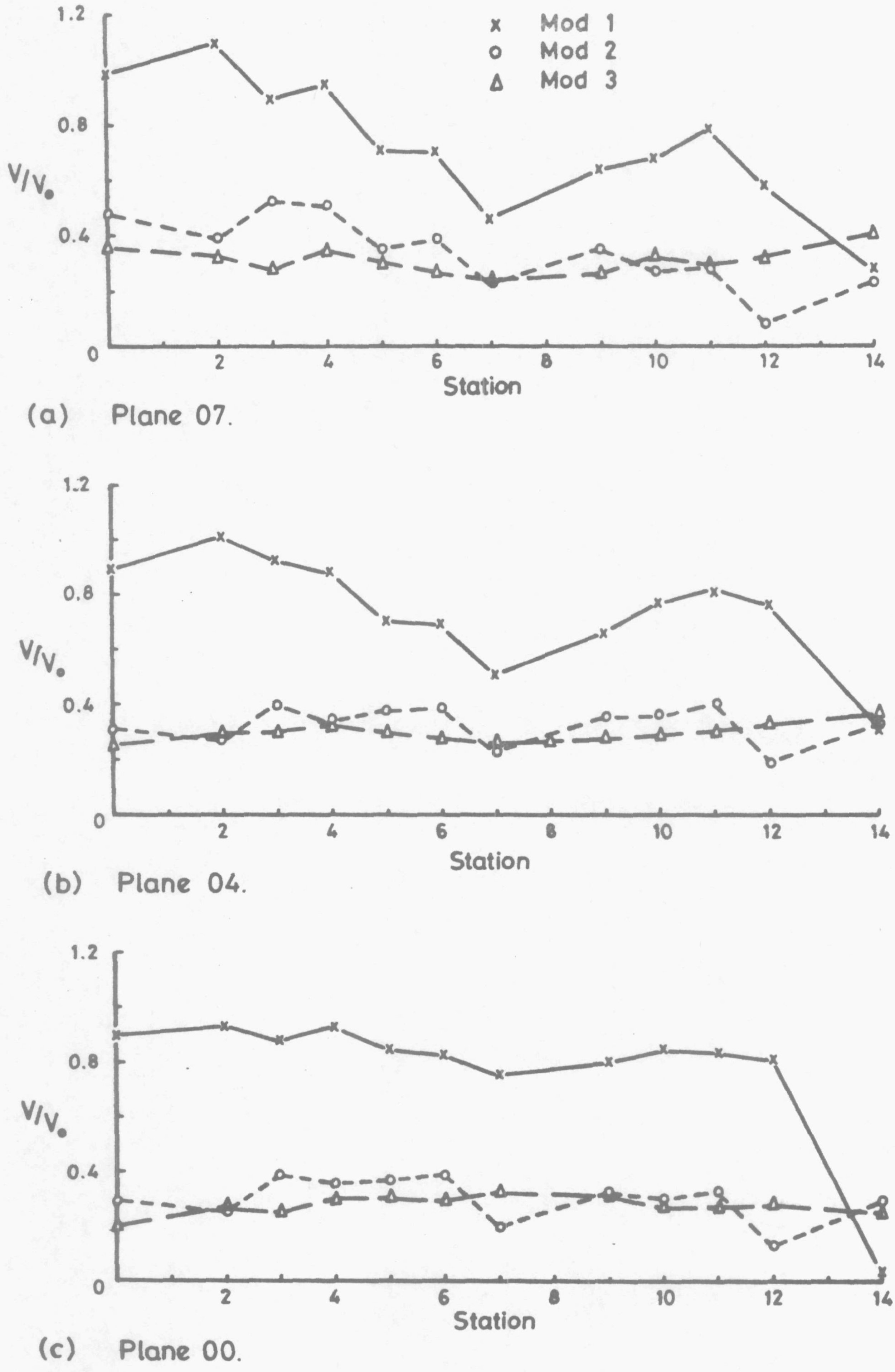

Figure 31. Effect of the modifications on swirl.

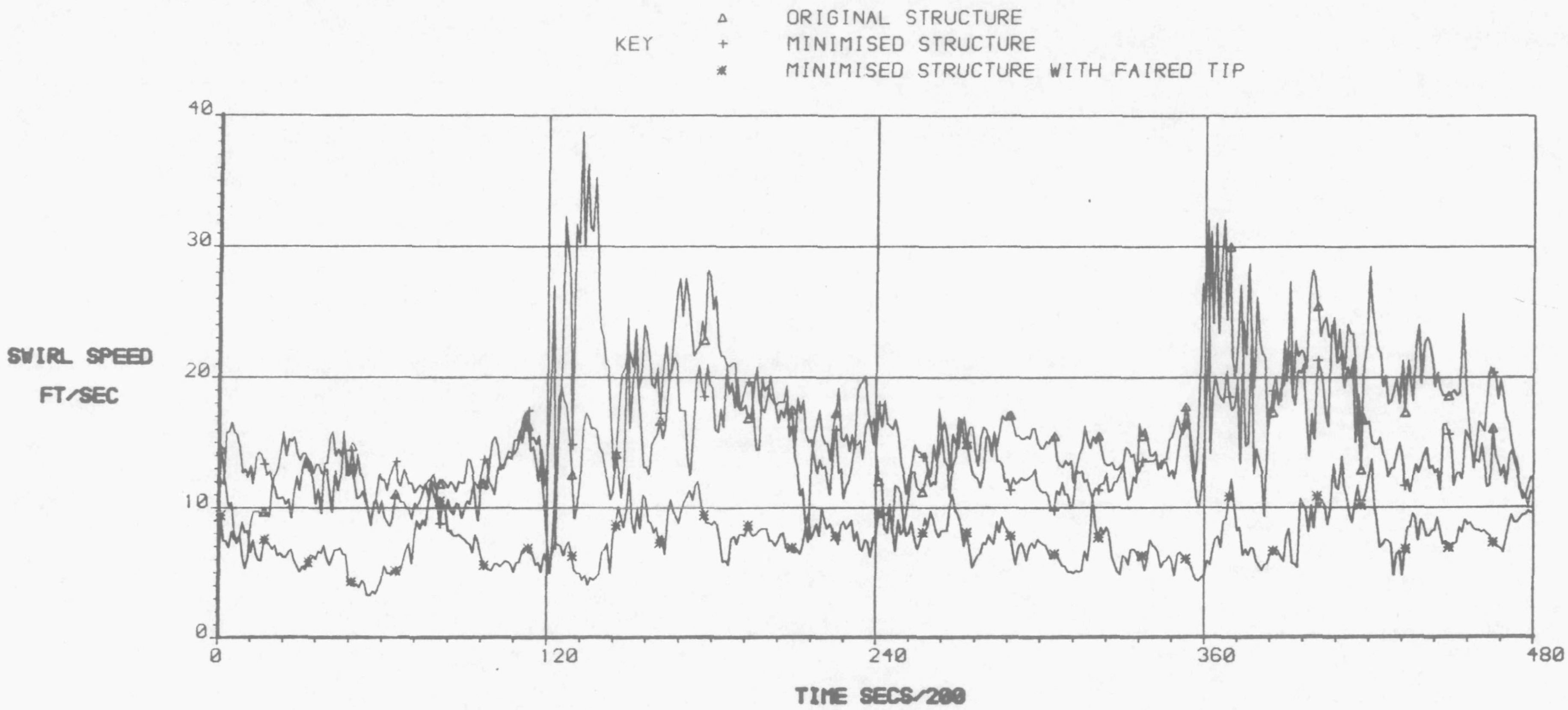

FIG 32 Effect of modifications on swirl at station 0700

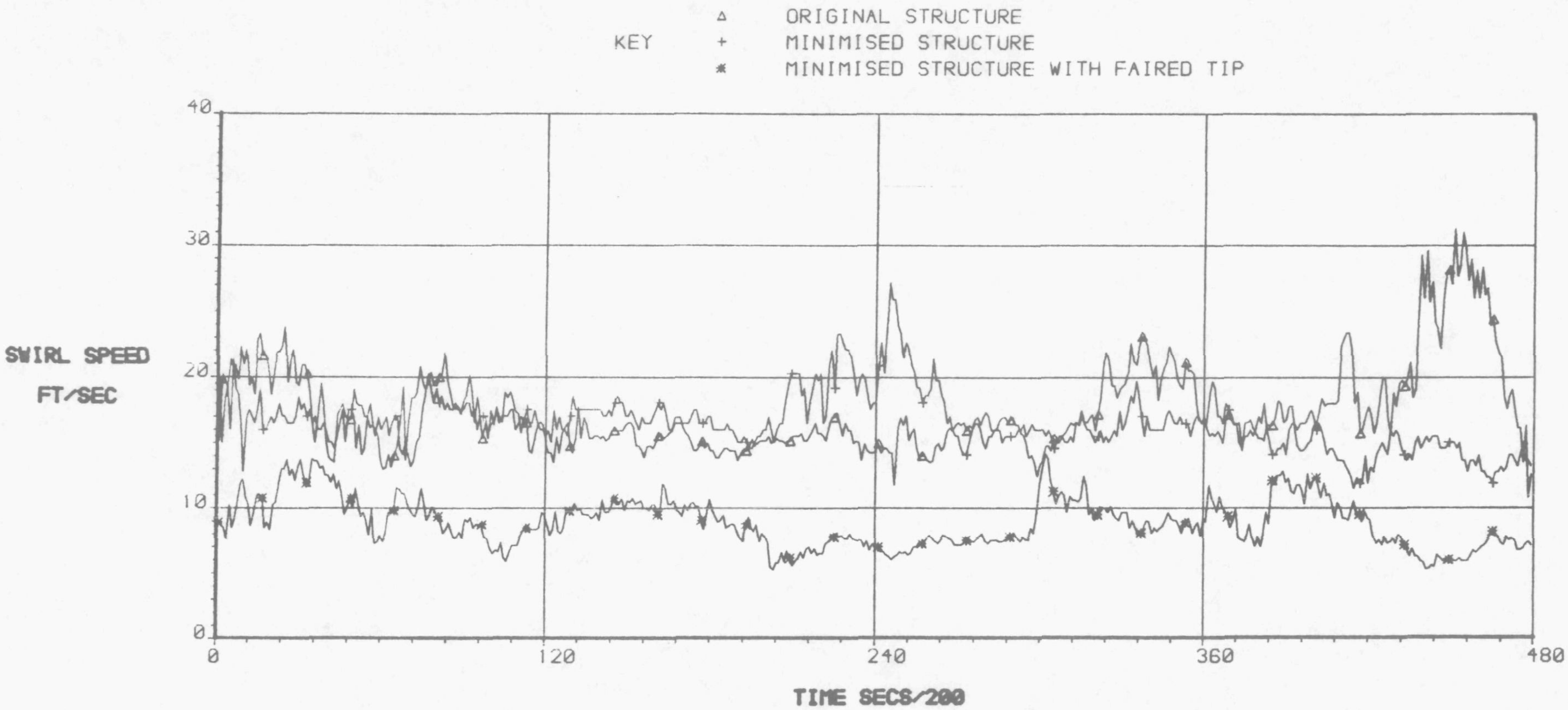

FIG 33 Effect of modifications on swirl at station 0704

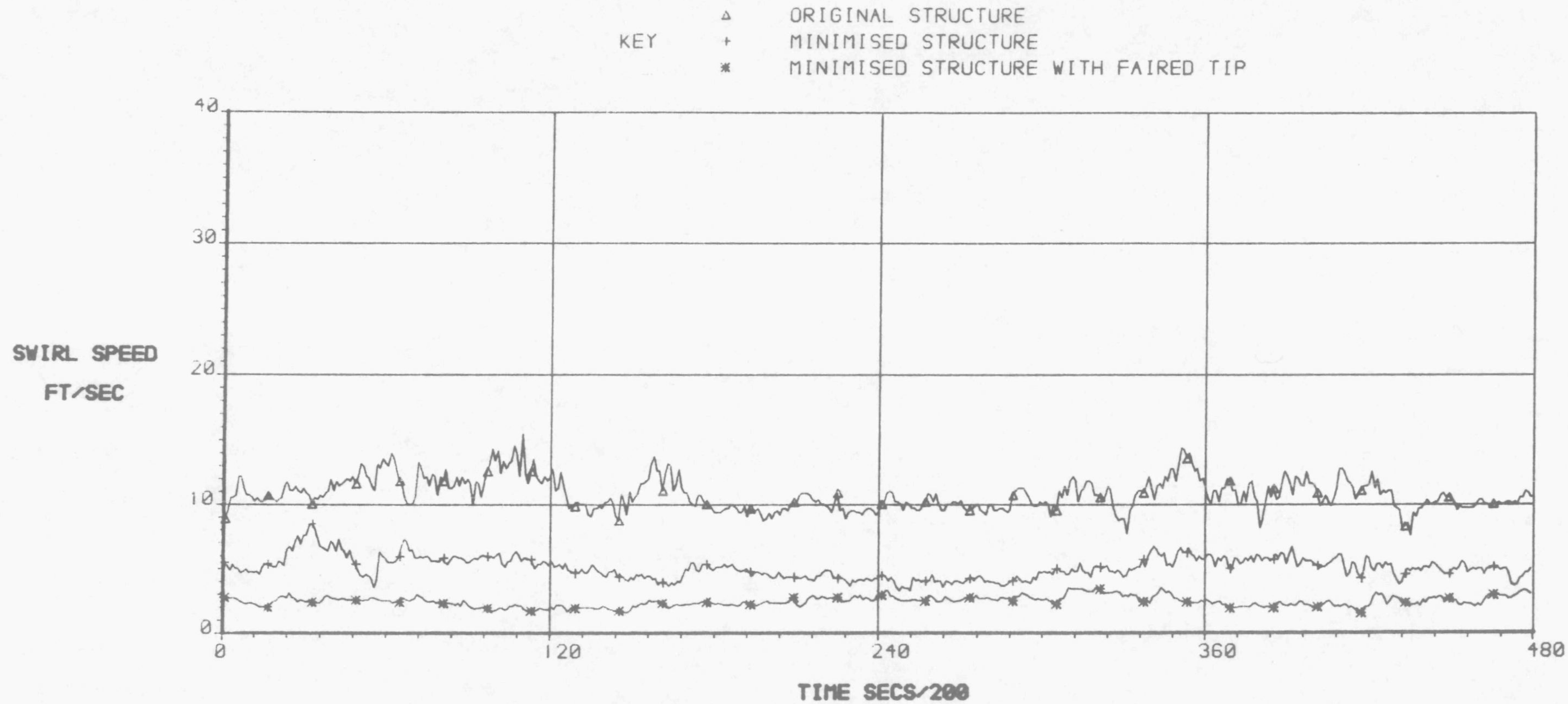

FIG 34 Effect of modifications on swirl at station 0707

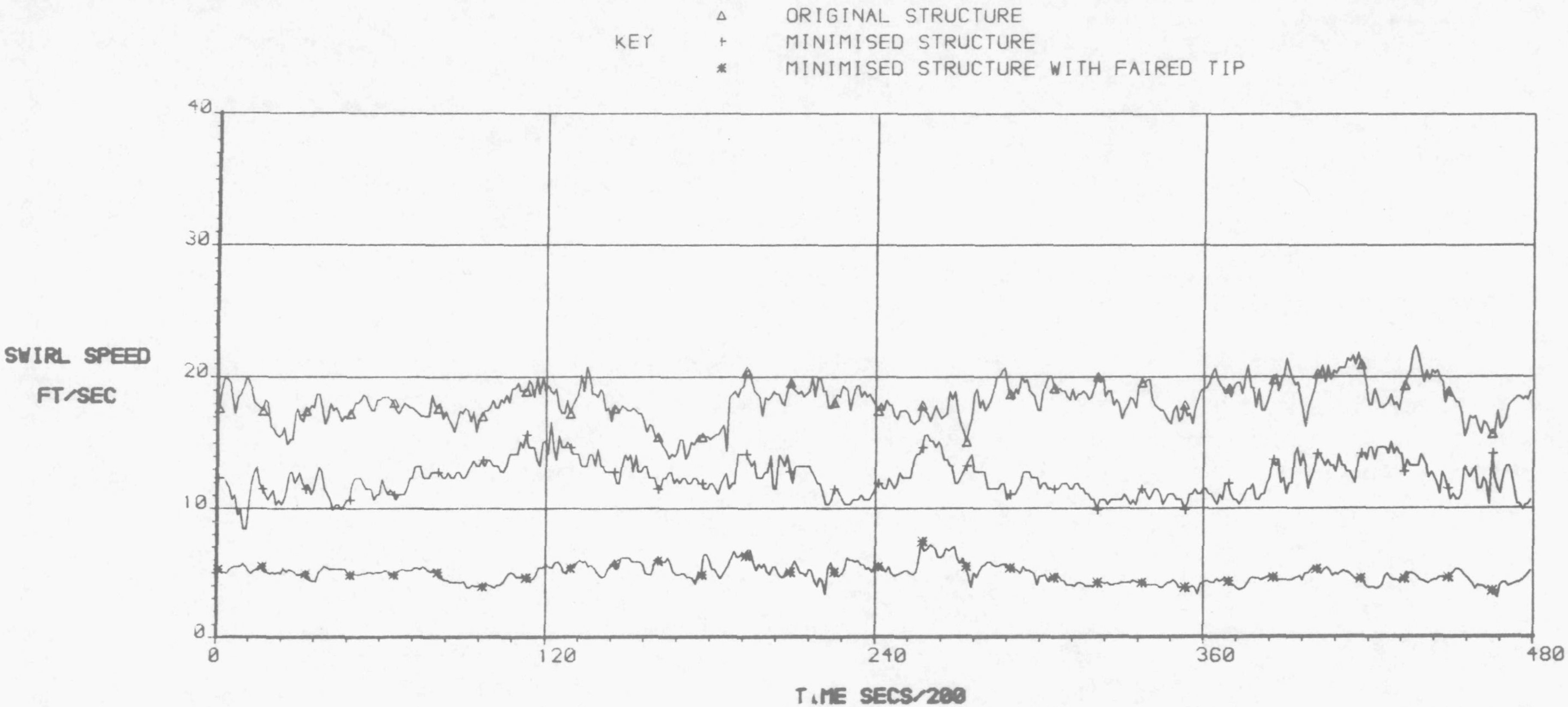

FIG 35 Effect of modifications on swirl at station 0710

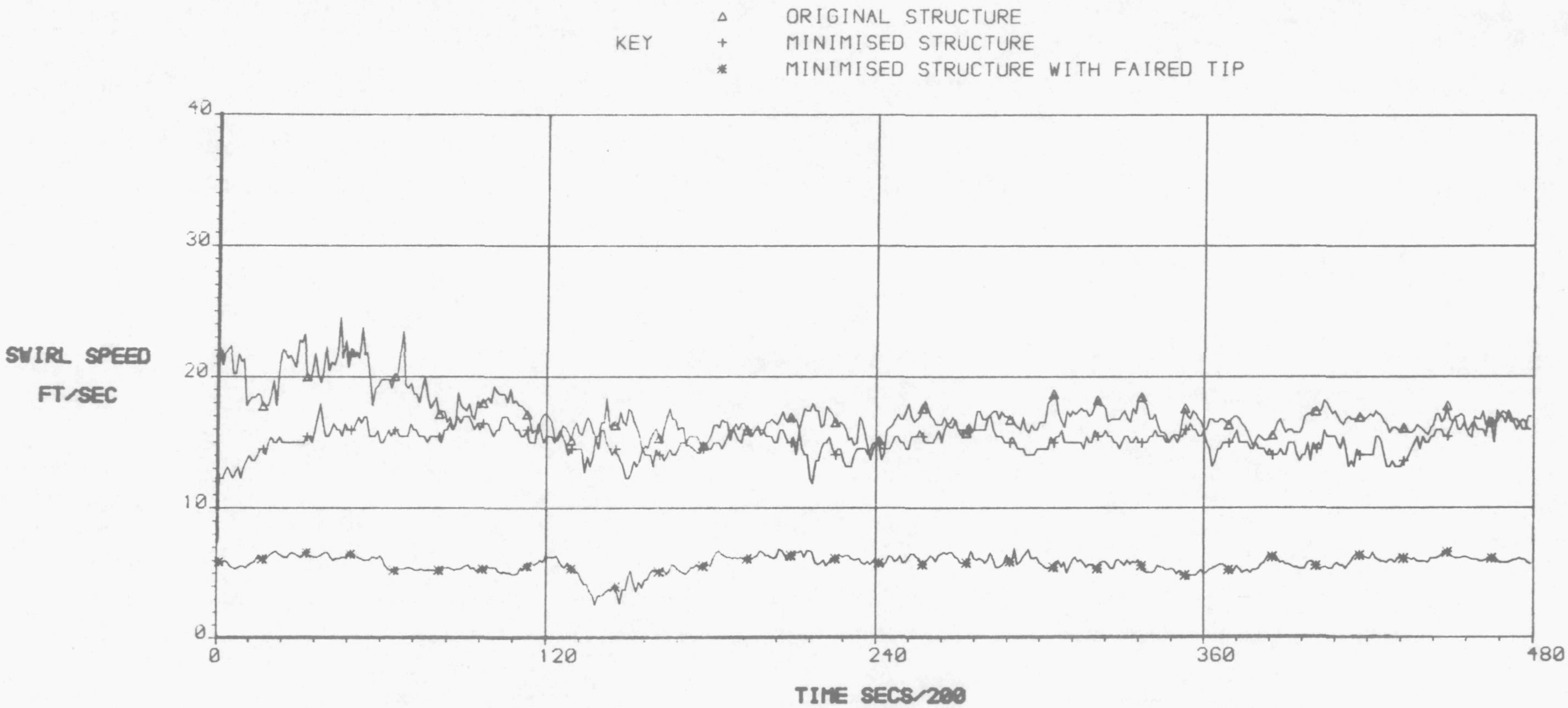

FIG 36 Effect of modifications on swirl at station 0404

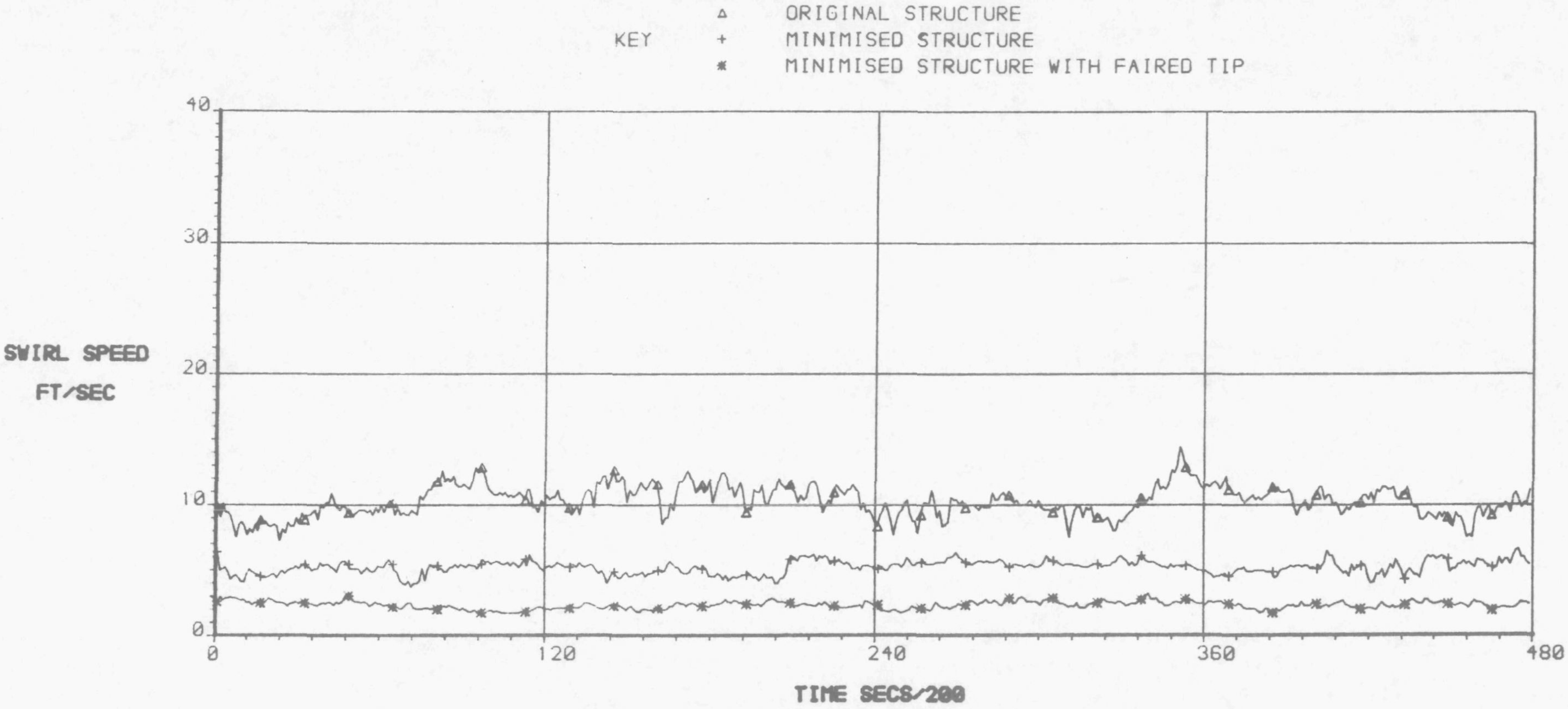

FIG 37 Effect of modifications on swirl
at station 0407

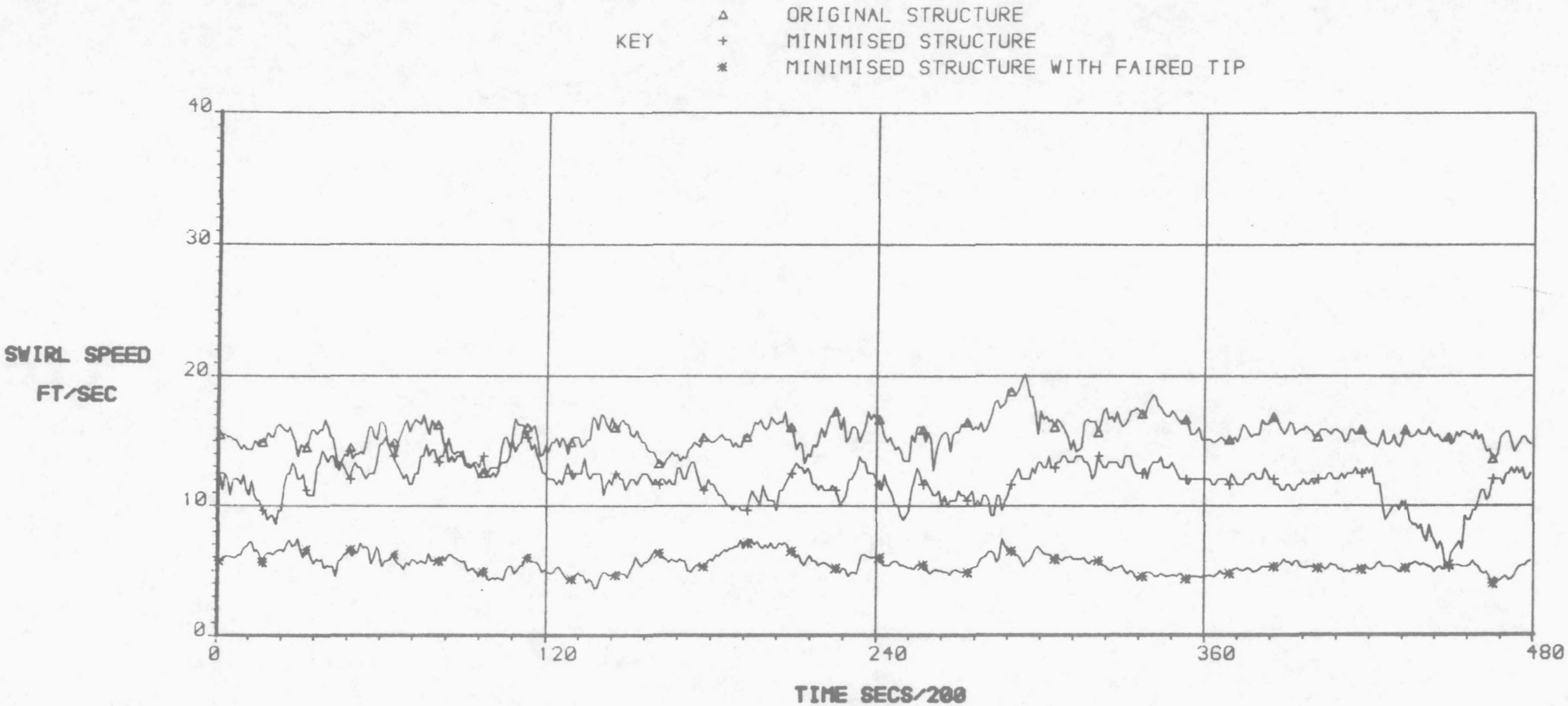

FIG 38 Effect of modifications on swirl at station 0410

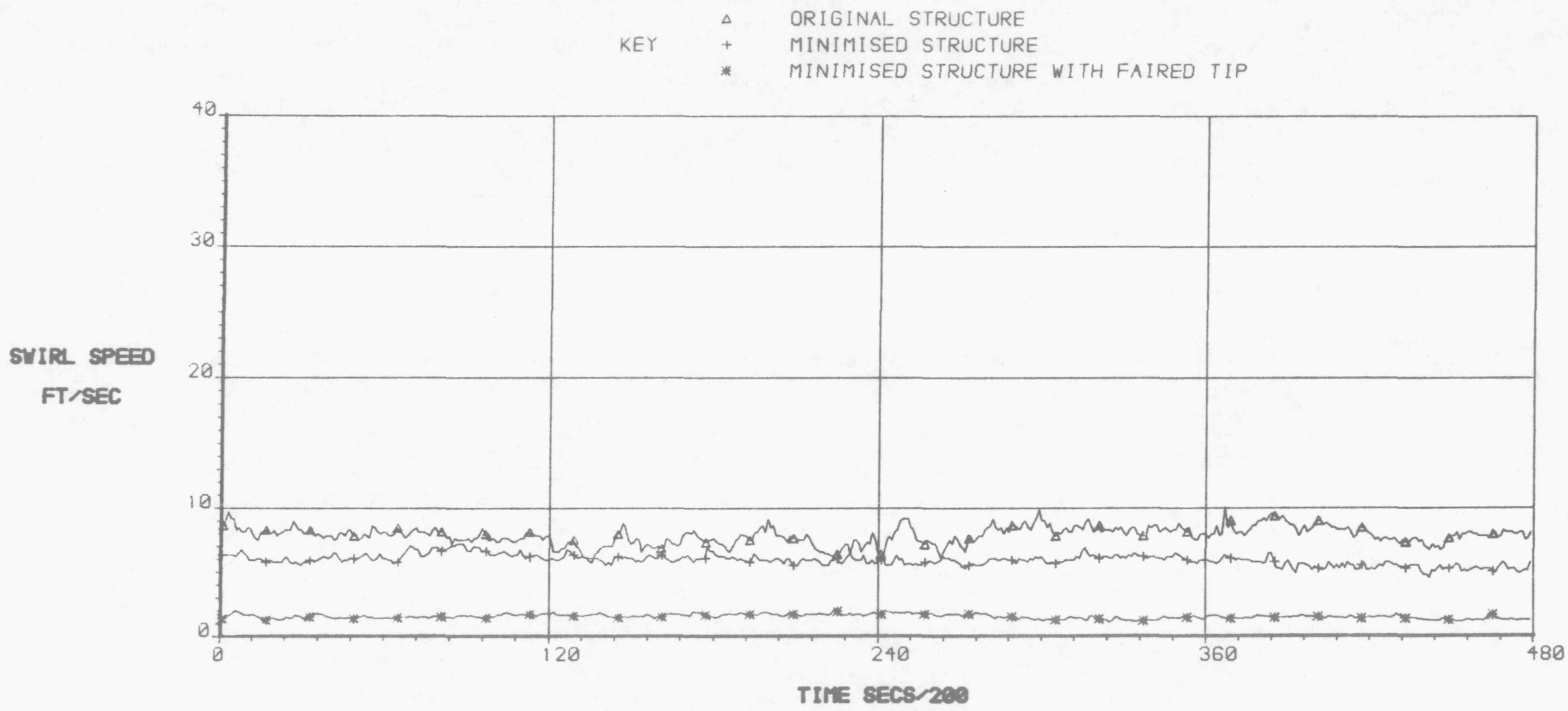

FIG 39 Effect of modifications on swirl at station 0007

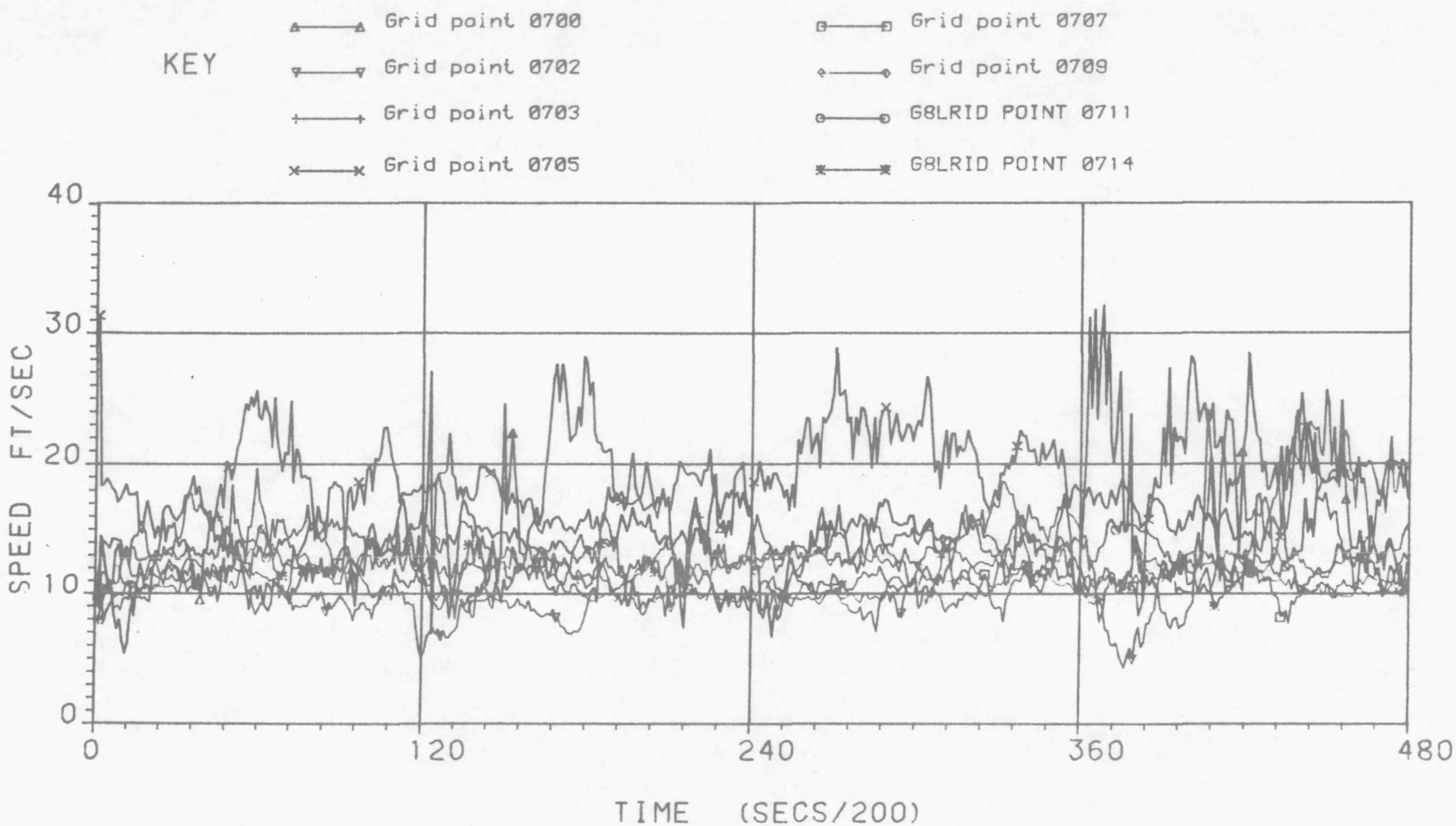

FIG **40**. VARIATION OF SWIRL SPEED WITH TIME AT STATIONS 0700, 0702, 0703, 0705, 0707, 0709, 0711, 0714 WHIRLING ARM IN ORIGINAL CONDITION

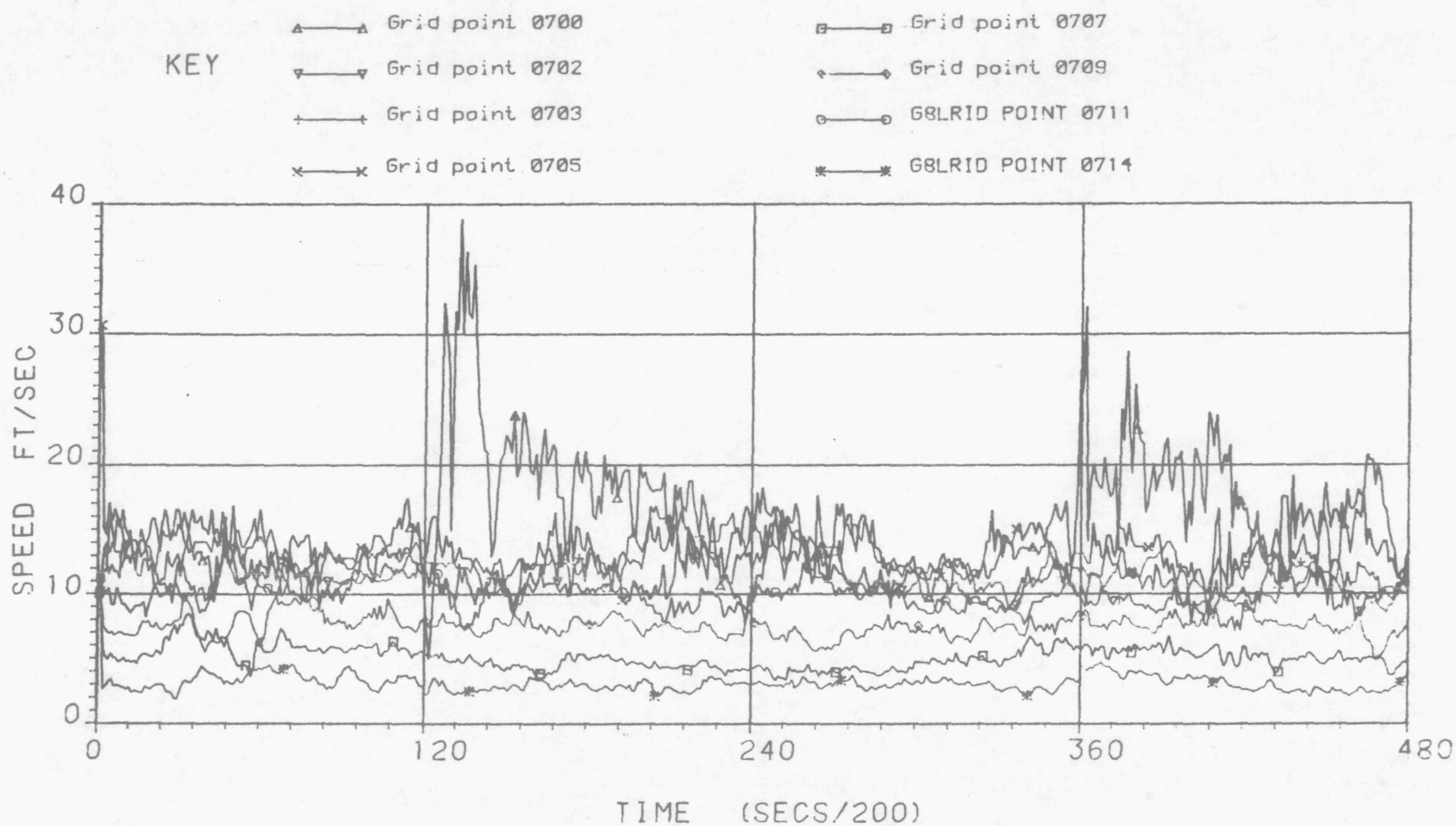

FIG 41. VARIATION OF SWIRL SPEED WITH TIME AT STATIONS
0700, 0702, 0703, 0705, 0707, 0709, 0711, 0714
WHIRLING ARM MOD 1. UNFAIRED MINIMUM STRUCTURE

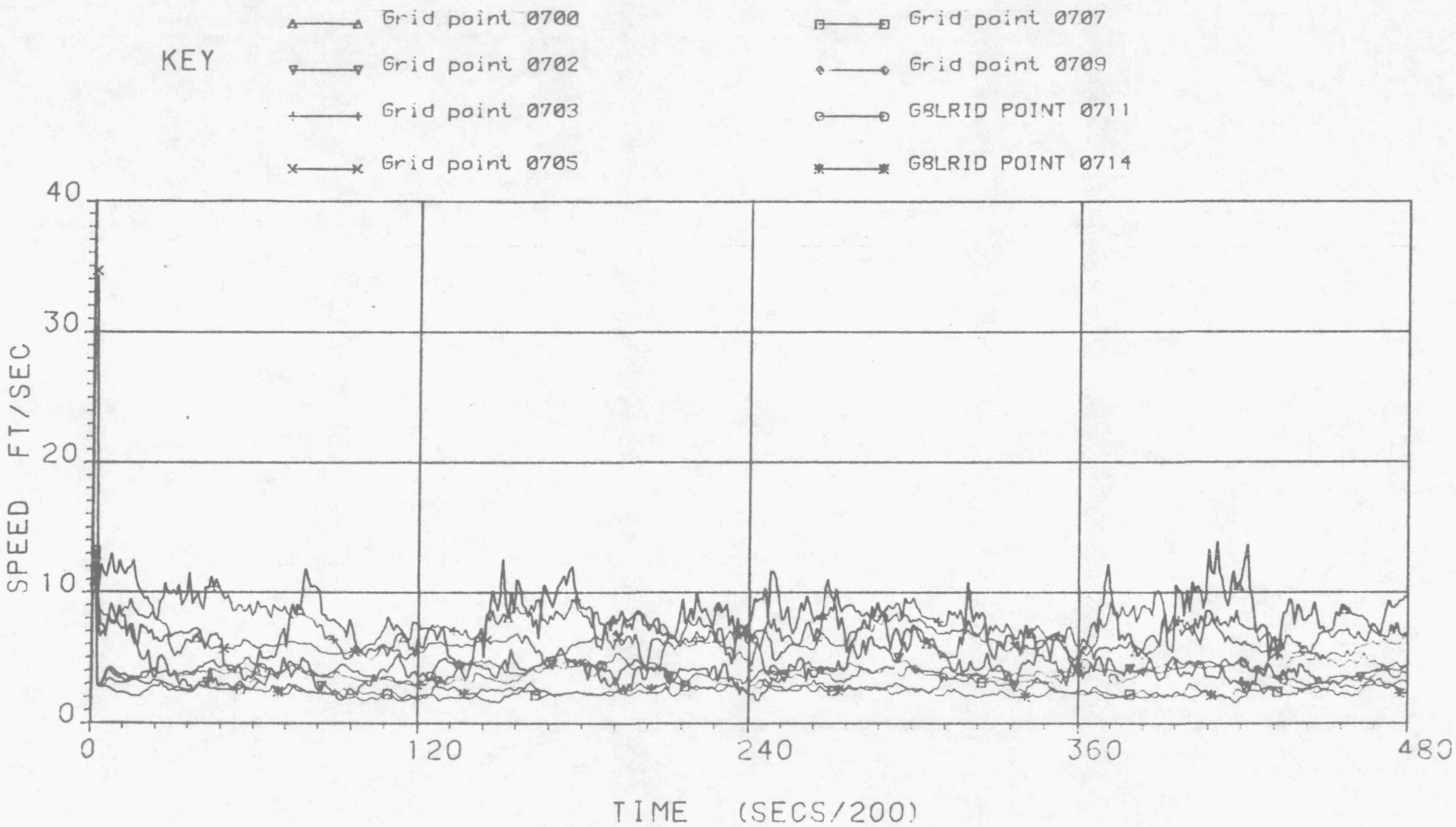

FIG **42**. VARIATION OF SWIRL SPEED WITH TIME AT STATIONS
0700, 0702, 0703, 0705, 0707, 0709, 0711, 0714
WHIRLING ARM MOD 2. MINIMUM STRUCTURE WITH FAIRED TIP

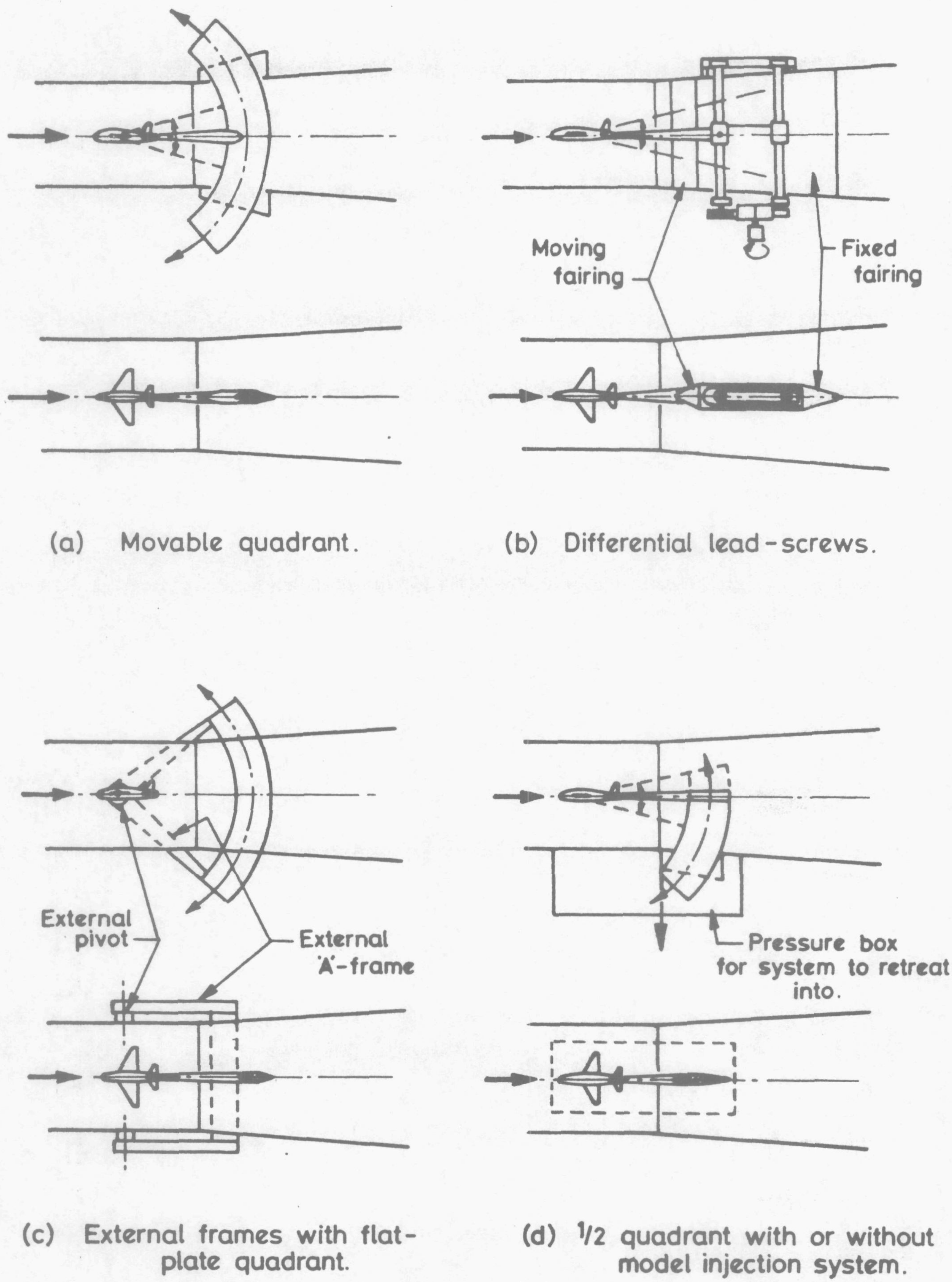

Figure 43. Possible methods to alter pitch of sting mounted models.

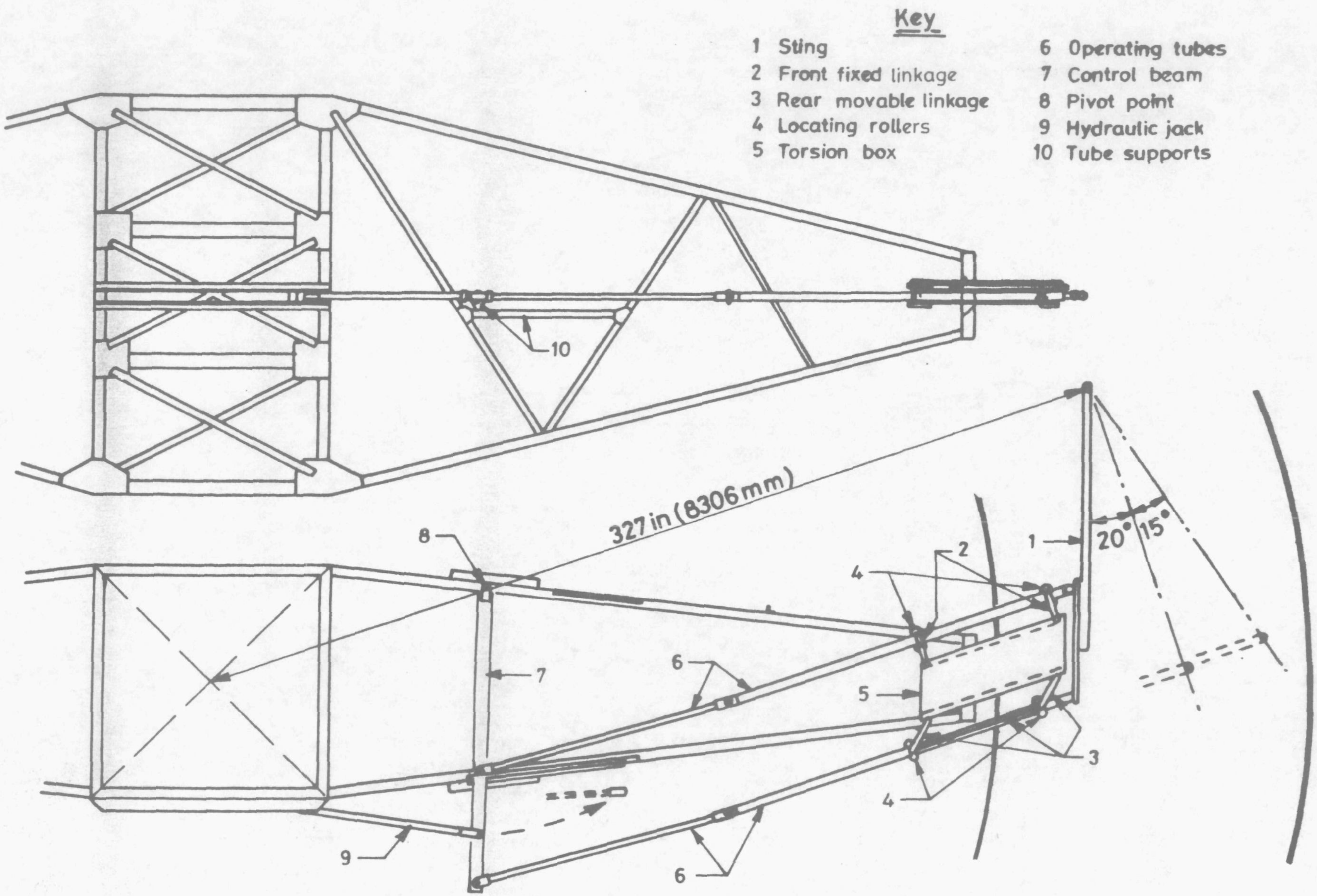

Figure 44. Pitch change linkage

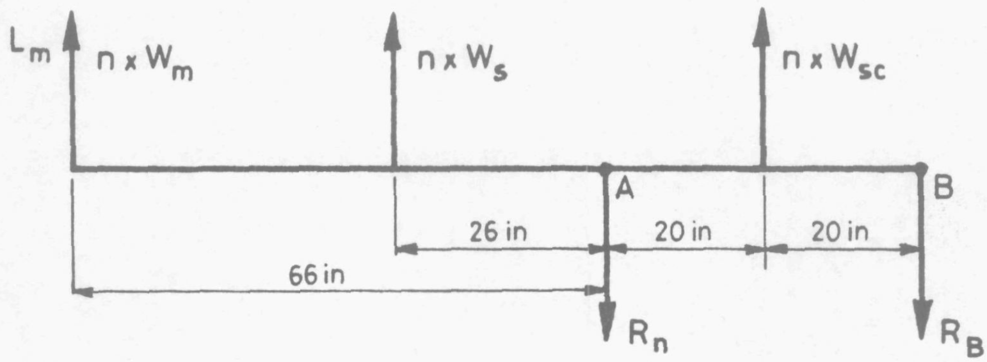

W_m = model weight $\quad$ L_m = lift on model

W_s = weight of sting $\quad$ W_{sc} = Weight of sting carrier

n = 'g' loading

Taking moments about A

$$(nW_m + L_m) \times 66 + nW_s \times 26 - nW_{sc} \times 20 + R_B \times 40 = 0 \qquad (1)$$

Resolving outwards

$$L_m + nW_m + nW_s + nW_{sc} = R_A + R_B \qquad (2)$$

Case	n	L_m	W_m	W_s	W_{sc}	R_A	R_B
1	10	100	10	30	200	2025	475
2	10	100	20	30	200	2290	310
3	10	100	20	100	200	3445	- 145
4	10	100	20	100	50	2695	- 895
5	10	100	20	200	50	4345	-1545
6	10	5	5	30	50	890.75	-35.75

N.B. For simplicity the 'g' loading has been taken as a mean value. The actual variation of 'g' at maximum extension is shown in table 4.

Figure 45. Horizontal loads imposed on the pitch linkage by the model and sting support system.

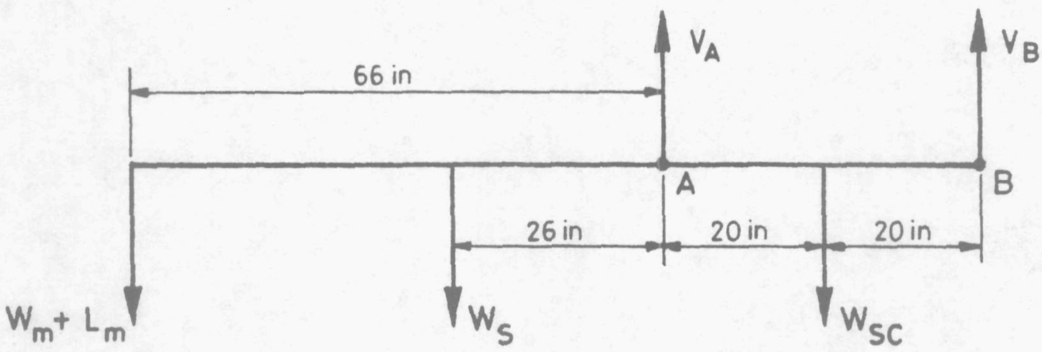

W_m = model weight L_m = Lift on model

W_s = weight of sting W_{sc} = Weight of sting carrier

Taking moments about A

$$(W_M + L_M) \times 66 + W_s \times 26 - W_{sc} \times 20 + V_B \times 40 = 0 \tag{1}$$

Resolving downwards

$$W_M + L_M + W_s + W_{sc} - V_B = V_A \tag{2}$$

Case	L_m	W_m	W_s	W_{sc}	V_A	V_B
1	100	10	30	200	441	-101
2	100	20	30	200	467.5	-117.5
3	100	20	100	200	583	-163
4	100	20	100	50	508	-238
5	100	20	200	50	774	-404
6	5	5	30	50	101	- 11

Figure 46. Vertical loads imposed on the pitch linkage by the model and sting support system.

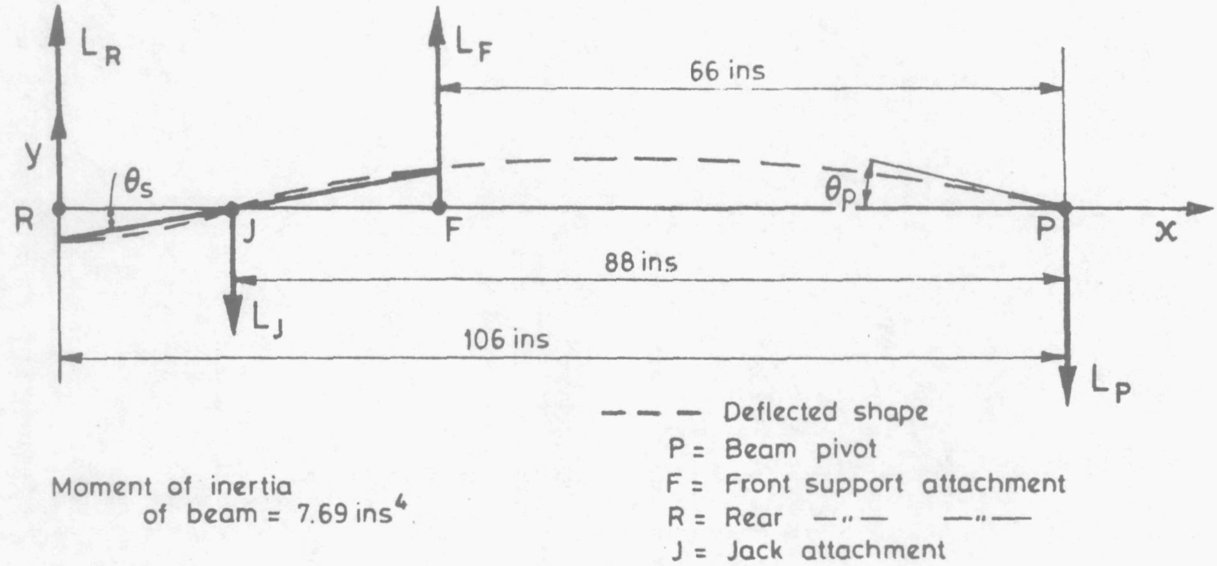

Definition of axes etc.

The jack attachment point, J, and the beam pivot point, P, are considered to be fixed and determine the 'x' axis; the 'y' axis is as shown above. The normal beam bending moment equations are applied with the forces and constraints shown. The leads at the front and rear pivots consist of the centrifugal loads on the support and connecting tubes in the fully extended position at 31.8 rpm, together with the loads defined in Fig. 45 for various model lifts and weights and sting weights. The centrifugal load of the front support tubes is 1173 lb and of the rear tubes is 1310 lb. N.B. No allowance has been made for the centrifugal loads on the control beam as these are small compared with the other loads.

Case	L_R(lb)	L_F(lb)	L_J(lb)	L_P(lb)	y_R(ins)	y_F(ins)	Θ_s°	Θ_p°
1	1784.8	3197.7	4548	434	-0.017	0.052	0.10	0.12
2	1619.8	3462.7	4548	534	-0.034	0.066	0.14	0.15
3	1164.8	4617.5	4866	916	-0.095	0.121	0.31	0.27
4	414.8	3867.7	3400	882	-0.107	0.120	0.33	0.26
5	-235.3	5517.7	3855	1427	-0.194	0.199	0.56	0.43
6	1274.0	2063.5	3082	255	-0.005	0.029	0.05	0.07

Figure 47. Deflection of control beam under various loading conditions.

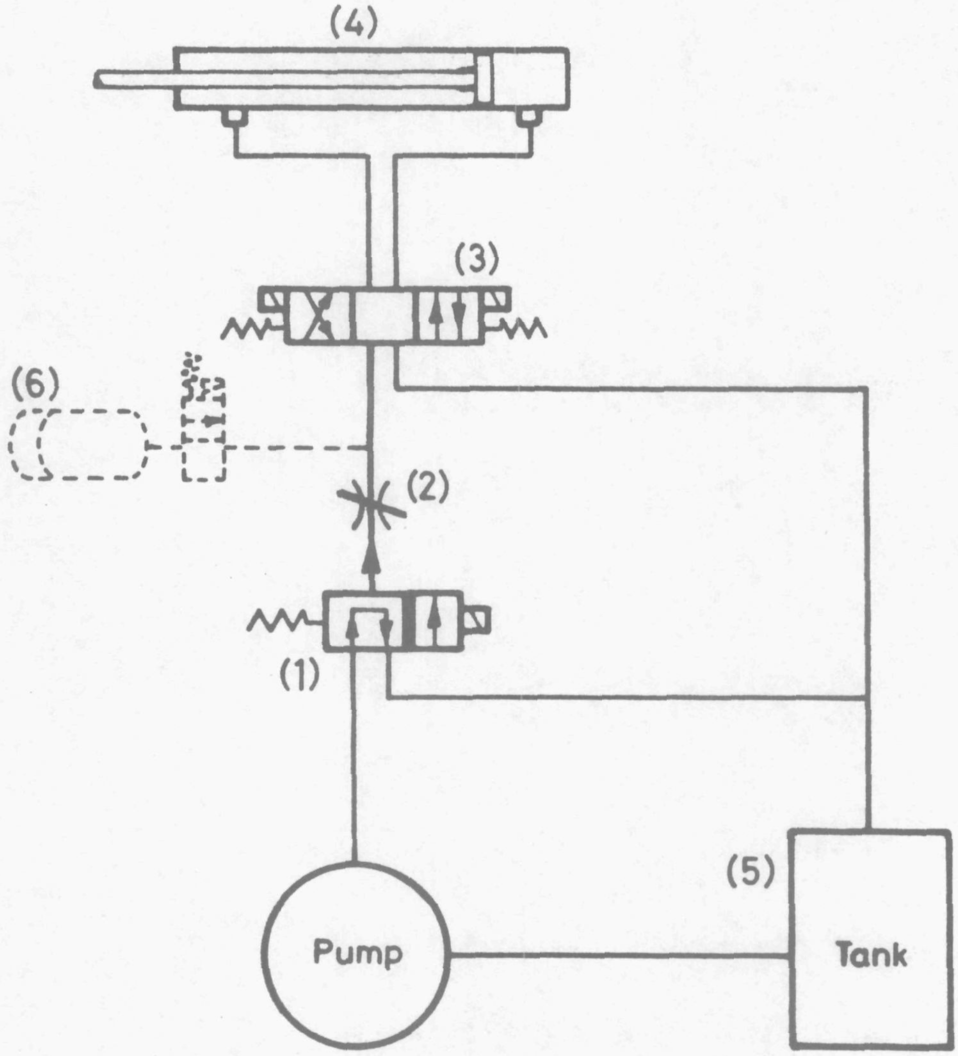

1. Isolating solenoid valve controlled by pump motor contactor.
2. Adjustable flow control valve.
3. Solenoid valve controlling direction of ram movement (ram isolated in neutral position).
4. Double acting ram.
5. Oil tank baffled to ensure pump suction is always submerged when whirling-arm is rotating.
6. Optional high pressure hydraulic reservoir and control solenoid valve for ultra rapid operation of jack.

Figure 48. Control circuit for ram moving control beam.

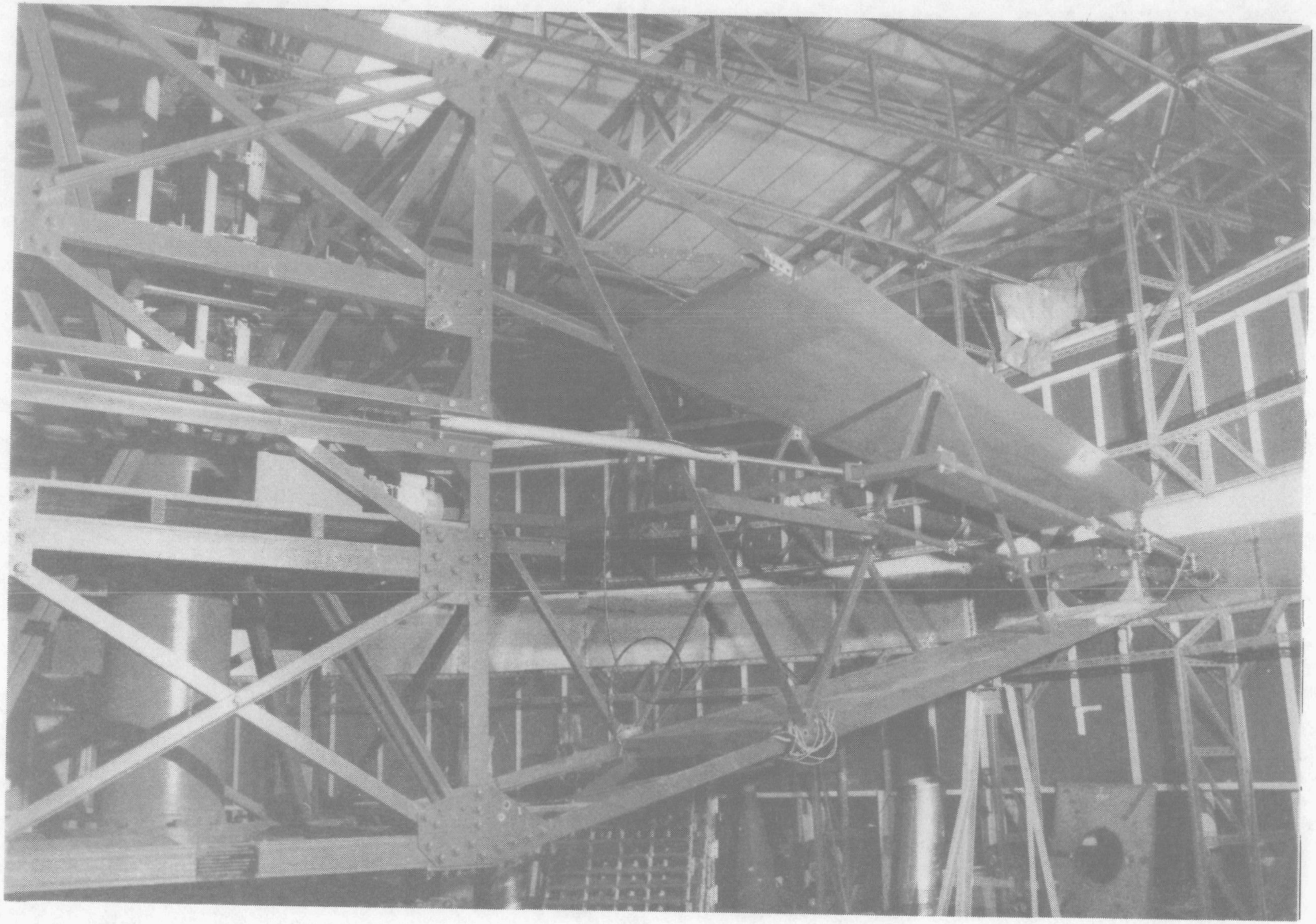

Figure 49. Model support system operating linkage. C of A Whirling Arm.

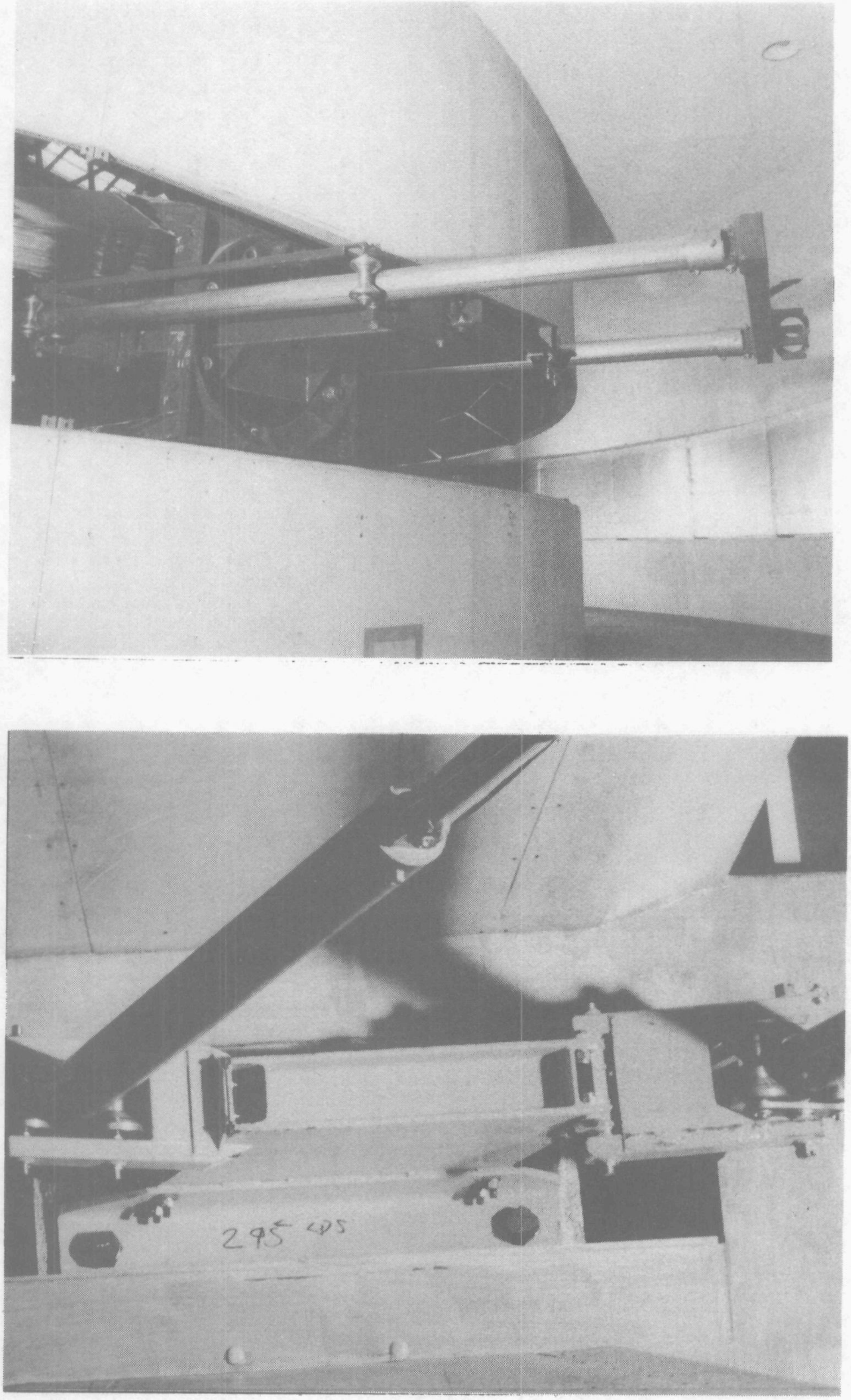

Figure 50. Torsion box and linkage. C of A Whirling Arm.

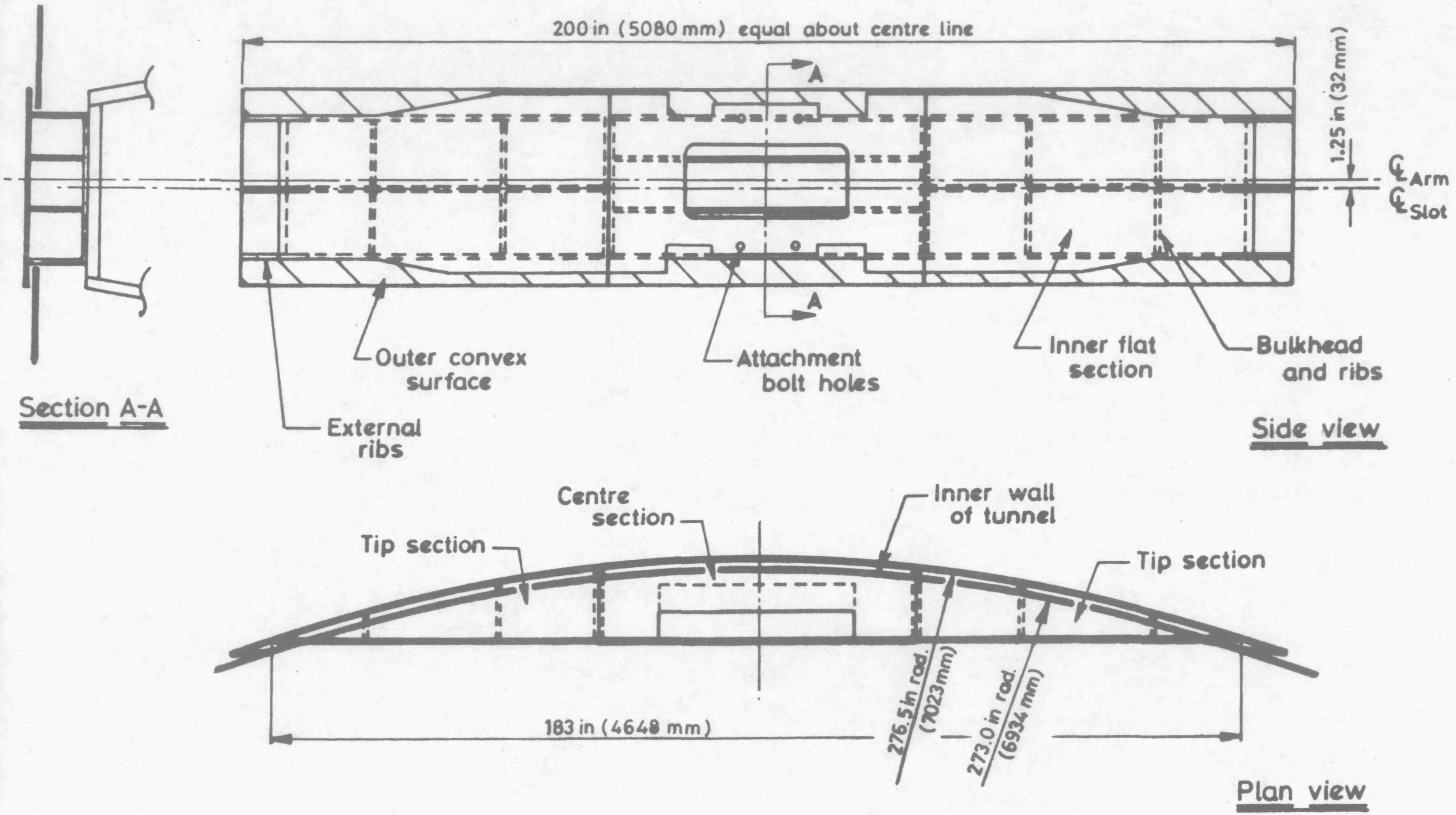

Figure 51. Labrynth tip fairing.

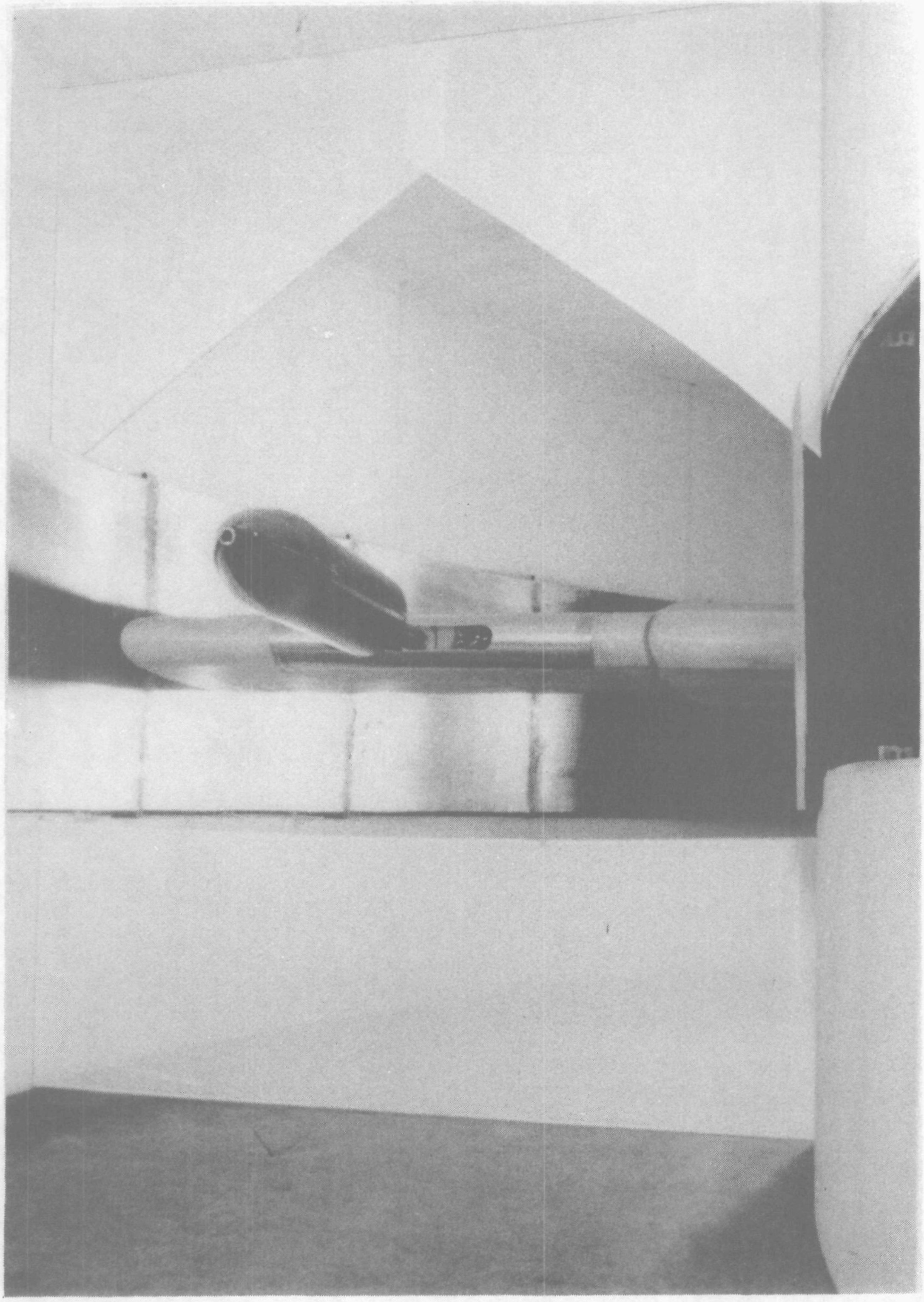

Figure 52. Test chamber . C of A Whirling Arm.

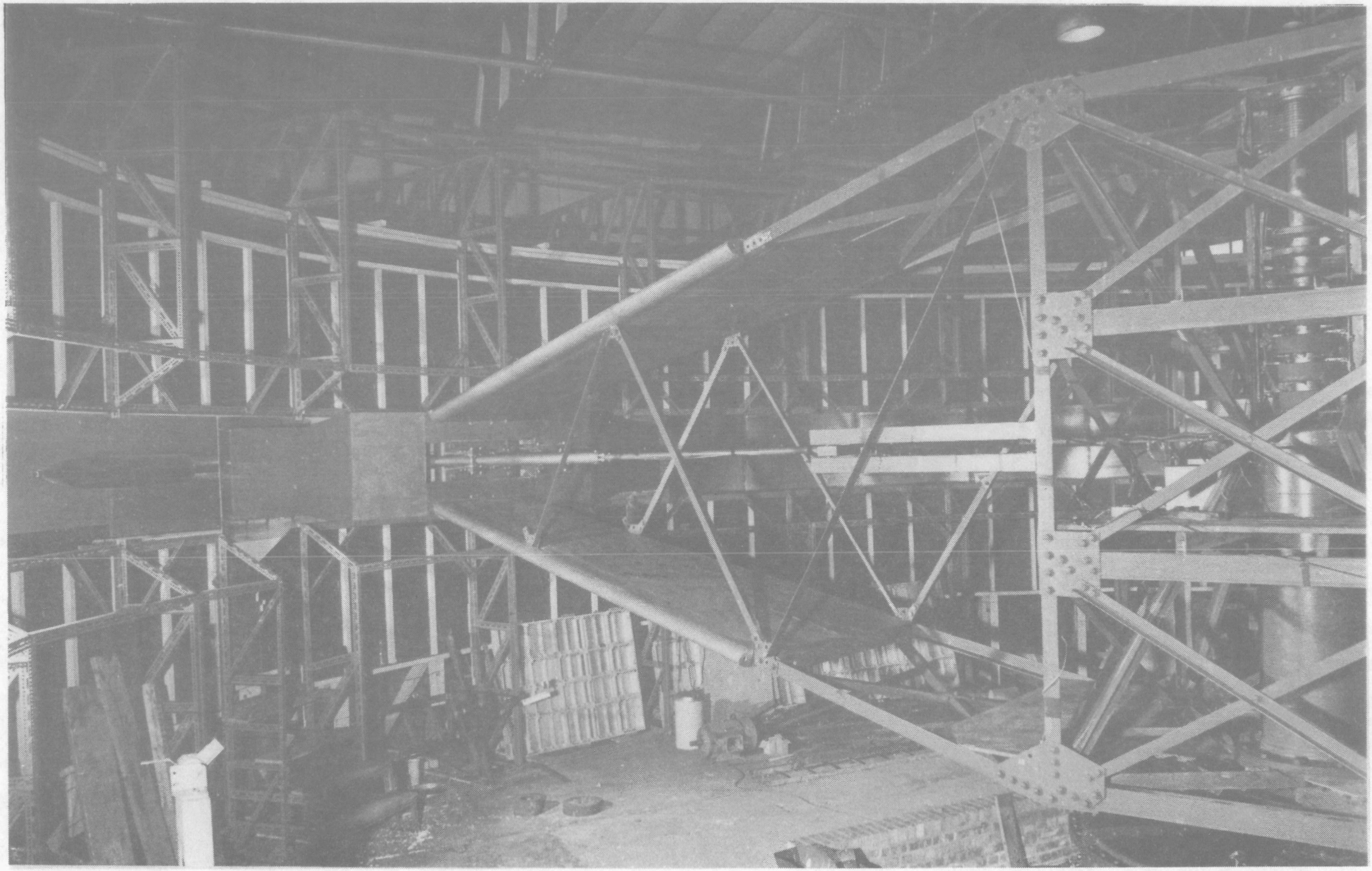

Figure 53. General view. C of A whirling arm.

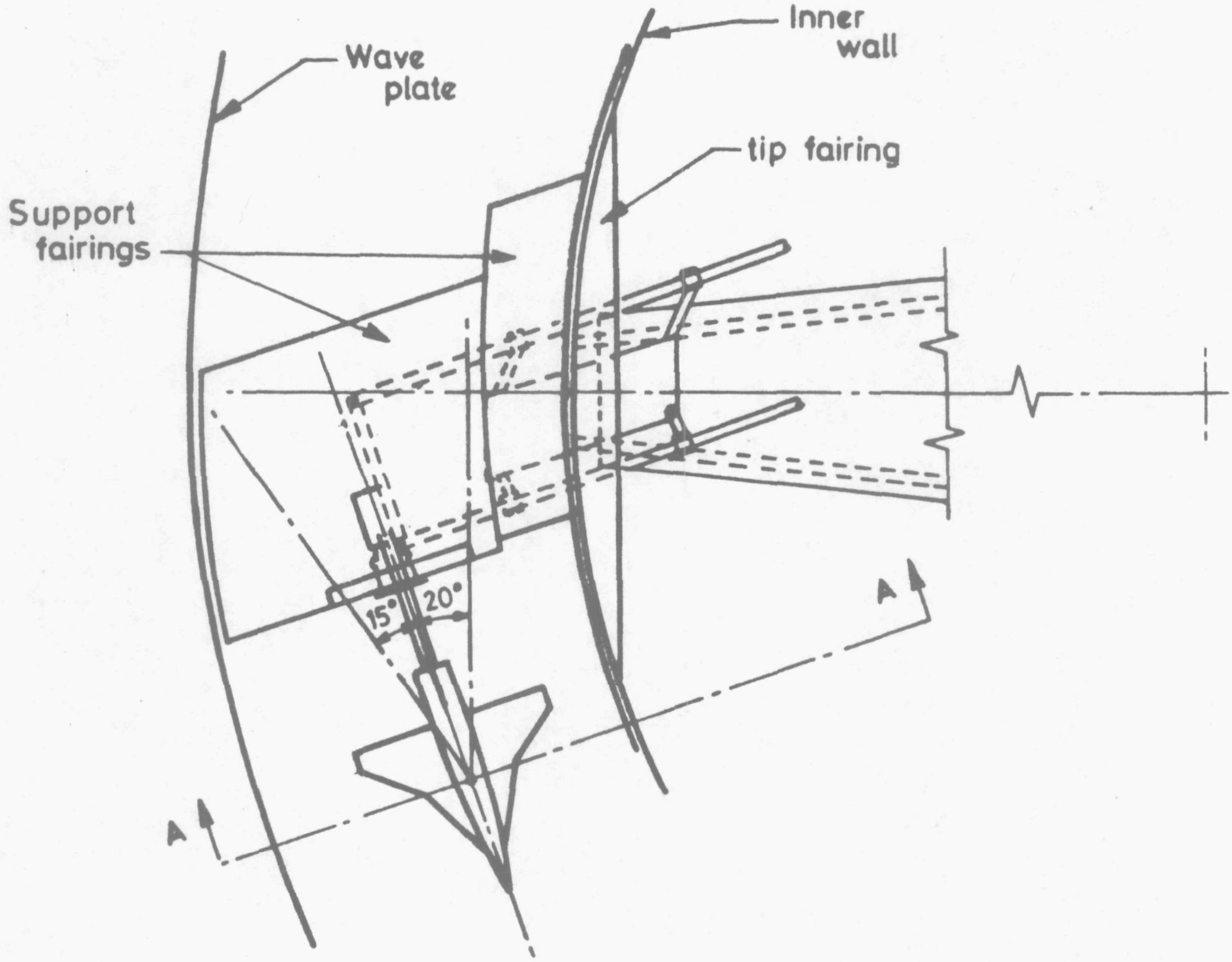

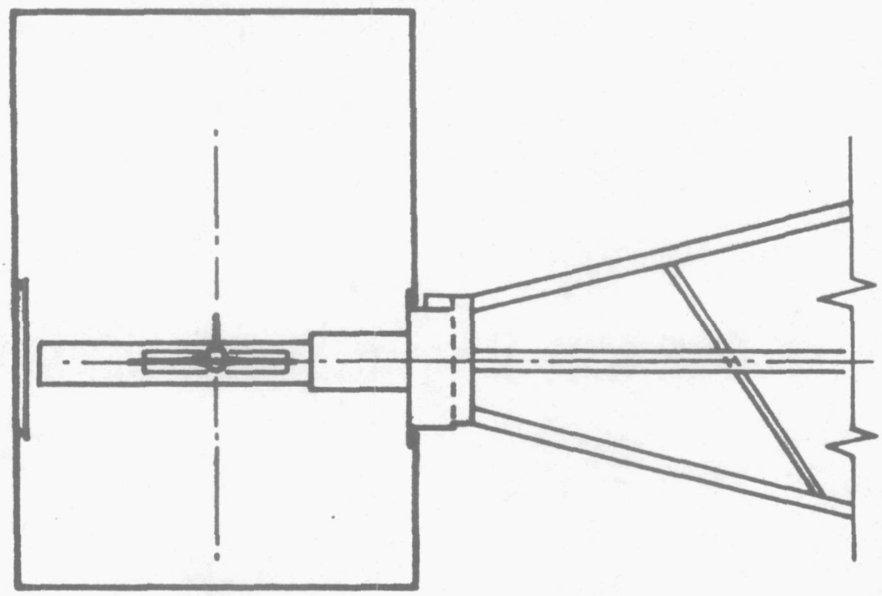

Section A-A

Figure 54. Fairings over model support system.

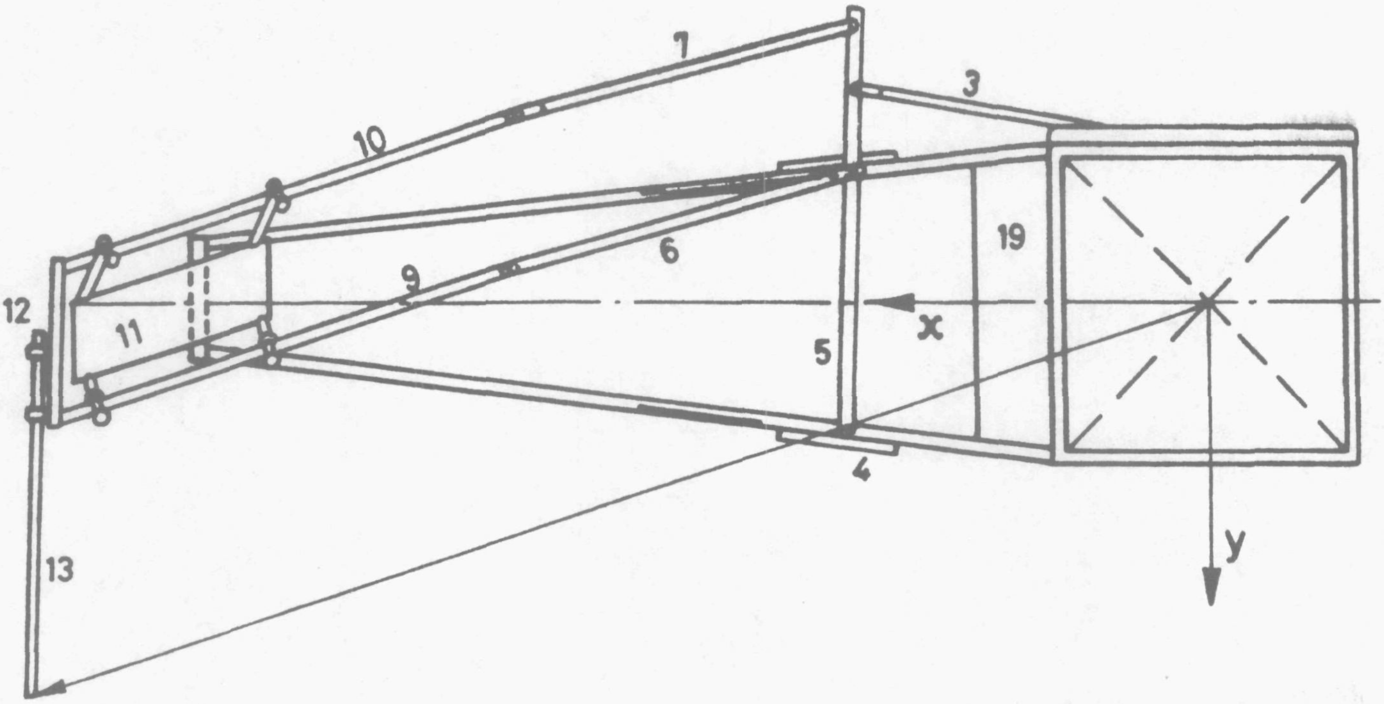

Item	W lb	x ft	$\bar{y}$ ft	W×x	W×$\bar{y}$
1. pump etc	112	1.8	-2.1	201.6	- 235.2
2. jack attachment	15	2.9	-3.5	43.5	- 52.5
3. jack	70	7.5	-3.6	525.0	- 252.0
4. pivot support	80	6.0	+3.0	480.0	+ 240.0
5. control beam	88	9.3	-1.8	818.5	- 158.5
6. front tube	40	13.1	-1.7	524.0	- 68.0
7. rear tube	40	14.0	-5.0	560.0	- 200.0
8. control beam support	30	10.0	-2.8	300.0	- 84.0
9. front support	120	21.6	+1.5	2592.0	+ 180.0
10. rear support	120	22.5	-1.5	2700.0	- 180.0
11. torsion box	340	23.0	+0.3	7820.0	+ 102.0
12. sting support	52	27.3	+1.9	1420.0	+ 98.8
13. sting	30 (est)	26.8	+4.8	804.0	+ 144.0
Totals	1107			18788.6	- 465.4
14. Instrumentation platform	110	4.75	+0.0	522.5	+ 0.0
15. Support fairing in test chamber	63	26.5	+0.6	1669.5	+ 37.8

C.G. of items 1 - 13 is at x = 16.97 ft, y = -0.42 ft
Balance weight secured to tip frame at x = -22.0 ft is 854 lb positioned at y = +0.55 ft

ALL dimensions refer to datum position of model support (0°)

N.B. Sketch shows innermost position (+20°)

Figure 55. Component weights and C.G. details to determine balance weight.

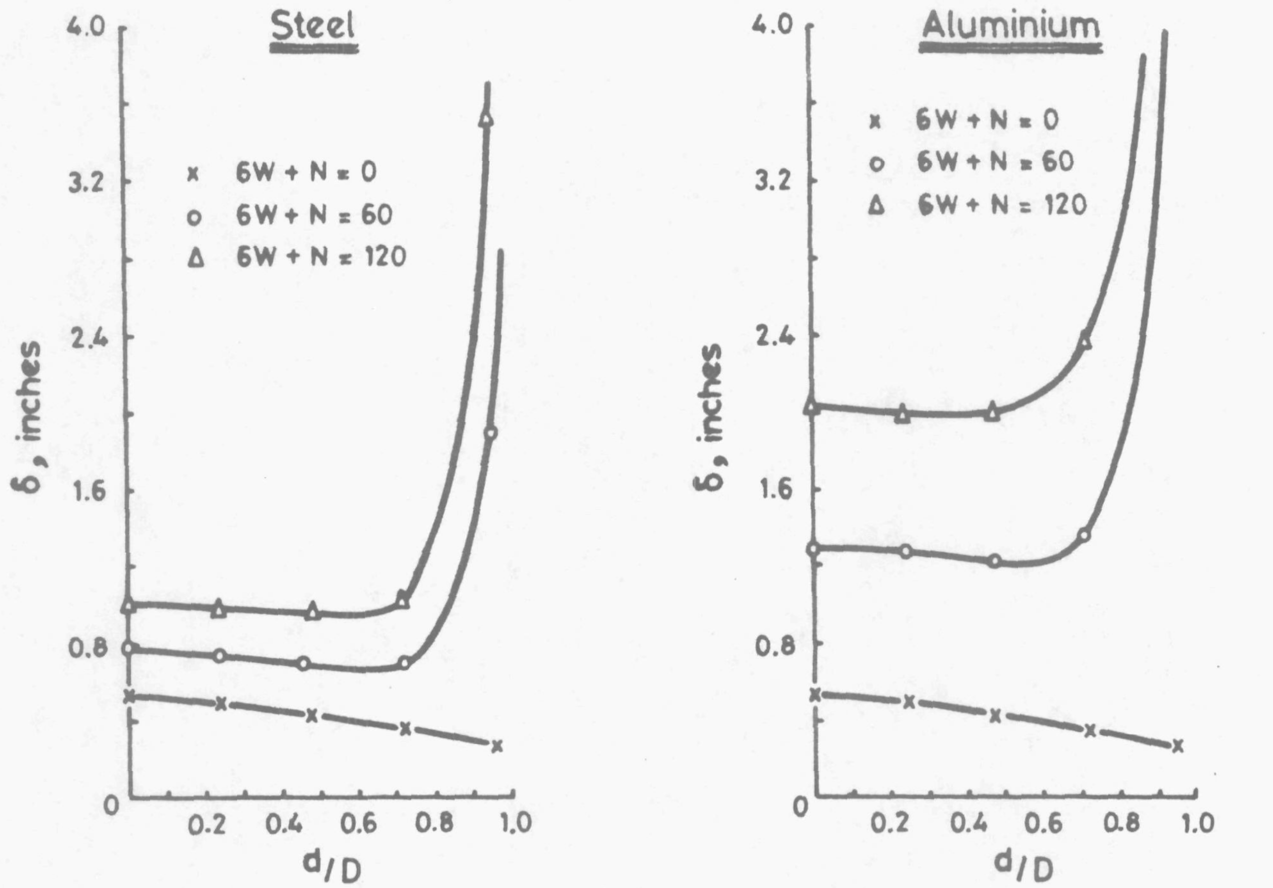

(a) Sting outside diameter = 2.0 inches , sting length = 66.0 inches

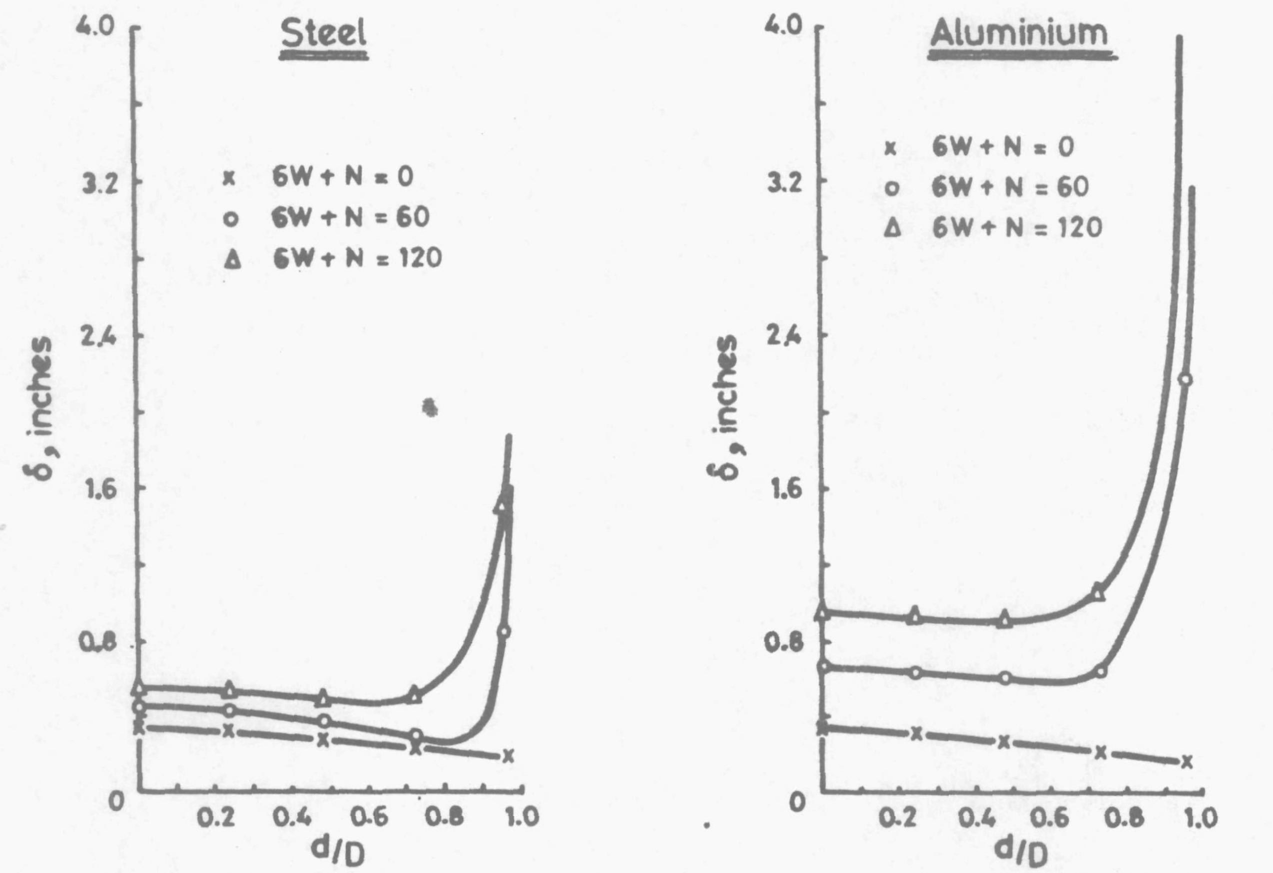

(b) Sting outside diameter = 2.5 inches , sting length = 66.0 inches

Figure 56. Variation of sting tip dispacement with loading under 6g conditions.

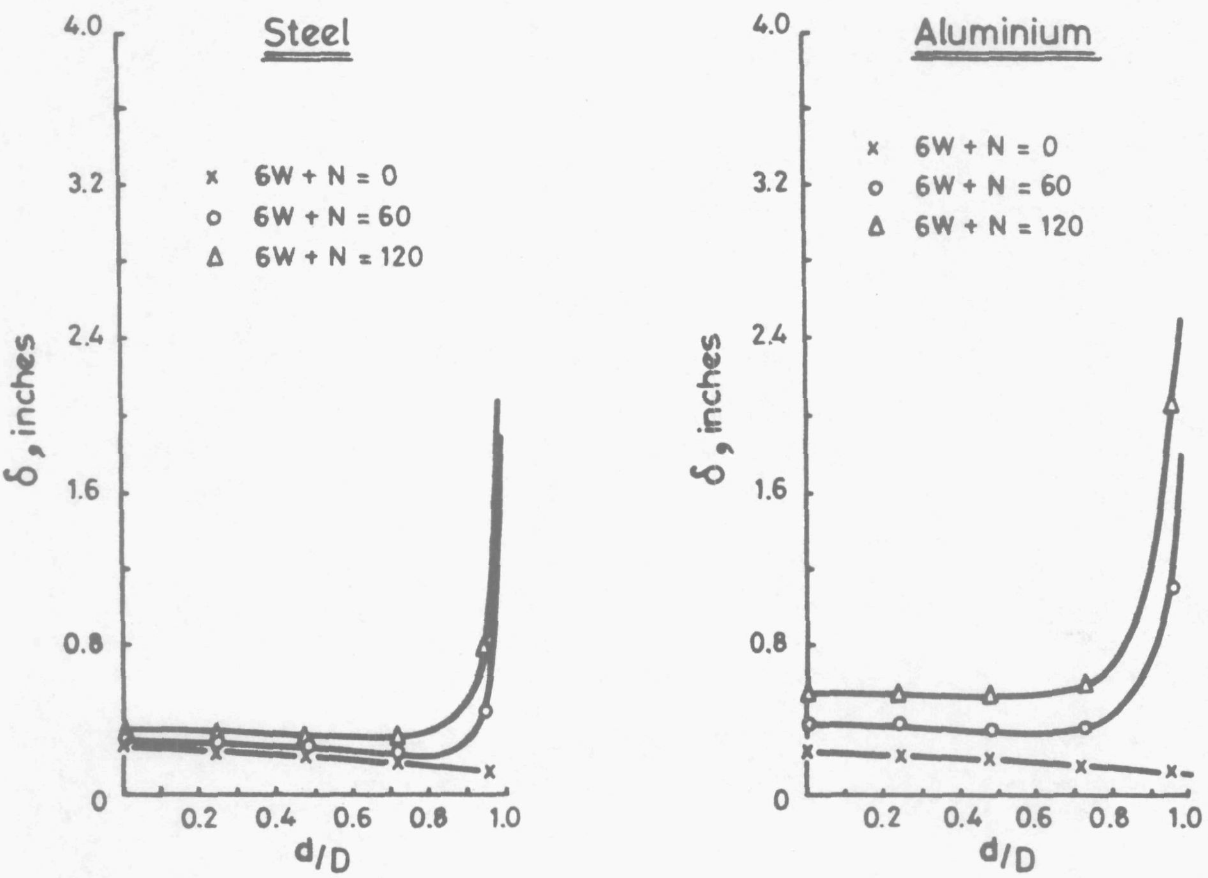

(c) Sting outside diameter = 3.0 inches , sting length = 66.0 inches

Figure 56.(cont.) Variation of sting tip displacement with loading under 6g conditions.

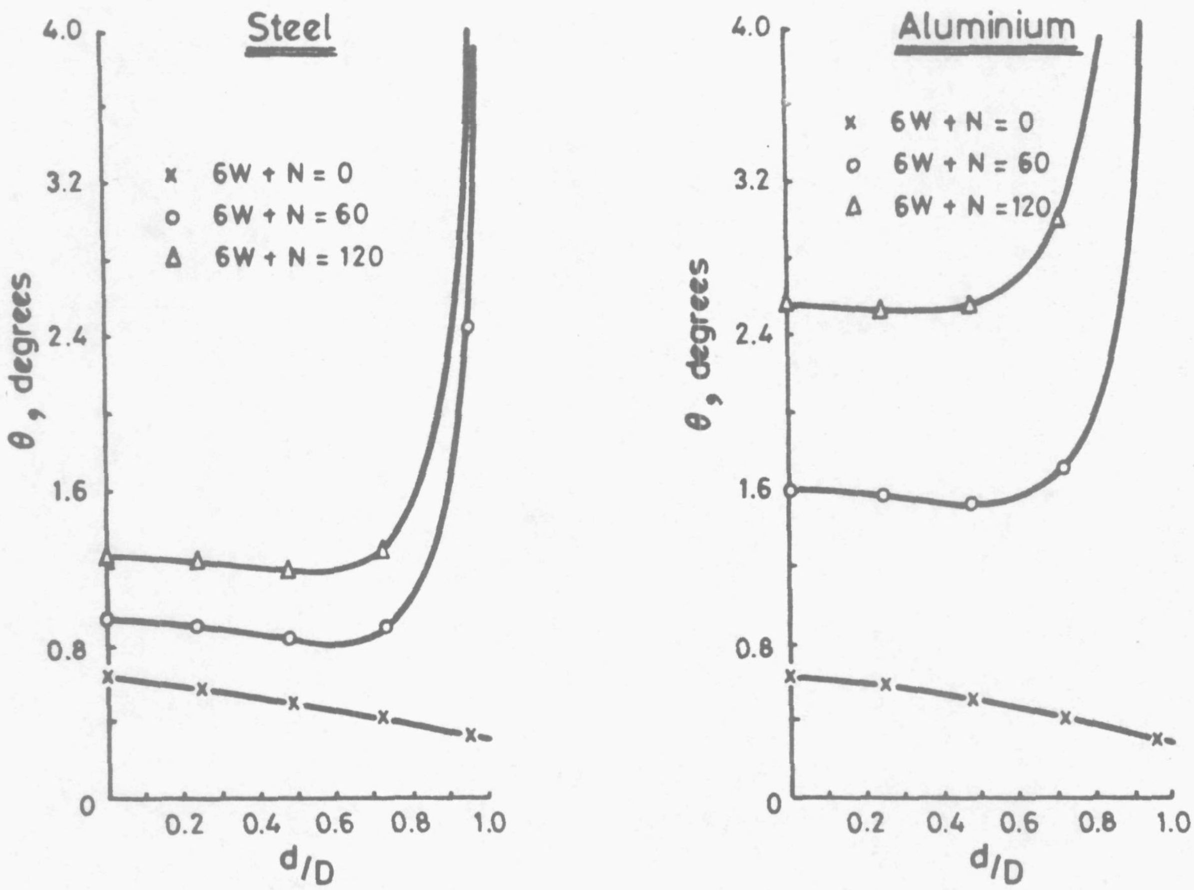

(a) Sting outside diameter = 2.0 inches , sting length = 66.0 inches

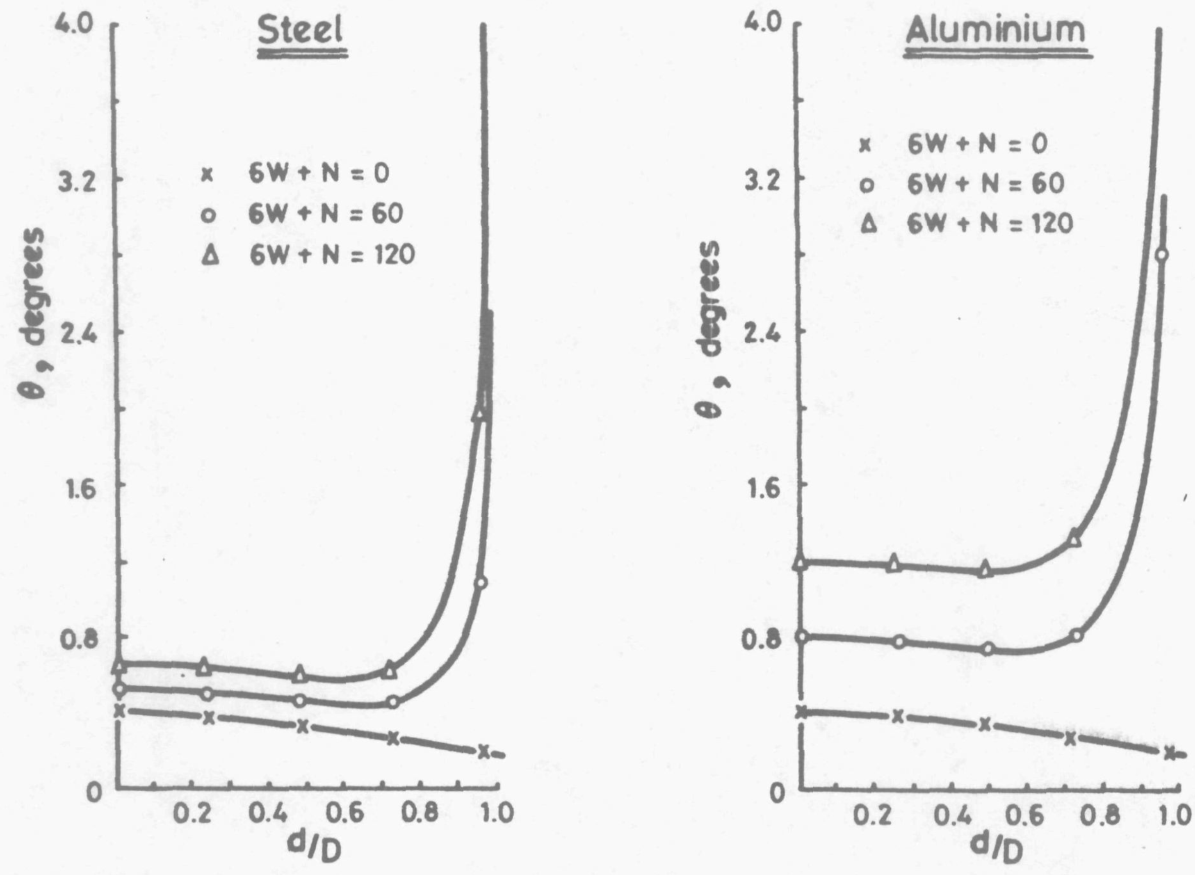

(b) Sting outside diameter = 2.5 inches , sting length = 66.0 inches

Figure 57. Variation of sting tip inclination with loading under 6g conditions.

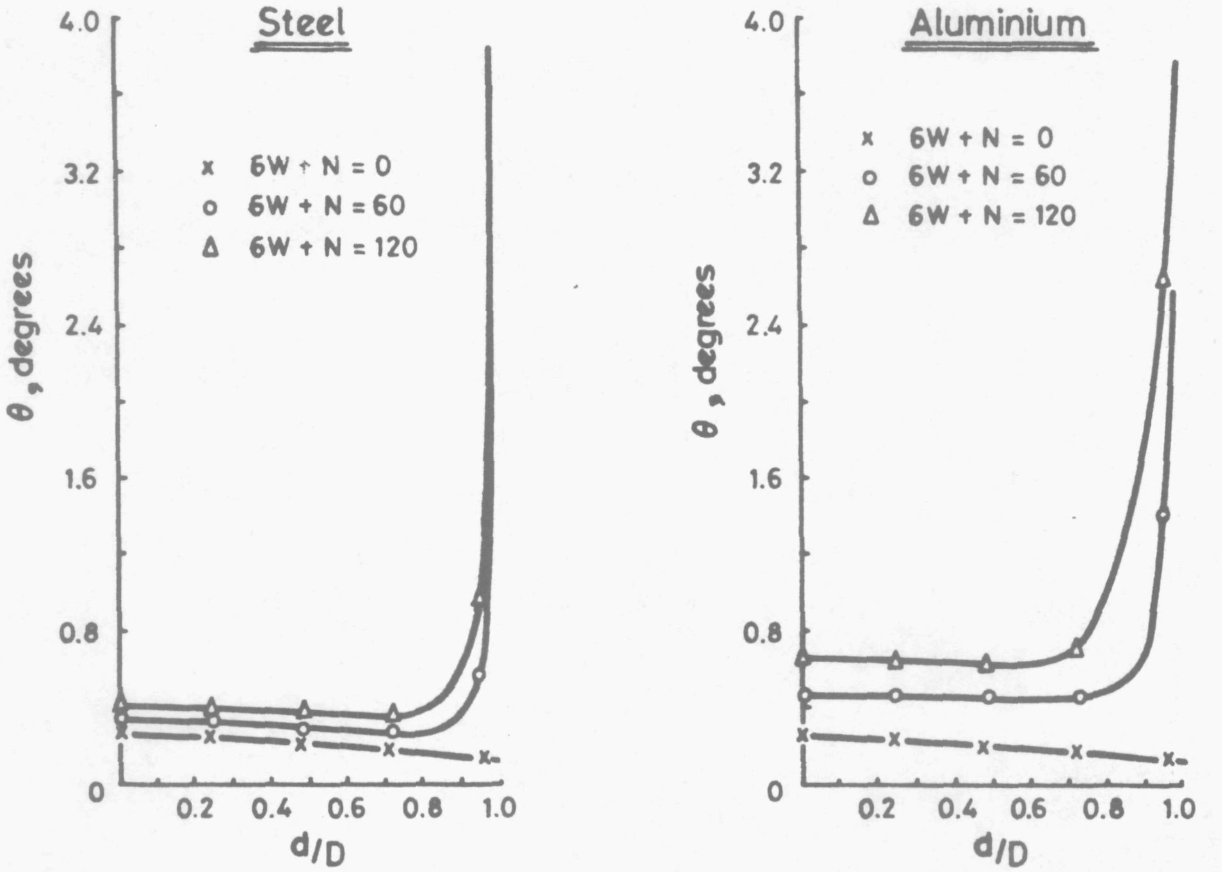

(c) Sting outside diameter = 3.0 inches, sting length = 66.0 inches

Figure 57.(cont.) Variation of sting tip inclination with loading under 6g conditions.

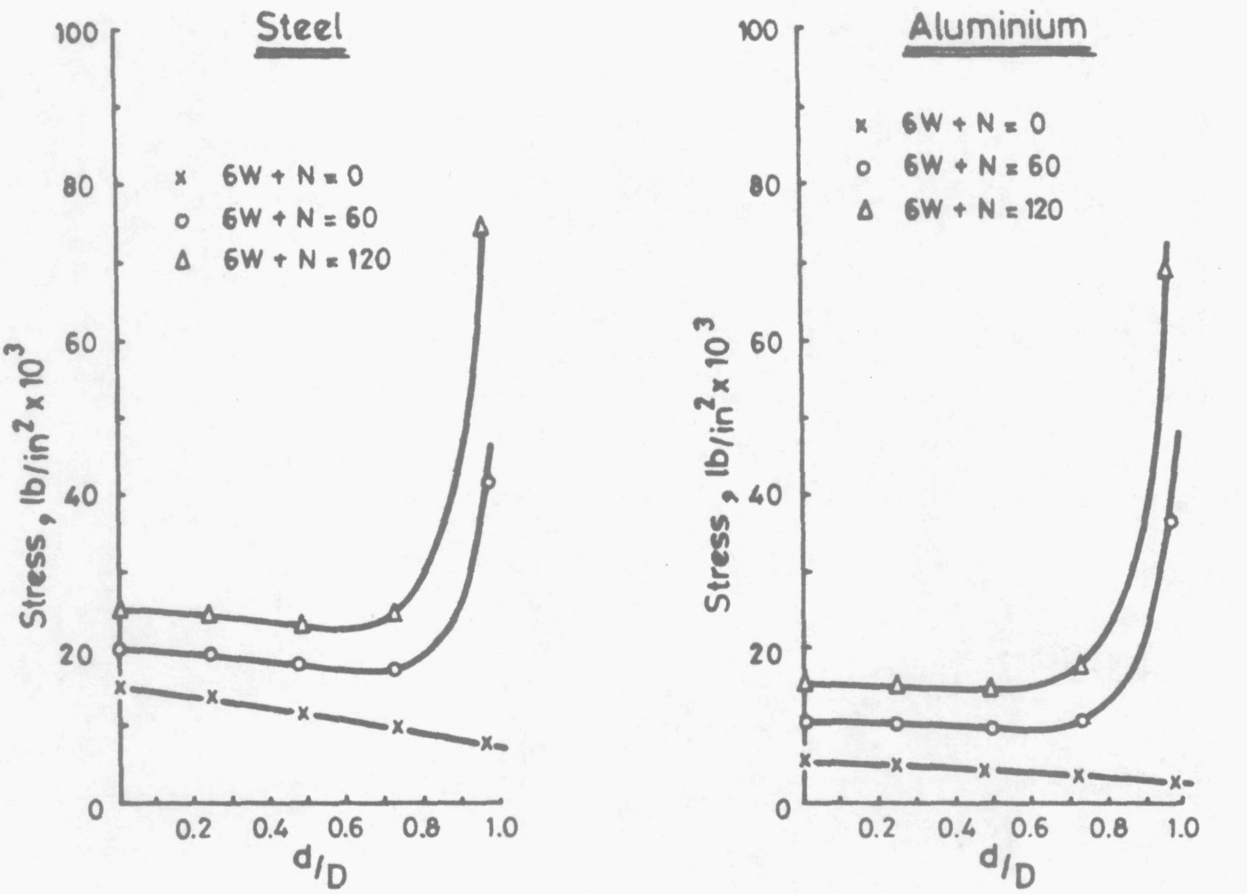

(a) Sting outside diameter = 2.0 inches , sting length = 66.0 inches

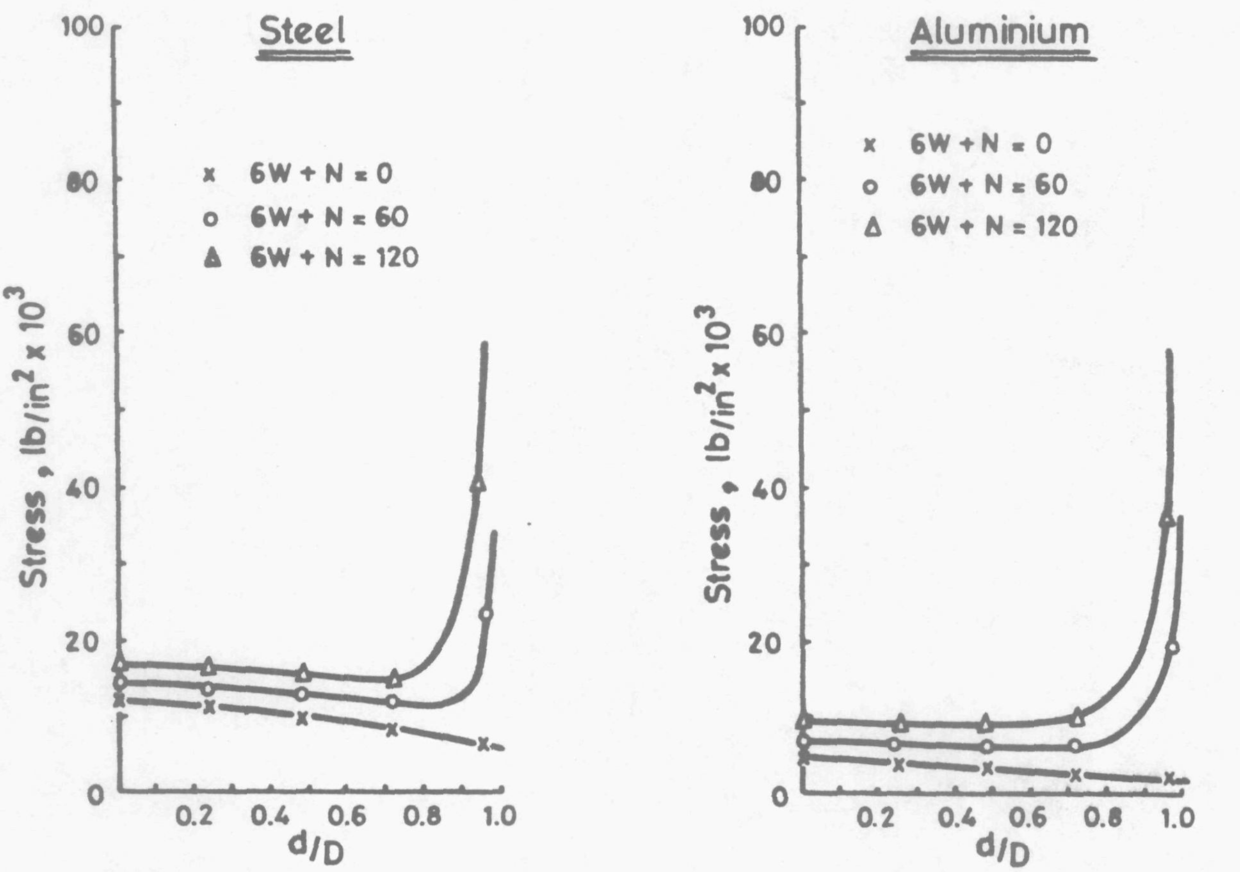

(b) Sting outside diameter = 2.5 inches , sting length = 66.0 inches

Figure 58. Variation of sting root stress with loading under 6g conditions.

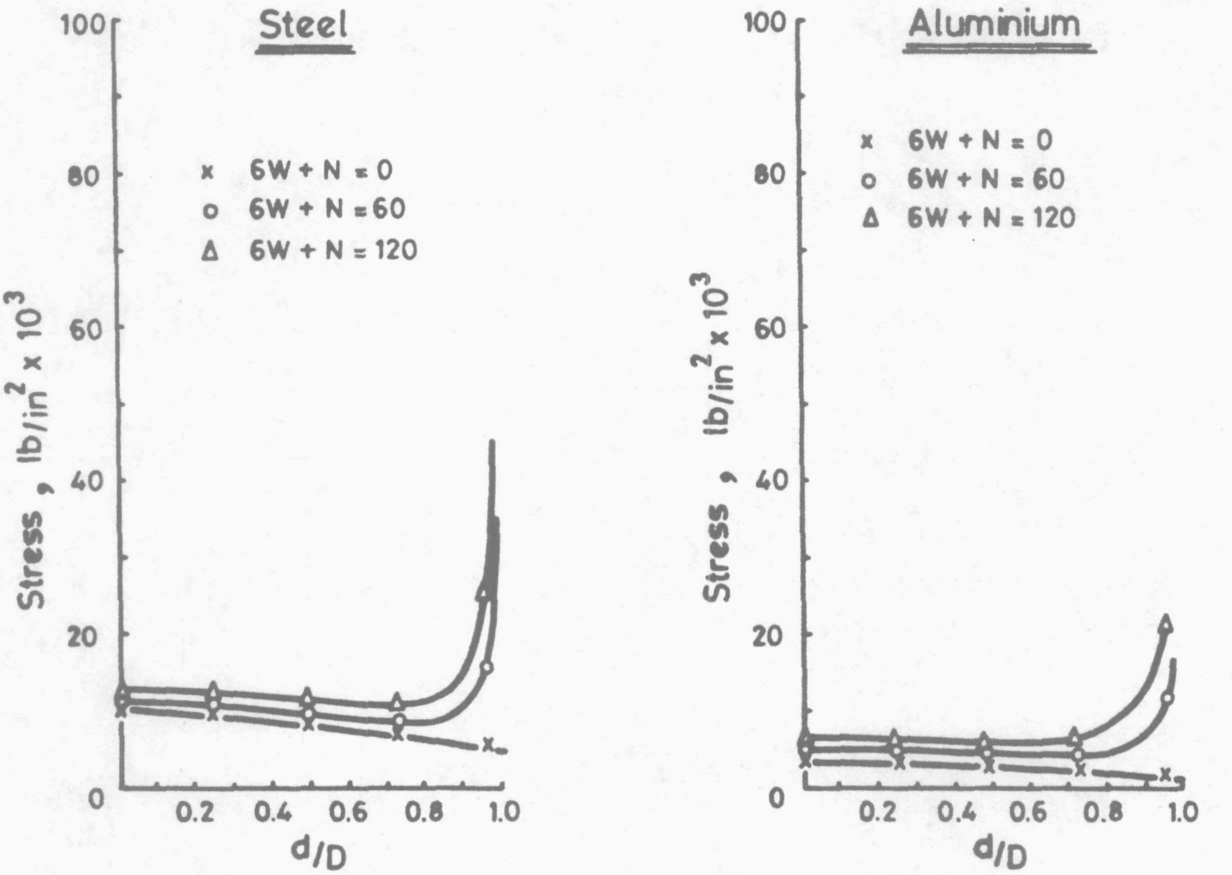

(c) Sting outside diameter = 3.0 inches , sting length = 66.0 inches

Figure 58.(cont.) Variation of sting root stress with loading under 6g conditions.

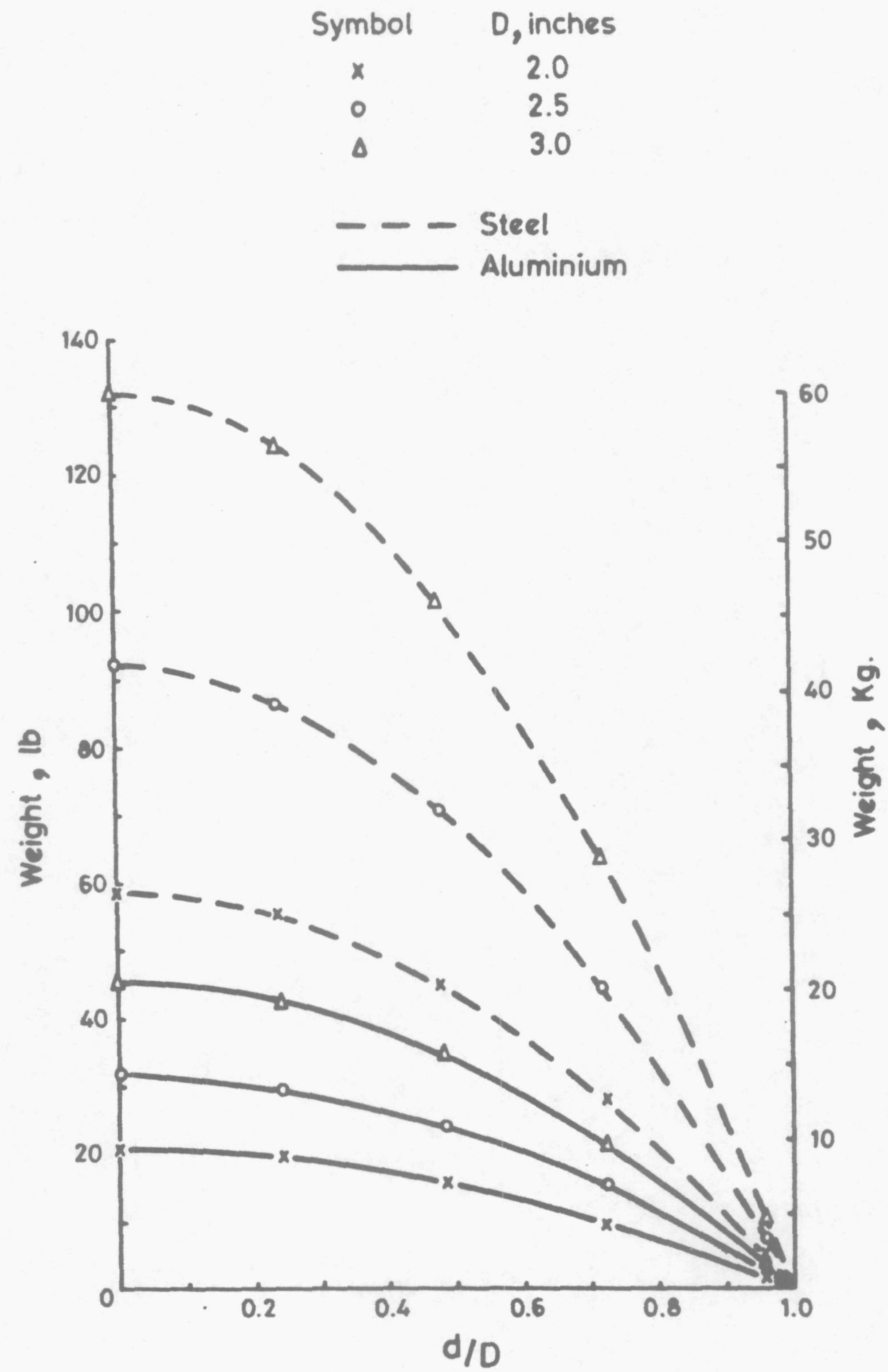

Figure 59. Weight characteristics of constant diameter steel and aluminium tubes 66.0 inches (1.676 m) long.

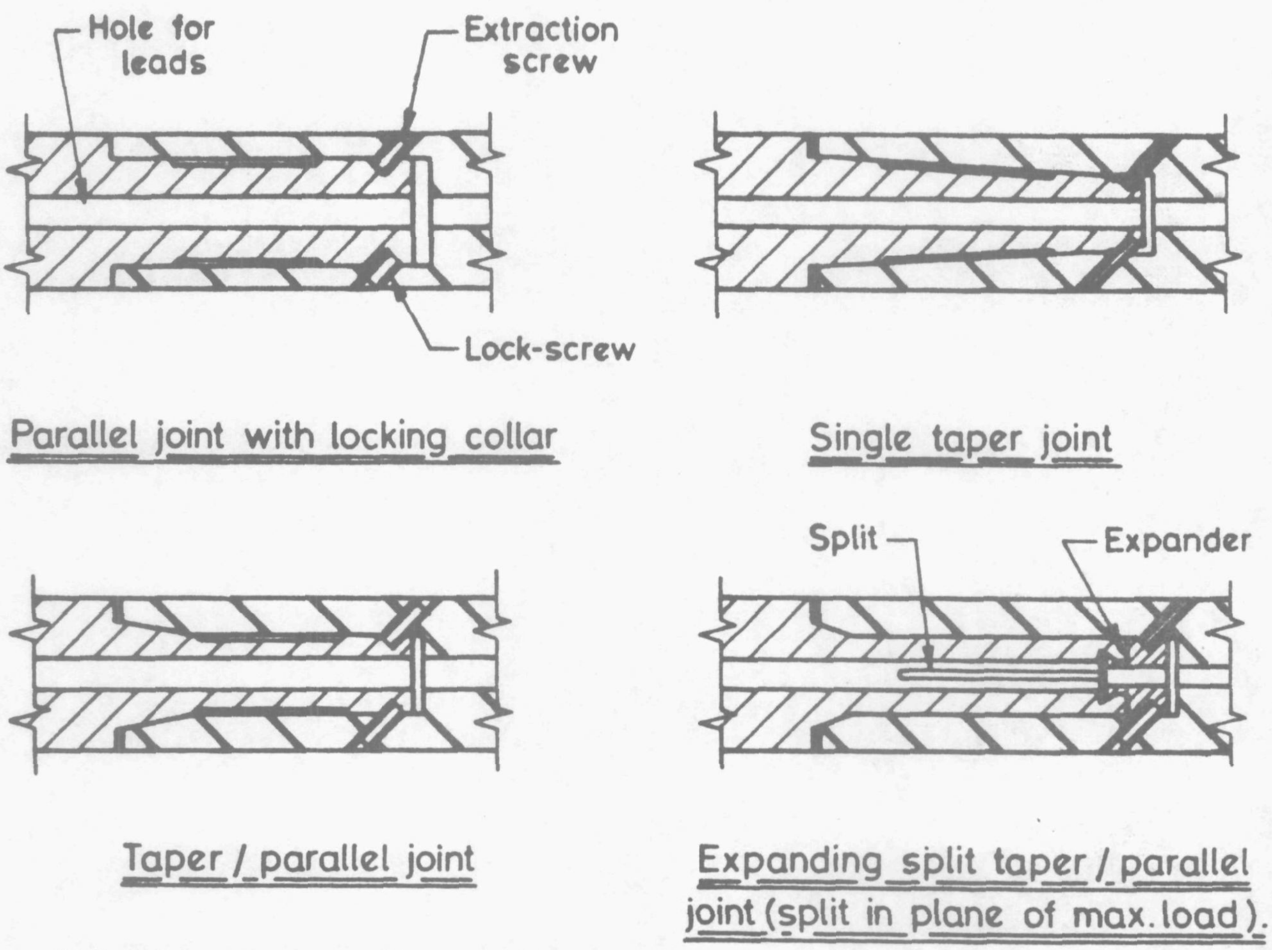

(a) Common sting joints.

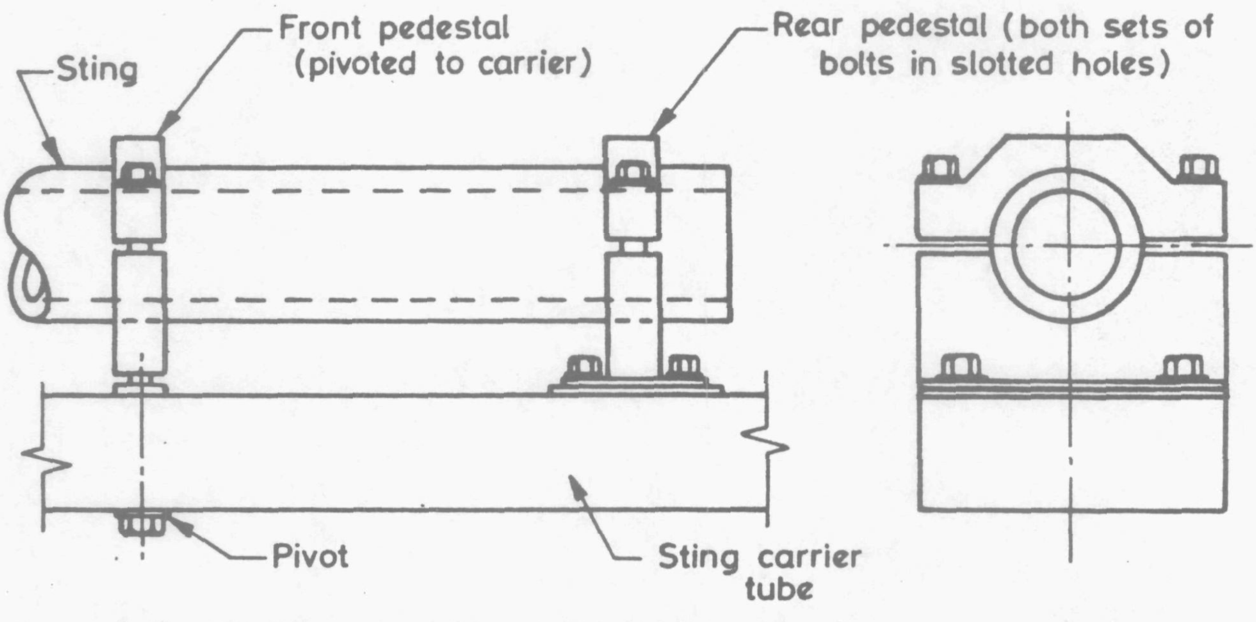

(b) Design used on Whirling Arm.

Figure 60. Sting attachment to carrier tube.

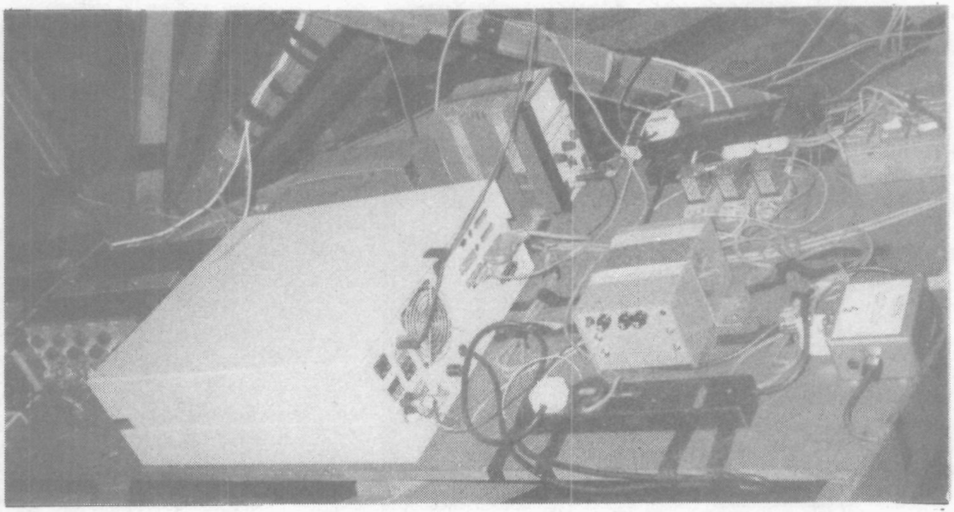

a) Midas and Scanivalve control system.

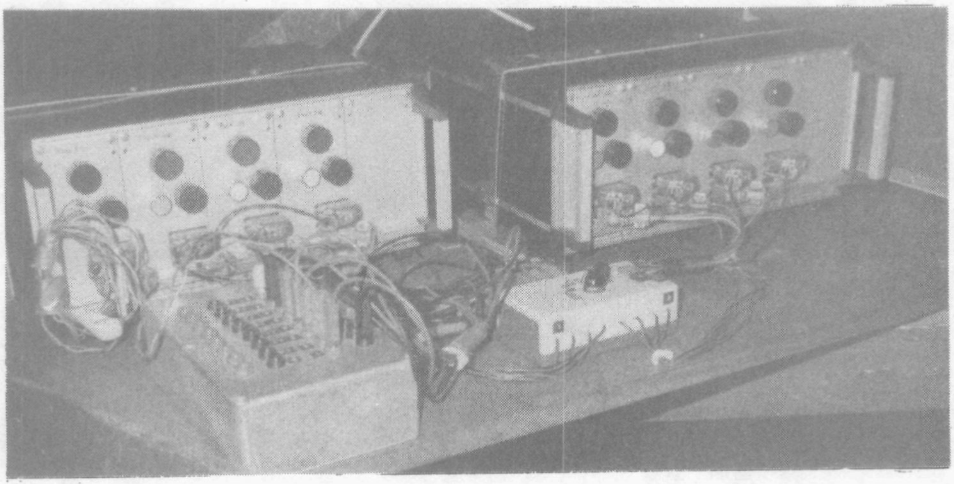

b) Analogue signal conditioning system.

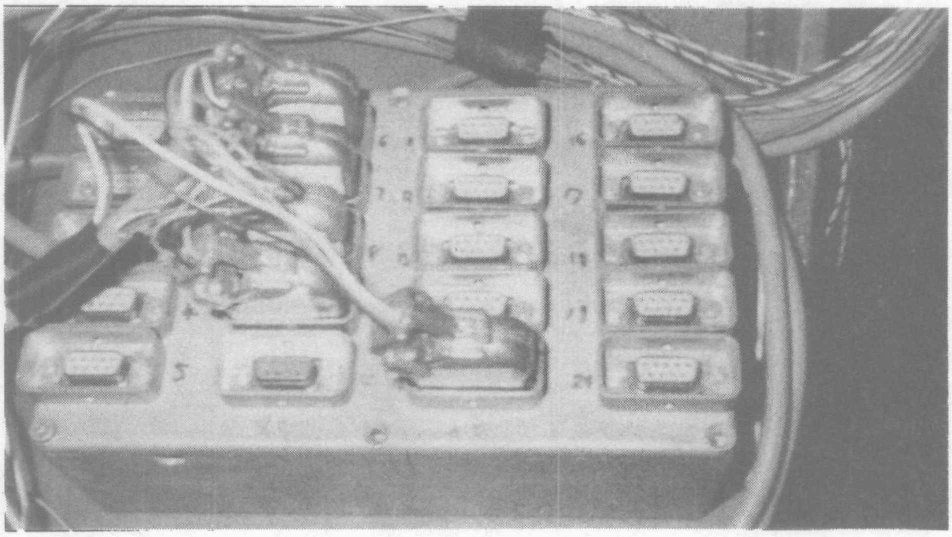

c) Distribution board.

Figure 61. Instrumentation platform.

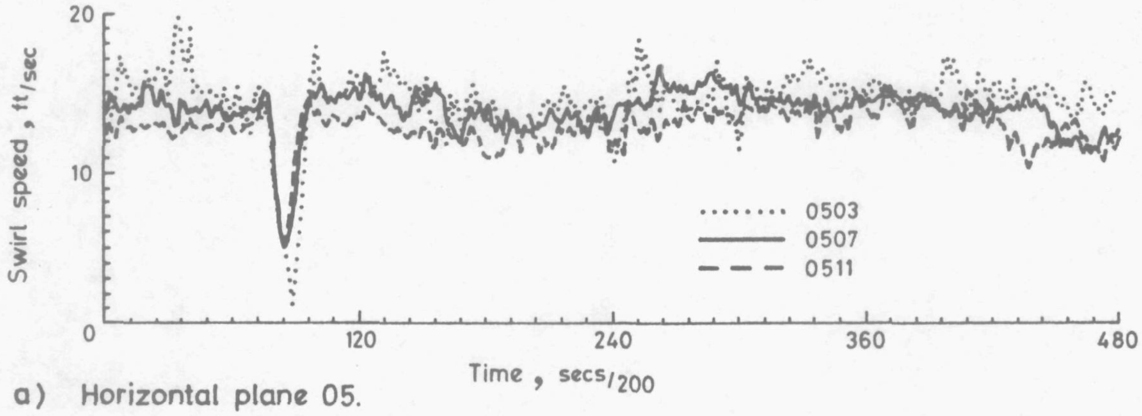

a) Horizontal plane 05.

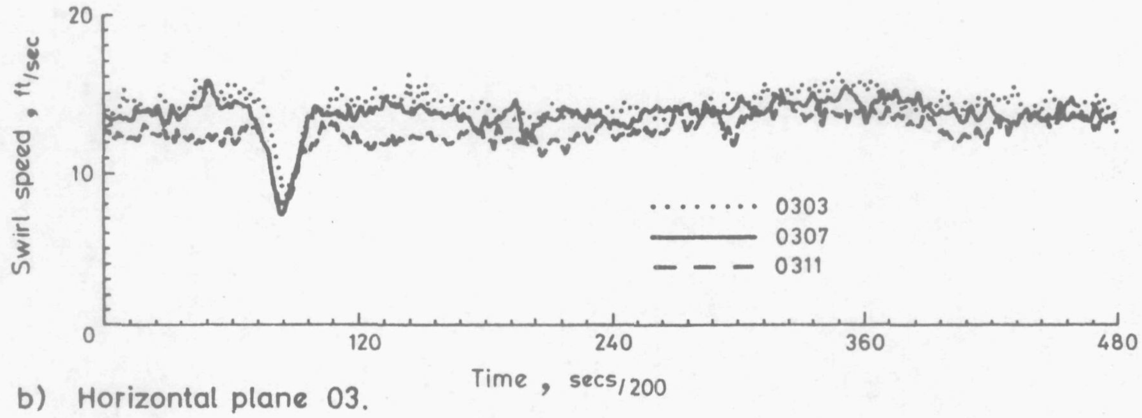

b) Horizontal plane 03.

Figure 62. Swirl distributions.

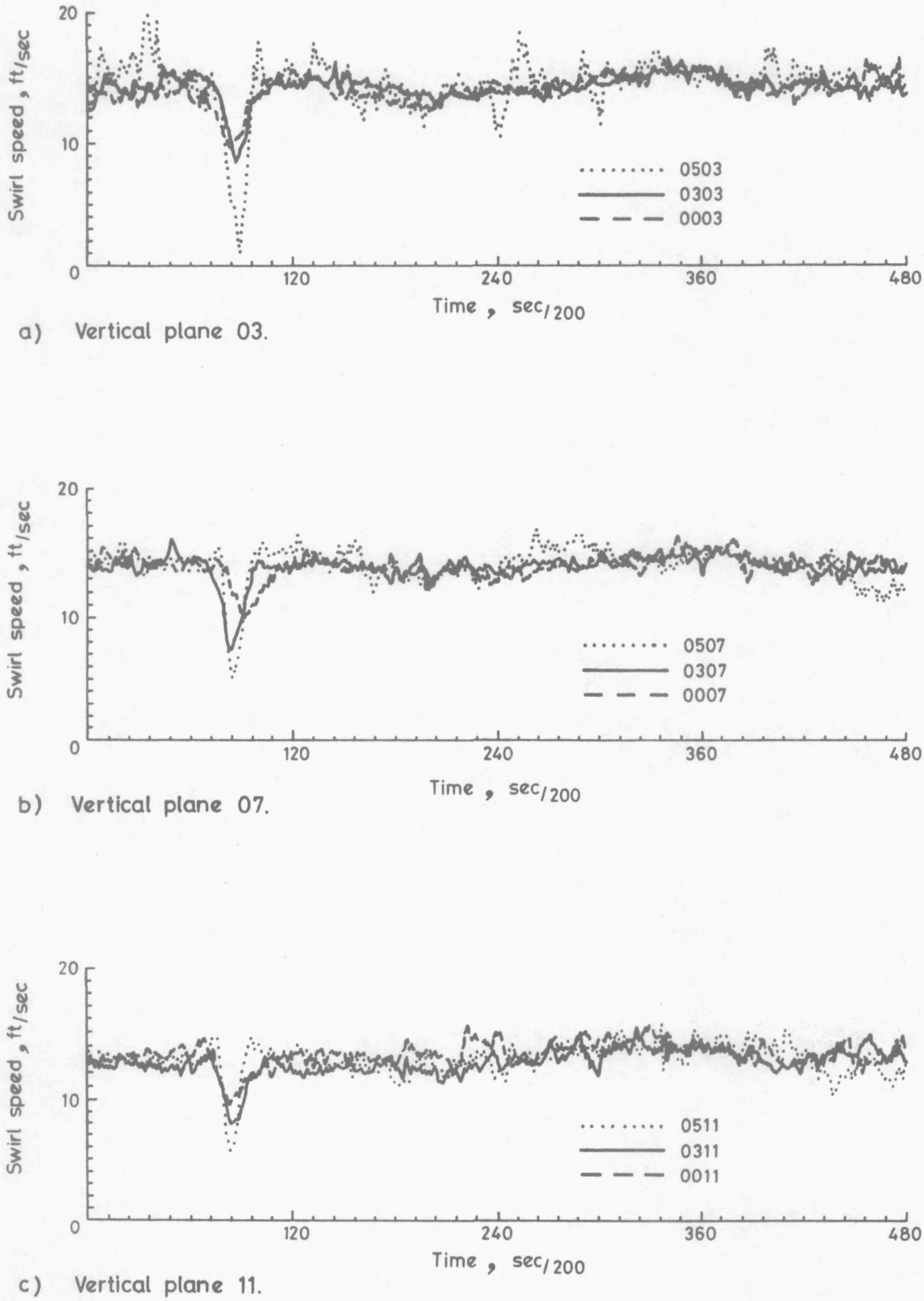

Figure 63. Swirl distributions.

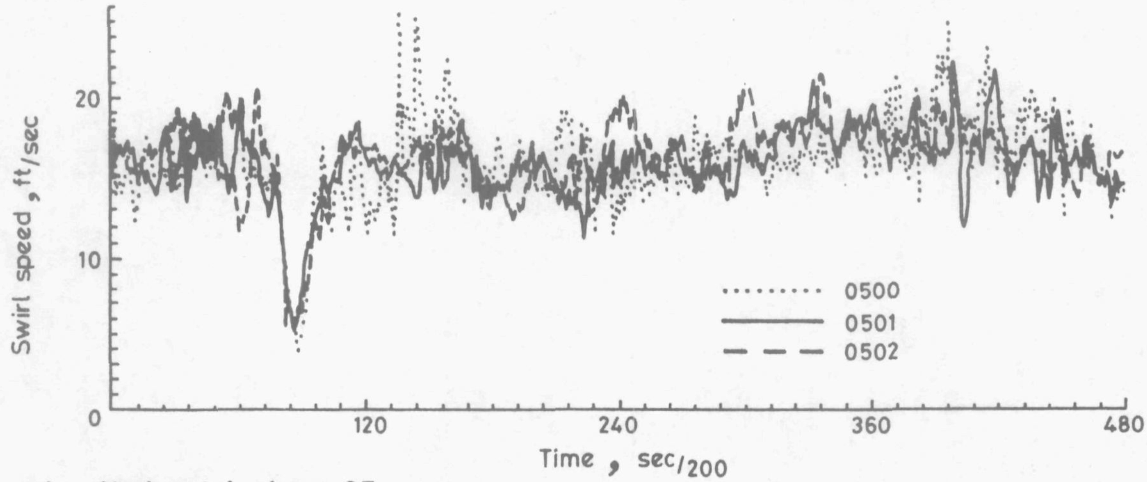

a) Horizontal plane 05.

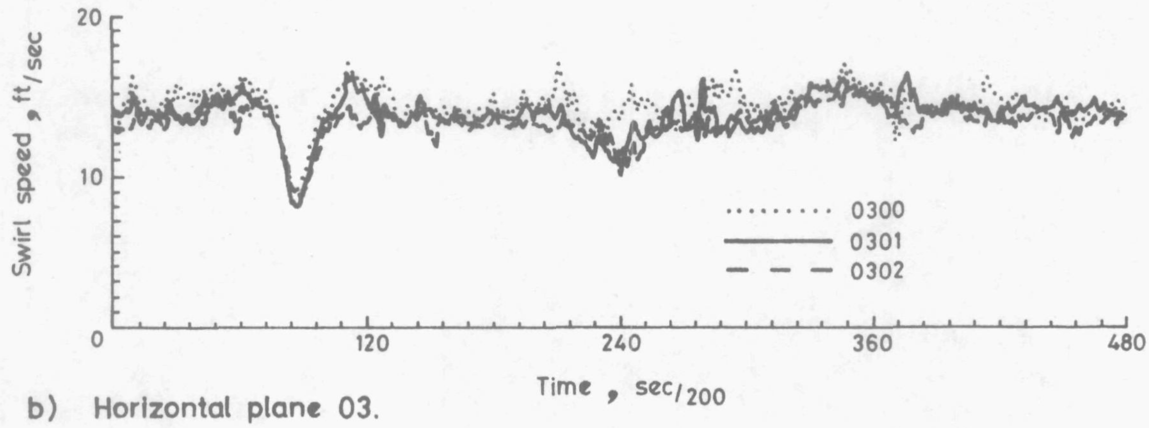

b) Horizontal plane 03.

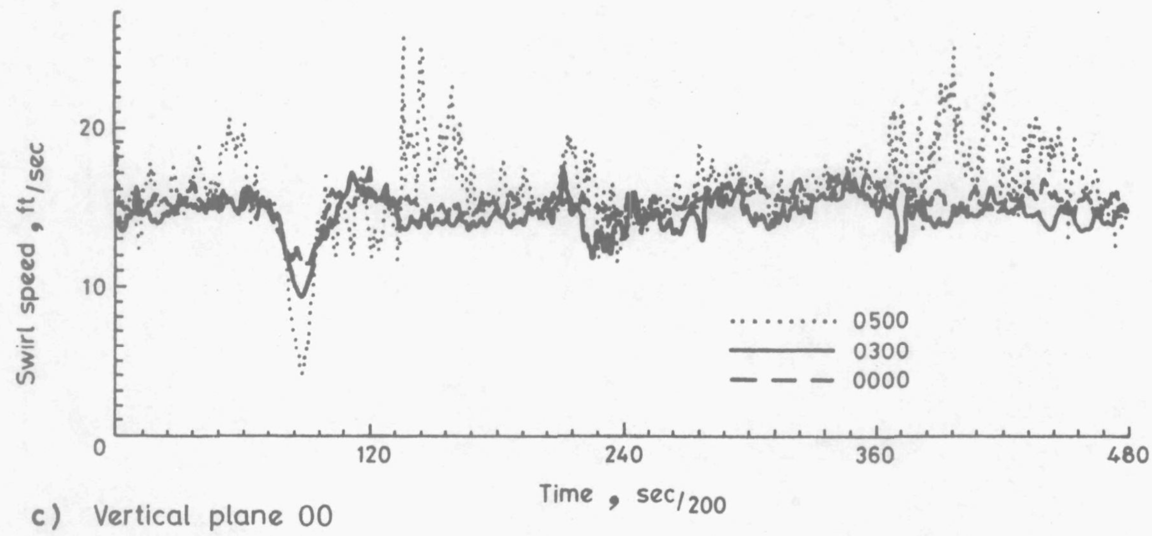

c) Vertical plane 00

Figure 64. Swirl distributions near the wall.

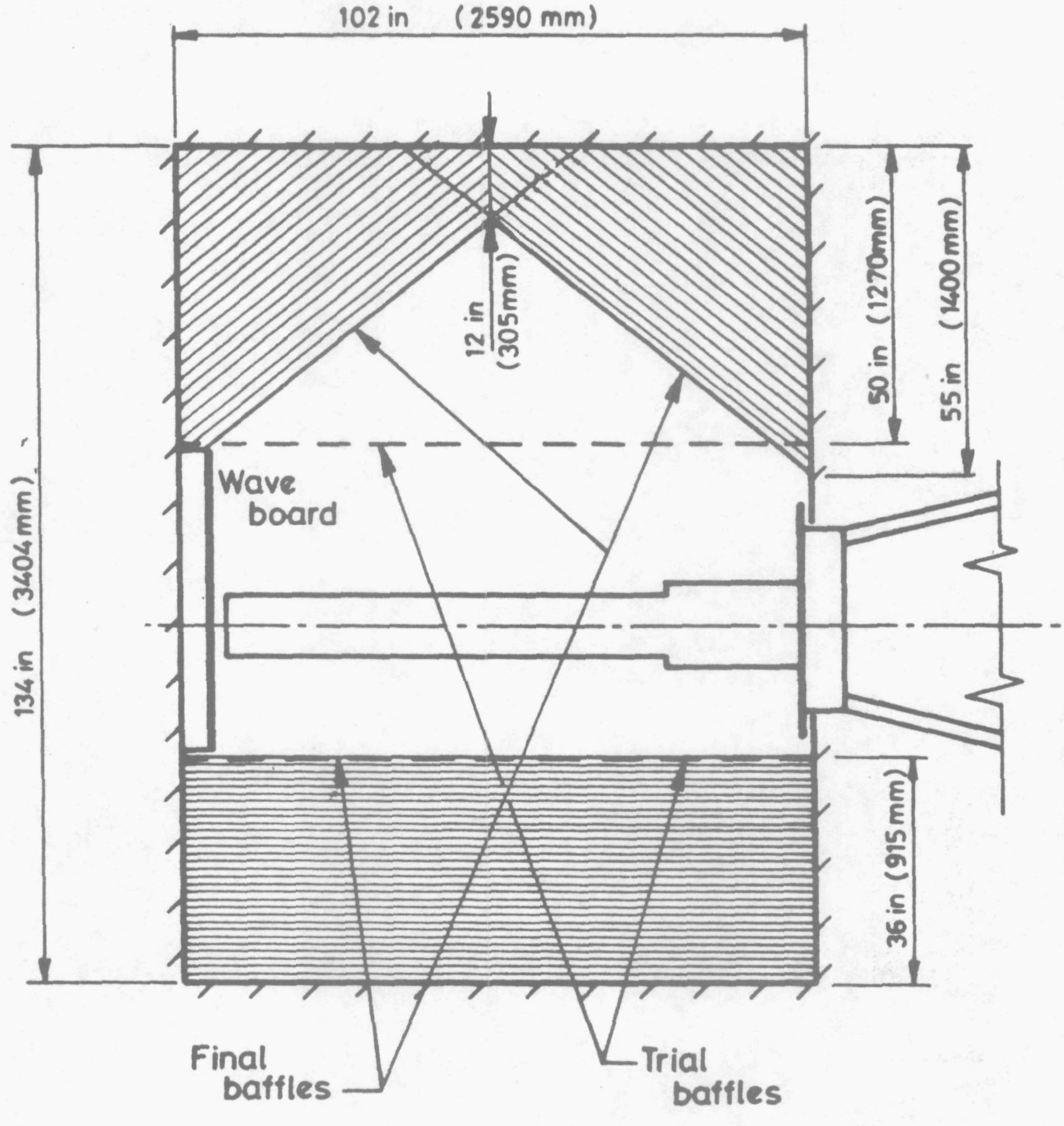

Trial installation :- 2 sets at 180° apart.
Final installation :- 6 sets at 60° apart.

Figure 65. Porous baffles installed in the Whirling Arm.

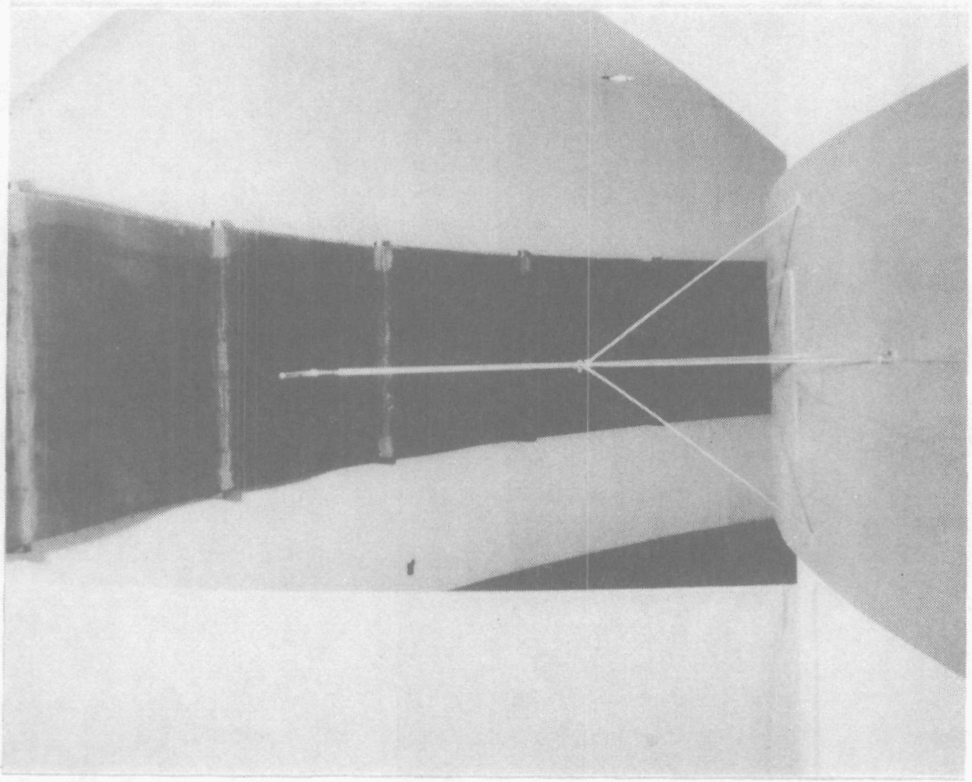

(a) Pitot-static measuring approach speed.

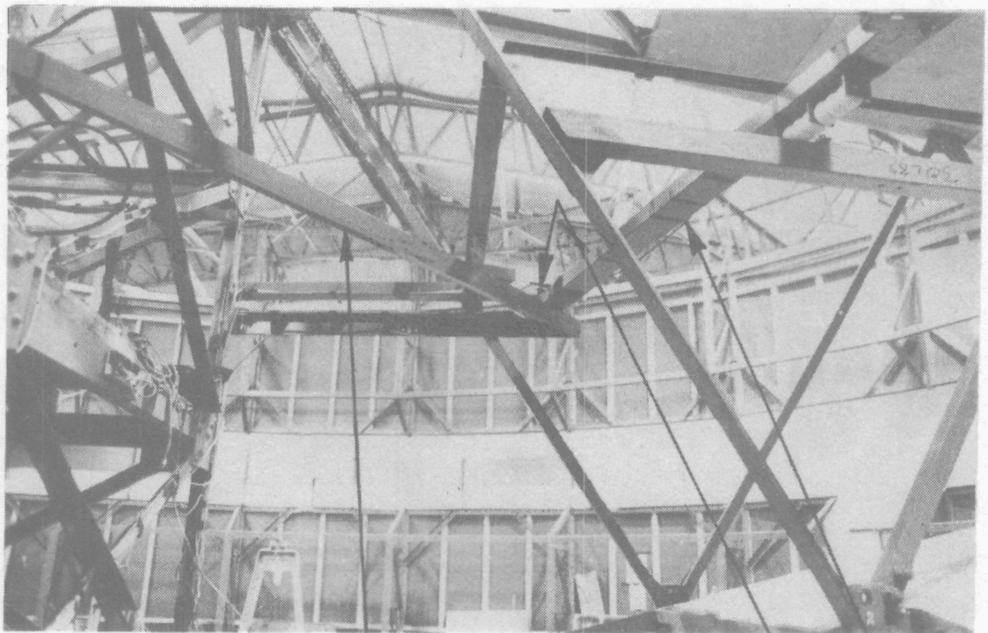

(b) Reinforcement of control beam pivot.

Figure 66. C of A Whirling Arm, measurement of approach speed and pitch angle.

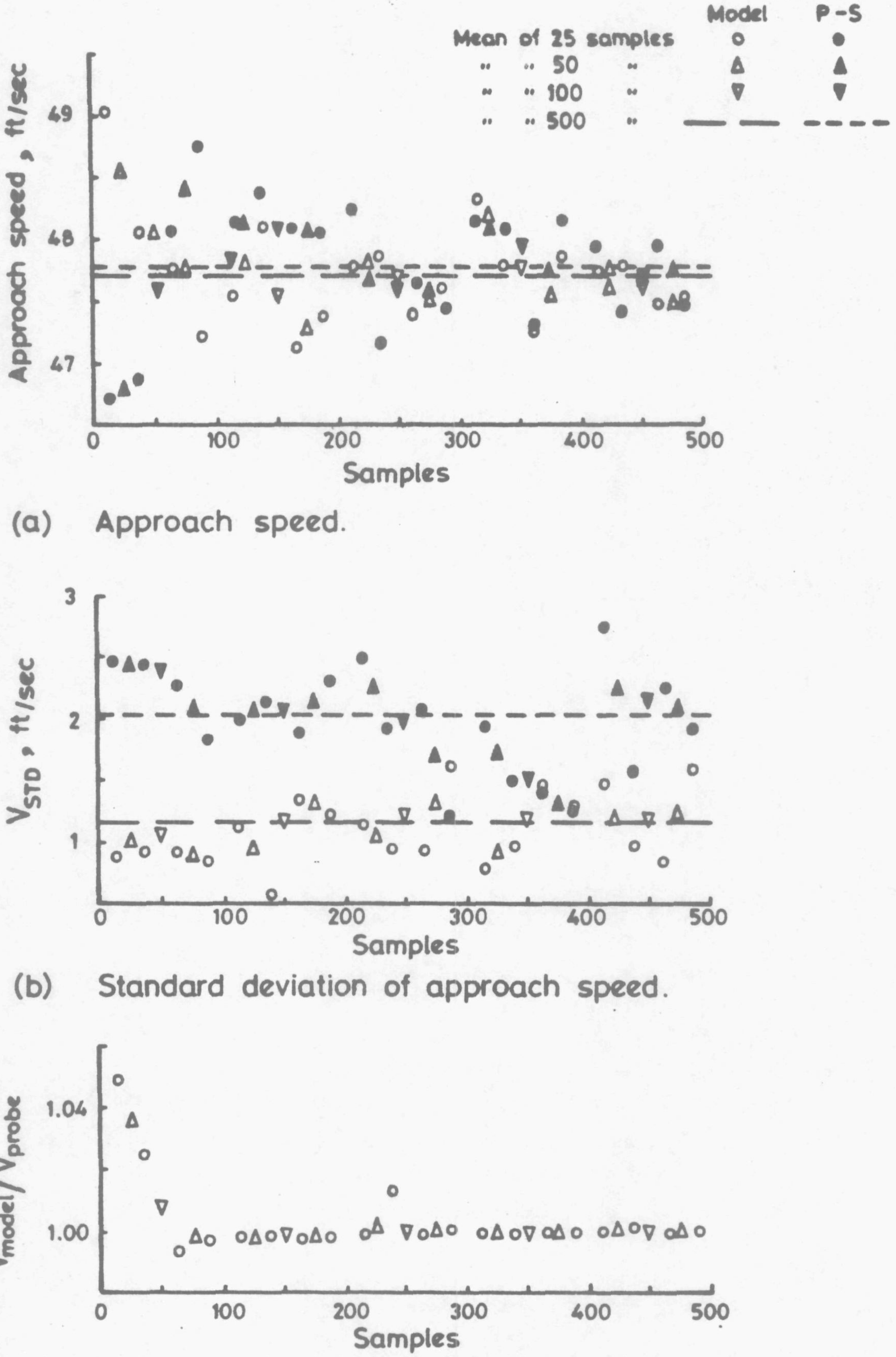

(a) Approach speed.

(b) Standard deviation of approach speed.

(c) Ratio of approach speeds at model and pitot-static probe.

Test speed = 18.42 r.p.m. = ft/sec at model radius.

Figure 67. Effect of group size on measurements of approach speeds at the model and pitot-static probe.

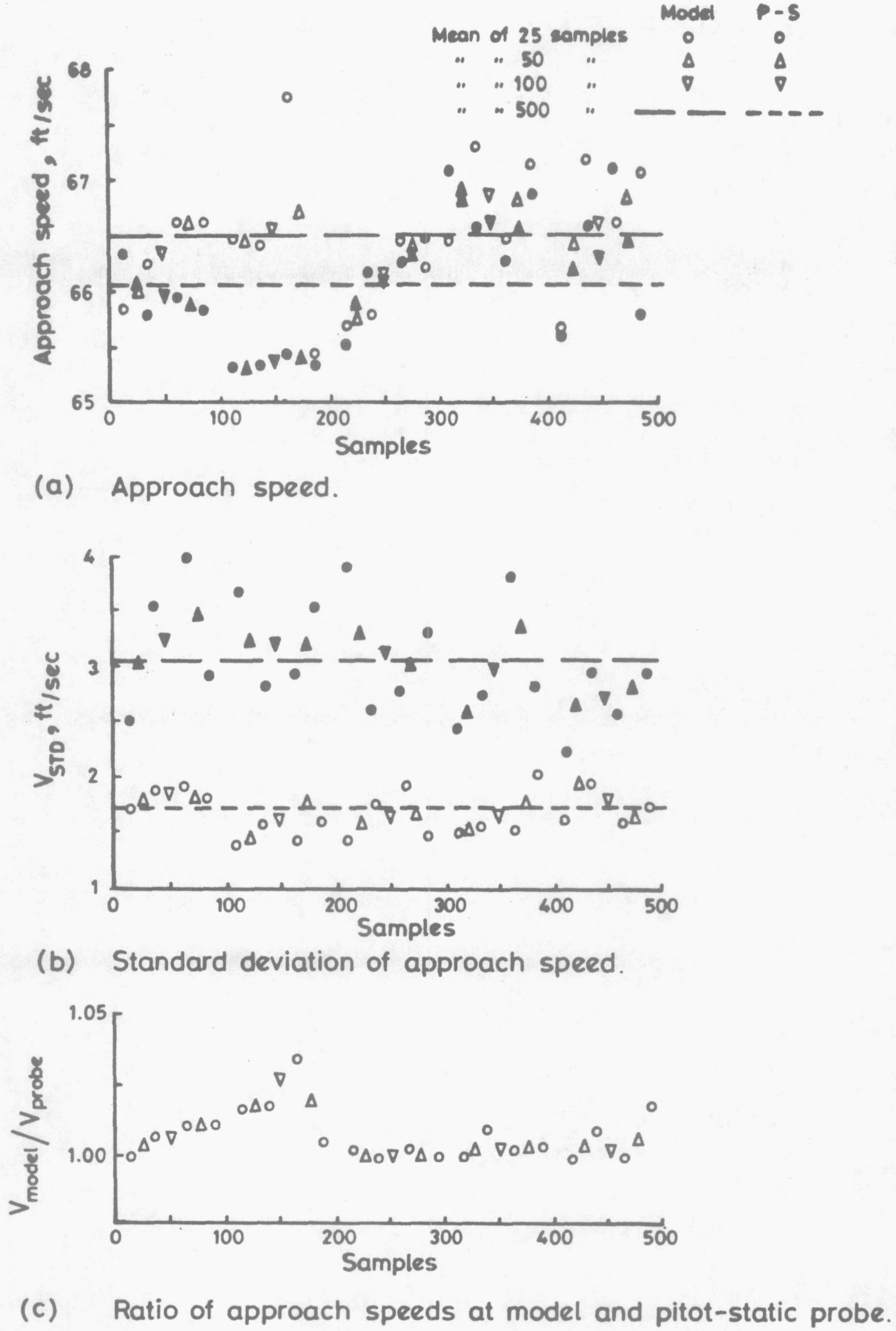

Test speed = 25.59 r.p.m = ft/sec at model radius.

Figure 68. Effect of group size on measurements of approach speeds at the model and pitot-static probe.

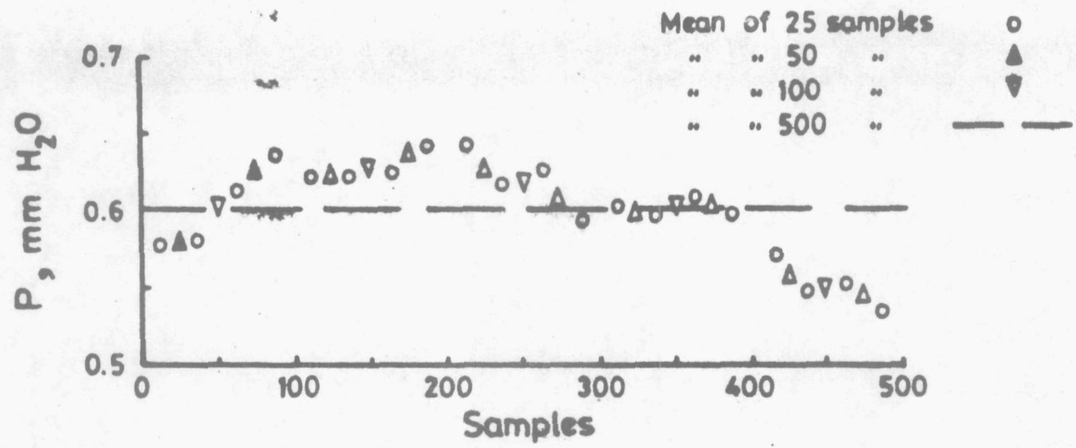

(a) Model static tapping.

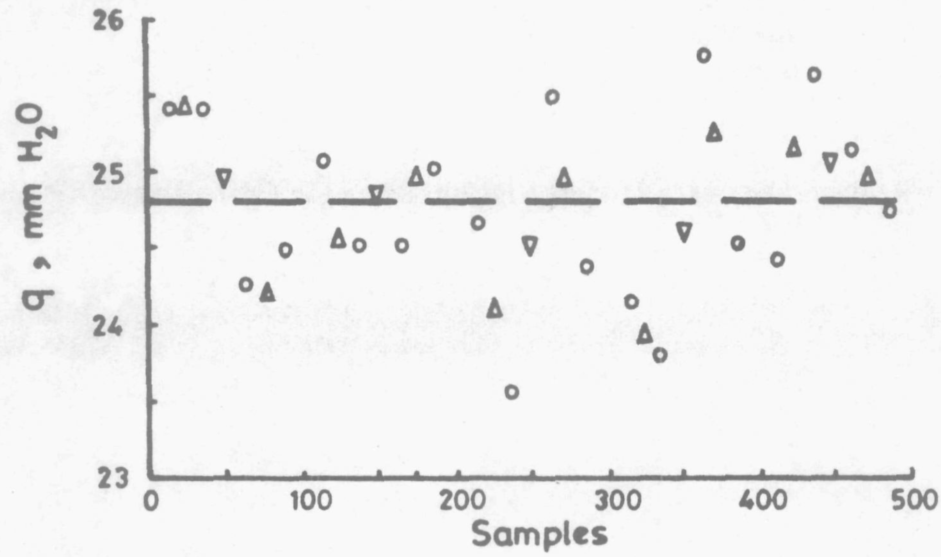

(b) Pitot - static probe.

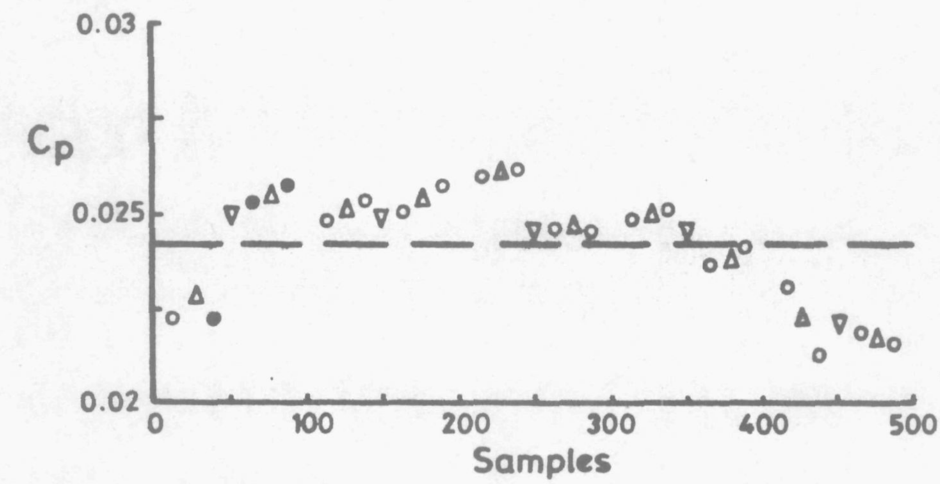

(c) Pressure coefficient C_p at model pressure tapping.

Figure 69. Effect of group size on measurement of mean pressures and C_p.

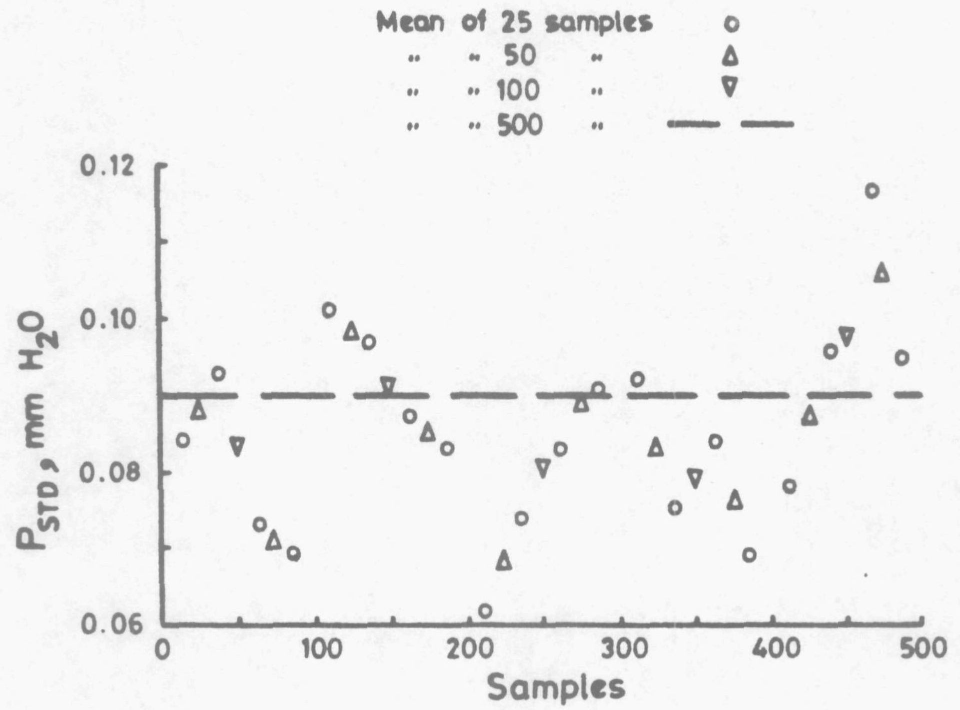

(a) Model pressure tapping.

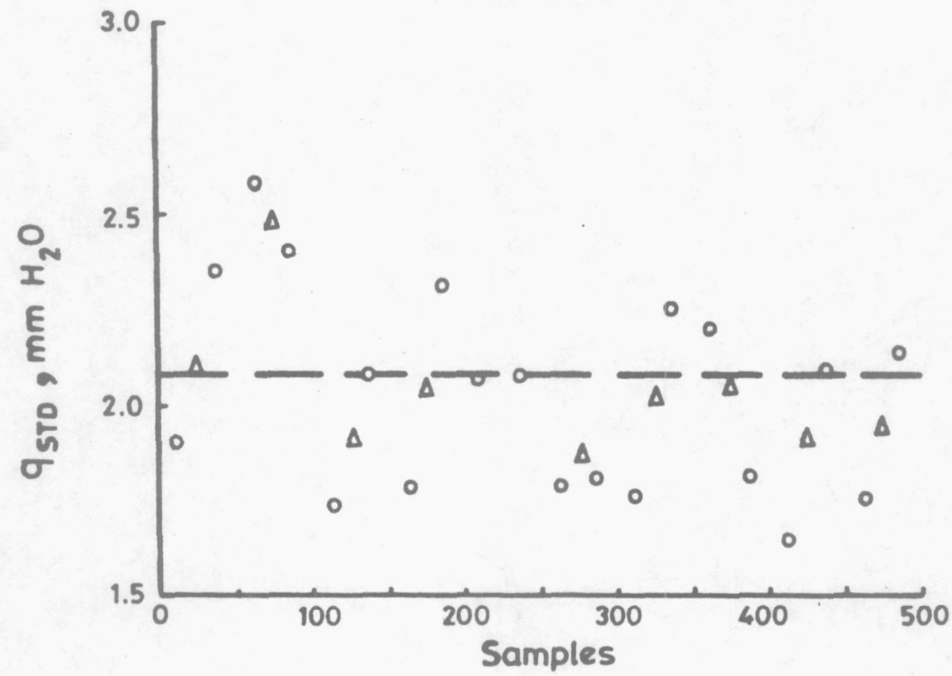

(b) Pitot-static probe.

Figure 70. Effect of group size on the standard deviations obtained when measuring pressures.

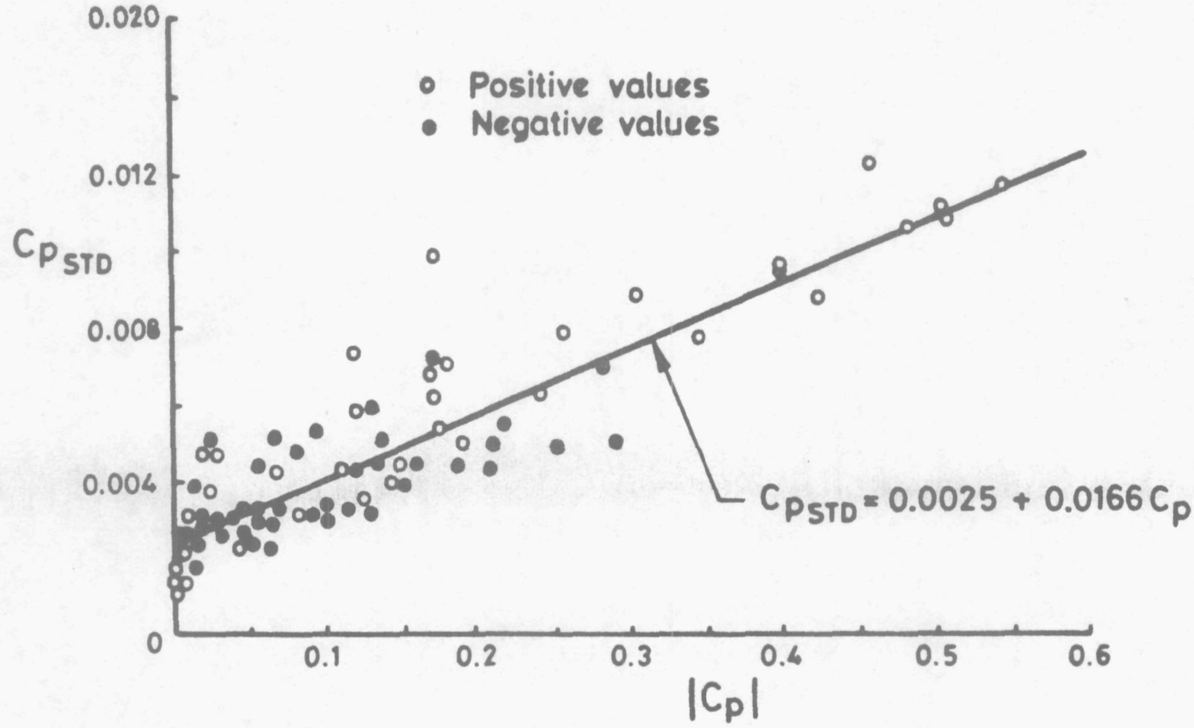

(a) Variation of the standard deviation with C_p.

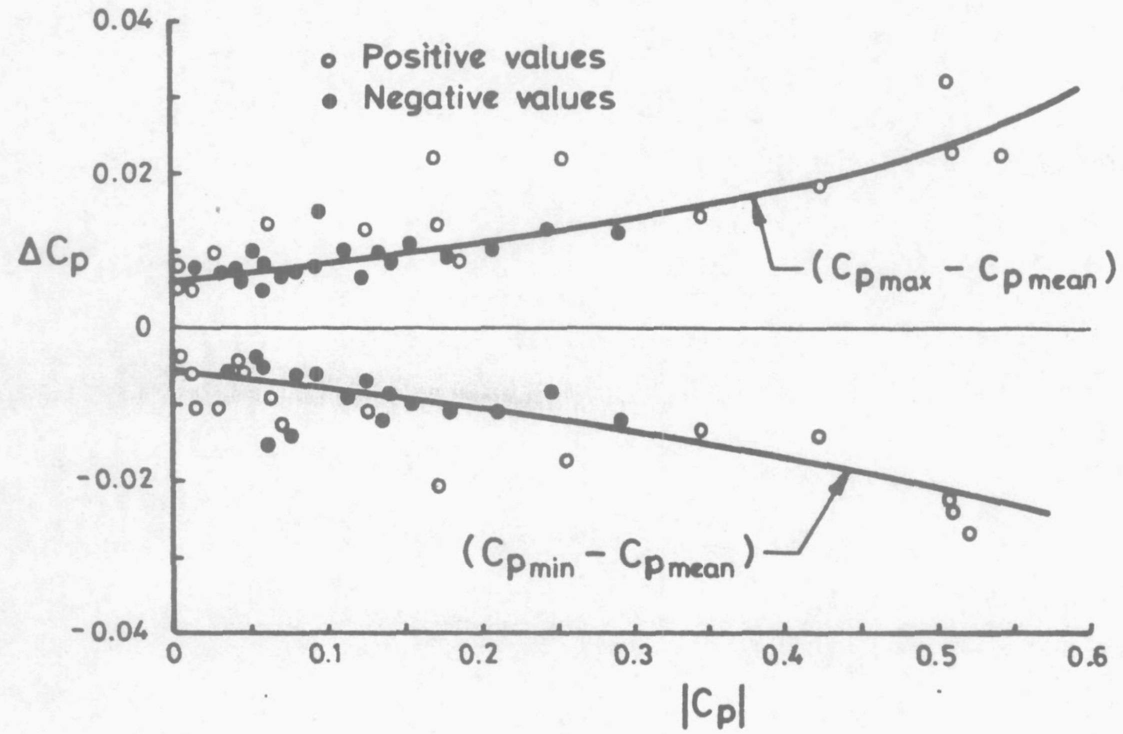

(b) Spread of C_p values relative to the mean value.

Figure 71. Repeatability of C_p measurements, arm speed = 25.46 rpm